Assessment of Drought and Crop Yield: A Climate Change Perspective

Submitted in partial fulfilment of the requirement for the award of the degree of

Doctor of Philosophy

by

Soumyashree Dixit

Roll No. 717002

Supervisor

Prof. K.V. Jayakumar

DEPARTMENT OF CIVIL ENGINEERING
NATIONAL INSTITUTE OF TECHNOLOGY
WARANGAL-506004, INDIA
June 2022

APPROVAL SHEET

This dissertation work entitled "**Assessment of Drought and Crop Yield: A Climate Change Perspective"** by **Ms. Soumyashree Dixit** is approved for the degree of Doctor of Philosophy.

Examiners

_____

_____

_____

Supervisor

Prof. K V Jayakumar
Department of Civil Engineering, NIT Warangal

Chairman

Professor & Head
Department of Civil Engineering, NIT Warangal

Date:

NATIONAL INSTITUTE OF TECHNOLOGY WARANGAL

CERTIFICATE

This is certify that the thesis entitled "**Assessment of Drought and Crop Yield: A Climate Change Perspective**" being submitted by **Ms. Soumyashree Dixit** for award of the degree of Doctor of Philosophy to the Faculty of Engineering and Technology of National Institute of Technology Warangal is a record of bonafide research work carried out by her under my supervision and this thesis has not been submitted elsewhere for award for any other degree.

(K.V. JAYAKUMAR)
Thesis supervisor
Emeritus Professor
Department of Civil Engineering
National Institute of Technology Warangal

DECLARATION

This is to certify that the work presented in the thesis entitled "**Assessment of Drought and Crop Yield: A Climate Change Perspective**" is a bonafide work done by me under the supervision of **Prof. K.V. Jayakumar** and was not submitted elsewhere for the award of any degree.

I declare that this written submission represents my ideas in my own words and where others' ideas or words have been included, I have adequately cited and referenced the original sources. I also declare that I have adhered to all principles of academic honesty and integrity and have nor misrepresented or fabricated or falsified any idea/data/fact/source in my submission. I understand that any violation of the above will be a cause for disciplinary action by the Institute and can also evoke penal action from sources which have thus not been properly cited or from whom proper permission has not been taken when needed.

Soumyashree Dixit

Roll No. 717002

Date: 01/06/2022

ACKNOWLEDGEMENTS

The research work and the current thesis are outcomes of constant inspiration and help from a number of persons at various spheres of my association. I would like to convey my sincere gratitude to each and every one for their respective assistances.

With great pleasure and proud privilege, I express my deepest gratitude to my thesis Guide and Supervisor **Prof K.V. Jayakumar**, for his encouragement, constructive criticisms, timely advice, and patience throughout the course of this research work. Your keen interest and concern towards the successful completion of this research work, made me to overcome all the obstacle and proceed with the work. You always made me realise my strengths and capabilities which made me more responsible towards the work. I thank you for distilling the thesis to get a more refined one, even at the far end. **Thanks a lot sir.**

I am very much thankful to **Prof. P. Rathish Kumar** Head, Department of Civil Engineering for his constant support and encouragement.

I take immense pleasure to thank all the members of my Doctoral Scrutiny Committee, **Prof. N. V. Umamahesh**, **Dr. K Venkata Reddy** and **Dr. R. S. Selvaraj** for their detailed review, constructive suggestions and excellent advice during the course of this research work.

I am sincerely thankful to my faculties Late Prof. E. Venkata Rathnam, Prof. P. Anand Raj, Shri. V. N. Kameswara Rao, Dr. Vema Vamsi Krishna, Dr. Manish Pandey and Dr. Litan Kumar Ray for their support in my PhD course.

I am grateful to my contemporary research scholars Mr. Chinmay Kumar Das, Dr. Pritam Das, Mr. Sandip Khobragade, Mr. Ajit Kumar Mohanty, Mr. V Mainikanta, Mr. Nikhil Teja, Mr. Rudraswamy G K, K Satish Kumar, Dr. A. Uday Kumar and Dr. Seenu P Z for their constant support during my journey.

I place on record my special thanks to my friends Ms. Shubhangi Padhi, Mrs. Barsa Nayak, Mr. Satya Nayak, Mr. Sukesh Ranjan Mohanty, Mr. Aditya Shankar Kar, Mr. Rashmi Ranjan Swain, Mr. Jitendra Bhanja and Mr. Abhilash Khuntia for providing constant encouragement and moral support throughout my life. I acknowledge their love and affection towards me.

I take this opportunity to express my special heartfelt thanks to my husband Mr. Debanjan Pathak, who provided moral support throughout my PhD work and helped me in completing my work successfully.

The affection and prayer of my parents, especially my mother and my parents-in-law can never be forgotten at this juncture. Above all, I humbly acknowledge the grace and blessings of God Almighty, which enlightened my path throughout.

(SOUMYASHREE DIXIT)

CONTENTS

LIST OF TABLES

LIST OF FIGURES

LIST OF ABBREVIATIONS

AIC	Akaike Information Criterion
BC	Bias correction
CC	Canopy Cover
CCCR	Centre for Climate Change Research
CC_x	Maximum canopy cover
CDC	Canopy decline coefficient
CFM	Change factor of mean
CGC	Canopy growth coefficient
Chsq	Chi-square
CMIP5	Coupled Model Intercomparison Model Project Phage 5
CMIP6	Coupled Model Intercomparison Model Project Phage 6
CORDEX	Coordinated Regional Climate Downscaling Experiment
CRU 4.03	Climate Research Unit 4.03
CVM	Cramer-von Misses
CWA	Cross Wavelet Analysis
CWC	Central Water Commission
CWP	Cross Wavelet Power
CWS	Cross Wavelet Spectrum
DEM	Digital Elevation Model
ENSO	El Nino Southern Oscillation
EQM	Empirical Quantile Mapping
E_s	Soil evaporation
ET_a	Evapotranspiration
FAO	Food and Agriculture Organization
GAMLSS	Generalized Additive Model in Location, Scale and Shape
GCMs	Global Climate Models
GDC	Growth decline coefficient
GDP	Gross Domestic Product
GLDAS	Global Land Data Assimilation System

GoF	Goodness of Fit
HI	Harvest Index
HI_o	Reference harvest index
HRUs	Hydrologic Response Units
IITM	Indian Institute of Tropical Meteorology
IMD	Indian Meteorological Department
IOD	Indian Ocean Dipole
IPCC	Intergovernmental Panel on Climate Change
ISMR	Indian Summer Monsoon Rainfall
KS	Kolmogorov-Smirnov test
LULC	Land Use and Land Cover
MDI	Multivariate Drought Index
MEI	Multivariate ENSO Index
MK	Mann Kendall
MLE	Maximum likelihood estimation
MME	Multi-model ensemble
MSDI	Multivariate Standardised Drought Index
NSE	Nash-Sutcliffe Efficiency
NSPI	Non-stationary Standardized Precipitation Index
PCC	Pairwise Copula Construction
PET	Potential Evapotranspiration
RCMs	Regional Climate Models
RCPs	Representative Concentration Pathways
RDI	Reconnaissance Drought Index
REA	Reliability Ensemble Averaging
RMSE	Root Mean Square Error
RTDI	Reconnaissance Trivariate Drought Index
SOI	Southern Oscillation Index
SPEI	Standardised Precipitation Evapotranspiration Index
SPI	Standardised Precipitation Index

SRTM	Shuttle Radar Topography Mission
SSI	Standardised Soil moisture Index
SSPs	Socio-economic Shared Pathways
SST	Sea Surface Temperature
SUFI-2	Sequential Uncertainty Fitting-2
SWAT	Soil Water Assessment Tool
SYRS	Standardised Yield Residual Series
T_r	Transpiration
WP*	Water Productivity
XWT	Cross Wavelet Transform

ABSTRACT

The ecological and socio-economic development of a region are directly or indirectly related to the natural resources like water. Spatial and temporal changes on the water budget for a particular region are due to the combined response of changes in the land cover, meteorology, geological features, morphological characteristics like basin slope and topography, climate change and anthropogenic activities. Climate change is a global phenomenon having varying degree of regional effects. Assessment of the adverse consequences of climate and anthropogenic effects on drought for proper allocation and risk management is a challenging issue for the water managers. Further, modulating effect of climate has far-reaching influence on agriculture, environment, social factors and natural extreme calamities like flood and drought with an intensified severity. Droughts in India affect food production, gross domestic product (GDP), livelihood, and socio-economic condition of a large population associated with agriculture. Droughts are a complex natural hazard, and the intensity, frequency, and duration of droughts are increasing in India and around the world, resulting in immense industrial, agricultural, and economic losses each year. Drought is generally defined as an abnormally prolonged dry period when the amount of rainfall is below the normal level (meteorological drought), soil moisture below the threshold level (agricultural drought) or there is deficit amount of water storage and runoff (hydrological drought). In the recent decades, long and severe droughts have triggered significant losses and lasting changes in vegetation conditions, owing to climate change, and the increasing demand for water resources. Future drought projections can be helpful for the development of efficient adaptation strategies by assessing the influence of climate change impacts on water resources Drought severity, intensity, onset and termination characteristics must be investigated in the river basin scale.

The principal tools for the assessment of climate change projections of drought regimes are the Global Climate Models (GCMs) and Regional Climate Models (RCMs). There is an existence of gaps between the GCM realization and hydrological features in spatial and temporal scale and hence the GCMs are not able to efficiently simulate the hydro-meteorological processes in a finer scale. Compared to the observed parameters, raw outputs from GCMs are commonly biased with systematic errors, and resolution of GCMs are too coarse to be used as inputs for drought management. GCM forecasts based on bias correction techniques need post processing before using the model outputs for drought prediction. It

has been well documented that the drought will be affected by the changes in the monsoonal system over India and accordingly the economy of the country will be influenced by the climate change. Hence, the spatial extent, occurrences, onset and withdrawal of drought events must be monitored based on the long-term climate projections by using suitable and reliable indices to provide water planners correct information to take appropriate disaster response measures. Globally, the water demand is increasing with the increase in population and their need with rapidly developing cities, industries and agriculture which lead to decrease in the availability of freshwater resources. Therefore, the hydrological alterations attributed to climate change must be investigated for accessing water availability and sustainable development especially the agricultural country like India.

The study is focussed on Godavari River Basin (GRB) to understand the alteration in the drought phenomenon for future scenarios. In the initial part of the thesis, The Standardised Precipitation Evapotranspiration Index (SPEI) at 3-month time scale was calculated using Climate Research Unit 4.03 (CRU 4.03) precipitation, minimum and maximum temperatures data sets. The drought magnitude and characteristics are determined using SPEI, which considered both precipitation and temperature data as input variables. The Mann Kendall (MK) trend analysis was performed to identify the trend associated with drought characteristics. The basin was divided into six homogeneous regions using K-means clustering algorithm. Reliability Ensemble Averaging (REA) method was used for ensemble averaging of RCMs. The drought frequency analysis was carried out using trivariate copula for reference and future time period. Variations in the drought characteristics were observed in the future scenarios with respect to the reference period. Drought duration, severity, and peak for different climate divisions showed increasing trend in future time period especially in case of Representative Concentration Pathway (RCP8.5) scenarios. The return periods of future droughts based on weighted average RCMs climate models under the two scenarios showed the possibility of more frequent drought in the far future (2053-2099) than in the past (1971-2017).

The second part of the thesis deals with the non-stationary drought index development and their risk assessment. It is well known that the stationarity is the basic assumption in the statistical interpretations of time series in hydrologic processes. Stationarity refers to the parameters of the climate that are invariant with time and space and free of trends. Stationary property is questionable in the context of global warming and anthropogenic changes in climate. The outcome of environmental changes exhibits non-

stationary behaviour in climatic parameters and hence indicators have been developed for identifying drought status in non-stationary conditions which can help in better management of water resources. Under variable climatic conditions, the conventional Standardized Precipitation Index (SPI) and Reconnaissance Drought Index (RDI) are inadequate for predicting extreme drought characteristics. Non-stationary Standardized Precipitation Index (NSPI) and Non-stationary Reconnaissance Drought Index (NRDI) are, therefore, developed by fitting non-stationary distributions. The Generalized Additive Model in Location, Scale and Shape (GAMLSS) framework, with time varying location parameters considering the external covariates, was used to fit the non-stationary distributions. Multivariate ENSO Index (MEI), Southern Oscillation Index (SOI), Sea Surface Temperature (SST), and Indian Ocean Dipole (IOD) were considered as external covariates for the non-stationary drought assessment. The performances of stationary and non-stationary models are compared. The study also concentrated on the trivariate and the Pairwise Copula Construction (PCC) models to estimate the drought return periods. The comparison of two copula models revealed that the PCC model performed better than the trivariate Student's t copula model. The recurrence intervals for drought events are different for trivariate copula model and PCC model. This study showed that non-stationary drought indices will be helpful in the better estimation of the drought characteristics under the changing climatic scenario.

The single variable dependent drought cannot adequately define the onset and withdrawal characteristics of the droughts. A Multivariate Standardised Drought Index (MSDI) is developed in the present study based on precipitation and soil moisture using bivariate copula function. Reconnaissance Trivariate Drought Index (RTDI) is also developed combining precipitation, soil moisture and evapotranspiration. MSDI and RTDI represent meteorological and agricultural droughts by linking the climate status in an effective way. The best fitted copulas obtained for bivariate and trivariate analysis are Frank and Student's t copulas respectively. The two drought indices were developed and tested to study the onset and withdrawal characteristics of drought and their trends. Cross Wavelet Analysis (CWA) was performed to identify the substantial effect of large-scale climate anomalies on the derived drought indices. The large-scale climate factors like Sea Surface Temperature (SST), Multivariate ENSO Index (MEI), Southern Oscillation Index (SOI), Indian Ocean Dipole (IOD), and Indian Summer Monsoon Rainfall (ISMR) are considered in this study. ENSO, IOD and ISMR showed significant influences on the drought variability. The 3-month MSDI is significantly influenced by ISMR while SST showed a

significant teleconnection with RTDI-3. The SST showed a strong influence on both 6-month MSDI and 6-month RTDI. This study is robust and reliable for future drought assessment and will provide a great platform to develop warning criteria on onset and termination of droughts.

Water availability and streamflow are very sensitive to the variation in the amount of rainfall and temperatures. Hence, the evaluation of climate change impact on streamflow and water balance pattern will be helpful in designing and managing the water resources system in an efficient way. This study focusses on the methodology to estimate the climate change impacts on water balance components in Wainganga and Indravati basins, sub-basins of GRB. A well-known and semi distributed model, Soil Water Assessment Tool (SWAT), has been implemented to model the streamflow for the reference and future periods using the ensemble Coupled Model Intercomparison Model Project Phage 6 (CMIP6) Global Climate Model (GCM) outputs considering four socio-economic shared pathways (SSP126, SSP245, SSP370 and SSP585). The bias corrected GCM outputs were ensemble based on Reliability Ensemble Average (REA) techniques. The ensemble model is given as an input to the SWAT model for generation of future water balance structure of these basins. Global sensitivity analysis was performed using Uncertainty in Sequential Uncertainty Fitting (SUFI-2) algorithm to obtain the most critical parameters. The model performance measures like Nash-Sutcliffe Efficiency (NSE) and coefficient of determination (R^2) were obtained for both calibration and validation were 0.83 and 0.85 and 0.73 and 0.76 respectively. Projected mean annual precipitation and minimum and maximum temperatures show a significant increment in the future scenarios. Wainganga and Indravati basins are expected to have a large inter-annual variation in streamflow pattern. Particularly, the variation in the streamflows are expected to have a significant increment in the monsoon period at the outlet station. The outputs from the time-series model showed a higher variation in streamflow, evapotranspiration and soil moisture especially in the high emission scenarios (SSP585). The developed hydrological model is capable of obtaining the future changes in future water availability and demand in a basin scale by considering the GCM data.

In context of climate change, studies on multivariate drought assessment and the climate change impact on a river basin scale are limited in India. Drought monitoring is a challenging subject due to its dependence on different climatic variables. To overcome this, a copula based probabilistic multivariate drought index (MDI) has been developed which simultaneously represents the meteorological, hydrological, and agricultural drought

phenomenon. The four variate Archimedean copula was used in this study to integrate the precipitation, evapotranspiration, soil moisture and streamflow. Hydrologic variables like evapotranspiration, soil moisture and streamflow were simulated using the SWAT model. The future MDI is also analysed to identify the impact of climate change on drought phenomenon using CMIP6-GCMs under four SSPs. Drought characteristics like severity and duration are evaluated to identify the present and future drought events. The precipitation and minimum and maximum temperatures were identified to have increasing tendencies in the future scenarios. Most of the future scenarios showed lower drought duration and severity when compared to the reference period. The drought duration and severity are likely to decrease in the future time scales especially under the high emission scenarios. The present study used a novel approach to examine the drought from various perspectives and the study will be useful for drought mitigation and adaptation strategies over the basin.

It is reported that that the impact of climate change will affect the drought pattern in India. Cropping pattern, cultivation period and crop productivities are vulnerable to drought onset and offset criteria. Therefore, it is inevitable to assess the crop-drought relationship in the perspective of climate change for sustainable development in agricultural practices. Aurangabad district, in Upper Godavari region, is considered as the study area. In this study, the temporal evolution of Standardised Yield Residual Series (SYRS) was investigated in the study region and then the impact of de-trended Standard Precipitation Evapotranspiration Index (SPEI) on different crops were studied. Crop simulation for three the handful of crops namely maize, cotton and wheat was carried out using calibrated AquaCrop model considering the datasets for the period of 1998-2014. The future crop yield is projected by considering the bias corrected CMIP6-GCM outputs under four SSP scenarios (SSP126, SSP245, SSP370 and SSP585). The outputs from the simulation indicated that there is high increase in crop yield especially in the SSP585 scenario. The increase in crop productivity could be attributed to the favourable thermal range, increased CO_2 concentration and increase in water productivity of crops. De-trended SPEI has a moderate association with the SYRS at different crop productivity phases. The yield-response to drought also varied among crops: the greatest yield-drought correlation was for wheat and the least for maize during study period. Cotton is expected to be more sensitive to drought onset in future. The approach adopted in the study can help the stakeholders to better understand the impact of drought on the agricultural ecosystem, the key to minimize drought-related yield losses.

CHAPTER 1
INTRODUCTION

1.1 General

Droughts are ecological and environmental calamities and have attracted attention of the agricultural scientists, environmentalists, hydrologist and meteorologists and other experts. Droughts may occur in any climatic zone, including locations with high and low precipitation. Deficiency in the amount of precipitation triggers the drought condition in the region over a prolonged period of time, such as a season or a year. High temperatures, wind velocity, low relative humidity, and rainfall characteristics, like the distribution of rainy days during the agricultural production cycle, rainfall intensity and duration, and initiation and termination, are factors which influence drought incidence. The demand for water has increased dramatically as a result of population expansion and the development of agricultural technology, energy, and industrial sectors, with water shortages happening virtually every year in many regions of the world. Water scarcity has been exacerbated by other issues such as climate change and contamination of water supplies. In recent years, floods and droughts had been experienced with higher peaks and severity levels. The period between extreme events seems to have become shorter in certain regions. Droughts influence both surface and groundwater resources, resulting in reduced water availability, deteriorated water quality, failure in crop, reduced range production, reduced power generation and altered ecosystems, among other things. Droughts have quantitative effect on water resources due to change in climate modulating the hydrologic regimes. Runoff transports sediment, organic matter, and nutrients to surface waters, but this pathway is disrupted during droughts. Droughts are extremely important when it comes to water resource planning and management.

1.2 Drought Definitions

Drought onset begins with alteration in hydro-meteorological phenomenon such as lack of precipitation, soil moisture, and runoff and the increased evapotranspiration. Although there are no particular definitions of drought, but they can be well-defined with several perspectives, like conceptual or operational droughts (Wilhite and Glantz, 1985). Conceptually, droughts are classified as meteorological, hydrological, and agricultural droughts, respectively, depending on a lack of precipitation, a lack of water in reservoirs,

lakes, and river streams, and lack of soil moisture. (Mishra and Singh, 2010). Then meteorological drought further slides to the hydrological drought eventually leading to the agricultural drought (Hao and Singh, 2015). Another type of drought namely, socio-economic drought is caused by a shortage of water mostly affecting the supply and demand of water for the people. Operational drought regimes can be defined as the identification of the onset, withdrawal, duration and severity of drought events. Operational definitions aim at providing precise drought-related information to support an effective early warning system. Drought definitions must be consistent in order to eliminate any ambiguity in establishing drought policy making choices (Mukherjee & Mishra, 2018). Some of the commonly used definitions are:

i. Drought is defined as "the proportion of years when crops fail due to a lack of moisture." United Nations Food and Agriculture Organization (FAO, 1983)
ii. Drought is defined as "a sustained, prolonged deficiency in precipitation." (World Meteorological Organization, WMO, 1986).
iii. Drought is a natural occurrence that occurs when precipitation is considerably below average recorded levels, resulting in serious hydrological imbalances that disrupt the production systems (UN Convention to Combat Drought and Desertification, UN Secretariat General, 1994).
iv. Drought is defined as a considerable deviation from an area's usual hydrologic conditions (Palmar, 1965).
v. Drought is defined as deficiency in precipitation, while in often it may originates due to high temperature or evapotranspiration (Hao et al. 2018).

1.3 Drought Indices

Since there are no universal definitions of droughts, drought indices can be used as the best tools to analyse the occurrence of droughts (Hao and AghaKouchak, 2013). Thus, based on long-term climatic forecasts and reliable indicators, the spatial extent, occurrences, commencement, and withdrawal of drought events must be monitored to provide water resource planners with accurate information to plan and implement suitable disaster response measures. The relevant decision-making systems depend on widely established indicators to quantity the physical aspects of drought (intensity, duration, and severity). Drought indicators are developed to track the hydro-meteorological cycles and are used frequently in monitoring drought mechanism (Mukherjee et al. 2018). In a broader

sense, drought indicators are the comprehensive aggregation of parameters such as precipitation, soil moisture, streamflow, evapotranspiration, groundwater levels and reservoir levels. Drought indices, on the other hand, are single numeric values computed from a variety of hydro-climatic factors that impact drought, and hence have a major advantage over raw data when it comes to defining drought features. Different types of drought indices have been developed by concentrating on the stochastic nature of climate and human activities. For instance, Standardised Precipitation Index (SPI, Mckee et al. 1993); Standardized Runoff Index (SRI, Shukla and Wood, 2008), Standardized Precipitation Evapotranspiration Index (SPEI, Vicente-Serrano et al. 2010), and Reconnaissance Drought Index (RTDI, reference) are some of the indices developed in the past studies.

1.4 Droughts as Natural Hazards

Drought is a type of natural hazard that is aggravated by scarcity of water. A natural hazard is a naturally occurring phenomenon that will have a detrimental effect on livelihood of people or the environment. Drought is a particularly pernicious climatic disaster since it develops slowly and frequently affects the people. It can have enormous effects when the severity and duration upsurge over time, making it one of the expensive natural disasters. Drought involves a variety of eco-hydrological and socioeconomic consequences, including decreased water shortages, crop and livestock loss, higher food costs, migration, and indirect health effects. The physical processes of drought are very nonlinear and include certain feedback mechanism, and its influence spreads unevenly across numerous levels, making it difficult to quantify objectively.

Droughts are complicated by the fact that they are dependent not only on the atmospheric processes, but also on the hydrological mechanisms that provide moisture to the atmosphere. Once dry hydrologic circumstances are established, the positive feedback of the drought process sets in, with moisture depletion from top soil layers increasing evapotranspiration (ET) rates and lowering atmospheric relative humidity. Lower relative humidity means there is lower possibility of rainfall, as it will be more difficult for a typical low pressure system to attain saturation levels over the region. Only the disturbances bringing adequate moisture from outside the arid zone will be able to bring enough precipitation to overcome the drought situation. Droughts are the most serious natural disaster considering the number of people impacted (Wilhite, 2000). It's difficult to anticipate drought onset or termination. The impacts of a drought develop gradually over

time and can persist over a prolonged time period. As a result, a drought is commonly described as a creeping event. Defining a drought is difficult and this leads to uncertainty in drought prediction. Unlike losses caused by other natural disasters, the consequences of droughts are non-structural and spread across wide geographic regions. A drought, unlike floods, hurricanes, earthquakes, and tornadoes, impacts water bodies and water resources structures, but it seldom causes structural damage. Finally, unlike other natural disasters, droughts can directly originate due to anthropogenic activities, with aggravating variables such as over-farming, excessive irrigation, urbanisation, deforestation, over-exploitation of available water, and erosion negatively reducing the land's ability to catch and store water.

1.5 Drought Propagation under Climate Change

Climate change, according to the Intergovernmental Panel on Climate Change (IPCC), is defined as a change in the mean and/or variability of its parameters over time caused by natural and human activities. Recently, IPCC revealed a picture of aggravating occurrence of extreme weather events, explicitly intense hot extremes, marine heat waves, extreme precipitation, hydrological and agricultural drought (IPCC, 2021). Natural and anthropogenic climatic forcings cause internal fluctuations in many elements of the Earth's system. IPCC AR5 reported an unprecedented rise in global temperature of the atmosphere in the last few decades, which had substantial negative feedback on climatic parameters, ecological, chemical and hydrological cycle over the globe. As a consequence of variations in the climatological parameters, changes are anticipated in the water availability and related climate extremities like flood and drought of the river basins. Climate change-induced warming has clearly accelerated the hydrological processes, first by raising the available energy for ET and, second, by raising temperatures and hence the water holding capacity of the atmosphere. As a result, severe climatic phenomena such as droughts become more intense, widespread, and protracted.

The additional heat from global warming has expedited the drying process, which is anticipated to result in more severe, prolonged, and extensive droughts in the future compared to the current climate situation. Furthermore, increases in drought intensity in future climates are caused by mean state change in a warming world. Consequently, once the climate conditions are favourable for drought, further climate change worsens the problem by adding modest quantities of heat that can raise the temperatures and ET. Moreover, due to limited moisture availability over land, such climate conditions experience substantial increase in sensible heat fluxes during a limited supply of latent

energy fluxes, further raising the land surface temperature. Further, a stronger association between warmer and drier conditions has been found to enhance the chance of concurrent heat and drought occurrences. As a result, temperature, which directly controls the ET, should be seen as a significant contributor to drought episodes under global warming scenarios.

Drought quantification cannot be completely understood just on the basis of natural climatic variability since anthropogenic impact has a substantial role in both generating and propagating drought occurrences. Drought, along with a rise in water demand for domestic, agricultural, and energy sectors in densely populated areas, might constitute a substantial concern for the future. A fair evaluation of drought must include such consequences as a resulting from increased anthropogenic influences. Other factors, like as precipitation, infiltration loss, and runoff, in addition to temperature, have a considerable role in the incidence of drought. Hence, drought indices should assimilate all these factors to quantify drought characteristics in the context of non-stationary climate.

1.6 Climate Change, Drought and other Factors Affecting Crop Production

Climate change has put excessive pressure on the hydrosphere due to which the water regime is expected to change creating an impact on global water supply and demand. Changes in water cycles have a significant impact on agriculture production considering traditional farming practises. Despite strong evidence of hydrological cycle amplification, its impact on agricultural output is difficult to predict because it is dependent on frequency and severity of drought events. IPCC observed that climate change is emerging as a major challenge faced by the human beings and the natural ecosystems. Drought phenomenon had an intensifying and prolonged effect during the 20^{th} century, predominantly connected to deficit precipitation and increase in temperatures (IPCC, 2007). Due to the dual force of change in climate and anthropogenic interventions, drought characteristics will have prominent alterations in the future and can cause severe damage to crop production. According to Dai (2011), global drought had increased since the 1970s due to decreased precipitation in arid regions of South Asia, Africa, Eastern Australia and Southern Europe. He also observed that with respect to the changing climate, losses due to drought will increase all over the world. Moreover, uneven distributions of rainfall and dry months may affect the crop production. Drought footprints have certain relationship with the crop productivity, which are rarely been reported, hence deserve further investigation. Aridity

has a significant impact on agricultural productivity, resulting in lower grain production. Drought and its relationship to crop characteristics are complicated because the increasing occurrence of drought phenomena caused by climate variability affects production, financial, and market factors.

Influence on precipitation on climate change is not the only factor affecting availability of water; increased ET due to longer growth periods and warmer temperatures could increase crop irrigation requirements. Water shortage is a key stumbling block for global agriculture and food security, resulting in rising food costs. Increased demand for fresh water for cases such as urbanisation, energy projects, and biofuel production, will further limit its availability for agricultural cultivation. Moreover, the per-capita growth in water for crop production due to amplified consumption protein and calories, as well as growing food demand due to population expansion, caused stress on already depleted water resources. Crop production has been restricted beyond its current level as a result of rising water demand and dwindling water supplies. As a result, efforts must be made to improve agricultural practices and adopt novel irrigation management systems in order to conserve water for increasing crop water productivity. Further, improving rain-fed farming through better precipitation, soil moisture, and soil fertility management has the potential for substantial increase in crop productivity. Improving agronomic water supplies through improved systems, minimising surface drainage, using drip irrigation, creating water storage facilities, using wastewater, and judicious use of groundwater would be beneficial to the long-term viability of irrigated agriculture.

1.7 Justification for Taking up the Problem for the Study

Climate change affects hydrological cycle, agricultural production and sea surface temperature (SST) patterns. The drought dynamics had an intensifying and prolonged effect during the 20^{th} century, predominantly subjected to decrease in precipitation and increase in evapotranspiration due to global warming. Due to the dual force of change in climate and anthropogenic interventions, the drought characteristics are expected to have significant alterations in the future. The drought decision makers have to formulate appropriate policy framework to minimize the impacts of drought hazard on the overall development of the country. Against the foregoing background, this study seeks to contribute to impact of climate change on drought and multivariate assessment of drought

characteristics, enhancing resilience to climate change impact, drought preparedness and sustainable environmental management in vulnerable areas.

Single valued drought indices are inadequate for a qualitative identification of the drought phenomenon as multiple climatic parameters are interconnected. The abnormal rising of temperature and evapotranspiration create flash drought indicating that precipitation alone cannot be a reliable entity in the study related to global warming phenomenon (Won et al. 2020). To deal with these limitations, multivariate drought indices are needed to be developed considering agricultural, meteorological and hydrological drought simultaneously.

Agriculture is facing difficulties due to a number of causes, including greater competition for land, water, and labour from non-agricultural industries, as well as increased weather unpredictability. The latter, which is linked to global warming, will cause significant seasonal and yearly changes in food output. Even now, all agricultural commodities are susceptible to similar fluctuations. Droughts, floods, tropical cyclones, heavy precipitation events, hot extremes, and heat waves have all been known to create havoc on agricultural productivity and farmers' livelihoods. Over the past few decades, drought has become the paramount threat to agronomy in several parts of the globe (Potopová et al. 2015). Water scarcity due to droughts frequently affect the capability of plant canopies to absorb the radiation which, in turn, diminishes the crop productivity. However, the relationship between climate variability and crop yield is not consistent. It varies from region to region and from one crop type to another. Hence this study is an attempt to assess the crop-drought relationship, in the perspective of climate change, which will be helpful in validating the crop response to drought relationship.

1.8 Scope and Objectives of the Study

The main aim of the research is to examine the effect of climate change on drought on with a specific focus on the Godavari River Basin (GRB). The broad idea is to systematically investigate the effects of climate change on drought and crop. The goal is to extract a much more nuanced perspective on climate change perceptions, impacts, and related reactions in order to improve long-term formal or planned interventions at the local level to address climate change impacts and environmental degradation. Apart from this, studies on the crop-drought relationship considering the climate change would help understand the effect of drought on crop productivity for future scenarios. With this background, following major objectives have been identified for the research work:

i. Assessment of Standardised Precipitation and Evapotranspiration Index (SPEI) and its variations based on climate phenomenon considering the Regional Climate Models (RCMs).
ii. Development of Non-stationary Standardized Precipitation Index (NSPI) and Non-stationary Standardized Reconnaissance Drought Index (NRDI) based on large scale climate indices as covariates. Analysis of the trivariate drought return period based on copula models and Pair-wise Copula Constructions (PCC).
iii. Development of Multivariate Standardized Drought Index (MSDI) and Reconnaissance Trivariate Drought Index (RTDI) based on bivariate, trivariate copula analysis.
iv. Multivariate Drought Index (MDI) development using four variate copula approach. Assessment of impact of climate change on MDI.
v. Development of AquaCrop model and prediction of future crop yield. Analysis of the crop-drought relationship considering the effect of climate change to determine the effect of drought on crop characteristics.

The study incorporates different drought indices and analysing them for the GRB. Non-stationary drought assessment has also been carried out considering the large-scale climate indices as covariates. Further, the multivariate drought characterisation for GRB has been conducted to obtain the drought return period of a particular area. The variability of climate and its impact on drought is also considered in the study. Apart from this, the study incorporated the crop-drought relationship considering the changing climate aspects. The research is an attempt to address following questions regarding the drought, climate and crop interrelation of GRB and the sub-basins of GRB.

i. What are the drought characteristics and how they are varying spatially? Are there any effects of climate change on drought?
ii. To what extent the drought return period is expected to change with respect to climate?
iii. Are there any streamflow and other climate parameters affected by climate change?
iv. Are there any relationships between crop and onset and offset of drought with changing climate?

The study offers a state-of-the-art approach for crop modelling and analysis for addressing the various questions.

1.9 Research Gaps Identified

Based on the review of literature, the following gaps were identified:

i. Limited studies have been carried out by considering soil moisture in multivariate drought assessment.
ii. India is highly affected by large scale climate oscillations. Nonstationary aspect of drought have not been assessed considering these indices on a river basin scale. The PCC model has not been used for drought frequency analysis.
iii. Individual drought indicators are generally insufficient for characterising complex drought conditions and impacts. Multivariate drought indices that combine multiple associated variables and indices for combined drought characterisations need to be developed. However, multiple drought-related variables and indices have not been explored in the study area.
iv. Crop development and phenological characteristics are highly sensitive to drought events. Studies on crop production and its relation with drought with changing climate have not been explored.

1.10 Significance of the Study

This study considered the Godavari River Basin (GRB), the second largest river basin in India covering the states of Maharashtra, Madhya Pradesh, Telangana, Andhra Pradesh, Karnataka, Odisha and Chhattisgarh. This basin is highly vulnerable to drought. In the GRB, which is depleted of natural resources, changes in flow regime, flood and drought, as well as the underlying causes and impact on agriculture, have frequently drawn attention towards climate change responses at the river basin scale. Apart from a lack of knowledge, gaps, and misconceptions about climate change and its effects on regional agriculture have continued to undermine efforts in the region to achieve environmental sustainability, climate mitigation, and adaptation.

Shah and Mishra (2020) reported that the real time drought assessment in India has been a challenging task due to the lack of near-real-time observations. There are major difficulties in detecting the onset and withdrawal of droughts. The information regarding the drought indices are not readily available to state governments. Indian river basins are highly vulnerable to extreme calamities like drought (Pathak and Dadamoni, 2020; Poonia et al. 2021; Kumar et al. 2021).

IPCC observed that climate change has emerged as one of the major challenges faced by the human beings and the natural ecosystems. It is reported that the drought phenomenon had an intensifying and prolonged effect during the 20th century, predominantly connected to deficit precipitation and increase in temperatures (IPCC, 2007).The overall aim of the study is to obtain a comprehensive evaluation of historical and future droughts in the GRB by incorporating the potential associations of drought characteristics.

There are several ecologically and economically significant special ecosystems in this region, but the assessment of their impacts on agriculture had received relatively less attention. Agriculture in these areas is multifaceted, encompassing rice farming, horticultural crops, plantations, fisheries, and dairy. As a result, it is necessary to investigate the impact of climate change on crop productivity in this region.

The drought and its relation to crop characteristics are complex as the growing occurrence of drought phenomenon resulting from climate variability affect the production, financial and market factors. Novelty point of view, the drought impacts on crop productivity considering the climate change has not been explored in Indian region. Therefore, the present study is an attempt to investigate the linkage between climate change, drought and crop yield.

1.11 Organisation of the Thesis

After introducing the problem taken up for the study and discussing about the significance of the problem, the objectives of the study are introduced in Chapter 1. A detailed review of the literature related to various methods of drought assessment, impact of climate change on drought, rainfall-runoff modelling approaches, crop modelling and crop-drought relationship with varying climate are presented in Chapter 2.

Chapter 3 presents the methodology related to the assessment of drought, impact of climate change on drought, hydrological modelling, and multivariate drought assessment, crop modelling and assessment of crop drought relationship. Further, the description of the study area, data needed and available for the study area are also presented in this Chapter.

Chapter 4 contains the results of impacts of climate change on drought on a river basin scale, non-stationary assessment of drought and its comparison with stationary drought indices. Further, multivariate drought index development and impact of climate change on multi variate drought are explained. Impact of climate change on crop productivity and crop drought relationship status are also discussed in this Chapter.

Chapter 5 presents the summary of the study, the conclusions arrived, recommendation from the study and suggestions for further research activities. This Chapter also reports the contribution from this study.

CHAPTER 2
LITERATURE REVIEW

2.1 General

Climate change affects hydrological cycle, agricultural production, sea levels and sea surface temperature patterns. The extent, frequency and occurrences of extreme calamities such as droughts and floods could be attributed to the global changes in climatic pattern (IPCC, 2013). Drought events have paramount concern in river basin scale across the globe. Over the last few decades, drought has evolved as the major threat to agriculture in several parts of the globe considering the climate change. Hence, it is necessary to evaluate the effect of climate change on drought condition and the agricultural productivity. Several drought indices have been developed to facilitate the water managers for evaluating the impact of drought on the agricultural productivity and to minimize the crop failure in different stages of crop growth. Literatures related to evolution of different drought indices considering the univariate drought indices to multivariate drought indices and their assessment were reviewed. Various models to evaluate the climatic change, the evolution and analysis of impact of climate change on drought and associated risk were also critically reviewed. Then works on projections of climate change scenarios on hydrology using outputs of climate models through different hydrological modelling are reviewed. Various types of crop models and their features and impact of climate change on crop phenology are studied. Finally, studies related to the crop-drought relationship and the impact of drought on crop failure in various stages of crop development are also reviewed and presented. This chapter reviews the various published literatures on drought, climate change impact on drought, hydrological model crop yield prediction, and crop-drought relationship to arrive at a proper methodology to be adopted for the study.

2.2 Drought Types and Indices

The drought phenomenon is linked to lack of precipitation, soil moisture, runoff, and increased evapotranspiration. Droughts can be defined from a variety of perspectives, such as conceptual or operational droughts, despite the fact that there are no specific definitions (Wilhite and Glantz, 1985). It is conceptually defined in terms of drought regimes, which include meteorological, agricultural, hydrological, and socio-economic drought occurrences. The duration, severity, peak, intensity, commencement, termination, area covered, and

frequency of drought occurrences can all be used to establish operational drought regimes (Mishra and Singh, 2010). Drought hazard is defined by the Food and Agriculture Organization (FAO, 1983) as "the proportion of years when crops fail due to a lack of moisture." Drought is defined by the World Meteorological Organization (WMO, 1986) as "a sustained, prolonged deficiency in precipitation." Changes in the monsoonal system over India have been widely documented as having an impact on drought, and accordingly the economy of the country will be influenced by the climate change (Mishra et al. 2020b; Kumar et al. 2021a). Based on long-term climate projections and reliable indices, the spatial extent, occurrences, onset, and withdrawal of drought episodes must be monitored to give water resources planners with accurate information for implementing appropriate disaster response measures.

2.2.1 Meteorological drought

The term "meteorological drought" refers to lack of precipitation over a long period of time. Some of the most regularly used meteorological drought indicators are Standardised 1precipitation Index (SPI, McKee et al. 1993), Palmer Drought Severity Index (PDSI, Palmer, 1965), Reconnaissance Drought Index (RDI, Tsakiris et al. 2007), and Standardised Precipitation Evapotranspiration Index (SPEI, Vicente-Serrano et al. 2010). SPI is frequently used to track meteorological drought with negative SPI values signifying drier-than-normal circumstances. Because the precipitation process dominates meteorological drought, this type of drought is frequently predicted using a medium to long-range climate forecast (Gupta and Jain, 2018). Since the water deficit may affect other components of the hydrological cycle, the prediction of meteorological drought is crucial in the prediction of other types of droughts. The meteorological drought generally triggers other types of droughts affecting the groundwater in the region (Mishra & Sing, 2010). Tirivarombo et al. (2018) have reconstructed SPI and SPEI and observed that both indices can pick up temporal variation of droughts. They also suggested that evapotranspiration due to temperature change played a major role in drought assessment. Sharma et al. (2021) investigated the drought characteristics over the Nepal Himalaya using the SPI and they observed that the spring and autumn drought events were slightly greater than summer and winter droughts.

2.2.2 Hydrological drought

Hydrological drought is defined based on the deficit in the streamflow, surface runoff, and reservoir water demand and groundwater profile. Various hydrological drought indicators including Standardized Runoff Index (SRI, Shukla & Wood, 2008), Palmer

Hydrologic Drought Index (PHDI, Palmer, 1965), runoff or streamflow percentile and reservoir level (Hayes et al. 2011) been developed in the past. Despite the fact that drought is caused by a lack of precipitation, the evolution of physical forms of drought from meteorological to hydrological to agricultural drought is a complicated mechanism. Although the hydrological drought mechanism is linked to an antecedent shortfall in precipitation, other factors such as reduced water storage, snow accumulation, topography, morphology, and other catchment characteristics also have an impact on drought mechanism. Overall, both climate and catchment features influence the occurrence of hydrological droughts.

2.2.3 Agricultural drought

Agricultural drought refers to a situation when the available water is not able to meet the crop water requirement. This type of drought is generally defined based on the deficit of root zone soil moisture that can affect plant developmental stages and crop productivity. The agricultural drought is mainly caused due to the insufficient amount of precipitation or increased evapotranspiration resulting from increment in the thermal regime from the bare soil and plant. Various agricultural drought indicators have been developed globally such as the Crop Moisture Index (CMI) (Palmer, 1965), Soil Moisture Deficit Index (SMDI, Narasimhan & Srinivasan, 2005), and Standardized Soil Moisture Index (SSI, Hao & AghaKouchak, 2013) and Vegetation Condition Index (VCI; Liu & Kogan, 1996).

2.2.4 Socio-economic drought

The socio-economic drought is related to the supply and demand of water to serve the population that includes the features of the other drought conditions. It highlights the strong association among drought and anthropogenic activities. The frequency of physical events, societal vulnerability to water shortages and water demand triggers the onset of drought (Wilhite, 2000). For the assessment of water scarcity, certain indicators like Social Water Stress Index (SWSI, Shafer & Dezman, 1982) have been constructed that can assess the water use, supply, and vulnerability.

2.3 Multivariate Drought Indices

Proper drought management requires the background knowledge of magnitude and occurrences of drought based on multiple variables. Different types of drought indices have been developed by concentrating on the stochastic nature of climate and the human activities. The traditional single variable drought indices reflect only a specific type of drought, viz.,

meteorological, hydrological, or agricultural drought. Further, single valued drought indices are probably inadequate for identification of the drought phenomenon since the various climatic parameters are interconnected. The single valued drought indices neither indicate the different climatic variable deficit nor quantify the drought condition because they depend on multiple variables (Rajsekhar et al. 2015). For example, the only variable which is used for finding the SPI is the precipitation. However, the dependency only on precipitation, neglecting the ground related variables and evapotranspiration may narrow down the effectiveness drought monitoring. Since the abnormal rising of temperature and evapotranspiration create flash drought, it indicates that precipitation alone cannot be a reliable entity in the study related to global warming phenomenon (Won et al. 2020). Therefore, the traditional forms of drought monitoring need to be updated to consider all the possible climatic features to define the environmental conditions. To overcome the drought assessment of single-valued drought index, multiple drought indices were developed by various researchers. Indices like Standardized Precipitation Evapotranspiration Index (SPEI, Vicente-Serrano et al. 2010) and Reconnaissance Drought Index (RDI, Tsakiris et al. 2007) have gained popularity by combining multi scalar properties of climate variables. Keyantash & Dracup (2004) considered all forms of droughts to develop the Aggregated Drought Index (ADI), which included all possible real-time input variables like precipitation, soil moisture, reservoir storage, streamflow, and evapotranspiration and snow. Rajsekhar et al. (2015) demonstrated a Kernel Entropy Component Analysis (KECA) to construct a Multivariate Drought Index (MDI). Multivariate Standardized Reliability and Resilience Index (MSRRI) that combined the information of Inflow-Demand Reliability Index (IDRI) and Water Storage Resilience Index (WSRI) was developed by Huang et al. (2016). Liu et al. (2020) evaluated the MSRRI for the Northwest China region. MSRRI was also used to evaluate the socio-economic drought in the Upper Yellow river basin (Guo et al. 2019).

2.4 Non-stationary Aspects of Drought

Traditional approaches used for the assessment of drought conditions assumed stationarity which were no longer valid under modulating effects of climate, human activities and the changing pattern of environment. Previous researches showed that regional hydrological variability and catastrophic occurrences such as droughts and floods are linked to global climate phenomena (Kahya & Dracup, 1993). Some researchers had established a correlation between global climate indicators and climatic conditions in India. Sea Surface Temperature (SST) oscillations and Indian Summer Monsoon Rainfall (ISMR) exhibited a

substantial association, according to Sahai et al. (2003). The spatial and seasonal changes of rainfall over the Ganges and Brahmaputra basins based on the ENSO events and Indian Ocean Dipole (IOD) modes were investigated by Pervez & Henebry, (2014). Tamaddun et al. (2019) discovered the impact of El Nino Southern Oscillation (ENSO) on north Indian precipitation, temperature, and potential evapotranspiration (PET) during the monsoon season. At a global scale, Hao et al. (2018) qualitatively assessed the association between the occurrence of compound dry and hot events and ENSO for the warm season. Zhang et al., (2020) identified that that the cold phases of the Pacific Decadal Oscillation (PDO) during the La Niña events (i.e., negative Multivariate ENSO Index) were the reason behind the intensified short-term concurrent hot and dry extreme (SCHDE) events in southern parts of South America and Australia. For accounting the climate forcings, Jha et al. (2021) assessed the association between ENSO, Atlantic Multidecadal Oscillation (AMO) and IOD on extreme precipitation events over 24 major river basins of India. Das et al. (2020a) qualitatively examined the tele-connection of eight large-scale climatic oscillations such SST, IOD, Southern Oscillation Index (SOI), Arctic Oscillation (AO), Multivariate ENSO Index (MEI), North Atlantic Oscillation (NAO), PDO, and Indian Summer Monsoon Index (ISMI) on monthly precipitation over six different homogeneous regions in India. Global variations in the large-scale climate oscillations also showed significant teleconnections with drought events (Wang & Kumar, 2015; Guo et al. 2019). Trenberth et al. (2014), in their study, observed that the major drought events in different parts of the world were influenced by ENSO events. The cross-correlations between ENSO events and Nonparametric Multivariate Standardized Drought Index (NMSDI) were investigated using the Cross Wavelet Analysis (CWA) analysis by Huang et al. (2016). In the Indian context, the positive ENSO showed substantial impact on the drought frequency over the country (Shah & Mishra, 2020). Kumar et al. (2021b) used CWA approach to identify the association between large scale climate oscillations with the drought characteristics focussing on groundwater over south Indian river basins. Gupta & Jain (2021) analysed the influence of ENSO events on dry/wet conditions over India considering indices such as SPI and SPEI. It can, hence, be summarised that covariates provide greater insight into the factors of climate that influence the distribution of climatic parameters over time.

It is well known that the stationarity is the basic assumption in the statistical interpretations of time series in hydrologic processes. Stationarity refers to the parameters of the climate that are invariant in time and space and free of trends (Wang et al. 2015).

Property of stationarity is questionable in the context of global warming and anthropogenic changes. The outcome of environmental changes exhibits non-stationary behaviour in climatic parameters. Hence indicators should be developed for identifying drought status in non-stationary conditions for better management of water. However, the large-scale climate indices based on ENSO events cannot be neglected in the computation of nonstationary drought indices (Bazrafshan & Hejabi, 2018) because the precipitation pattern and its hydro-meteorology are influenced by the global scale climate indices.

Standardized Non-stationary Precipitation Index (SnsPI) was developed by Russo et al. (2013) and further used by Wang et al. (2015). This index deals with the time varying mean, as an extension of the stationary SPI. Past studies used the Generalized Additive Model in Location, Scale and Shape (GAMLSS) model developed by Rigby & Stasinopoulos (2007) for the modelling of non-stationary events (Villarini et al. 2009; Lopez & Frances, 2013; Debele et al. 2017). Many studies have been carried out in the past for the non-stationary drought analysis (Osorio & Galiano, 2012; Wang et al. 2015) using GAMLSS model.

Rashid & Beecham (2019) developed NSPI using GAMLSS framework in South Australia. They have incorporated climate indices like SOI, Niño3.4, PDO, Southern Annular Mode (SAM) and DMI as external covariates to capture the non-stationary property of drought. They specified that non-stationary model can capture the rainfall variability better than a stationary model. In addition, they have suggested that NSPI is better than a traditional stationary SPI (SSPI) for assessing the drought properties.

Das et al. (2020b) constructed the Non-stationary Standardised Precipitation Index (NSPI) by considering large scale oscillations using the GAMLSS model in the Himalayan states of Sikkim and Uttarakhand. The nonstationary drought index exhibited fairly good result as compared to the stationary drought index.

A non-stationary Standardized Runoff Index (SRI_{NS}) was developed by Jehanzaib et al. (2020) using GAMLSS framework for the Han river basin of South Korea. At different time scales, they assessed the relative contributions of meteorological (precipitation, temperature) and human (water consumption for social development needs, and water consumption induced by check dams) factors to hydrological drought. They identified a shift in the streamflow series after the 1990s. Furthermore, the change point was detected in the streamflow series after 1990s. Additionally, they observed significant decrease in

streamflow and precipitation pattern. The potential evapotranspiration increased in a higher rate after the change point in the watershed.

Zhang et al. (2021) developed a Non-stationary Meteorological and Hydrological Drought Index (NMHDI) by integrating the NSPI and NSRI at the Huaxian station in the Weihe river basin in China. They developed the NSPI and NSRI considering climate and anthropogenic factors, as covariates. The NMHDI was calculated after using the time-varying copula model to characterise the temporal dependency structure of precipitation and runoff. Comparing the NMHDI and MHDI, the study revealed that the non-stationary model performed better than the stationary model in recreating precipitation and runoff changes. In the case of NMHDI, frequent extreme drought occurrences were detected. The improved performance of the NMHDI had an ability to respond to the continuously changing environment.

Shao et al. (2022) used a GAMLSS-based non-stationary standardised runoff index (NSRI) in conjunction with meteorological and human-induced water consumption as covariates to estimate hydrological drought in the Wuding river basin, China. They compared how well SRI and NSRI performed in detecting drought events. The NSRI recognised more severe and extreme droughts, and it had a significant advantage in detecting hydrological drought by considering human influence.

2.5 Climate Change Implications

The varying global climate alters the hydrological cycle leading to the variability in frequency of extreme events, availability of water, irrigation water use, and quality of fresh water resources. Anthropogenic changes induce climate change causing increase in CO_2 concentration and other atmospheric heat-trapping gases, resulting in global warming conditions. Due to the increase in surface heating, there must be the strong anticipation of escalation in PET. This will possibly modulate and rise the actual evapotranspiration demands in plants, provided adequate root zone moisture is available. So, potential changes in moisture regimes and precipitation trigger warming situations as part of energy goes into increasing temperature over dry land. Changes in atmospheric circulation would certainly affect the extreme phenomenon like flood and drought (Mishra et al. 2020a).

2.6 Downscaling Methods for Climate Projections

General Circulation Models (GCMs) are the feasible and credible tools widely used to predict the changes in atmospheric variables under climate change scenarios (Anandhi et

al. 2008). GCMs are physically-based models, which represent atmospheric and oceanic dynamics (Angeles et al. 2007). The GCM projections are well simulated at a coarser resolution i.e. at continental and hemispherical scale; however, the regional impact analysis requires the variables at finer scale. GCMs have typically low spatial resolution of approximately 100-250 km and they are inadequate for regional impact studies especially for analysing the changes in extreme events (Fowler et al. 2007; Sharma et al. 2017). Hence, in order to analyze the impact of climate change, large scale climate variables should be linked to the hydrologic variables at a regional scale. Downscaling methods can be used to derive local to regional scale information from large-scale spatial and temporal scales. These could be dynamic or statistical. The dynamical downscaling generates finer resolution output based on atmospheric physics over a region using GCM as a boundary (Teutschbein et al. 2012). Statistical downscaling methods establish an empirical relationship between the outputs of the GCMs with observed climate data (Fan et al. 2021).

2.6.1 Dynamic downscaling

Dynamic downscaling refers to the use of high-resolution regional simulations to dynamically extrapolate the effect of large-scale climate processes to regional or local scales. This uses a limited area high-resolution models such as Regional Climate Models (RCMs) which are driven by large scale and lateral boundary conditions from a GCM to produce higher resolution output (Tiwari et al. 2017; Torma et al. 2015). RCMs are frequently used to analyse the impact of climate change on hydrology on the watershed because of their higher resolution. The resolution of RCMs is around 12-50 km and it accounts for the sub-GCM grid scale forcing (e.g. complex topographical features and land cover heterogeneities in a physically-based way). RCM outputs have been used by many researchers for the quantitative and qualitative assessment of future climatic extreme events including drought regimes (Wang et al. 2011; Huang et al. 2015). Due to higher spatial resolution output, RCMs provide a better description of topographic phenomena. Further, the finer dynamical processes in RCMs produce more realistic mesoscale circulation pattern. Some of these studies which used dynamical downscaling in hydrological researches are discussed in this Chapter.

Giorgi & Mearns (1991) compared the empirical and GCM nested limited area modelling techniques and discussed the advantages, disadvantages, limitations, and variability of their use. They observed that, though such models are capable of encompassing the wide range of climate variability and atmospheric phenomenon, they are complex and

expensive. Leung et al. (2003) studied the capability of the RCM in the analysis of hydrologic variable like precipitation as well as inter annual variability such as mesoscale ENSO anomalies over Western United States. Poul et al. (2016) examined the effect of land use land cover (LULC) changes on the ISMR using weather research and forecasting (WRF) coupled with Community Land Model (CLM4.0). Gu et al. (2012) predicted the future climate change by using RegCM4, a regional climate model, for East and South Asia. The result indicated that the Yangtze river basin will witness changes in extreme precipitation and drought events and it potentially increased risks of both floods and droughts at the same time. Verma & Bhatla (2021) used RegCM4 to dynamically downscale the summer monsoon system over the South Asian Coordinated Regional Climate Downscaling Experiment (SA CORDEX) domain and observed that the model performed well in identifying the properties, spatial distributions, and trends associated with dry spell during ENSO phases. The RegCM4 RCM was employed to dynamically downscale future climate variables driven by the GCM Flexible Global Ocean-Atmosphere-Land System Model Grid-Point Version 3 (FGOALS-g3), under multiple SSP scenarios over the CORDEX East Asia Phase II domain. Considering both spatial pattern correlation and biases, the downscaled model improved simulating the precipitation over China than the FGOALS-g3 GCM (Zou & Zhou, 2021). Gao et al. (2022) used simulations of the WRF model with both Kain-Fritsch and Grell cumulus convective parameterisation approaches to perform ensemble dynamical downscaling of precipitation across China. They found that the model captured the precipitation signals better.

2.6.2 Statistical downscaling

Statistical downscaling, in contrast to the computationally demanding dynamical downscaling, provides a straightforward solution by establishing empirical relationships between GCM climate variable and local climate. These relationships can be established without involving the mass and energy exchange between the land and atmosphere. The relationships hold good for future changed climate scenarios as the selected predictors completely represent the changing climate signals. There are several statistical downscaling approaches which established statistical links between large-scale climate and the observed local-scale climate data. Broadly, the statistical downscaling approaches are categorised into three diverse groups: weather generators, transfer function and weather typing (Ghosh and Mujumdar, 2008). In the case of weather generator approach, local scale climate time series are reproduced by replicating the statistical properties of observed climate. Similarly, in the

weather typing approach, regional variables are organised according to distinct classes of atmospheric circulation, and climatic scenarios are then generated by utilising Monte Carlo simulation and resampling techniques to get a sequence of weather classes. The most popular downscaling method is the use of a transfer function, which is a regression-based downscaling method (Tripathi et al. 2006). A basic linear regression is commonly utilised to establish the link between one large-scale predictor and one local predictand. To obtain the predictor–predictand connection, Linear and nonlinear regression, Artificial Neural Network (ANN), canonical correlation, and other techniques have been utilised to obtain the predictor and predictand relationship. ANN-based downscaling approaches, in particular, have gained popularity due to their ability to capture nonlinear interactions between predictors and predictands (Ghosh and Mujumdar, 2008).

Wilbey et al. (2002) developed a well-organized regression-based Statistical Downscaling Model (SDSM) to downscale daily scale meteorological data (precipitation and temperature). Ghosh & Mujumdar (2008) used machine learning techniques such as support vector machine (SVM) and relevance vector machine (RVM) to forecast monthly monsoon streamflow across the Mahanadi river basin in Odisha, India. Raje & Mujumdar (2011) compared several downscaling algorithms, including SVM, K-nearest neighbour (KNN), and conditional random field. Their findings indicated a rise in average daily precipitation for the majority of the stations. Lin et al. (2017) used the KNN algorithm to construct a new spatio-temporal downscaling approach for hourly rainfall. SDSM, in integration with two bias correction methods, was employed to project the climate variables such as daily maximum temperature, mean temperature and minimum temperature over the Loess Plateau, China (Fan et al. 2021). Tabri et al. (2021) compared four statistical downscaling methods namely bias correction (BC), change factor of mean (CFM), quantile perturbation (QP), and an event-based weather generator (WG) to assess the impact of climate change on drought in the future (2071-2100) compared to a baseline period (1971-2000) for the Uccle region of Belgium. Ensemble CMIP6-GCMs were subjected to downscaling, with four future scenarios of SSP1-2.6, SSP2-4.5, SSP3-7.0, and SSP5-8.5. The QP technique surpasses the others in recreating the amplitude and monthly pattern of the reported drought indicators.

2.6.3 Bias correction in climate change analysis

Inherent biases in RCMs due to systematic model errors are caused by imperfect conceptualisation, discretisation and spatial averaging within grid cells. Andréasson et al.

(2004) showed that these biases were not only for precipitation but also for temperature. The common biases were the occurrence of too many wet days with low-intensity rainfall or erroneous prediction of severe temperatures (Ines & Hansen, 2006). Other biases include general under/over-estimation of precipitation and improper seasonal fluctuations of precipitation. (Teutschbein et al. 2012). Several bias correction methods have been developed to downscale climate variables from climate models (Chen et al., 2011; Chen et al. 2019). These methods range from simple scaling approaches to sophisticated methods employing probability mapping or weather generators. They were originally designed to downscale GCM data, but can also be applied to adjust RCM-simulated temperature and precipitation. Regardless of the fact that RCM simulations are increasingly being used in hydrological climate-change impact assessments, their application is challenging due to the potential existence of biases. To deal with these biases, several studies have been undertaken, ranging from simple scaling to more intricate ones (Fang et al. 2015; Guo et al. 2019; Tong et al. 2021). Bias correction techniques have been used widely for post processing the climate model output prior to application for impact studies (Wood et al. 2004; Ashfaq et al. 2010; Piani et al. 2010; Ngai et al. 2017)

2.7 Comparison between Coupled Model Intercomparison Project Phase 5 (CMIP5) and Coupled Model Intercomparison Project Phase 6 (CMIP6) GCMs

Researchers across the world began generating new scenarios to examine how climate would evolve during the latter parts of the 21st century. The Representative Concentration Pathways (RCPs) were developed to represent the many phases of greenhouse gas emissions and other radiative forcings that may affect the future. Four routes were developed that span a wide range of forcing (2.6, 4.5, 6.0, and 8.5 watt/m^2), but they do not have any socio-economic "narratives". To connect a wide range of research communities including climate change mitigation and adaptation activities, the 6th IPCC assessment report (AR6) developed the Shared Socio-economic Pathways (SSPs), based on five narratives that depict major socio-economic patterns that might affect society in the future. The four SSPs are SSP126 (2.6 W/m^2 radiative forcing, low end of the range of future forcing pathways), SSP245 (medium end of the range of future pathways 4.5W/m^2 (radiative forcing), SSP370 (representing the medium to high end of the range of future forcing pathways, 7.0 W/m^2 radiative forcing) and SSP585 (high end of the range of future pathways, 8.5 W/m^2 radiative forcing). The probable greenhouse gas concentration assuming

the population, economic, GDP, educational growth and LULC changes, and the climate mitigation efforts from the ScenarioMIP were considered in the SSPs. SSPs were used in CMIP6 models allowing for enhanced future impact assessments with better parametrisation. These climate predictions considering new set of emission and land use scenarios were developed using Integrated Assessment Models (IAMs) based on both SSPs and RCPs (O'Neill et al., 2016).

Various studies have been carried out considering the CMIP5 to examine extreme events (Ahmadalipour et al. 2017; Gaitán et al. 2020). However, CMIP6 has an improvised parameterisation that can efficiently model climate projections (Eyring et al. 2016). A study by Gusain et al. (2020) showed that CMIP6-GCMs are more efficient compared to CMIP5-GCMs in simulating the Indian summer monsoon. Further, Chen et al. (2020) and Wang et al. (2020) reported that the ISMR is likely to increase in future climate scenarios based on CMIP6-GCMs. A recent study used CMIP6-GCMs to evaluate different drought events over India (Rajbanshi & Das, 2021). Further, CMIP6 models have also gained popularity world-wide among many research communities to deal with climatic variations and for assessment of extreme events (Chen et al. 2020, Aadhar & Mishra, 2020, Zhai et al. 2020, Ukkola et al. 2020, Hirabayashi et al. 2021). Future analysis of long term and short-term drought events based on CMIP6-GCMs could effectively be used for improvement of sustainable management practices like drought resistant measures, water storage, land and groundwater management practices, dealing with agricultural production and livestock insurance etc. These can efficiently tackle the negative impacts of droughts in future.

2.8 Multi-Model Ensemble (MME)

Ensemble approaches based on different climate models, data sets, or members of the same model can effectively model the uncertainty in hydro-meteorology estimation (Raftery et al., 2005). Typically, the ensemble average method is capable of synthesising single information from several members and outperforms all or most of the individual characteristics. Duan et al. (2021) reported that the ensemble average strategies can explore a variety of skilful forecasts and improve the predictive abilities from the viewpoint of either a point forecast or a density forecast. In particular, probabilistic ensemble approaches that could effectively synthesize outputs from different GCMs and RCMs and hydrological models were getting increased attention in various studies (Adhar & Mishra, 2020; Zhai et al. 2020; Mishra 2018). The key of probabilistic ensemble method such as Bayesian Model Averaging (BMA) was to quantify the weights according to each climate model and to

generate predictive distributions of variable of interest (Xu et al. 2018; Ma et al. 2018). Besides, multi-model-ensemble weights can also be assigned to climate models in terms of some weighting criteria such as the Reliability Ensemble Averaging (REA) that can quantify accuracy of the climate models for impact analysis on hydro-meteorology (Sengupta & Rajeevan, 2013; Choudhary et al. 2018; Tegegne et al. 2020). In probabilistic MME methods like the REA, convergence criteria in multi-model predictions of future changes are also regarded crucial for model selection.

2.9 Copula Analysis

Copulas are widely used for capturing the association between two or more random variables (Salvadori & De Michele, 2004; Grimaldi & Serinaldi, 2006; Kumar et al. 2021b). A copula is highly useful for implementing efficient algorithms for more realistically simulating joint distributions. Copulas, in fact, can model the dependence structure using marginal distributions. These functions can derive joint distributions for more than one dependent random variable irrespective of their probability distributions (Ganguli & Reddy, 2013).

2.9.1 Types of copulas

Various families of copulas exist: (i) Meta-elliptical families (Normal and Student's t copula), (ii) Archimedean copula families (Gumbel, Frank, Clayton, and Ali-Mikhail Haq), (iii Extreme Value copula families (Gumbel, Tawn, Husler-Reiss and t-EV), and (iv) other families (Farlie-Gumbel-Morgenstern and Plackett). Among these families, meta-elliptical and Archimedean copulas are used in hydro-meteorological studies. Meta-elliptical **c**opulas consider that the elliptical distributions are very useful in different applications since they have several properties of the multivariate normal distribution. Originally Archimedean copulas appeared in the study of probabilistic metric spaces. Archimedean families have been popular choices for dependence models because of their simplicity and generation properties (Nelson 2006).

2.9.2 Applications of copulas in hydrology

Copulas have wide application in hydro-meteorological studies. The results of frequency analysis may be over or under-estimated in the case of univariate analysis which provide limited evidence of the dependencies among extreme hydrological events. Copula functions have the capability to model the conventional multivariate distributions incorporating their nonlinear dependency measures of variables (Sklar, 1959). Salvadori et

al. (2011) considered flood peak, volume and initial water levels of the dam to estimate the multivariate flood quantiles using copula functions. Meta-elliptical copulas were applied to flood variables (as peaks, durations and volumes) for the analysis of the return period at Romaine river in Québec (Genest & Favre 2007). Bivariate distributions of monsoon rainfall in various meteorological subdivisions in India were estimated by Ghosh (2010). Reddy & Ganguli, (2012) applied Archimedean copulas like Clayton, Frank, Ali-Mikhail-Haq and Gumbel-Hougaard to model the bivariate flood frequency analysis of annual peak flow-volume, and volume-duration pairs. Filipova et al. (2018) developed an approach for selecting different copulas for modelling the joint probability of flood peak and volume for 27 catchments in Norway.

2.9.3 Joint probability distribution and multivariate return period analysis of droughts based on copula theory

Droughts are complicated natural events, and therefore a single variable cannot provide a thorough assessment of droughts (Shiau et al. 2007). Instead of using typical univariate analysis to measure drought characterization, determining the joint distribution of drought variables was found to be a better way to describe drought features (Mishra & Singh, 2010). Due to existence of mutual dependencies between random variables, a univariate probability distribution was insufficient to model the multivariate aspects of a drought event that can be defined by duration, severity, peak, and intensity. The computed return period for a hydro-meteorological system with two or more random variables was not equivalent to the actual return period of drought (Hawkes et al. 2002). Simply analysing the duration or intensity of a drought will result in an overestimation or underestimation of risk while performing drought frequency analysis (De Michele et al. 2005). As a result, analysing the complicated hydro-meteorological phenomenon requires a multivariate stochastic analysis (Grimaldi & Serinaldi, 2006). The multivariate analysis is based on: (i) fitting a suitable marginal distribution to hydro-meteorological parameters; (ii) estimation of related parameters; and (iii) assessment of multivariate return periods considering associated properties (Chebana & Ouarda, 2011). Nelson (2006) and Salvadori et al. (2007) provide more information on the theoretical background and use of copulas.

The analyses of drought properties play a satisfactory role in monitoring the negative impacts on water resources and agriculture (Oguntunde et al. 2017). Drought characteristics like severity, duration and peak must have a dependence structure. Considering SPI, Shiau & Modarres (2009) reported that the complex drought phenomenon can be categorised by

three dependent properties, viz. severity, duration and frequency. Further, they implemented the copula functions to develop a probabilistic approach to obtain relationship between drought severity-duration and frequency (SDF) at 2 gauge stations in Iran. Analytically derived SDF curves represent a function of univariate distribution of severity and duration. Moreover, the study showed that if any modulation in precipitation exists in humid region, the drought severities might be higher in the region.

Song and Singh (2010) used meta-elliptical copulas such as Gumbel-Hougaard, Ali-Mikhail-Haq, Frank, and Clayton copulas to develop trivariate return periods of drought considering duration, severity, and interval time, and the best-fit copula for trivariate drought analysis was chosen. Ma et al. (2013) estimated the drought return period by considering duration, severity, and peak based on Gaussian and Student's t copulas in the Weihe river basin, China.

Chen et al. (2013) used SPI time series to determine drought parameters such as duration, severity, interval time, and minimum SPI values. To develop four-dimensional joint distributions that reflect the dependence structure of drought events, suitable marginal distributions were fitted. The joint return period based on the drought properties were computed and investigated in the upper Han river basin, China using Archimedean and meta-elliptical copulas.

The spatio-temporal variability of meteorological drought conditions for the western Rajasthan, which is the most drought prone region in India considering 6-month SPI (SPI-6) was investigated by Ganguli & Reddy (2013). From spatio-temporal analysis of SPI-6, they observed that frequency of droughts showed increasing tendency at the central part the region. Gumbel-Hougaard, Frank and Plackett copulas were used for modelling bivariate dependence between drought properties like intensity and areal extent. On the basis of upper tail dependence and goodness-of-fit tests, Gumbel-Hougaard copula was identified as the best fit model for representing the dependence status of drought properties. Further, conditional return periods were also estimated based on the best fit copula model. Drought intensity-area-frequency (I-A-F) curves which could be helpful in risk evaluation of droughts in the region were also developed.

Saghafian & Mehdikhani (2014) investigated dependence structures between severity–peak, duration–severity and duration–peak considering different copula functions. The generated copula-based joint distributions were also used to calculate the trivariate return period. The suggested model was tested using data from a synoptic station in Qazvin,

and the findings were compared to empirical probabilities. The study revealed that that copulas are useful models in exploring the dependency among drought variables.

Trivariate copula model was used by Xu et al. (2015) to calculate regional drought frequency, incorporating the duration of drought events, the area affected by drought, and the intensity of the drought in Southwest China. The best fit copula model was chosen using several methods depending on goodness of fit. From the results, they observed that the copula-based return period incorporates the combined effects of drought duration, affected area and severity, which are reliable drought statistical measurements and the 2009–2010 drought was found to be the most severe drought in this region which had a return period of about 94 years.

SPI was assessed for identifying drought duration and severity by Mortuza et al. (2019). In order to estimate the regional frequency analysis, copula models were used by obtaining appropriate marginal distributions for the drought properties. The study was carried out over Bangladesh. They classified the country into three homogeneous regions using fuzzy clustering algorithm. The future drought was also projected and properties of drought were used to obtain drought occurrence in the region. They found that the standard univariate frequency analysis under/overestimated the output of bivariate drought frequency analysis. Overall, they identified that more frequent and severe droughts occurred in the western side of the country.

Poonia et al. (2020) implemented a bivariate copula-based approach for understanding the combined occurrence of drought duration and severity by considering SPI, SSI and SRI. Franck, Gumbel and Plackett were used for modelling dependence structure among copula model over India. Further, they have analysed the joint dependence of drought properties in order to derive exceedance probabilities and return periods. After investigation, they identified that the Western and Central India were vulnerable to drought conditions while the South Indian river basins showed more frequent but less severe events.

Multivariate analysis of drought properties was widely accepted in hydro-meteorological studies for better understanding of risk, return period and for detecting the warning criteria of extreme events (Mishra & Singh, 2009; Hao & Singh, 2015; Das et al. 2020b, Gupta et al. 2020, Zhao et al. 2021).

2.9.4 Vine copula/Pairwise Copula Construction (PCC) model

Several past studies indicated that the vine copula model was more flexible in handling the higher dimension copulas by extending the bivariate copula to higher

dimensions. The basic idea of vine copulas is to construct high dimensional copulas based on a stage-wise mixing of bivariate copulas by decomposing the full density function into a product of low-dimensional density functions. The higher dimensional multivariate Student's t copula was not adequate to model the complexity in the dependence structure of extreme event variables. Because of this limitation of higher dimensional copulas, an efficient way of copula construction method was introduced for a highly dependent structure to model the complex pattern called vine or pair-copula (Bedford & Cooke, 2001; Aas et al. 2009). A trivariate discharge modelling considering flood duration, peak and severity was carried out by Song & Kang (2011) using pair-copula construction. A vine copula model was constructed to analyse the flood frequency using variables like peak discharge, duration and volume (Gräler et al. 2013). Daneshkhah et al. (2016) developed a multivariate pair copula model by using the flood properties in Beas river of the Himalayan region indicating that the Himalayan rivers are highly affected by the monsoon fluctuations and stored snow cover. Muthuvel & Amai (2021) developed quad-variate models encompassing SPI, SRI, SSI, and Standardized yield residual Series (SYRS) using the vine copulas. They have also reported that the vine-copula model performed better than the elliptical and symmetric Archimedean copula.

2.9.5 Copula based multivariate drought indices

Copula based multivariate approaches have proven to be a reliable way for assessing the drought phenomenon, and these approaches are gaining significant recognition in the field assessment of multivariate drought analysis. A Joint Drought Index (JDI) using copula for obtaining the joint probabilities while considering precipitation and streamflow in the State of Indiana, USA, was introduced by (Kao & Govindaraju, 2010). Hao & AghaKouchak (2013) used a 2-dimensional Frank copula based Multivariate Standardised Drought Index (MSDI) considering both meteorological as well as agricultural droughts in California and North Carolina. Ma et al. (2014) developed a Composite Drought Index (CDI) using monthly precipitation, temperature and soil moisture by merging PDSI and Standardised Palmer Drought Index (SPDI) through a potential moisture departure probabilistic approach. Shah & Mishra (2019) developed an Integrated Drought Index (IDI) by combining a number of drought indices using copula SPI (meteorological drought), SSI (agricultural drought), SRI and Standardized Groundwater Index (SGI, hydrological drought). Copula-based Joint Drought Index (CJDI) developed by Won et al. (2020) combines the properties of SPI and Evaporative Demand Drought Index (EDDI).

2.10 Hydrological Modelling and Impact Analysis

The global climate has changed significantly since pre-industrial times due to the major anthropogenic interventions, threatening the sustainability of natural resources at regional scale. Climate change has extensive influence on agriculture, environment, water availability, and ecosystems, social and economic factors. IPCC AR5 reported an unprecedented rise in global temperature of the atmosphere in few decades, which will substantially impact the climatic, ecological and chemical parameters and hydrological cycle over the globe. As a consequence of variations in the climatological parameters, changes are anticipated in the water availability and related climate extremities of the river basins. Therefore, the hydrological alterations attributed to climate change must be investigated for assessing water availability and for sustainable development especially for the agricultural country like India (Nilawar & Waikar, 2019). Hydrological response simulations based on climatic conditions are useful in understanding the hydrological phenomenon in a better way. This approach provides a bigger picture of the spatio-temporal changes of hydrological variables for creating the inter-linkages with the climate in the future. Hence, based on the water balance modelling approach, a qualitative assessment of changes in water resources can be carried out under influence of climate and human activities. Hydrological models have proven to be efficient tools to assess the adverse effect of climate change. These models can be externally provided by climatic parameters that can assess the probable changes in the streamflow of a specific river basin. The main factors affecting hydrological regimes are climate and land use/cover change. Given the wide range of options, correctly quantifying the effects of climate and land use/cover changes on streamflow within a specific watershed becomes critical.

Generally, the conceptual hydrological models are categorized into three types - semi-distributed, lumped and deterministic - based on the ability of the model to conceptualize input variables with the catchment characteristics like LULC, soil type, slope, etc. Physically-based, spatially-distributed hydrological models are not only able to quantify the spatial variability of hydrological parameters, but also simplify the simulation of state variables and external fluxes. Variable Infiltration Capacity (VIC) model (Liang et al., 1994), Genie Rurala 4 parameters Journalier (GR4J) (Perrin et al. 2003), Hydrologiska Byråns Vattenbalansavdelning (HBV) model (Begström and Forsman, 1973) and MIKE 11 NAM (Danish Hydraulic Institute, 2017) were used in various studies for the assessment of impact of climate change on streamflow.

Li et al. (2013) examined the impact of climate change on streamflow pattern across the Yarlung Tsangpo river (YTR) basin in the south-eastern Tibetan Plateau rivers which strongly affect the hydro-meteorology of southern and eastern Asia. In the watershed scale, two hydrological models, viz. SIMHYD and GR4J, were used to analyse the monthly and annual streamflow. Further, the hydro-meteorology of the basin was analysed using outputs from 20 GCMs. The historical streamflow was efficiently simulated by two rainfall-runoff models for the eight catchments in the YTR basins based on the statistical measures and the visual observations. The results of the study predicted a rise in mean annual future precipitation and runoff across the region. According to the findings, the streamflow in the middle reaches of the YTR and its two tributaries in the basin showed increasing tendencies.

A simple and efficient hydrologic modelling-based approach using calibrated and validated VIC model to isolate the impacts of climate change and LULC change on the streamflow of Upper Ganga basin in India was quantified by Chawla & Mujumdar (2015). This approach had three scenarios. Initially, the streamflow response to LULC changes were assessed under invariant climate. In the second scenario, the response of streamflow with change in climate was analysed by neglecting the variations in LULC. Finally, the integrated effect of climate and LULC changes were estimated over the streamflow of the basin in the third scenario. Based on the results obtained from the three scenarios, quantification of isolated impacts of land use and climate change on streamflow was addressed. The results of the case study revealed that the integrated effect showed more significant impact compared to their isolated impacts. Further, the sensitivity of streamflow was high in urban areas and moderate in cropland areas. It was observed, based on the isolated effects of land use and climate change, that climate has a more dominant impact on streamflow in the region.

Das & Umamahesh, (2018) assessed the impact of climate change streamflows over Wainganga river basin using the VIC model. Uncertainties associated with bias corrected GCMs were treated using REA. Associate uncertainties in flood return levels considering the projected streamflows were modelled using Bayesian analysis through Metropolis-Hastings algorithm. Furthermore, uncertainty increases with the climate change forcings moving from RCP4.5 to RCP8.5. The time variability of uncertainty was considered indicating that the uncertainty in the projected return levels are likely to increase in future scenarios.

Impact of climate change on streamflow regime of Mahanadi river basin was analysed by Bisht et al. (2020) considering projected and bias corrected climate scenarios of 9 GCMs achieved from CMIP5 models. Prior to generating the streamflow regimes for future period, Integrated MIKE 11 NAM-HD, was implemented at Hirakud and Mundali gauging sites. Streamflow was analysed using projected ensemble mean of simulated streamflow from different GCMs. Under projected climate scenarios, the results revealed that the mean monthly streamflow showed increasing tendencies during the period 2070-2099. Daily high flows also showed increasing tendency in magnitude and frequency at the end of 21st century while occurrences of low flows were observed to be decreasing significantly under future climate scenarios.

The impact of climate change on the hydrology were analysed for the Jhelum catchment, western Himalayas using VIC model by Jasrotia et al. (2021). Comparison among future periods, showed increasing tendency of streamflow from 2020 to 2080, then slightly decreased towards the end of 2080-2100. Results showed that streamflow projections are highly influenced by precipitation projections in the catchment.

Tehrani et al. (2021) studied hydrological impacts of climate change over Nerang river catchment using MIKE 11 model. An integrated modelling framework was developed which combined a hydrologic model, a reservoir-based model, and a hydrodynamic model on a catchment scale. The multi-model ensemble was investigated considering 8 GCMs of the CMIP5 under RCP 4.5 and RCP 8.5. For the future period, GCM projections exhibited slight decrease in the median of monthly daily inflow in the upper part of the catchment. The results from hydrodynamic model also revealed that sea level rise is projected to have significant impact on water level variations at two river flooding alert sites.

Recently, Tarek et al. (2021) investigated the impact of climate change on streamflow pattern by considering all combinations of precipitation and temperature. The streamflow was simulated and projected based on two lumped hydrological models (HMETS and GR4J) using 10 CMIP5-GCMs under RCP8.5 scenario for the 2071-2100. The uncertainty sources for GCMs were evaluated by variance decomposition method. Furthermore, the sources of uncertainties for precipitation were reduced by considering four best performing reference datasets but continued as the main source of uncertainty for streamflow. Results showed that over the reference period, all precipitation and temperature datasets provided good streamflow predictions. Selection of reference dataset for climate change impact studies was essential, since minor changes between datasets over a common

reference period can propagate to generate huge amounts of uncertainty in future streamflows.

SWAT model is extensively utilized to address the impact due to climate change, on hydrological processes and extreme events in Indian river basins (Swain et al. 2020). SWAT, can therefore, be considered an appropriate model to visualise the connectivity of climate variation with the streamflow in Indian rivers basins. SWAT is a complex physically-based, continuous model and was designed to forecast the impact of watershed management practices on hydrology, sediment, water quality and agriculture production on the gauge and ungauged basins. The model simulates a watershed by dividing it into sub-basins which are further subdivided into Hydrologic Response Units (HRU). For each HRU in every sub-basin, SWAT simulates the soil water balances, groundwater flow, lateral flow, channel routing, evapotranspiration, crop growth and nutrient uptake, pond and wetland balances, soil pesticide degradation and in-stream transformation nutrients and pesticides (Anand et al., 2018; Visakh et al. 2019; Qi et al. 2020; Samimi et al. 2020; Dash et al. 2020).

Abbaspour et al. (2015) used SWAT model to simulate the hydrologic regime for sub-basin scale of Europe. This study contributed essential understanding into continental water resources quantity and water quality at a sub-basin scale with a monthly time interval. An improved version of SWAT model was used to predict the impacts on watershed hydrology and water quality for two watersheds in the Midwest USA (Raj et al., 2016). The study of Lin et al. (2015) showed a varying change in runoff among three time scale (i.e. daily, monthly and annual) and three catchments in the Jinjiang river basin under land use change scenarios using SWAT model.

Zhang et al. (2016) integrated SWAT and SDSM to assess the streamflow regime in the Xin river basin, China. The impact of climate change was studied using downscaled GCMs (BCC-CSM1.1, CanESM2, and NorESM1-M) under 3 RCPs. The study revealed that SWAT model accurately depicted hydrological aspects on annual, daily, and monthly periods. It was shown that while temperature is expected to rise in the future, there would be greater uncertainty in precipitation estimates, with large differences amongst GCMs under different RCPs.

Bhatta et al. (2019) quantified the impact of climate change on water balance of Tamor river basin in the eastern Himalayas of Nepal. The response of SWAT was evaluated with changing the number of sub-basins, HRUs, and elevation bands. Future climate was projected by considering three different time windows i.e. 2030s, 2060s, and 2080s, based

on an ensemble of 5 linearly bias corrected CMIP5-GCMs and 4 RCMs under both RCP4.5 and RCP8.5 and then used as input SWAT for simulating the future streamflows in the watershed scale. It was observed that under RCP8.5 scenarios, future climate might reduce streamflow by more than 8.5 % during latter half of 21st century.

Nilawar & Waikar (2019) attempted to quantify the climate change effect on hydrology and sediment concentration in the Purna river basin, India, considering SWAT model and 3 RCMs under RCP 4.5 and RCP 8.5. Both RCPs showed a significant increase in precipitation and temperature when compared to the baseline scenario. Under RCP 4.5 and 8.5, average monthly streamflow is expected to increase by 24.47 to 115.94 $m^{3/s}$, while average monthly sediment concentration is expected to increase by 32.58 to 162.96 mg/l. Significant increase in streamflow and sediment was observed from June to September at the basin outlet.

An integrated framework was developed by Guo et al. (2019) considering the combined effect of land use/cover and climate variations in future time scale to assess how isolate and combined model would impact on streamflow regime in the Xinanjiang basin, East China. The inter-model uncertainties were evaluated using 5 bias-corrected and downscaled GCM forecasts under 3 different RCPs for the climate change conditions. Three land use/cover change scenarios based on Cellular Automata - Markov (CA-Markov) were predicted, representing a variety of trade-offs between ecological protection (EP) and urban development (UD). The projected land use/cover and GCM simulations were given as input to SWAT to analyse the combined and isolated impact of two attributes on the streamflow. It was observed from the study that the streamflow projected under land use/cover changes showed disagreement with the streamflow change solely under climate change. However, the land use/cover changes basically drove the streamflow pattern when compared to climate change which may reduce the impact triggered due to change in land use/cover.

The changes in streamflow regime was projected by Mishra et al. (2020b) in the Godavari River basin (GRB). An integrated framework was developed considering three hydrological models, 4 GCMs, and 2 RCPs (2.6 and 8.5). The integrated framework highlighted differences in annual flow and high flow. High flow frequencies were anticipated in the future period with respect to baseline period. For the impact assessment, the comprehensive evaluation of hydrological models predicted increases in mean, high flows, as well as the frequency of high flows, at all four gauge sites in the GRB. The projected increases are higher under RCP 8.5 in the far future (2071–2100).

Veettil & Mishra (2020) studied linkages between key climate, catchment and morphological variables with the hydrological phenomenon within a complex system of water resources. A conceptual modelling framework was developed by integrating SWAT and statistical models for investigating the probable impact of catchment, climate and morphological variables on hydrological drought (SRI) in watersheds of Savannah river basin. SRI was developed for short term, medium term, and long-term events to examine the drought variables and their changes with climate. However, it was discovered that linear models based solely on climate characteristics may be incapable of predicting the duration of multiscale hydrological droughts. The integration of catchment and morphological variables to statistical models can significantly enhance the performance. Furthermore, among the morphological variables studied, stream order appears to have a substantial influence on the duration of short, medium, and long-term droughts in the research area.

2.11 Drought in the Perspective of Climate Change

Climate change affects agricultural production, hydrological cycle, sea levels and SST patterns. The extent, frequency and occurrences of droughts could be attributed to the global changes in climatic pattern (IPCC, 2013). Further, the modulating effect of climate has far-reaching influence on agriculture, environment, social factors and natural extreme calamity like drought with an intensified severity (Trenberth et al. 2013). Considering the effect of human activities and climatic parameters across the globe, a substantial increase in drought severity in future due to global warming is predicted by Ahmadalipour et al. (2017). The spatial and temporal increase in drought with a greater severity level were identified across India by Mishra and Singh (2010). On a global scale, the climatic alterations are being used extensively for the assessment of drought in the 21st century (Dai, 2012; Xu et al. 2015; Masud et al. 2019; Thilakarathne and Sridhar, 2017). The spatial and temporal increase in drought situation with greater severity level were identified all over India (Mishra and Singh, 2010; Sharma and Goyal, 2020; Rehana and Naidu, 2021).

Drought conditions were assessed and analysed by Adhar & Mishra (2018) using 5 CMIP5 GCMs under the warming climate in India and identified increase in drought severity and occurrences in the recent decades over the region. It has been documented that the drought will be affected by the changes in the monsoonal system over India and consequently, the economy of the country will be influenced by climate change (Shah & Mishra, 2020a; Kumar et al. 2021a). Moreover, terrestrial ecosystems are highly vulnerable

to unexpected rapidly occurring droughts which are called as ‘flash droughts. These droughts trigger serious threat to crop productivity and vegetation in India (Poonia et al. 2022).

Wang et al. (2011) investigated impacts of climate change on meteorological, hydrological and agricultural droughts. Initially, meteorological drought (SPI) was reconstructed based on daily climate inputs from RCMs driven by 3 GCMs. Further, at the catchment scale in Central Illinois, these anticipated climate inputs were fed into a hydro-agronomic model. Based on the model output, agricultural drought (standardised soil water index, SSWI) and hydrological drought (SRI) were constructed at the catchment scale. The drought characteristics such as duration, intensity and frequency, and the drought propagation from meteorological to agricultural to hydrological systems were analysed for historical and future periods and then compared accordingly. SSWI showed extreme drought conditions and was more sensitive to climate variations compared to SPI or SRI. It was reported that for this region, the intensity, duration and frequency showed increasing patterns from meteorological to agricultural to hydrological drought situation. SSWI and SRI are likely to change significantly due to the nonlinear hydrological response to variation in temperature and precipitation.

The study by Leng et al. (2015) investigated the climate change impact on meteorological, hydrological and agricultural droughts and their propagations, in the perspective of SPI, SSWI and SRI, respectively. Daily climate forecasts from 5 GCMs were given as input to the VIC model for investigating future hydrological changes in China under the RCP8.5. In comparison to the baseline period, it was found that future drought events will be more severe, longer, and frequent. Further, when compared to long-term droughts (duration $>$ 4 months), the frequency of short-term meteorological and hydrological droughts (duration $<$ 4 months) tend to increase, whereas the converse is anticipated for agricultural droughts.

A probabilistic multi-model dual-index dual-scenario framework was implemented by Ahmadalipour et al. (2017) to evaluate drought properties while characterizing the uncertainty associated in projected drought in warming condition. Drought properties were assessed based on SPI and SPEI considering 21 readily available downscaled GCMs generated by NASA (NEX-GDDP) under RCP4.5 and RCP8.5 scenarios. The major drought attributes were used for characterization and then investigated through combined effects of precipitation and temperature variations. The study revealed significant aggravation of future

drought severity and extent in the western United States, trending towards more frequent and intense summer droughts in the contiguous United States.

Gupta and Jain (2018) projected SPI, Standardized effective Precipitation Evapo-Transpiration Index (SP*ETI) and SPEI and then droughts were analysed for 21st century using precipitation and temperature data obtained from RCMs under RCPs 4.5 and 8.5 over India. These indices were developed and used for drought characterization in the region. Drought homogeneous regions were derived based on the K-means clustering algorithm. The major highlights of the study are: (i) the projected rise in temperature directly accelerate the evapotranspiration which in turn affect the drought dynamics in future scenarios; (ii) in the near future, the Northern part of India will be more prone to drought severity and frequency; (iii) however in the far future, most parts of the country, except a few south-eastern states, are likely to face an escalation in drought severity and frequency; (iv) areal extent of droughts showed increasing tendencies in the historical period and is further likely to increase in the future scenarios in most regions in the country.

Bisht et al. (2019) evaluated drought properties of SPEI for future climatic scenarios in different time windows across India. The future time was divided into three time windows. viz., near-future (2010-2039), mid-future (2040-2069), and far-future (2070-2099) and then compared with the reference period (1976-2005). Further, quantile mapping bias corrected MME of 9 CMIP5 GCMs were used to project future drought conditions for different homogeneous regions in India such as North East (NE), Hilly (HR), North West (NW), Central North East (CNE), West Central (WC), and Peninsular (PS). The study revealed that the projected drought severity, duration, occurrences, and the average length are expected to increase in the warming scenarios.

Precipitation data from Global Precipitation Climatology Centre (GPCC) were used by Ahmed et al. (2019) to construct SPI for historical period. Further, 7 downscaled CMIP5-GCMs under four RCP scenarios, such as RCP2.6, RCP4.5, RCP6.0 and RCP8.5 were taken for precipitation projection in the future. The concept of SVM and quantile mapping were used for downscaling and bias correcting the GCMs. Furthermore, the historical and future droughts were characterised based on projected SPI for different crop growing periods. The drought Severity-Area-Frequency (SAF) curves were prepared for historical as well as future scenarios. During historical period, SAF curves showed that for equal values of drought severity, bigger areas were influenced by drought conditions with higher return periods. However, projected droughts for future revealed increasing areal extent for lower severity

and return period while the decrease in affected area for higher severity and return period droughts, were also observed.

For highlighting the drought risk in the future, Gupta et al. (2020) examined the spatio-temporal analysis of drought frequency and hazard over India. In order to compute the future values of SPEI, the meteorological data from RCMs under RCP 8.5 were used. Further, an improved copula-based framework was applied to develop severity-duration-frequency (SDF) curves for the region. The study area was divided into five different homogeneous regions based on fuzzy clustering algorithm. An improved fuzzy clustering-based drought Modified Drought Hazard Index (MDHI) was also developed to assess the risk associated in different homogeneous region. From the results, it was observed that the drought frequency showed increasing pattern for all the regions except for Region 2, i.e., Western Ghats. It was found that drought severities linked with durations are expected to increase significantly with the progression of time. The SAF curves were also analysed and these curves revealed higher probability of a larger areal extent of drought in different regions of the country.

Meteorological drought indices such as SPI and SPEI attributes were analysed by Gaitán et al. (2020) for historical as well as future scenarios for the Aragon region in Spain. Future drought episodes were generated based on 9 Earth System Models (ESMs) and 2 RCPs corresponding CMIP5 model. Further, drought episodes were evaluated considering three main aspects: spatial extent, duration and magnitude. Major contributions of their study were: (i) the projected SPI hardly showed any changes in future compared to normal values; (ii) the projected SPEI showed clear increasing trend of drought episodes at the end of 21st century; (iii) drought indices for future scenarios reflected the most populated areas (the Ebro Valley and the SW of the region) are going to experience the longest and most intense drought periods.

Kumar et al. (2020) examined the potential changes in drought properties of SPI-12 to understand future drought risk in GRB, India. Four homogeneous drought regions were identified using a fuzzy c-means clustering approach. For the homogenous regions of basin, the 12-month SPI was estimated using precipitation data from IMD and GCM-MIROC-ESM-CHEM. For different homogeneous regions, SDF and SAF were constructed using various copula functions. Moderate to severe drought episodes are expected to increase in future periods. For this region, the SDF curves were concave upwards which indicated that

the severities are expected to increase in the future periods, while steeper curves for SAF indicated high variability in topography and hydrological properties in the basin.

Rajbanshi and Das (2021) investigated the spatio-temporal variations of meteorological (SPI) drought patterns for the future considering SSPs (viz., SSP1-2.6, SSP2-4.5, SSP3-7.0, and SSP5-8.5) considering 10 CMIP6-GCM simulations in India. The observations from the study were: (i) observed period (1951-2014) indicated that the summer monsoon drought events were more evident and significantly affected the crop productivity; (ii) the most severe droughts occurred for the years when El Nino events (equatorial Eastern Pacific Ocean (EPO) sea surface temperature (SST)) were negatively correlated with the SPI events; (iii) Future projection (2071–2100) from the selected models indicated the more frequent droughts in the SSP1-2.6 and SSP2-4.5 in comparison to SSP3-7.0 and SSP5-8.5.

2.12 Crop Modelling and Impact of Climate Change on Crop Yield

A study by Kumar (2016) showed that global warming with its negative impacts was affecting the root zone soil moisture during critical crop growth stages. Cropping pattern, cultivation period and its productivities are vulnerable to climate change, due to partial or complete crop failure because of scanty or more amount of precipitation. Deb et al. (2015) reported that the agricultural sectors are highly prone to climate change due to the association amongst plant phenology and meteorological variables. Uneven distributions of rainfall and dry months may affect the crop production. Further, changes in plant phenology, respiration, transpiration and photosynthesis are likely to affect agricultural productivity as CO_2 concentrations and temperatures rise. This, in turn, could increase water stress and consequently, food security. India being an agrarian country is likely to be affected substantially due to the adverse consequences of climate change (Das et al. 2020c).

Climate change footprints also have certain relationship with the crop productivity, which have rarely been reported, and hence deserve further investigation. The climate change influence on crop yield is expected to be more intense over future periods due to increase in intensity, magnitude and distribution of rainfall, decrease in soil moisture, relative humidity, higher temperatures, and consequently higher evapotranspiration. Crop model is an important tool for studying future clime change effect on crop production and its counter measures. Future climate change impact on crop yield and its countermeasures can be studied using crop models. Crop models have shown great potential in evaluating the impact of climate change on crop water consumption and irrigation requirements at both the

local and regional scales, and it provides new analytical abilities for water resource management planners to help them make better decisions. Crop modelling approach had been established and gained popularity among scientific research community (Holzworth et al. 2015). Crop growth models generally simulate the relationship between plant phenology and environmental situation to forecast the anticipated production of crop. These models can be implemented for prediction of crop yield with respect to climate change and understanding crop responses in field trials and circumstances. These can be helpful in crop management and agronomic decision making, as well as to study the potential impacts of climate change on food security. Many such models have been developed over the past decades and prominent examples are Decision Support System for Agro-technology Transfer (DSSAT), (Jones et al. 2003), Agricultural Production Systems sIMulator (APSIM), (Holzworth et al. 2018), WOrld FOod STudies (WOFOST), (van Diepen et al. 1989); Cropping Systems Simulation Model (CROPSYST), (Stockle et al. 2003) and Simulation of Evapotranspiration of Applied Water (SIMETAW#), (Mancosu et al. 2016). Some hydrological models like SWAT, (Santhi et al. 2001) and Distributed model for Runoff, Evapotranspiration, and Antecedent soil Moisture simulation (DREAM), (Manfreda et al. 2005) were also used in various studies to improve the simulation for both at local and regional scale.

Water is critical for agricultural productivity, and it has long been recognised as a major limiting factor in crop development. AquaCrop is a well-known crop simulation model developed by the Food and Agriculture Organization (FAO), (Hsiao et al., 2009; Steduto et al. 2009). Steduto et al. (2009) characterised the model as a "canopy-level and engineering kind of model, primarily concentrating on modelling the achievable crop biomass and harvestable yield in response to the water availability". The goal of the model was to employ fewer parameters while yet preserving accuracy, simplicity, and resilience. In this model, the primary driver for yield production modelling is water. Moreover, the modelling technique must work with modifying the simulated yield by considering water limiting variability or conditions. This model has been widely used by researchers to model the biomass and yield all over the globe for different crops (Bird et al. 2016; Farahani et al. 2009; Abedinpour et al. 2012; Nyathi et al. 2018). In the context of India, Dubey et al. (2017); Kumar et al. (2014) and Pawar et al. (2017) had used the AquaCrop model to simulate various crops under different climatic and management conditions.

Bocchiola (2013) studied the effect of climate change on crop productivity of maize considering and response of water footprint to possible variations of weather variables as case study of the Po valley of Northern Italy. The maize production was simulated using validated CropSyst model for the period 2001-2010. Then, the water footprint (the absolute and specific (kg/yield) water evapotranspiration during growing season), was estimated under three different irrigation conditions, such as: (i) no irrigation, (ii) manual irrigation at fixed dates, and (iii) automatic irrigation on demand. It was observed from the study that under future scenarios, the temperature is expected to increase and amount of precipitation is expected to decrease. These create a decrease in crop productivity and increase in evaporative demand of crops which boils down to higher irrigation demand.

Shrestha et al. (2017) used the crop growth model DSSAT (CERES-Rice) to calculate the possible impact of climate change on rice productivity for the Nam Oon Irrigation Project in Northeast Thailand. Field experiments were performed to collect crop phenology data, which were then used to set up and evaluate the model. Under RCP 4.5 and RCP 8.5, the water footprint and evaporative demand of crops during the growth phase were calculated using bias-corrected outputs of different RCMs. A significant increase in the water footprint was observed for KDML-105 and RD-6 rice varieties under various scenarios compared to the baseline period. The opposite condition was depicted by the ChaiNat-1 variety which showed decrease in projected water under two scenarios. High increase in blue water footprint is expected in future period, as a consequence high increase in the irrigation water requirement due to high evaporative demand of plants.

The variations of yield of major crops such as wheat, barley and maize in the Banas river basin, in the Rajasthan state of India were investigated in a perspective of climate change (Dubey & Shrama, 2018). Based on the AquaCrop model, the simulated yield showed a good agreement with the observed yield. Furthermore, based on climate forecasts from CORDEX-SA (CNRMCM5, CCSM4, and MPI-ESM-LR) under RCP4.5 and RCP8.5 for the future period, the calibrated model was utilised to analyse the likely variance in agricultural output due to the influence of climate change and CO_2 concentration. Crop yields are predicted to rise in the future as a result of climate change.

Pranuthi & Tripathi (2018) investigated the crop productivity in the perspective of climate change based on bias-corrected PRECIS RCM data in the Haridwar district of Uttarakhand, India. Further, DSSAT CERES rice model was used to simulate the rice yield at Haridwar district. For undertaking this study, the future yield was projected by providing

PRECIS RCM weather data under different RCP CO_2 emission scenarios. The study showed that the rice productivity of Haridwar is expected to decrease by 31.7 kgs/ha/year in the future scenario and could be attributed to increase in maximum temperature which will not be favourable for crop growth.

Raoufi & Soufizadeh (2020) investigated the impact of anthropogenic and climate changes on the productivity of rice genotype behaviour for deep understanding of crop yield change in northern Iran. The future meteorological variables were given as input to the AquaCrop-Rice model to examine the sensitivity of genotypic in rice under varied CO_2, precipitation (± 20%), and temperature (+ 1 °C, + 2 °C, + 3 °C, + 4 °C) under different RCPs (2.6, 45, and 8.5). Results from the study indicated that increased CO_2 concertation and temperature were favourable for rice growth while the change in precipitation was no longer significant. However, under RCP8.5 scenarios and +1 °C temperature change lead to highest increase in aboveground biomass. Nevertheless, phenological behaviour and length of the vegetative phase were accelerated by increased temperature.

Das et al. (2020c) simulated the yields for three different crops (rice, wheat and maize) using calibrated AquaCrop with an observed period of 17 years (1998–2015) over Sikkim, India. Further, the future crop yield for three crops were estimated using bias-corrected climate scenarios from four GCMs under RCP4.5 and RCP8.5 scenarios. The model showed that the mean yield is expected to increase in the future period (2021-2099). The increase in mean yield can be attributed to a favourable temperature profile, an increase in CO_2 concentration, the study area's high elevation, and the absence of major water stress during crop growth seasons.

SIMETAW# model was implemented to evaluate the impact of climate change on crop productivity with two new versions ((SIMETAW_GIS platform) and (SIMETAW_R)) in semi-arid area of Southern Europe (Masia et al. 2021). These two versions were accomplished to estimate water consumption by crops and irrigation demand in regional and local scales. The methodological framework was used to calibrate and validate the model SIMETAW_R in ten experimental sites. SIMETAW_GIS model performance was evaluated in Mediterranean countries. Further, the meteorological inputs from GCMs under RCP4.5 and RCP8.5 scenarios were given as inputs to model for estimating the on maize, wheat, and wine grape sensitivities and water requirements in under the influence of future climate conditions (2036–2065). From the results, it was found that for Mediterranean countries, water requirements for three crops are expected to increase under climate change scenarios.

Recently, Quan et al. (2022) implemented the calibrated SPACSYS and DSSAT-CERES-Maize models to evaluate the application of six methods under future climate considering two-year field data. Three mulching measures, namely transparent film, black film, and no film conditions, as well as two fertilisation levels, namely high and low, were evaluated in the study. Both models were calibrated and validated, and the anthesis and maturity dates of maize, as well as the ultimate biomass, yield, and soil water content (SWC), were compared to measured values. In comparison to DSSAT, the SPACSYS model accurately predicted maize and SWC growth under nitrogen stress. 27 GCMs were used for assessing the impact of climate change on crop growth driven by DSSAT and SPACSYS models with different irrigation schemes (I1, I2, I3) and four irrigation ratios (T1, T2, T3, T4) under future decades (2040s and 2080s). It was highlighted that the I1T1 scenario considering transparent film mulching created the maximum maize production. The I3T4 scenario retained constant production in the 2040s while it showed decreasing tendencies by 20% in far future (2080s). Consequently, I3T4 scenario require the optimum management practices aimed to better maize production in this region.

Shirazi et al. (2022) used AquaCrop to evaluate the influence of climate scenarios yield of winter wheat and summer maize productions considering downscaled climate data driven by SDSM and CanESM2 under RCP4.5 and RCP8.5. The study area taken up for investigation was in the Huang-Huai-Hai Plain (3H Plain). The results indicated that the potential yield of wheat and maize were estimated to increase in the future time scale compared to baseline period. Higher increase in wheat yield was detected in the Shandong and north-eastern parts of Henan. However, the water budget during the wheat growth period is expected to have deficit tendency in the northern part of 3H Plain while the maize growth period showed improvement in central and southern parts of the 3H Plain.

2.13 Crop and Drought Relationship

Climate extremes, such as droughts and hot events, may result in reduced crop productivity threatening regional and global food security. Uneven distributions of rainfall and dry months may affect the crop production. Further, drought footprints have certain relationship with the crop productivity, which have rarely been reported. Over the last few decades, drought has evolved as the paramount threat to agronomy in several parts of the globe (Leng and Hall, 2019; Potopová et al. 2015). Thus, investigations related to the hazard of droughts on the crop productivity have become a supreme concern for the governance of comprehensive mitigations and prevention strategies (Potop et al. 2012). Water scarcity due

to drought frequently affect the capability of plant canopies to absorb the radiation which has a detrimental effect on crop productivity. Further, the impact of drought on quantity of cultivation, significantly depend on the type of crops, developmental phases of crop, genetic characteristics of the specific crop and the properties of soil (Karim and Rahman, 2015). It has been reported that the association between climate variability and crop yield varies for different regions and various crop types. Muthuvel & Amai (2021) specified that crop yield variations owing to drought can be estimated using yield anomalies like the Standardized Crop Yield Index (SCI), yield data detrended by using first difference approach)/ Standardized Yield Residuals Series (SYRS, yield data detrended by fitting linear regression model). Detailed information on the impact of drought on the crop growth for different seasons can be efficiently captured by considering the SPEI (Potopová et al. 2015). Droughts can influence an agrarian country's economy and food security by diminishing crop production, in addition to creating an ecological imbalance.

Researchers from different parts of the world have attempted to investigate the drought impacts on crop productivity but still more studies are needed to be conducted focussing the influence of drought on crop production worldwide. A copula-based model was implemented for the assessment of drought impression on terrestrial vegetation in China by obtaining the correlation between Normalized Difference Vegetation Index (NDVI) and the SPEI at varying timescales (Fang et al. 2019). The response of crop anomalies to SPEI, and Vegetation Condition Index (VCI) and Temperature Condition Index (TCI) distinctly were analysed by Ribeiro et al. (2019). Feng & Hao, (2020) investigated the likelihood of occurrences of dry, hot, and compound dry-hot events triggering the decrease of maize yield. Additionally, they identified the occurrence of compound events becomes higher as the crop yield reduces. Feng et al. (2019) investigated the association between variability of maize production and compound dry-hot events based multivariate copula functions.

Potop et al. (2012) explored the impact of two multi-scalar dry and wet spells of SPI and SPEI on different crops in the low land regions of the Czech Republic. The finding revealed that the SPEI from April to September and detrended SYRS series of root vegetables had reasonably significant negative relationship. However, more frequent dry episodes throughout the growing period of brassica vegetables and fruits had negative consequences. Even the longest dry spell (early spring droughts) had no effect on bulb vegetables during sowing period.

Potopová et al. (2015) investigated the impact of SPEI at different time scales on crop productivity for 11 agricultural crops with different growth cycles in the Czech Republic. The crops with different growth cycles taken up for the study were spring wheat, spring barley, winter rye, oilseed rape, winter wheat, winter barley, oats, maize, potatoes, sugar beet and grapevine. The study showed that variations in crop responses to various SPEI lags were derived via correlation studies between drought-crops. However, during crucial growth periods of the crops, the monthly detrended SPEI exhibited strong correlation with SYRS. Based on the study, drought risk defined in terms of the SPEI at 1-, 3-, and 6-month lags was becoming more of a concern during the early stages of root and tuber crops.

Wang et al. (2017) proposed a quantitative approach for assessing the influence of multi-scale drought (SPEI) on wheat yields in the Huang Huai Hai (3H) Plain. Winter wheat was estimated at 28 locations on the 3H Plain using the calibrated Environmental Policy Integrated Climate (EPIC) crop growth model. The relationship between multi-scale SPEI and winter wheat series was further investigated using a crop growth process model. The study findings revealed that wheat yields calculated using calibrated EPIC was a reliable crop yield predictor in the region. Further, in the year 2000, a large water shortage was detected, and the degree of yield reduction did not always link to the change in water deficit.

A study by Liu et al. (2018) analysed the drought events based on SPEI and inspected the drought and crop (winter wheat and summer maize) association in the North China Plain (NCP). It was reported that the annual changes in the detrended SPEI can explain a huge variation in winter wheat and summer maize yields in the region. Further, the link between yield series and SPEI series with different lags varied significantly; the most related time scale increased as the development stage of winter wheat progressed. The relationship between the winter wheat SYRS and detrended SPEI in three sub-periods were continuously strong and constant, while the relationship between the summer maize SYRS and detrended SPEI had considerably reduced at all time scales, apart from 1-month lag.

Masud et al. (2020) investigated the crop-drought connectivity between (SPEI/MSDI) and three important cereal crops (spring wheat, barley, and canola) in a large agricultural command region in western Canada. In terms of agricultural impact assessment, both indices performed similarly; however, the MSDI performed better in the early growing season for wheat and barley, demonstrating strong crop production sensitivity to soil moisture deprivation. The study summarized that the association between detrended drought

indices and the yield series depend upon timescale, geographic location, and crop growing period.

A recent study by Muthuvel & Amai (2021) developed three concurrent drought indices and their influence on agricultural yield series (SRYS), using a copula-based multivariate method in India. The drought properties were computed based on MSDI that includes the three isolated drought indices using the Gaussian copula. Some of the severe concurrent drought years such as 2002, 1987, 1972, and 1965 caused considerable yield losses in Kharif season crops of groundnut, millet, and rice. The study summarized that although the single valued droughts caused mild losses in yield, the concurrent droughts triggered high losses in yield which further seems to grow to exceptional losses.

2.14 Gaps in the Literature and Summary

An overview of different forms of drought, types of drought indicators, non-stationary aspect of drought analysis, and multivariate aspect of drought analysis based on the changing climate, crop yield prediction and impact of drought on crop prediction is presented in this chapter. Based on discussions on drought analysis, it can be justified that the antecedent meteorological droughts may evolve into hydrological and/or agricultural droughts, coexisting as concurrent droughts. In a changing environment, where the hydro-meteorological parameters such as precipitation, streamflow, soil moisture and groundwater may show non-stationary behaviour, traditional drought indicators based on the principle of stationary hypothesis often failed to identify and assess nonstationary drought events.

All these indices consider only one specific physical form of drought: hydrological, meteorological, or agricultural. This might not be adequate to get a comprehensive idea of the drought condition since the drought is dependent on multiple variables. It can, hence, be concluded that the drought status indicated by one drought index might not be consistent with the findings obtained by using a different drought index. To overcome these limitations, a group of indices that considers multiple variables to represent drought were constructed and these hybrid drought indices provide a stronger correlation with actual physical impacts. Based on the literature study, copula-based Multivariate Drought indices considering the meteorological, agricultural and hydrological droughts were capable enough to replicate the actual drought mechanism.

Literatures on the climate change and MME method suggest that various sources of biases are present in the climate models which need to be further corrected using suitable bias correction techniques. Various sources of uncertainties are associated with the climate

models and it is essential to reduce these uncertainties by considering a suitable weightage average technique.

In the past few decades, due to continuous intervention with the environmental landscape in the form of land use practices (water diversions, deforestation, local agriculture practices, industrialization etc.) there is a need to quantitatively assess the future climatic scenario for initiating and effectively undertaking the adaptation strategies for safe and sustained agricultural growth. Based on the critical review of literature on impact of climate change on drought studies, it can be concluded that droughts are likely to become more common as global warming worsens during this century. Therefore, accurate studies of future projections at a local level are crucial. That is to say, both climate and man-made causes play a role in exacerbating droughts. When they do occur, the increased heat from global warming is projected to accelerate the rate of drying, causing drought to develop more quickly and with higher intensity. Further, it can be noted that a significant increase in potential evapotranspiration would cause a prolonged dryness in most of the regions during the twenty-first century. Hence, the spatial extent, occurrences, onset and withdrawal of drought events must be monitored based on the long-term climate projections using reliable indices to provide water resources planners with correct information to take appropriate disaster response measures.

The multivariate aspect of the drought has been studied in various literatures but the climate change aspects to project multivariate drought indices have not been taken into consideration.

Based on the literature of hydrological modelling, it is observed that hydrological modelling has become an integral part of climate change assessment which incorporates the physical parameters of a region. Therefore, physically based hydrological models with high resolution meteorological variables can be used to simulate the streamflows. Further, SWAT model can simulate the water balance components in well manner.

Crop growth models, such as AquaCrop, are useful in determining the influence of climate change on crop output based on forecasts from global circulation and regional climate models. Hence, this model could be used to generate future crop yield on the basis of changing climate.

The impact of drought on agricultural production depends not only on the severity of the event itself, but also on the time of the event and the vulnerability of the natural systems that experience it. Similar extreme weather could have differing outcomes depending on the

crop development stages and the vulnerability of the exposed system. Thus, identifying the spatio-temporal variation of the drought impacts on agriculture and constructing a quantitative relationship between drought and agriculture losses could provide policy makers and stakeholders with scientific information regarding which agricultural areas are most vulnerable and sensitive to drought.

CHAPTER 3

METHODOLOGY

3.1 General

This chapter presents the methodology adopted in this research. Various data required for the assessments of drought and its characteristics in Godavari River Basin (GRB) and its sub basins are presented. The SPEI is developed and drought characteristics are projected for the future scenarios using RCM models. GAMLSS model is implemented to obtain the non-stationary drought indices such as Non-stationary standardized Precipitation Index (NSPI) and Non-stationary Reconnaissance Drought Index (NRDI), considering the large-scale climate indices as external covariates. Multivariate drought indices such as MSDI, RTDI and MDI are developed as a part of the study. The MSDI considered the combined drought status of precipitation and soil moisture while RTDI considered the three variables such as precipitation, soil moisture and evapotranspiration. The teleconnection between large scale climate indices and drought indices (MSDI and RTDI) in GRB are also obtained using Cross Wavelet Analysis (CWA). SWAT model is developed and then calibrated and validated using SUFI2 algorithm based on the streamflow data. The other climate parameters like soil moisture, evapotranspiration and streamflow are generated for future scenarios considering the CMIP6-GCMs. Along with a copula-based four variate MDI considering the climate variables were assessed for future scenarios. AquaCrop model is used to evaluate the future changes in the crop yield under different climate scenarios. Finally, the crop and drought relationship is obtained using Kendall's τ correlation between Standardised Yield Residual Series (SYRS) and Standardized Precipitation and Evapotranspiration Index (SPEI).

3.2 Study Area

The area taken up for the study is the GRB lying in the central and southern part of India. The Godavari river, originating in the Nashik district of Maharashtra, flows for a length of 1,465 km toward east, draining many states of central and peninsular India, eventually emptying into the Bay of Bengal. Covering a drainage area of 312,812 km^2, it is one of the major river basins of India. GRB is mainly dominated by the south-west monsoon rainfall which is generally erratic with wide temporal and spatial variation in rainfall. The average annual rainfall of the basin is about 1100 mm. South-west monsoon has a direct

influence on agriculture in the region, which is more vulnerable to extreme weather events. Hence, irrigation, amounting to approximately 95% of the water use, has high priority in this basin. The extreme events in this basin and various anthropogenic activities bring extra pressure on the water resources. So, a comprehensive drought assessment is needed to be carried out for identifying the drought variability with respect to the changing climate. GRB consists of eighth major sub-basins. Different sub-basins of GRB were taken up to meet the objective of the study. For the first two objectives, the whole GRB is considered. Third objective considered Wainganga and Indravati basins. Fourth objective considered the Aurangabad region as the study area which is part of Upper Godavari sub-basin. A map of the study area is given in Fig. 3.1.

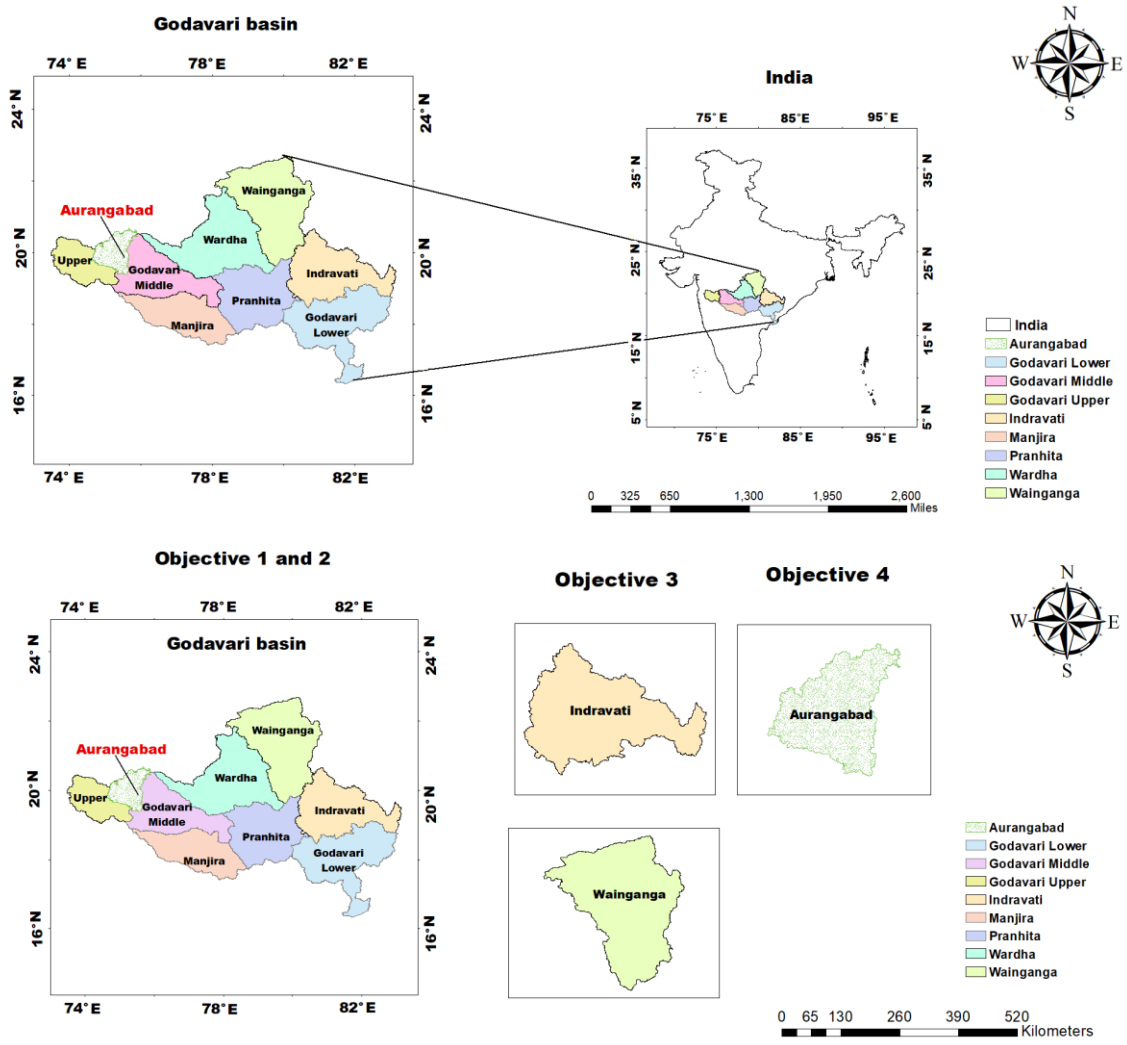

Fig.3.1 Map of the study area

3.3 Data Needed and Available for the Study

This section comprises of different types of data needed for the study and their source. The data includes Climate Research Unit Time Series (CRU TS) data, Global Land Data Assimilation System (GLDAS) VIC soil moisture data, Indian Meteorological Department (IMD) data, RCMs, and CMIP6-GCMs, geospatial data like Digital Elevation Model (DEM), soil map, Land Use and Land Cover (LULC) map and crop details. The following sections explain these.

3.3.1 Climate Research Unit Time Series (CRU TS) data

This study used 0.5°×0.5° monthly gridded precipitation and evapotranspiration data sets acquired for a period of 39 years (1980-2018) from CRU TS 4.03 (https://data.ceda.ac.uk/badc/cru/data/cru_ts/cru_ts_4.03). CRU TS monthly climate anomaly 0.5º x 0.5º gridded dataset are derived based on the Angular Distance Weighting (ADW) method over all the land domain in the world except Antarctica. The evapotranspiration data for the same time period were downloaded and extracted to a particular location. CRU data was utilised for the temperature-based derivation of potential evapotranspiration (PET) (Harris et al. 2014). Gridded rainfall, evapotranspiration and temperature data have been extensively used in various hydro-climatological analyses in different parts of the world (Zarch et al. 2015; Krishnan et al. 2018). The climate data were extracted and regridded by using bilinear interpolation method to GRB scale.

3.3.2 RCM data

Daily precipitation, minimum and maximum temperature projections for the years from 2053 to 2099 were obtained from Centre for Climate Change Research (CCCR), Indian Institute of Tropical Meteorology (IITM), Pune, India (https://cccr.tropmet.res.in/home/cordexsa_datasets.jsp) database. 5 RCMs under RCPs 4.5 and 8.5 with a spatial resolution of 0.44º were downloaded from the site given in Table 3.1. All the RCM datasets were regridded to CRU grids under the same spatial and temporal resolution for analysing the future dry and wet spells. The sources of various models used are presented in Table 3.1.

Table 3.1 RCM model sources

Sl. No.	Model	Source
1	ACCESS 1-0	Australian Bureau of Meteorology
2	GFDL-ESM2G	Geophysical Fluid Dynamics Laboratory
3	MPI-ESM-LR	Max Planck Institute Earth System Model
4	CCSM4	Community Climate System Model
5	CNRM-CM5	Canadian Earth System Model

3.3.3 Indian Meteorology Department (IMD) data

Daily observations such as precipitation, minimum and maximum temperature from Indian Meteorological Department (IMD) were collected for the period from 1951to 2018. The precipitation data were developed based on 6955 rain gauge stations all over India with a resolution of 0.25 x 0.25 (Pai et al. 2014). Similarly, maximum and minimum temperature data were developed using 395 quality-controlled measuring stations and available at a resolution of 1^{o} x 1^{o} (Srivastava et al. 2009). Spatial uniformity was ensured by converting the temperature data to a resolution of 0.25 x 0.25 using the bilinear interpolation method.

3.3.4 Large scale climate indices

Large-scale climate indices have an effect on a non-stationarity aspects of drought phenomenon. The non-stationary drought indices were computed based on the association with four large-scale climate indices such as Indian Ocean Dipole (IOD), Southern Oscillation Index (SOI), Sea Surface Temperature (SST) and Multivariate ENSO Index (MEI) and are presented in Table 3.2.

Table 3.2 Large-scale climate indices and their data site

Large-scale climate indices	Links
SOI	http://www.bom.gov.au/climate/current/ soihtm1.shtml
SST	http://www.esrl.noaa.gov/psd/gcos_wgsp/Timeseries/Data/nino34.long.anom.data
MEI	http://www.esrl.noaa.gov/psd/enso/mei.ext/ table.ext.html
IOD	http://www.jamstec.go.jp/frcgc/research/d1/iod/DATA/dmi.monthly.txt

3.3.5 Soil moisture data

Assessment of drought indices requires sufficiently long historic observations to obtain a reliable evaluation of drought phenomenon. The Global Land Data Assimilation System (GLDAS) VIC soil moisture data has been used in many studies and proved to be a reliable source to assess the soil moisture drought anomalies (Mishra et al. 2014). The soil

moisture data for the period from 1980 to 2018 was downloaded from the GLDAS VIC data sets for further computation of SSI.

3.3.6 Hydrological data

Daily observed streamflow data from the two gauging stations located at Pathagudem in the Indravati River Basin (IRB) and Ashti in the Wainganga River Basin (WRB) were obtained from Central Water Commission (CWC) for the period 1966 to 2018.

3.3.7 Geospatial data

DEM, LULC, soil and slope maps are the main geospatial datasets used as an input for the SWAT model. The Shuttle Radar Topography Mission (SRTM) DEM has a resolution of 30 m at the equator. DEM has been used as an input in SWAT model for delineating watershed and for topographic parameterization for the watersheds of IRB and WRB. The Globeland30 LULC datasets were downloaded from the link (http://www.globallandcover.com/defaults_en.html?src=/Scripts/map/defaults/En/browse_en.html&head=browse&type=data). Madhusoodhanan et al. (2017) reported that the Globeland30 data set showed least bias and performed well for Indian subcontinent. The LULC data was reclassified as SWAT database to form the model simulation. Global soil map is downloaded from the link (https://swat.tamu.edu/data/india-dataset/). The slope map was generated from the DEM. The DEM, LULC and soil maps for Wainganga and Indravati river basins are shown in Fig.3.2.

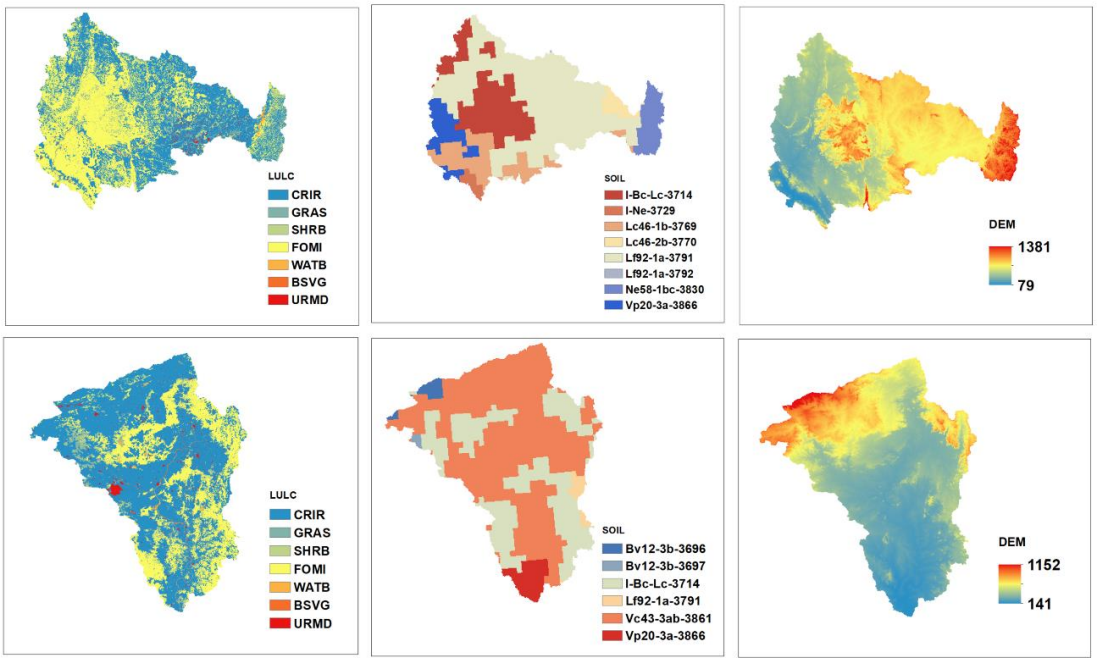

Fig. 3.2 DEM, LULC and soil maps for Wainganga and Indravati river basins

3.3.8 CMIP6 model data

Daily precipitation, and maximum and minimum temperature data from 5 CMIP6-GCMs were bias corrected using Empirical Quantile Mapping (EQM) method for South Asia and Indian sub-continent on a river basin scale (Mishra et al. 2020a). For the GRB scale, the daily precipitation, maximum and minimum temperature data for historical (1951-2014) and future (2015-2100) periods for four SSPs (SSP126, SSP245, SSP370, and SSP585) were obtained from the website (https://zenodo.org/record/3874046#.YOQWg0kzZPa). The sources of CMIP6 model data are shown in Table 3.3.

Table 3.3 CMIP6 GCM models and their sources

Sl. No.	Model	Source
1	ACCESS-CM2	Commonwealth Scientific and Industrial Research Organisation and Australian Research Council Centre of Excellence for Climate System Science
2	BCC-CSM2-MR	Beijing Climate Centre Climate System Model
3	CanESM5	Canadian Earth System Model
4	INM-CM4-8	Russian Institute for Numerical Mathematics Climate Model
5	MPI-ESM1-2-HR	Max Planck Institute Earth System Model

3.3.9 Crop characteristics, management and soil information

Cotton, maize and wheat are the three widely planted crops, chosen to examine the influence of drought with respect to climate change on agricultural production. The data sets of annual yield datasets for the crops during base period (1997-2014) were obtained from https://data.gov.in/resources/district-wise-season-wise-crop-production-statistics-1997.

The maize crop is a C4 photosynthetic plant and is one of the major cereals in the region. Maize is cultivated as a Kharif crop in the study area with the crop period from April-September. It is cultivated when the mean temperature is greater than 15 °C. The maturation period of maize is around 80-110 days. Wheat and cotton are categorised as C3 plants and the growth could be related to the increase in atmospheric CO_2. Wheat is cultivated as a Rabi crop with the sowing in the months of October to September. For cotton, the growing period is from May to December. Table 3.4 presents the crop characteristics and development stages of the C3 and C4 plants.

The cropping pattern over Aurangabad region consists of rain-fed, single cropping and double cropping. For the study, rain-fed irrigation method is considered. Farm

mechanization adopted was weeds management. Sprinkler irrigation is opted for the study area. Based on the FAO soil classification, the type of soil dominated in Aurangabad regions is clayey and clayey loam soils.

3.4 Potential Evapotranspiration (PET) Estimation

Various empirical methods and tools available to estimate the PET indirectly are Thornthwaite method (Thornthwaite, 1948), Hargreaves method (Hargreaves and Samani 1985), Penman-Monteith method (Monteith 1965, Penman 1948), and Modified Penman-Monteith method (Yang et al. 2019). However, a realistic PET can be estimated using Penman-Monteith's equation (Aadhar and Mishra, 2020). This method considers the climate variables such as temperature, humidity, wind speed and solar radiation. However, precipitation, maximum and minimum temperatures variables are taken considered in the present study. Therefore, Hargreaves method is chosen to estimate the PET demand as it is recommended as the most reliable method after the Penman-Monteith's equation (Subburayan, 2011) given in Eq. 3.1. The outputs from this method are comparable with the Penman-Monteith formula with lesser number of climate data (Subburayan et al. 2018).

$$PET = 0.00938(T_{max} - T_{min})^{0.5}(T_{mean} + 17.8)R_a \quad (3.1)$$

where, T_{mean}, T_{max} and T_{min} are the monthly mean, maximum and minimum air temperature respectively in °C and R_a is represented as the extra-terrestrial radiation (MJ m^{-2} d^{-1}).

Table 3.4 Crop characteristics and developmental stages of crops in Aurangabad region

Crop	Maize	Cotton	Wheat
Growing period	April-September	May-December	October-February
Root depth, m	0.3-1.2	0.3-0.8	0.3-1.5
Crop coefficient	1.05	1.1	1.1
Base temperature °C	8	12	15
Upper temperature °C	30	35	35
Sowing to emergence, days	6	13	13
Sowing to maximum rooting depth, days	107	97	90
Sowing to flowering, days	66	97	99
Flowering stage, days	13	53	25
Sowing to start senescence, days	108	131	124
Sowing to maturity (length of crop cycle), days	132	230	165

3.4.1 SPEI computation

In the current global warming situation, the effect of temperature and evapotranspiration must be considered for assessing the meteorological drought. Therefore,

the widely used SPEI is computed, in the present study for future drought assessment, based on the resulting water balance (P-PET) from precipitation (P) and PET series. SPEI is estimated to investigate the effects of climate change on drought in the context of global warming. This index is obtained by fitting the Log-normal probability distribution to the water balance i.e. the difference (x_i) between time series of P and PET for the month (i) as given in Eq. 3.2.

$$x_n^k = \sum_{i=0}^{k-1} P_{n-1} - (PET)_{n-1} \quad (3.2)$$

where P_{n-1} is represents the monthly rainfall time series and $(PET)_{n-1}$ represents the monthly evapotranspiration time series.

The probability distribution function for the x series is given in Eq. 3.3.

$$f(x) = [1 + (\frac{\tau}{x - \gamma})^{\delta}]^{-1} \quad (3.3)$$

where x is considered as the difference between the precipitation and evapotranspiration, τ, δ and γ are scale, shape and location parameters, respectively. The CDF values from fitted distribution are then standardized for obtaining SPEI as given by Eq. 3.4.

$$SPEI = W - \frac{p_0 + p_1 w + p_2 w^2}{1 + q_1 w + q_2 w^2 + q_3 w^3} \quad (3.4)$$

where,

$$W = \begin{cases} \sqrt{-2\ln(f(x))} & \text{if } 0 \le f(x) \le 0.5 \\ \sqrt{-2\ln(1 - f(x))} & \text{if } 0.5 \le f(x) \le 1 \end{cases} \quad (3.5)$$

where, $p_0 = 2.515517$, $p_1 = 0.802853$, $p_2 = 0.010328$

$q_1 = 1.432788$, $q_2 = 0.189269$, $q_3 = 0.001308$.

3.4.2 Drought characteristics

Drought characteristics can be identified using the Run theory analysis. A run is defined as the values below a preferred truncation level by considering the positive and negative run (Yevjevich, 1967). In the present study, a value of -0.8 is considered as the threshold value below which all the values are taken as drought events. This study considered three drought characteristics namely drought duration (D), peak (P) and severity (S). The drought duration is the interval between the onset and offset of drought for a particular threshold level. The drought peak is computed as the absolute lowest index value reached

by the drought time series throughout the period of a run. A simple arithmetic sum of deficit volume for each month under a certain drought duration can be defined as the drought severity.

3.4.3 Detection of monotonic trend using Mann-Kendall (MK) trend test

Positive and negative trends associated with the drought characteristics are investigated using the non-parametric MK trend test and Sen's slope estimator for both historical and future periods. The S-statistics are used in MK test as suggested by Mann (1945) and Kendall (1975). If there exists any positive difference between data points, then the S-statistics increase by 1 and vice versa while zero difference represents that S-statistic is constant. The S-statistic is given by Eq. 3.6.

$$S = \sum_{k}^{n-1} \sum_{m=k+1}^{n} \mathrm{Sgn}(x_j - x_k) \tag{3.6}$$

x_j and x_k are data points in the time series linked with the Sgn is shown in Eq. 3.7.

$$\mathrm{Sgn}(x_j - x_k) = \begin{cases} +1 \text{ if} (x_j - x_k) > 0 \\ 0 \text{ if} (x_j - x_k) > 0 \\ -1 \text{ if} (x_j - x_k) > 0 \end{cases} \tag{3.7}$$

Positive S-statistic values indicate an upward trend while negative values indicate a downward trend.

The Z-statistic, as given in Eq. 3.8, is generally used to test the statistical significance of the detected trends in the data points.

$$Z_{stat} = \begin{cases} \dfrac{S-1}{\sqrt{\frac{n(n-1)(2n+5) - \sum_{m=1}^{r} t_m(t_m-1)(2t_m+5)}{18}}} & \text{if } S > 0 \\ 0 & \text{if } S = 0 \\ \dfrac{S+1}{\sqrt{\frac{n(n-1)(2n+5) - \sum_{m=1}^{r} t_m(t_m-1)(2t_m+5)}{18}}} & \text{if } S < 0 \end{cases} \tag{3.8}$$

where n is the total sample associated with the study, r is the number of tied groups in the data sets and t_m is the number of data points in the m^{th} tied groups. The results of the MK test give the hypothesis, H=1, which says that if there exists a statistically significant trend, the null hypothesis is rejected when $|Z-stat| > 1.96$. Throughout the study, the value of 1.96 is taken as a threshold value obtained from the standard normal table at 95% confidence level. The MK statistic is the identification of the direction associated with the detected trends. The magnitude of the trend can be determined using Sen's slope estimator (Sen, 1968).

3.4.4 Regionalization of drought characteristics

The GRB is divided into sub-regions based on the homogeneous drought characteristics. Since drought is considered a regional phenomenon, the drought studies must be carried out in a regional perspective. K-means clustering algorithm developed by MacQueen (1967) is used to achieve the best combination of sub-regions with each cluster being represented by its centroid. The attributes selected for the present study are latitude, longitude and drought characteristics to segregate the homogeneous regions. The mathematical form of K-means clustering is given in Eq.3.9.

$$C_k = \sum_{j=1}^{U} \sum_{i=1}^{V} \|P_n - O_m\|^2 \quad (3.9)$$

$\|P_n - O_m\|^2$ is the square of Euclidean distance between the n^{th} data points and m^{th} cluster centers, V is the total number of data points and U is the total number of clusters. K-means is an iterative clustering algorithm technique that aims to obtain the well segregated clusters given as below:

i. Initially, the data points are divided randomly among K-clusters and then each data point is allocated to its nearest cluster centers.
ii. Cluster centers are computed based on the averaging of the coordinates for specific clusters and each point is reassigned to the closest cluster centroid to obtain new clusters.
iii. The steps are repeated till the best result is obtained as the final result shows sensitivity to initial cluster centers.
iv. Two validation criteria, namely Silhouette Coefficient (SC) and Dunn Index (DI) are implemented to justify the total number of clusters as a consequence of K-means algorithm for obtaining the homogeneous climate regions (Roushangar and Alizadeh, 2018).

3.4.5 Linear scaling (LS) bias correction

The RCMs have systematic biases of climate model simulations relative to observations and hence, RCM model outputs cannot be used directly in impact assessment studies. Linear scaling (LS) bias correction method is implemented to adjust the RCM mean values (Fang et al. 2014). The monthly correction of RCM data is on the basis of the differences between observed and RCM data.

For precipitation correction is given by Eq. 3.10.

$$P_{corr} = P_{RCM} \times \frac{\mu(P_{obs})}{\mu(P_{RCM})} \quad (3.10)$$

For temperature correction is given by Eq. 3.11.

$$T_{corr} = T_{RCM} + \mu(T_{obs} - T_{RCM}) \quad (3.11)$$

where, P_{corr} and T_{corr} are the corrected precipitation and temperature, P_{RCM} and T_{RCM} are the RCM precipitation and temperature data, P_{obs} and T_{obs} represent the observed precipitation and temperature data.

3.4.6 Reliability Ensemble Averaging (REA)

The weights assigned to the climate models can be derived using an iterative algorithm called as REA by considering the observational data sets. The uncertainty generated from multiple RCMs/GCMs are addressed by REA approach developed by Giogi & Mearns, (2002). The algorithm for the proposed approach is as follows.

Step1: The CDF deviations of RCMs/GCMs from observational data sets are computed using Root Mean Square Error (RMSE) for entire GRB. The initial weights are computed using Eq. 3.12

$$W_k = \frac{1/RMSE_k}{\sum_{k=1}^{n} 1/RMSE_k} \qquad k = 1,2,\ldots,n \quad (3.12)$$

where n = number of RCMs/GCMs and W_k is represented as initial weight of k^{th} RCMs.

Step 2: The weighted mean CDF of RCMs/GCMs are computed using Eq. 3.13.

$$CDF_m^{RCM/GCM} = \sum_{k=1}^{n} W_k CDF_k^{RCM/GCM} \qquad k = 1,2,\ldots,n \quad (3.13)$$

where, CDF_m^{RCM} is represented as the RCM/GCM weighted mean, CDF_k^{RCM} is the future CDF of k^{th} RCM/GCM under a particular RCP scenario.

Step3: Inverse RMSE is computed and new weights are assigned and this procedure is repeated till the converged weights gets generate.

3.4.7 Multivariate copula analysis of drought properties

Univariate analysis of drought characteristics is not capable of determining the drought frequencies as it assumes that drought variables are interdependent on each other. Therefore, the trivariate drought analysis is incorporated using copula functions for the assessment of the dependence structure among the drought characteristics. In this study, peak (P), duration (D) and severity (S) are considered as dependent random variables to obtain the multivariate dependence structure. The joint distribution function $F(y_1 \ldots \ldots y_n)$ is given in Eq. 3.14.

$$F(y_1, \ldots \ldots, y_n) = C(u_1, \ldots \ldots u_n, \theta) \quad (3.14)$$

where C is the copula distribution function, associated with the copula parameter θ. $F_1, \ldots\ldots, F_n$ are the marginal distribution of random variables $(y_{1,} \ldots\ldots, y_n)$. The dependence between $y_{1,} \ldots\ldots, y_n$ is characterised entirely by the copula C that is invariant by monotonically increasing transformations of the margins. The copula function C is treated as a unique function only when the marginal distributions are continuous. The joint probability density function linked with the copula function C is given in Eq. 3.15.

$$f(y_{1,} \ldots\ldots, y_n) = f_1(y_1) \times \ldots\ldots \times f_n(y_n) \times c[F_1(y_1), \ldots\ldots\ldots, F_n(y_n)] \quad (3.15)$$

The probability density function $f_1(y_1), \ldots\ldots f_n(y_n)$ of the dependent variables are linked to the density function c as given in Eq. 3.16.

$$c(u_1, \ldots\ldots, u_n) = {\partial^n C(u_1, \ldots\ldots u_n)}\Big/{(\partial u_1 \ldots\ldots\ldots\ldots \partial u_n)} \quad (3.16)$$

where $u_1 = F_1(y_1)$,……., and $u_n = F_n(y_n)$

A trivariate distribution function, fitted to three dependent drought characteristics P, D and S with marginal CDFs F_P, F_D and F_S can be represented by a copula function that guarantees the existence of a unique function c such that all P, D and $S, \in R$. The trivariate joint probability distribution resulting in the parameter associated with the specified copula function is presented by Eq. 3.17.

$$f(P, D, S) = f_P(P) \times f_D(D) \times f_S(S) \times c[F_P(P), F_D(D), F_S(S)] \quad (3.17)$$

Different types of copula families, namely Frank, Gaussian, Gumbel, Clayton, and Student's t copula are used in many hydro-meteorological studies. The dependency status between the interrelated drought variables is represented by the respective copula parameter. In this study, the parameters of copula families are estimated using the maximum likelihood estimation (MLE) method based on its fitted marginal distribution. The best fitted copula is estimated based on the Goodness of Fit (GoF) measures, namely, Kolmogorov-Smirnov test (KS), Cramer-von Misses (CVM), and Chi-square (Chsq) tests as suggested by Genest et al. 2007). AIC criteria and the maximum likelihood function are also used to justify the best fitted copula model.

Various copulas are given in Eq. 3.18 to Eq. 3.22

Clayton: $C_\theta(\alpha, \beta) = \left(\alpha^{-\theta} + \beta^{-\theta} -\right)^{-\theta}$ for all $\theta\ (0, \infty)$ (3.18)

Frank: $C_\theta(\alpha, \beta) = -\frac{1}{\theta}\log\left(1 + \frac{(\exp(-\theta\alpha)-1)(\exp(-\theta\beta)-1)}{\exp(-\theta)-1}\right)$ for $\theta \in R\{0\}$ (3.19)

Gaussian: $C_\theta(\alpha, \beta) = \int_{-\infty}^{\varphi^{-1}(\alpha)} \int_{-\infty}^{\varphi^{-1}(\beta)} \frac{1}{2\pi\sqrt{1-\theta^2}} e^{\frac{2\theta uv - u^2 - v^2}{2(1-\theta^2)}} dudv$ (3.20)

Gumbel: $C_\theta(\alpha,\beta) = \exp\{-[-(-\log\alpha)^\theta + (-\log\beta)^\theta]^{1/\theta}\}$, for $\theta \in [1,\infty)$ (3.21)

Student-t: $C_\theta(\alpha,\beta) = \int_{-\infty}^{T_\gamma^{-1}(\alpha)} \int_{-\infty}^{T_\gamma^{-1}(\beta)} \frac{\Gamma\left(\frac{\nu+2}{2}\right)}{\Gamma\left(\frac{\nu}{2}\right)\nu\pi\sqrt{1-\theta^2}} \left\{1 + \frac{u^2+v^2-2\theta uv}{\nu(1-\theta^2)}\right\} dudv$ (3.22)

3.3.8 Drought risks assessment

The trivariate copula model is implemented to obtain the multivariate drought return periods for different climate divisions of GRB. The return period of a particular event can be used for designing the hydrologic projects which gives a qualitative and quantitative measure of risk associated with extreme events. The joint return period analysis is carried out by using the two probability cases, primary return periods ''T^{AND}'' and ''T^{OR}'' for the drought variables. The joint occurrence probabilities of drought severity (S), peak (P) and duration (D) that exceed a definite threshold level (i.e. S > s, P > p, D > d) related to the trivariate return for 'T^{AND}' and 'T^{OR}' are shown in Eq. (3.23) and (3.24)

$$T^{AND} = \frac{\mu}{P(S \geq s, D \geq d, P \geq p)}$$

$$= \frac{\mu}{1 - F_S(s) - F_D(d) - F_P(p) + F_{S,D}(s,d) + F_{D,P}(d,p) + F_{P,S}(p,s) - F_{S,D,P}(s,d,p)}$$

$$= \frac{\mu}{1-F_S(s)-F_D(d)-F_P(p)+C(u_1,u_2)+C(u_2,u_3)+C(u_3,u_1)-C(u_1,u_2,u_3)} \quad (3.23)$$

$$T^{OR} = \frac{\mu}{P(S \geq s, D \geq d, P \geq P)}$$

$$= \frac{\mu}{1-P(S \geq s, D \geq d, P \geq P)} = \frac{\mu}{1-F_{S,D,P}(s,d,p)} = \frac{\mu}{1-C(u_1,u_2,u_3)} \quad (3.24)$$

where, $F_P(p)$, $F_D(d)$ and $F_S(s)$ are the marginal CDF of severity, drought, and peak respectively Here, $\mu = N/n$ is expressed as the ratio of the total number of years (N) to the number of drought events (n) for the estimation of drought return period. T^{AND} denotes the joint return period of $P \geq p$, $D \geq d$ and $S \geq s$; and T^{OR} denotes the joint return period of $P \geq p$, $D \geq d$ or $S \geq s$.

3.5 Development of Non-stationary Reconnaissance Drought Index (NRDI) and Non-stationary Standardized Precipitation Index (NSPI)

The stationary RDI is calculated based on the assumption that the parameters related to initial values (δ_0) are constant with time. Under non-stationarity condition, some parameters of the distribution function of δ_0 can get changed. The initial value, δ_0, is taken

as the ratio of precipitation series to evapotranspiration series in different time windows (3-, 6- and 12-month), which can be computed using the Eq. 3.25.

$$\delta_0(t) = \frac{\sum_{j=1}^{n} P_j(t)}{\sum_{j=1}^{n} PET_j(t)} \quad (3.25)$$

Further, for computation of NSPI and NRDI, correlation analysis between the precipitation and global scale climate indices as well as the computed δ_0 values (3-,6- and 12- month) and the global scale climate indices of different lags (1-12) are performed using Kendall's method (Kendall, 1955) with a significance level of 0.05. The significant covariates from potential large-scale climate indices are evaluated from the best lags based on the minimum p-value. Further, NSPI and NRDI can be developed using the filtered covariates using the GAMLSS model.

3.5.1 GAMLSS model development

GAMLSS model used in this study was developed by Rigby and Stasinopoulos (2005). This model has been widely accepted to obtain the non-stationary parameters related to its parametric distribution varying linearly and nonlinearly with respect to the significant covariates. In the present study, random variable y_i (precipitation series / the ratio between aggregated precipitation and evapotranspiration series) was assumed to have a parametric cumulative distribution function. Related time varying parameters can be modelled as a function of selected covariates namely SST, SOI, MEI and IOD by using the GAMLSS model. Independent observations y_j, with j = 1,…., n have distribution function $f(y_j,\theta_i)$ where $\theta_i = \theta_1^i \ldots\ldots \theta_q^i$ vector of q distribution parameters which denote the location, scale and shape. The parameters of distributions are related to the monotonic link functions denoted by $g_k(.)$, where k = 1, ..., q, which creates a relationship between covariates and random variables using a semi-parametric additive model and outlined in Eq. 3.26.

$$g_k(\theta_k) = x_k \Psi_k + \sum_{j=1}^{J_k} h_{jk}(x_{jk}) \quad (3.26)$$

Here, x_k is a matrix that represents the explanatory variables of order $n \times j_k$ (length of the covariate vectors); θ_k (θ_{1k},……, θ_{jk^k}) are the vectors of parameters of length j_k, and $h_{jk}(.)$ is an additive function that is flexible in modelling the dependence of parameters of the response variable with relation to the explanatory variables x_{j_k}. Flexibility in modelling the dependence parameters on the covariates can be achieved using the linear or smoothing form of variation. The selected covariates based on the Kendall's τ lag correlation method for different time windows (3-, 6- and 12 - months) of precipitation as well as the series of initial

values (δ_0) are varied linearly with respect to the parameters (here μ_t is chosen as a time varying parameter) of the distribution.

For computing the NSPI for the drought status of a particular location, a two parametric Gamma distribution is fitted to the precipitation series with linearly varying location and constant scale parameter, ensuring a relationship between precipitation series and selected explanatory variables as shown in Eq. 3.29, using Eq.3.27 and 3.28.

$$y_t \sim \text{Gamma}(\mu_t, \sigma) \tag{3.27}$$

$$\mu_t = a_o + a_1 I_1(t) + a_2 I_2(t) + \cdots + a_n I_n(t) \tag{3.28}$$

where $a_o, \ldots\ldots, a_n$ are estimated mean coefficients for the linear variability for a particular location after fitting non-stationary Gamma distribution and $I_1, \ldots\ldots, I_n$ represent the explanatory climate variables at time t.

$$f(y_t, \mu_t, \sigma) = \frac{1}{(\sigma^2 \mu_t)^{1/\sigma^2}} \frac{y^{\frac{1}{\sigma^2}-1} e^{-y/(\sigma^2 \mu_t)}}{(1/\sigma^2)} \tag{3.29}$$

The cumulative distribution functions of the aggregated rainfall series were computed by fitting the non-stationary model and then transformed into standard normal values using Eq. 3.30.

$$\text{NSPI} = \varphi^{-1}\big(f(y_t, \mu_t, \sigma)\big) \tag{3.30}$$

where $f(y_t, \mu_t, \sigma)$ are the CDFs of the aggregated precipitation series y_t , is the aggregated precipitation at any time t, and φ^{-1} is the inverse CDF values.

Further, a non-stationary Log-normal distribution with linearly varying location parameter (μ_t) with time considering the respective covariates and with the constant scale parameter (σ), is fitted to the δ_0 values as shown in Eq. 3.31. and Eq. 3.32.

$$y_t \sim \text{LogNormal}\ (\mu_t, \sigma) \tag{3.31}$$

$$\mu_t = b_o + b_1 I_1(t) + b_2 I_2(t) + \cdots + b_n I_n(t) \tag{3.32}$$

where $b_o, \ldots\ldots, b_n$ are estimated mean coefficients for the linear variability for a particular location for the fitted non-stationary Log-normal distribution and $I_1, \ldots\ldots, I_n$ are the explanatory climate variables at time t.

Then using the time variant location parameter and the invariant scale parameter, the NRDI is estimated using the Eq. 3.33.

$$\text{NRDI}(t) = \frac{y_t - \mu_t}{\sigma} \tag{3.33}$$

Here, $y_t = \ln(\delta_0)$; μ_t is the time varying arithmetic mean and σ is the standard deviation of the observational variable.

The parameters for Log-normal and Gamma distribution are estimated by Rigby and Stasinopoulos (RS) algorithm in the GAMLSS framework. The distribution function f (y_j,θ_i) is selected based on the largest maximum-likelihood value. Generally, the quality of fitting is not justified by the maximum likelihood. Besides maximum likelihood, the selection of both the models (stationary and non-stationary) is evaluated in terms of lowest AIC values.

In NSPI and NRDI, the dry periods are represented as negative values while the wet conditions are shown as positive values. The classification of NSPI and NRDI is similar to the standard SPI and RDI. The drought characteristics can be identified using the Run theory analysis.

3.5.2 Multivariate dependence modelling using Pair-wise Copula Constructions (PCC)

Brechmann and Schepsmeier (2013) observed that exchangeable Archimedean copulas including multivariate Student's t copula and Normal copulas were not flexible enough to develop an accurate model dependent status among a larger number of variables. When the dimension of random variable increases, the construction of a copula becomes difficult. Regular vines are broadly categorised into two subsets i.e. D-vine and canonical vine (C-vine) (Kurowicka and Cooke, 2006, Aas et al. 2009). Vine is a flexible graphically represented tree-like structure that computes the pairwise construction of variables that are mutually dependent, called as PCC model. In the case of D-vine structure, the node has a link to more than two edges based on the number of random variables and basically, it forms a hierarchical trend structure from 1st to the nth node in the tree.

The D-vine structure is used to model joint probability related to the drought characteristics $P, D,$ and S with marginal densities F_P, F_D, F_S respectively. Similarly, a multivariate density function can be decomposed using a C-vine structure. C-vine is a tree-like structure where the main component is uniquely defined as the root node and the other variables are the branch nodes directly connected to the root with n-j edges. The D-vine structure can be converted to a C-vine structure by slightly modifying the structure. Here D-vine structure is selected for the joint density decomposition as shown in Eq. 3.34.

$$F(P, D,S) = f_P(P) \times f_D(D) \times f_S(S) c_{PD}\{F_P(P), F_D(D)\} \times c_{DS}\{F_D(D), F_S(S)\} \times c_{PS|D}\{F_{PD}(P|D), F_{SD}(S|D)\} \quad (3.34)$$

$c_{PD}\{F_P(P), F_D(D)\}$ represents the bivariate copula fitted between $F_P(P)$ and $F_D(D)$. $c_{PS|D}\{F_{PD}(P|D), F_{SD}(S|D)\}$ represents the bivariate copula fitted to the second tree variables $F_{PD}(P|D), F_{SD}(S|D)$.

Archimedean copulas like Gumbel, Clayton, Frank and the Meta-elliptical copulas namely Gaussian and Student's t copulas are used for finding the dependency parameter among the non-stationary drought variables. The D-vine pair copula structure is constructed between the drought characteristics by identifying the advantages of pair copula over the multivariate copula that can capture the entire dependency among the variables. Further, drought return period of NSPI and NRDI were computed.

3.5.3 Estimation methods for pair-copula models

The steps used in this study for pair copula construction are outlined as follows:

Firstly, the dependency measurement between drought characteristics like peak - duration, duration - severity and severity - peak are estimated using Kendall's τ and Spearman's ρ. Then, an appropriate D-vine model is chosen in terms of the dependency of variables. Graphical tools like Kendall plot (K-plot) and Chi-plots are useful for the optimum choice of bivariate copula models that are defined by Genest et al. (2007). The GoF tests, namely, the Vuong and Clarke tests, are applied to find the suitable copula family for this study (Vuong, 1989; Clarke, 2007). Commonly used AIC criteria to discriminate between models are also used in this study to find an optimum solution regarding the selection of copula family.

After deciding the pairwise copula models, the parameter estimation is conducted using the MLE method which maximises log-likelihood function. The process of parameter estimation for the three-dimensional distribution function for a vine structure is given in Eq. 3.35.

$$L(P, D, S|\theta) = f_P(P) \times f_D(D) \times f_S(S) \times c_{PD}\{F_P(P), F_D(D); \theta_{PD}\} \times c_{DS}\{F_D(D), F_S(S); \theta_{DS}\} \times c_{PS|D}\{F_{PD}(P|D), F_{SD}(S|D); \theta_{PS|D}\} \quad (3.35)$$

where $\theta = (\theta_{PD}, \theta_{DS}, \theta_{PS|D})$

$$l(P, D, S|\theta) = \log\{c_{PD}(F_P(P), F_D(D); \theta_{PD})\} + \log\{c_{DS}(F_D(D), F_S(S); \theta_{DS})\} + \log\{c_{PS|D}(F_{PD}(P|D), F_{SD}(S|D); \theta_{PS|D})\}$$

where $F_{PD}(P|D) = h(P, D, \theta_{PD})$ and $F_{SD}(S|D) = h(D, S, \theta_{DS})$

The parameters of the copula function can be estimated by choosing a particular tree structure. The first tree parameters can be estimated from the fitted copula between the pairwise variables in the first tree, then the second tree parameter and so on. The association

between the first tree and second tree can be achieved using conditional distribution function also namely h functions which are presented in Eq. 3.36 and Eq. 3.37.

$$h(P/D|\theta_{PD}) = \frac{\partial C_{P,D}[(F(P), F(D)|\theta_{PD})]}{\partial F(D)} \quad (3.36)$$

$$h(D/S|\theta_{DS}) = \frac{\partial C_{D,S}[(F(D), F(S)|\theta_{DS})]}{\partial F(D)} \quad (3.37)$$

where, $\partial C_{P,D}$ is the bivariate copula distribution function with parameter θ_{PD} specified for peak and duration whereas $\partial C_{D,S}$ is the bivariate copula distribution function with parameter θ_{DS}. The inverse of h function (h^{-1}) gives an inverse conditional distribution function of variables.

3.6 Computation of SPI, RDI and SSI

SPI, RDI and SSI for 3 - and 6 - month time scales are computed for the GRB. SPI follows the two-parameter (scale and shape parameter) Gamma probability density function. Gamma (Γ) probability distribution used to describe precipitation variation is given in Eq. 3.38.

$$G(x_n) = \frac{1}{\beta^{\alpha}\Gamma(\alpha)} x_n^{\alpha-1} \exp^{-x_n/\beta} \quad (3.38)$$

Gamma probability density function is applied to 3-month and 6-month moving average precipitation series in order to estimate SPI by involving a shape factor and a scale factor, denoted by α and β respectively. Wet periods are specified by positive SPI series, whereas a sequence of negative values denotes a dry period.

RDI was proposed by Tsakiris et al. (2007) with the concept that meteorological droughts show the water balance deficit between precipitation and output reference evapotranspiration. The initial value (a_k) is a combined form using a monthly time-step and can be computed in terms of 3-month and 6-month time scales. RDI is calculated using the Eq. 3.39.

$$a_k^{(i)} = \frac{\sum_{j=1}^{k} P_{ij}}{\sum_{j=1}^{k} PET_{ij}} \qquad I = 1 \text{ to } ...n \quad (3.39)$$

where P_{ij} and PET_{ij} are the precipitation and PET respectively of the j^{th} month of the i^{th} year. It is assumed that the standardised RDI follows Lognormal distribution as given in Eq. 3.40.

$$RDI_{st}(k)(i) = \frac{y_k^{(i)} - \overline{y_k}}{\sigma_{yk}} \quad (3.40)$$

where y_k is $\ln(a_k)$, $\overline{y_k}$ is the arithmetic mean of y and σ_{yk} is its standard deviation. The calculation of RDI_{st} for monthly time steps, which may contain zero-precipitation values, can be carried out by the lognormal approach.

SSI can be computed by using empirical probability function instead of a parametric Gamma function. Farahmand et al. (2015) derived the marginal probability of soil moisture from the GLDAS data site using the empirical Gringorten plotting position as given in Eq. 3.41.

$$P(X_n) = K = \frac{r-0.44}{n+0.12} \quad (3.41)$$

where 'n' is the total sample size and r is the rank of soil moisture data which have non-zero values and $P(X_n)$ is the empirical probability. The outputs of Eq. (3.39) and Eq. (3.41) can be transformed into the Standardised Index (SI) using Eq. 3.42.

$$SI = \emptyset^{-1}(K) \quad (3.42)$$

where $\emptyset$ is the standard normal distribution function and K is probability derived from Eq. 3.41. The computed SPI, SSI and RDI indices were further compared with the multivariate drought indices computed in this study.

3.6.1 Bivariate and trivariate drought indices

The presence of a unique copula is assumed in the analysis of copula, but the most important aspect to be noticed here is the selection of a suitable copula function (Nelson, 2006). The multivariate random vectors are demonstrated as $X = (X_1, \ldots\ldots\ldots, X_d)$ with margins of F_x being continuous and strictly increasing. $F(X_1, \ldots\ldots\ldots, X_d)$ is the joint probability distributions with margins as $Fx_1, \ldots Fx_d$. Then there must be a presence of unique copula C for all $X_1, \ldots\ldots\ldots, X_d \in [-\infty, \infty]$ which links the multivariate distribution and d dimensional copulas as given in Eq. 3.43

$$C_\theta(\alpha_1, \ldots\ldots, \alpha_d) = Pr\left(F_{X_1}(X_1) \leq \alpha_1, \ldots\ldots\ldots\ldots, F_{X_d}(X_d) \leq \alpha_d\right)$$
$$= F_x\left(F_{X_1}^{-1}(\alpha_1), \ldots\ldots\ldots, F_{X_d}^{-1}(\alpha_d)\right) \quad (3.43)$$

It can be noticed that the values of $X_1, \ldots\ldots\ldots, X_d$ are the inverse functions of $\alpha_1, \ldots\ldots\ldots\ldots, \alpha_d$

So $X_1 = F_{X_1}^{-1}(\alpha_1), \ldots\ldots\ldots\ldots\ldots\ldots\ldots\ldots, X_d = F_{X_d}^{-1}(\alpha_d)$

$$F(X_1, \ldots\ldots\ldots, X_d) = C(F_1(X_1), \ldots\ldots\ldots, F_d(X_d)) = Q \quad (3.44)$$

For Bivariate Case,

$$F(X_1, X_2) = C(F_1(X_1), F_2(X_2)) = Q \quad (3.45)$$

For Trivariate Case,

$$F(X_1, X_2, X_3) = C\left(F_1(X_1), F_2(X_2), F_3(X_3)\right) = K \quad (3.46)$$

Gumbel, Clayton and Frank copulas are used to obtain the joint probability distribution of variables based on their dependency phenomenon. Maximum Pseudo Likelihood (MPL) estimation method is used for estimating the copula parameters that imitates the dependence structure among the correlated drought characteristics. The best fitted copula is then estimated based on the GoF measures. AIC and the maximum likelihood function are used to justify the best fitted copula model. These criteria can be applied for obtaining the best fitted copula by comparing the p-values obtained from all the GoF tests (Genest et al. 2009).

3.6.1.1 *Development of Multivariate Standardised Drought Index (MSDI) and Reconnaissance Trivariate Drought Index (RTDI)*

The MSDI can be computed using the joint probability Q as given in Eq. 3.47.

$$\text{MSDI} = \varphi^{-1}(Q) \quad (3.47)$$

For the computation of RTDI, the joint probability given in Eq. (3.47) can be used. The link between the joint probability of K and the RTDI can be derived using Eq. 3.48

$$\text{RTDI} = \varphi^{-1}(K) \quad (3.48)$$

where φ^{-1} is the inverse standard normal distribution function. MSDI is formulated as the joint probability of precipitation and soil moisture while RTDI is the combined form of precipitation, soil moisture and evapotranspiration.

3.6.2 Cross Wavelet Analysis (CWA)

The combination of Cross Wavelet Transform (XWT) and the Cross Wavelet Spectrum (CWS) can be represented by CWA. CWA breaks down the time series into time and frequency domain and detects the significant association with other variables. This method identifies the combined teleconnection and the variations in the time and frequency domain of the pair time-series. Morlet wavelet is adopted as mother wavelet as it shows a good balance between time and frequency localization. Therefore, the CWA is implemented to examine the potential teleconnection between SOI/IOD/SST/MEI/ISMR events with both

MSDI and RTDI time series. The two-time series are taken as α_k and β_k and the XWT for these time series is shown in Eq. 3.49.

$$W^{\alpha\beta} = W^{\alpha} W^{\beta *} \tag{3.49}$$

where * denotes the complex conjugate and the Cross Wavelet Power (CWP) is denoted as $|W^{\alpha\beta}|$. The distribution associated with the CWP of α_k and β_k with the related power spectra P_n^{α} and P_n^{β} is given in Eq. 3.50.

$$D\left(\frac{\left|W_n^{\alpha}(s)\, W_n^{\beta}(s)\right|}{\sigma_{\alpha}\sigma_{\beta}} < p\right) = \frac{Z_v(p)\sqrt{P_n^{\alpha}\, P_n^{\beta}}}{v} \tag{3.50}$$

where $Z_v(p)$ is denoted as 95% the confidence level linked with the probability p. For more details regarding the CWA, the study by Grinsted et al. (2004) can be referred.

3.7 Hydrologic Model Set Up

SWAT has been chosen for the present study to simulate the hydrological fluxes of IRB and WRB and for assessment of drought events based on MDI. SWAT is a process based, semi-distributed basin scale model developed by United States Department of Agriculture (Arnold et al. 2012). Two sub-basins of GRB are selected i.e. Indravati basin and Wainganga basin for the application of SWAT. DEM is the basic input data used to delineate the watershed into number of sub-basins and each sub-basin is joined by a stream network. Each of the sub-basin is then further sub-divided into hydrologic response units (HRUs), based on homogeneous land use, soil, management and topographical features. All hydrological processes are simulated based on HRUs. Overall, 300 target HRUs were generated over the 23 sub-basins located in IRB while 280 target HRUs were generated over the 31 sub-basins in the WRB. The surface runoff was simulated by Natural Resources Conservation Service-Curve Number (NRCS-CN), considering daily precipitation, LULC characteristics, hydrologic soil groups and antecedent soil moisture condition. PET was estimated using Hargreaves equation. QSWAT with QGIS interface is used in the present study. Model simulations are carried out, considering the first 5-years as warm-up period (1961-1965) to initialize the important model processes and variables on a daily time step. The model is simulated with the continuous observed monthly streamflow data available at the IRB (1966 to 2013) and WRB (1966 to 2017) outlet stations (i.e. Pathagudem and Ashti gauge station). For IRB, calibration and validation were carried out for the periods of 1966 to 1997 and 1998 to 2013, respectively at Pathagudem station. Similarly, for WRB, the data of Ashti station was used for calibration (1966 - 2004) and validation (2005 - 2017). SWAT

calibration and validation were carried out using SWAT Calibration and Uncertainty Analysis Program (SWAT-CUP) using the Sequential Uncertainty Fitting-2 (SUFI-2) self-automated algorithm. More details regarding SWAT-CUP calibration and validation is presented in the result section.

3.7.1 Evaluation of Multivariate Drought Index (MDI)

A reliable and robust copula based multivariate drought index is proposed in this study. The unique marginal distributions of associative climatic variables can be efficiently preserved within the joint distribution, which in turn, would be capable of assessing the deficit status.

Step1: Marginal distribution and correlation

To assess the assimilated behaviour of meteorological, agricultural and hydrological droughts, the correlation between precipitation and SWAT simulated variables (PET, soil moisture and runoff) have been taken into consideration. The degree of correlation was calculated by Kendall-τ correlation approach with an assumption of monotonic association between climate variables, using the time series of 6-month moving average of climate variables. From Table 3.5 and Table 3.6, it can be observed that significant correlations are exhibited between climate variables like precipitation-streamflow, precipitation-soil moisture and streamflow-soil moisture. The evapotranspiration showed insignificant positive correlation with other climatic variables. Various types of distributions are fitted to the climatic variables for obtaining the marginal distributions.

Table 3.5: Kendall-τ correlations between climate variables in the Indravati river basin

Variables	Precipitation	Evapotranspiration	Soil moisture	Streamflow
Precipitation	1	0.008	0.93	0.54
Evapotranspiration	0.008	1	0.08	0.03
Soil moisture	0.93	0.08	1	0.38
Streamflow	0.54	0.03	0.38	1

Table 3.6**:** Kendall-τ correlations between climate variables in the Wainganga river basin

Variables	Precipitation	Evapotranspiration	Soil moisture	Streamflow
Precipitation	1	0.02	0.9	0.4
Evapotranspiration	0.02	1	0.04	0.07
Soil moisture	0.9	0.04	1	0.41
Streamflow	0.4	0.07	0.41	1

Step 2: Copula analysis

This study considered precipitation (P), evapotranspiration (E), streamflow (S_f) and soil moisture (S_m) for the development of MDI using four variate copula functions to examine the joint effects of associative parameters leading to probabilistic assessment of drought. By considering these as random variables, the dependency structure between multi-scalar climatic variables were obtained. F_P, F_E, F_{S_f} and F_{S_m} are the marginal distributions of P, E, S_f and S_m respectively. $F_{PES_fS_m}(P, E, S_f, S_m)$ denotes the cumulative distribution function (CDF) of the four-variate distribution with marginal CDFs as $F_P(P), F_E(E), F_{S_f}(S_f)$ and $F_{S_m}(S_m)$. The presence of the unique copula C for all real P, E, S_m and S_f is as shown in Eq. 3.51.

$$(P, E, S_m, S_f) = c\left(F_P(P), F_E(E), F_{S_f}(S_f), F_{S_m}(S_m)\right) f_P(P) f_E(E) f_{S_f}(S_f) f_{S_m}(S_m) = q \qquad (3.51)$$

where C is the copula function; $\left(F_P(P), F_E(E), F_{S_f}(S_f) \text{ and } F_{S_m}(S_m)\right)$ are the marginal CDFs of P, E, S_f and S_m respectively; $f_P(P), f_E(E), f_{S_f}(S_f)$ and $f_{S_m}(S_m)$ are the probability distribution functions (PDFs) of the random variables P, E, S_f and S_m respectively.

The MDI used to model the dependence between the climatic parameters can be obtained by Eq. 3.52, where φ is the standard normal distribution function.

$$MDI = \varphi^{-1}(q) \qquad (3.52)$$

Step 3: Optimal selection of copula

The optimal copula functions must be selected in order to represent dependence structure between climatic variables well. Clayton copula fitted well compared to Gumbel and Frank copulas based on the GoF measures. Hence, the Clayton copula was used in this study to obtain the joint behaviour of climate variables. The optimal parameters of copula functions were obtained by MPL parameter estimation criteria. The analytical expressions of n-dimensional symmetrical Clayton (C_C) is written as shown in Eq. 3.53.

$$C_c(P, E, S_f, S_m) = \left(P^{-\theta} + E^{-\theta} + {S_f}^{-\theta} + {S_m}^{-\theta} - 3\right) \qquad (3.53)$$

Wet events of MDI were identified by positive values and the dry events were identified by negative values. MDI was computed at 6-month time scales by aggregating all hydrological entities using 6-month moving average values. In addition, the drought characteristics like duration and severity are quantified based on the extensively used Run theory analysis.

3.8 Impact of Climate Change on Crop Yield and the Crop-Drought Relationship with Changing Climate

The methodology includes meteorological, soil and crop data collection and calculation of PET. Further, AquaCrop model is developed and crop yield is simulated for maize, cotton and wheat. For future period the crop yield is predicted. The changes in the yield with respect to observed period was investigated in the study. Further, crop-drought relationship is obtained considering the correlation between Standardized Yield Residual Series (SYRS) and SPEI in different lags. The methodological frame work is presented in Fig 3.3.

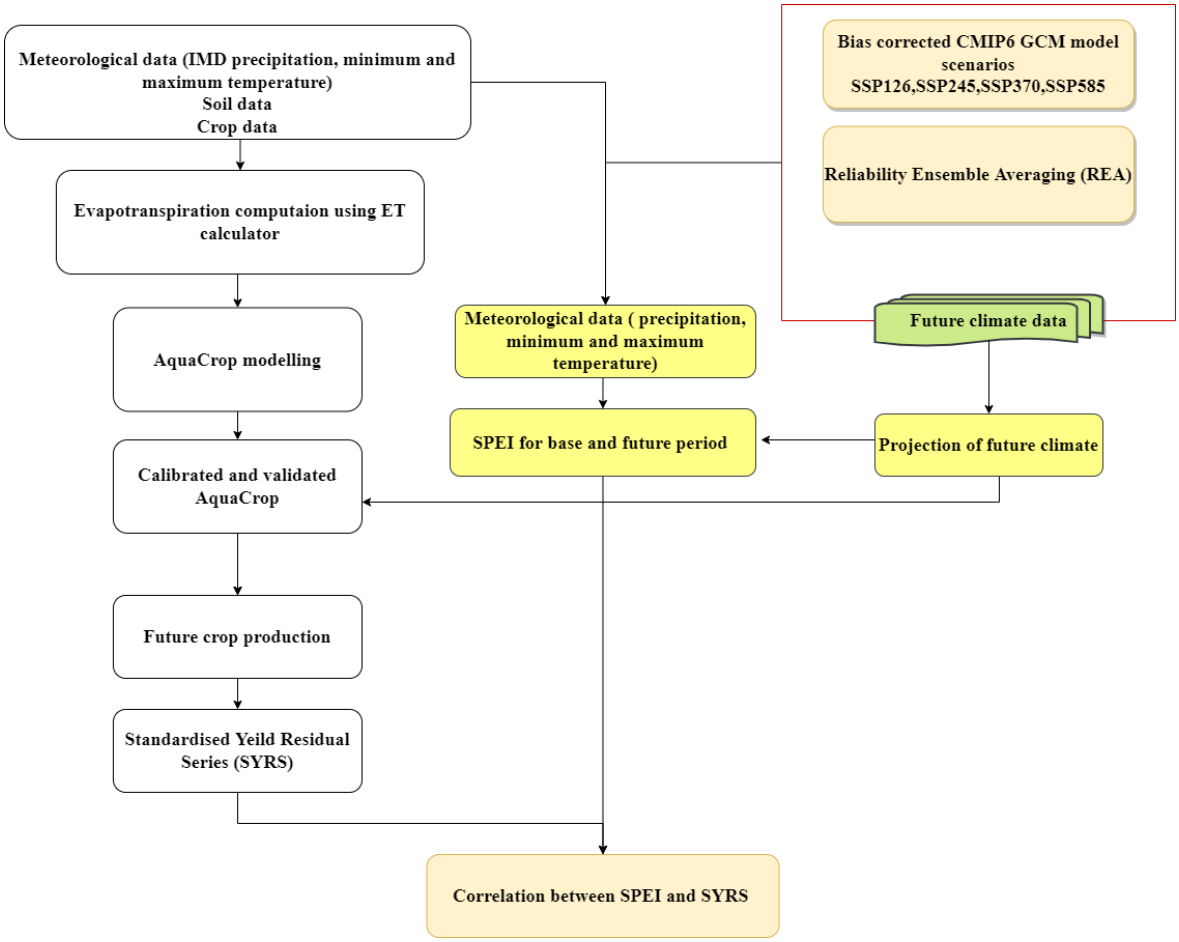

Fig 3.3. Methodological frame work for crop yield prediction and the crop-drought relationship

3.8.1 AquaCrop model development

AquaCrop generally simulates yield response to water (i.e. water productivity) considering robustness, simplicity and water condition regionally. The model was developed

based on the Doorenbos and Kassam (1979) hypothesis to obtain the yield response to water that led to the model evolution (Steduto et al. 2009). The main are features of the model are:
(i) Evapotranspiration (ET_a) consisting of two components, (a) soil evaporation (E_s); (b) transpiration (T_r).
(ii) The model uses Canopy Cover (CC) instead of Leaf Area Index (LAI), which is directly interrelated to loss of water.
(iii) Crop yield is simulated as a function of the total biomass (B) and harvest index (HI)
(iv) It reflects the normalised water productivity (WP*) as conservative parameter which would be appropriate for different environmental conditions (Foster et al. 2017)

The model includes of two types of parameters: (i) parameters that do not change with time, location and management practices, referred as conservative parameters; and (ii) non-conservative parameters basically varying with time, location and management practices (Montoya et al. 2016). Besides this, AquaCrop structures its soil-crop-atmosphere continuum by including (i) the soil and its water balance components; (ii) the plant development, growth and productivity; and (iii) the atmosphere considering the temperature regime, rainfall pattern, evaporative demand, and CO_2 concentration. The crop growth development based on the model is integrated with the soil water balance that provides an efficient platform to model different agricultural practices (Steduto et al. 2009). Water use can be estimated based on four stress parameters (K_s); stomatal closure, canopy expansion, aeration stress and early canopy senescence (Mabhaudhi et al. 2014). AquaCrop also computes E_s and T_r. The basic input components for model simulation are climate variables, crop parameters, management details, and soil properties to simulate the crop yield.

The biomass is simulated based on the cumulative transpiration (T_r) and normalised water productivity (WP^*) during the crop development stage as given in Eq. 3.54.

$$B = WP^* \times \sum T_r \quad (3.54)$$

The harvestable yield (Y) is a function of Biomass (B) and Harvest Index (HI) Eq.3.55.

$$Y = B \times HI \quad (3.55)$$

In this study, AquaCrop (version 5) is used to simulate the crop yield. Input variables required for the model are explained below. The water productivity (WP, kg m^{-3}) is the relationship between crop yield and evapotranspiration and is defined as the kg of grain yield produced per m^3 of water evapotranspired.

3.8.1.1 Climate Variables

ET_o is evaluated considering precipitation, maximum and minimum temperatures by using Hargreaves method. The CO_2 concentration during the base period recorded at Mauna Loa, Hawaii, while for future scenarios CO_2 concentration can be generated directly from the AquaCrop model.

3.8.1.2 Soil parameters

Many soil characters like the number and thickness of soil profiles (m) and saturation hydraulic conductivity (Ksat) (mm/day), Curve Number, field capacity (percent volume), permanent wilting point (percent volume), bulk density (gm/cc), total accessible water (mm/m) are used for assessment root zone soil moisture in a particular region is used in the study.

3.8.1.3 Crop management details

The non-conservative parameters are purely depended upon crop phenology and can be influenced by field management practices, planting mode, soil profile etc. The identification and calibration of cultivar-specific parameters are essential for the effective model development. Some of the major critical parameters including canopy coefficients (growth and decline), maximum canopy cover (CC_x), reference harvest index (HI_o), maximum effective rooting depth, sowing to flowering period, sowing to maturity period, air temperature stress (cold and hot stress) and crop coefficient were identified during calibration process. The canopy growth coefficient (CGC) estimates the time required to attain maximum canopy, whereas the canopy decline coefficient (CDC) displays the rate of decline of green canopy in late season. Under non-stressed conditions, the HI_o is defined as the ratio of mature dry yield mass to total dry above ground biomass. The minimum and maximum temperatures when the pollination process starts to fail are known as cold stress and heat stress, respectively. Due to non-availability of the irrigation scheduling data such as frequency of irrigation net application, depth of application; the irrigation management practices, rain-fed irrigation technique was adopted for wheat, cotton and maize cultivation.

3.8.1.4 Simulation of AquaCrop model and parameter selection

AquaCrop model was calibrated by adjusting the sensitive parameters to simulate the yield. The calibration and validation periods were different for different crops for the region, as presented in Table 3.9. The datasets were divided into calibration and validation period to optimise the model parameters without getting under/over fitted. Calibration is the process

of fine-tuning non-conservative model parameters in order to enhance the agreement between observed and simulated yields. To assess the robustness of the model for different crops and to enhance the model, sensitivity analysis was performed by changing soil, crop and climatic inputs. It is based on the trial and error approach where one parameter was selected as a base parameter and the other influencing parameters were changed according to the base parameter. The same parameters are generally taken in the validation process to identify the agreement between observed and validation period yield. The procedure was repeated until a close match between observed and simulated obtained. For future prediction of yield, the parameters obtained from the calibration process are utilised throughout the future time series.

3.8.1.5 Model evaluation criteria

Various statistics are available for evaluating the model performance and to compare the simulated and observed yields from the model (Heng et al. 2009; Steduto et al. 2009). The model was evaluated using two statistical measures such as coefficient of determination (R^2) and root mean square error (RMSE) and presented in Eq. 3.56. and Eq.3.57 respectively.

$$R^2 \frac{\sum y_{sim(i)} \times y_{obs(k)} - \sum y_{sim(k)} \times \sum y_{obs(k)}}{\sqrt{\sum y_{sim(k)}^2 - (\sum y_{sim(k)}{}^2)} \times \sqrt{\sum y_{obs(k)}^2 - (\sum y_{obs(k)}{}^2)}} \quad (3.56)$$

$$RMSE = \sqrt{\frac{\sum_{I=1}^{n} (y_{sim(k)} - y_{obs(k)})^2}{n}} \times \frac{100}{\overline{Y_{obs}}} \quad (3.57)$$

where $y_{sim(k)}$ is denoted as simulated yield for k^{th} period. $y_{obs(k)}$ is denoted as observed yield for k^{th} period and Y_{obs} represented as the mean observed yield. The calibrated parameters and the efficiency of the model for the three crops for different regions are presented in the next chapter.

3.8.2 Standardized Precipitation Evapotranspiration Index (SPEI)

Due to temperature rise globally, the climate change has become more vulnerable and plays a significant element in governing the drought occurrence. SPEI was initially computed for the historical period (1951-2014) and then the parameters of the log-normal distributions were transformed to future period (2025-2099) for different scenarios to compute SPEI.

3.8.3 Crop yield data detrending and standardisation

At a regional level, the agro-databases consists of annual yields of maize, cotton and wheat in Aurangabad region of the Upper Godavari region. Considering different growing seasons, and cultivation periods, these plants are classified as kharif and Rabi crops. Compared to Rabi crops, a comparatively short period of drought impacts on the yield of kharif crops. The sowing to harvest period was May to December for cotton and April to September for maize. The shortest growing cycles were taken for wheat (October to February).

The developments in agricultural practices such as increased amount of fertiliser applications, scientific cropping pattern and crop varieties, better tillage practices, better weed management, farming tools and seeding technologies, cause an increasing trend in the yield in the command area (Potopova et al. 2015). So, the obtained crop yield data cannot be directly used to establish a drought-yield relationship. Thus, the agricultural drought hazard should be presented by the residuals of the de-trended crop yield series (Potopova et al. 2015). Generally, to remove the biases caused due to non-climatic factors, the crop series are de-trend by means of linear regression. Thus, the weather parameters only will be reflected by the residual variation in crop yield series and the residuals signify the yield under normal climatic conditions. The variabilities of yield among the three crops were quantified by considering mean and standard deviations for different series. The same log-normal distribution is fitted to yield series. Then the yield residuals were standardised based on the Z-score transformation for each crop.

The SYRS is the standardised series that considers the long-term mean and standard deviation as zero and one, respectively. According to the theory of normal distribution, the SYRS values > -0.50 or < 0.50 are satisfying the normal condition of the series. SYRS values corresponding to -0.51 to -0.99 imply low yield losses, -1.00 to -1.49 moderate, and > -1.50 high yield losses. For computation of future SYRS, the log-normal distributions are transferred to obtain the SYRS considering the observed yield series for different crops.

Furthermore, the drought can reduce yields significantly, especially in rain-fed agricultural systems. A correlation analysis was performed to assess the impact of meteorological droughts on agricultural production. i.e., calculating the Kendall's τ correlation coefficient between SPEI series at different lags and crop yield during the growing season of crops (SYRS). The correlation analysis of SPEI series at different lags for both future and historical crop yield periods were conducted in this study. It should be

noted that for the most part, the historical time period was chosen based on observed agricultural yield data, which ranges from 1997 to 2014.

3.9 Summary

This chapter presents quantitative and qualitative assessments of drought and its characteristics in Godavari River Basin (GRB) and its sub-basins. RCM models were used to obtain the future changes of drought considering SPEI. Then non-stationary drought indices (NSPI and NRDI) were developed and compared with stationary drought indices (SPI and RDI) Copula based multivariate drought indices were developed to analyse the integrated effect of different climate parameters on drought. The AquaCrop model was developed and then future changes of maize, cotton and wheat were obtained based on CMIP6-GCMs. Based on the performance of these models, if found to be satisfactory, they can be used for generating and simulating the crop yield. Crop-drought relationship was obtained by considering SPEI and SYRS with changing climate scenario.

CHAPTER 4

RESULTS AND DISCUSSIONS

4.1 General

Methodology to meet the objectives of the study described in Chapter-3 is applied to the study area. The results pertaining to various objectives of the study are described in this chapter. As already discussed earlier, the first three objectives are applied to entire study area and for remaining two objectives part of study area is taken up. Results are presented in forms of graphs, box plots and tables followed by a thorough discussion.

4.2 Spatio-temporal Variation and Future Risk Assessment Using SPEI

CRU TS 4.03 TS precipitation, maximum and minimum temperature data were downloaded, and potential evapotranspiration was estimated using the Hargreaves method. SPEI for the GRB was used to conduct a comprehensive evaluation of historical and future droughts, incorporating potential associations of drought characteristics. Drought was assessed historically using SPEI, which considers multiple meteorological variables such as precipitation and evapotranspiration. The weighted average of the five RCMs, such as ACCESS 1-0, GFDL-ESM2G, MPI-ESM-LR, CCSM4 and CNRM-CM5 under RCPs 4.5 and 8.5 was calculated using the REA method. The K-means clustering algorithm was used to identify drought homogeneous regions. The M-K test approach was used to obtain the trend associated with drought characteristics for both historical and future periods. Copula functions were also used to estimate multivariate drought return periods. Changes in drought characteristics in the future periods were assessed using RCMs under RCP4.5 and RCP8.5 scenarios to gain a better understanding of the impact of future climatic variability on drought characteristics.

4.2.1 Performances of RCM models and uncertainty analysis

For future drought analysis, five linearly bias corrected RCMs were considered. Although RCMs are widely used for the assessment of extreme events with respect to climate change, there are uncertainties associated with the RCM simulated variables. The sources of uncertainty in climate models are associated with (i) their spatial and temporal scale, (ii) anthropogenic activities and GHG emissions under different scenarios.

The individual model and ensemble mean quantile plots for precipitation, maximum and minimum temperature are presented with in Fig. 4.1. Ensemble models were used to model the extreme and low precipitation events. For RCP4.5, the precipitation obtained from the ensemble mean performed well when compared to RCM models. The ensemble model for RCP8.5 scenario showed satisfactory performance for the precipitation series while high uncertainties were exhibited RCP4.5 scenario. Comparison of simulated and observed precipitation showed that models like CNRM-CM5 showed poor performance for RCP4.5 while ACCESS 1-0 showed poor performance for RCP8.5. From Fig. 4.1, it can be seen that the ensemble maximum and minimum temperature showed better performance under both the scenarios. For maximum temperature, the models that performed poorly are CNRM-CM5 and CCSM4 under RCP4.5. ACCESS 1-0 and GFDL-ESM-2G showed poor performance under RCP8.5 scenarios. The bias corrected RCMs were individually under/over estimating the climate parameters. Hence consideration of isolated models may increase the uncertainty in modelling the drought phenomenon. The REA approach provides a remedy to this problem by accounting for uncertainty caused by RCMs.

4.2.2 Spatial variation of reference and future climate parameters

Spatial maps are presented in this section for better understanding of variability experienced due to annual precipitation, dry days, and fluctuations in minimum and maximum temperature. The spatial distribution of mean annual precipitation is presented in Fig.4.2. The MPI-ESM-LR and ensemble model under RCP4.5 captured the extreme annual precipitation. Similarly, for RCP8.5, ACCESS1-0, MPI-ESM and ensemble model captured the extreme annual precipitation in the north-east part of the GRB. Further, for the mean annual precipitation, the ensemble model gave the uncertainty in each grid cell. The future time period, 2053 to 2099, showed a decrease in precipitation in western part of the GRB and an increase in the lower reaches of the basin. Significant variations in annual precipitation were more pronounced under RCP8.5. From Fig. 4.3, except CCSM4, the maximum temperature hot spots can be identified in the middle part of the basin for the various climate models. The average annual minimum temperature has a significant increasing trend in RCP8.5. The minimum temperature hot spots showed prominent increase in RCP8.5 (Fig. 4.4). The intensification in projected maximum and minimum temperature will cause increase in evapotranspiration. Nevertheless, increase in evapotranspiration, variation in precipitation and the increase in the dry spells for future

time period will further accelerate the drought phenomenon in the GRB due to global warming.

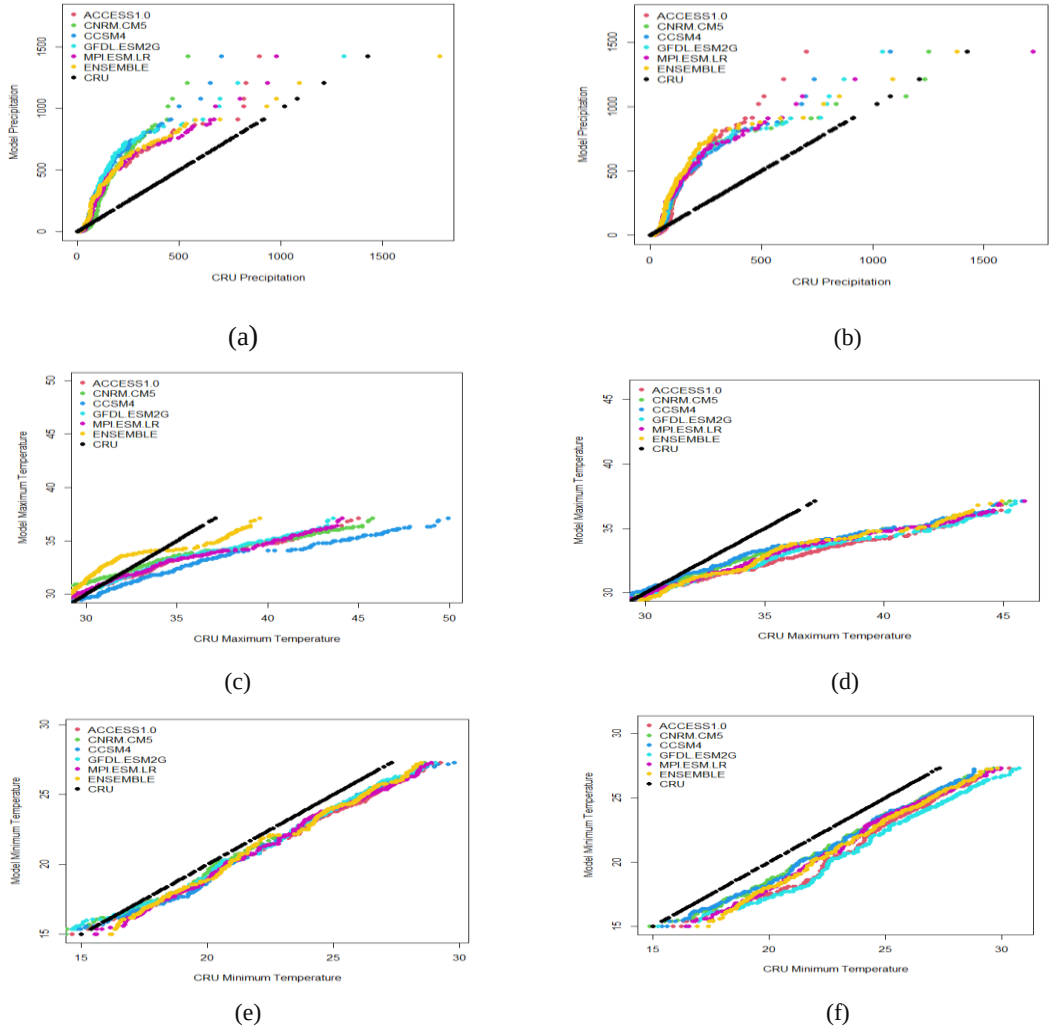

Fig 4.1 Quantile-Quantile plots for comparison of precipitation for (a) RCP4.5; (b) RCP8.5; Comparison of maximum temperature for (c) RCP4.5; (d) RCP8.5; Comparison of minimum temperature for (e) RCP4.5; (f) RCP8.5.

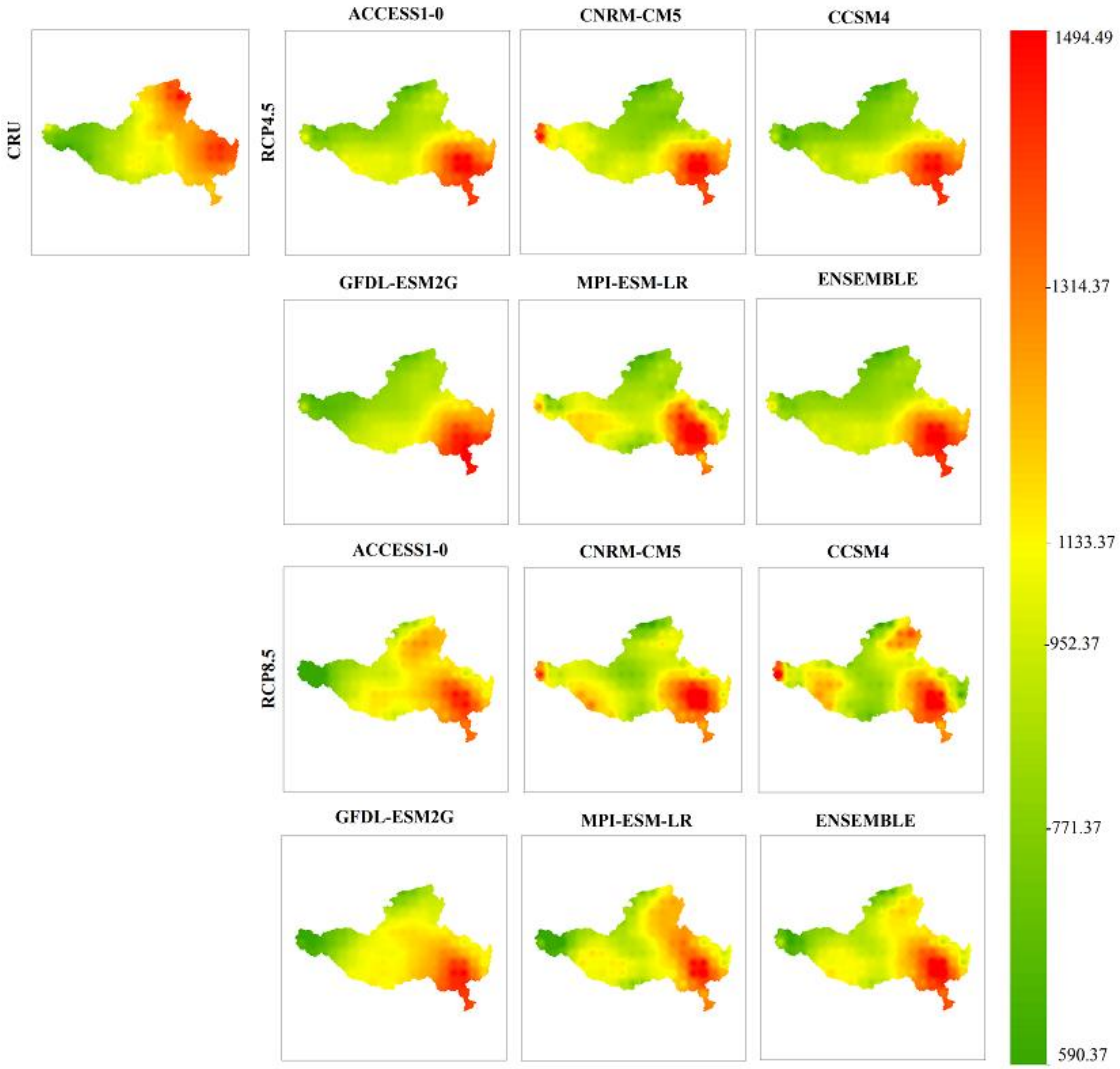

Fig. 4.2 Spatial variation of annual mean precipitation for reference period (1971-2017) and future time period (2053-2099)

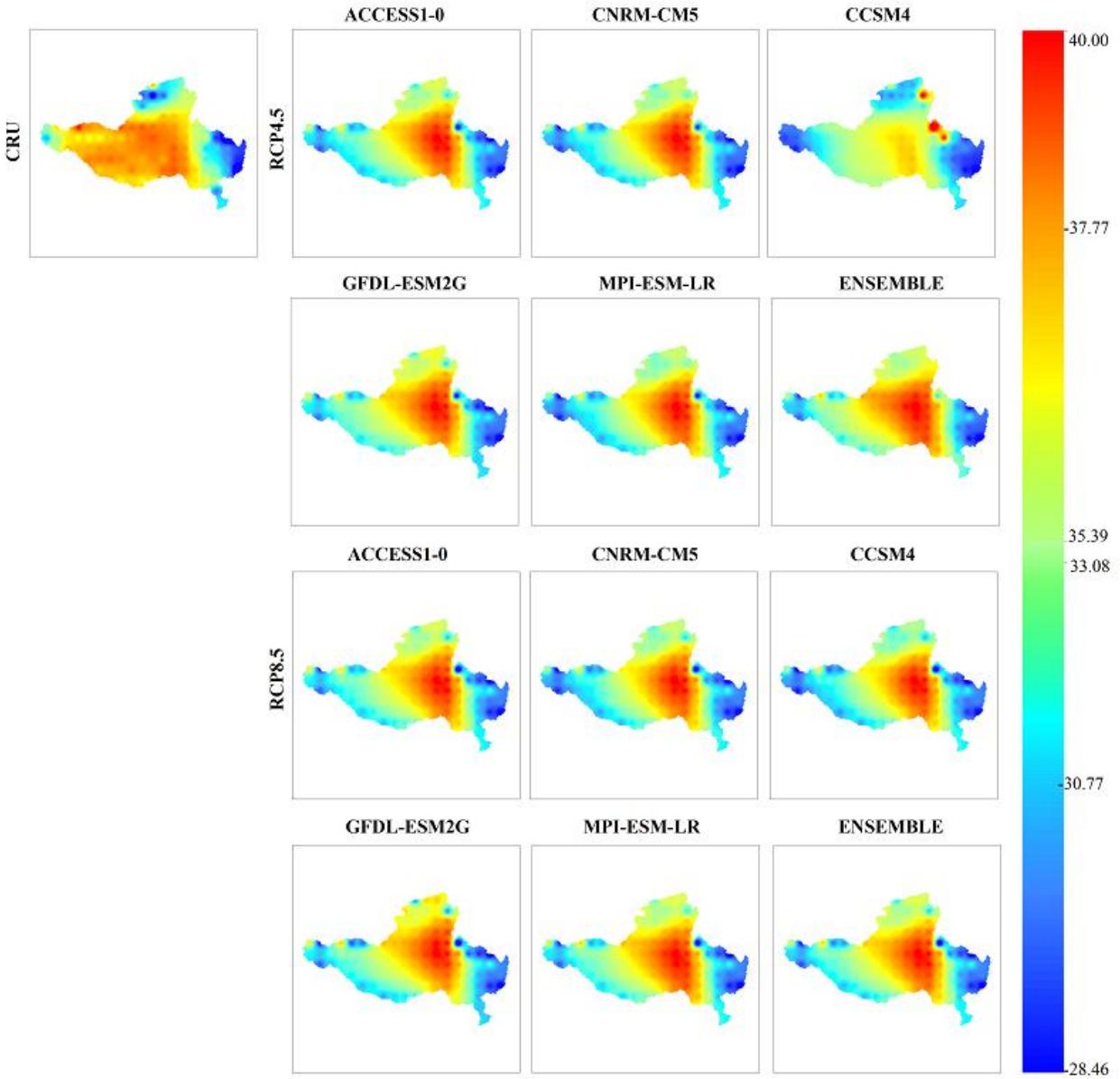

Fig. 4.3 Spatial variation of annual mean maximum temperature for reference period (1971-2017) future time period (2053-2099)

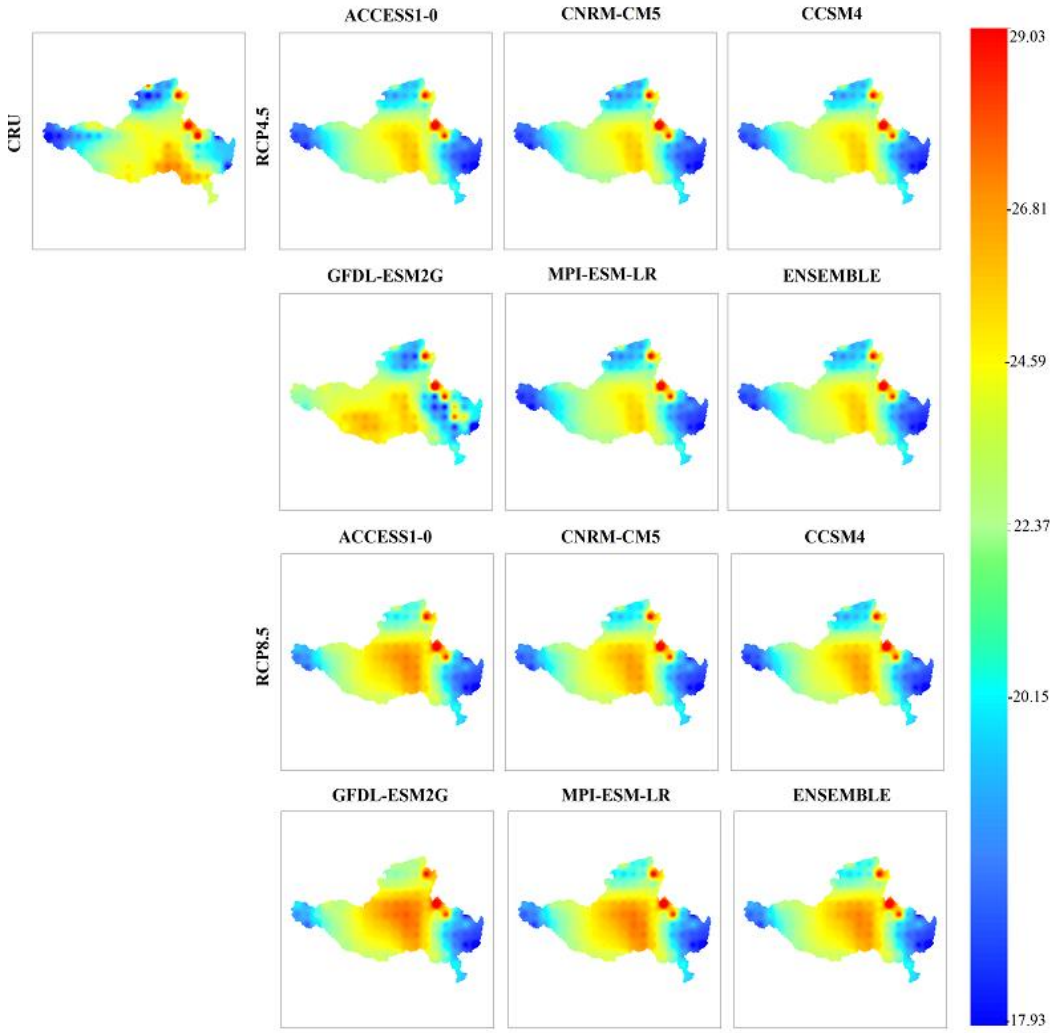

Fig. 4.4 Spatial variation of annual mean minimum temperature for reference period (1971-2017) and the future time period (2053-2099)

4.2.3 Identification of homogeneous drought regions

All the meteorological stations located in various climatological regions of GRB were used in this study. Some of these stations have been facing extremely vulnerable drought conditions in each season because of significant variability of rainfall among seasons. There were also variations in climatic variables based on their topographic existence. K-means clustering was used to identify the homogeneous drought regions. The division of total study area into homogeneous climate divisions (clusters) was advantageous in reducing the unwanted noise resulting from the grid-wise frequency analysis (Masud et al. 2017). For each cluster, the nearest data point to the respective cluster head was chosen to represent the data point to obtain the results. The cluster validation indices based on K-means techniques for the historical period are given in Table 4.1. From Table 4.1, the

number of clusters equal to 6 captured homogenous areas better in comparison to other cluster numbers as the values of Silhouette Coefficient (SC) and Dunn Index (DI) are higher compared to other cluster numbers. From Fig. 4.5, the number of grids in each climate division were as follows: a total of 21 grids in climate division I, 5 grids in climate division II, 4 grids in climate division III, 25 grids in climate division IV, 29 grids in climate division V, and 22 grids in climate division VI. The homogeneous regions using the drought features provide a clear foundation for further analyses of the drought events.

Table 4.1 Validation of clustering models based on reference dataset

	Number of clusters							
Validity index	3	4	5	6	7	8	9	10
DI	2.85	3.08	4.52	8.1	0	0.15	3.11	0.29
SC	0.377	0.454	0.33	0.511	-0.214	0.389	0.211	0.178

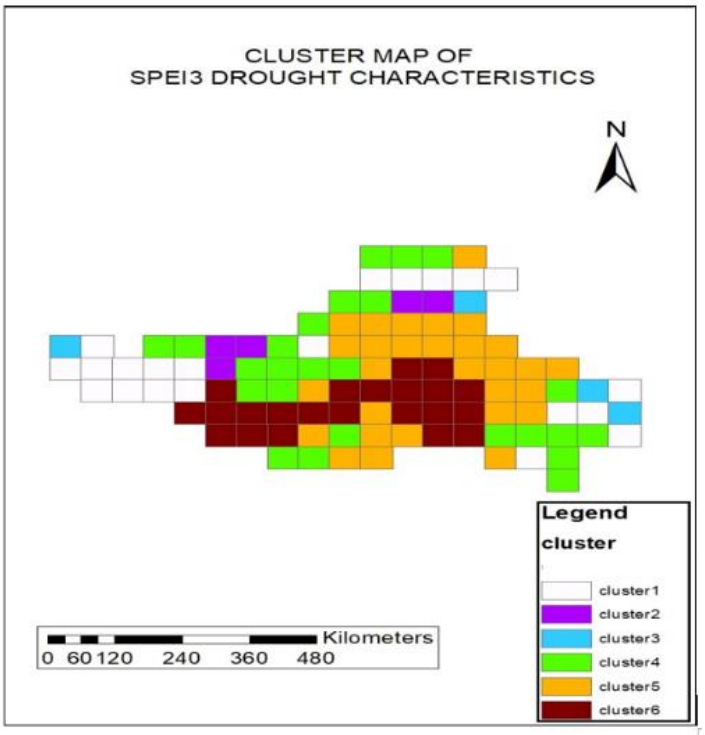

Fig. 4.5 Cluster Map of SPEI-3 drought characteristics

4.2.4 Comparison between historical and future droughts

Water resources are sensitive to droughts and the demand for water is mostly met by amount of precipitation. The prolonged droughts associated with increase in water demand under climate change will lead to further stress on water shortage. Pathak and Dodamani, (2019) stated that the 3-month time scales have shorter duration and creates a greater number of drought events, On the other hand, the 12-month time scale indicates

less drought events with higher durations. This study considered SPEI-3 for estimating the meteorological drought events. The drought characteristics for each grid cell were extracted using the observed and future SPEI series based on Run theory approach for return period analysis.

Drought events are directly related to high temperature and evapotranspiration. The study was carried out to determine how precipitation and evapotranspiration affect the future SPEI in the six climate divisions. The temporal changes of SPEI are presented in Fig. 4.6. Significant differences exist in signals between the SPEI time series generated using RCM outputs and the observed climatic data for all the six climate divisions. Higher peaks in signals were detected in RCP8.5 when compared with RCP4.5 and the reference period. The number of dry months were significant in case of RCP8.5 and RCP4.5. SPEI for RCP8.5 and RCP4.5 captured an early onset of drought. The projected SPEI signals exhibited more severe and persistence drought events. Due to increase in CO_2 and greenhouse gas concentration in future, the temperature and precipitation exhibit high fluctuations which have great influence on the behaviour of drought indices. SPEI time series of projected periods and reference periods differ from each other for different climate divisions showing an intensification of dry spells for future periods

In this section, projected changes of drought characteristics are evaluated based on the differences between the drought characteristics in future period and reference period. The projected characteristics are presented by means of density plots and box plots for different climate divisions and shown in Fig. 4.7 to Fig. 4.12. Significant changes in the density of drought characteristics were noticed between historical, RCP4.5 and RCP8.5 for different climate divisions. For climate divisions I, III, V and VI, higher densities were observed during the reference period compared to the future scenarios, whereas the magnitude of projected drought duration for RCP8.5 displayed higher density for climate division IV. RCP4.5 showed higher densities in projected drought duration for climate division II. Prominent deviations were also observed in the historical and future peak densities (Fig 4.7) for different climate divisions. The higher peak densities are observed for RCP 8.5 in case of climate division I and IV (Fig 4. 8). It was observed from the figures that RCP4.5 series showed higher peak densities for climate division II. In the case of climate division III and V, the reference time series showed high densities in peak. The density plots for severities for all climate divisions revealed the change in the probability densities for historical and future scenarios (Fig. 4.9). Larger differences in the projected

drought severities were observed for all the time periods in the climate divisions. Higher densities in case of severities were observed for climate division I, III, V and VI during the reference period (1971-2017), whereas, RCP8.5 and RCP4.5 showed higher densities for climate division IV and climate division II respectively. Hengade et al. (2018) stated that spatial and temporal variation of rainfall were observed in GRB under climate change scenarios whereas the evapotranspiration of the basin showed a huge increment due to increasing temperature in most part of the basin. It was also observed that there were huge variations in the climatic phenomenon of GRB under RCP8.5 than in RCP4.5. So, the evapotranspiration can intensify the drought phenomenon when the temperature is more for this river basin. Deficit precipitation and more evapotranspiration in future can impact the future drought phenomenon.

The variations in the drought characteristics were identified using box plots shown in Fig 4.10, Fig. 4.11 and Fig. 4.12 for six climate divisions. The historical and RCM-simulated weightage averaged drought durations were shown in Fig 4.10. Relative variances were observed between historical and future duration for different climate divisions. The climate divisions II and III showed higher durations in case of reference period, whereas for RCP4.5, the climate divisions I, IV, V and VI showed higher drought durations. Significant variations were also identified in the drought severity and peak between historical and future periods for the different climate divisions. High peaks were noticed in case of future periods. RCP4.5 displayed high peaks in climate divisions I, IV and VI whereas the RCP8.5 exhibited higher peaks in the other climate divisions II, III and V. The climate division II showed severe drought in case of historical period. RCMs tend to produce relatively more severe droughts when compared to historical drought. The drought severities showed high values in case of climate divisions VI for RCP4.5. Similarly, RCP 8.5 shows high values for climate divisions I, II, IV and V. Hence, it can be concluded that the changes in severities are more prominent in case of RCP4.5 and RCP8.5.

Deficient rainfall caused extreme drought condition in the GRB (Masroor et al. 2020). During the summer season, temperatures increased which can accelerate the drought condition. From spatial observation from Fig. (4.2) to Fig. (4.4), RCMs under RCP 4.5 and RCP 8.5 projected a change in drought pattern during 2053-2099 as there would be an increase in dry spells in GRB. The drought severity, peak and duration would increase in the future due to the effect of climate change for most of the climate divisions. So future

drought analysis will be helpful for water managers to understand the drought behaviour considering the variable climatic phenomenon.

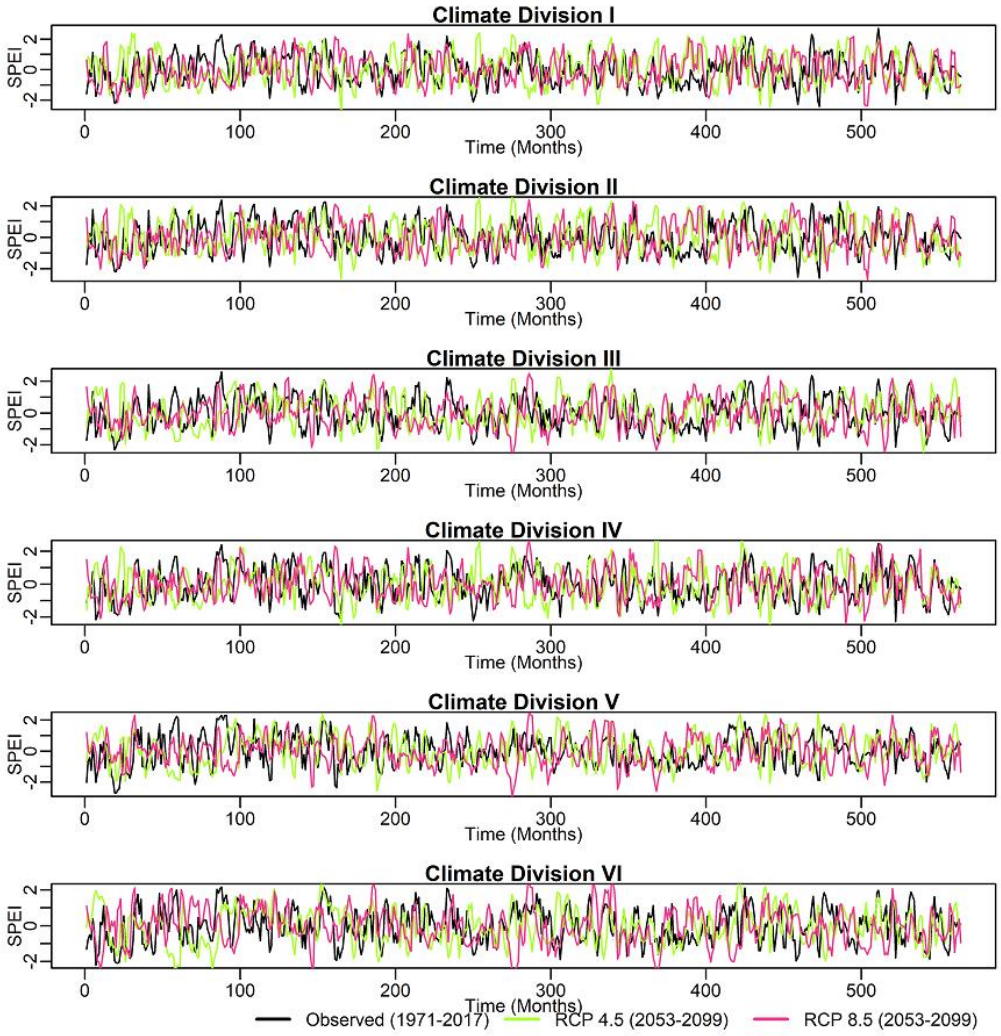

Fig 4.6 Comparison of SPEI time series for historical period (1971-2017) and future time period (2053-2099) under RCP4.5 and RCP 8.5

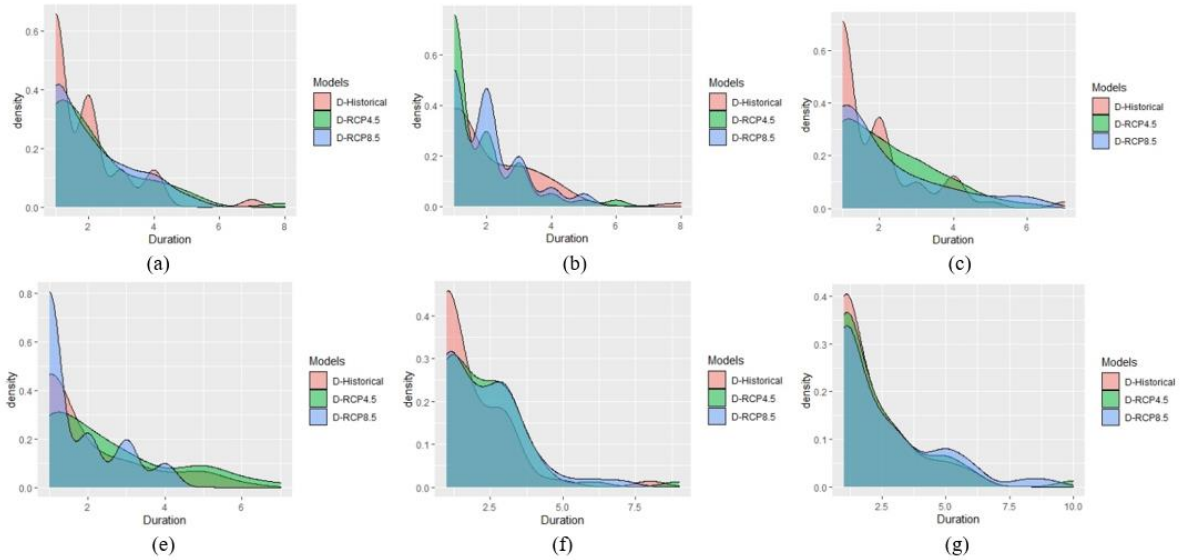

Fig. 4.7 Comparison of Probability Density of duration for historical period (1971-2017) and future time period (2053-2099) under RCP4.5 and RCP 8.5 for climate division, (a) I; (b) II; and (c) III; (d) IV; (e) V; (f) VI.

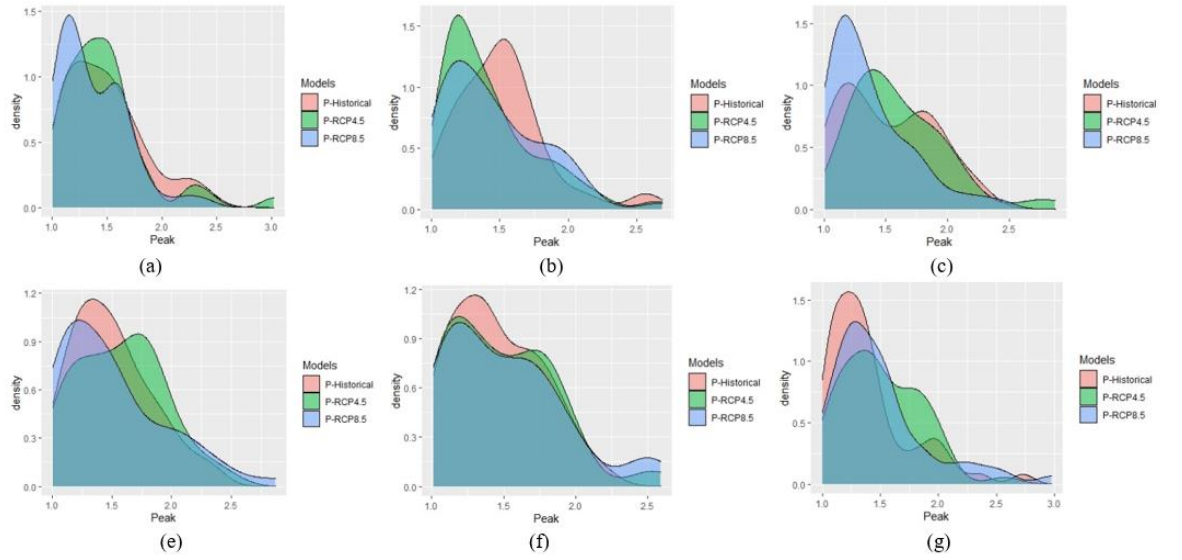

Fig. 4.8 Comparison of Probability Density of peak for historical period (1971-2017) and future time period (2053-2099) under RCP4.5 and RCP 8.5 for climate division, (a) I; (b) II; and (c) III; (d) IV; (e) V; (f) VI.

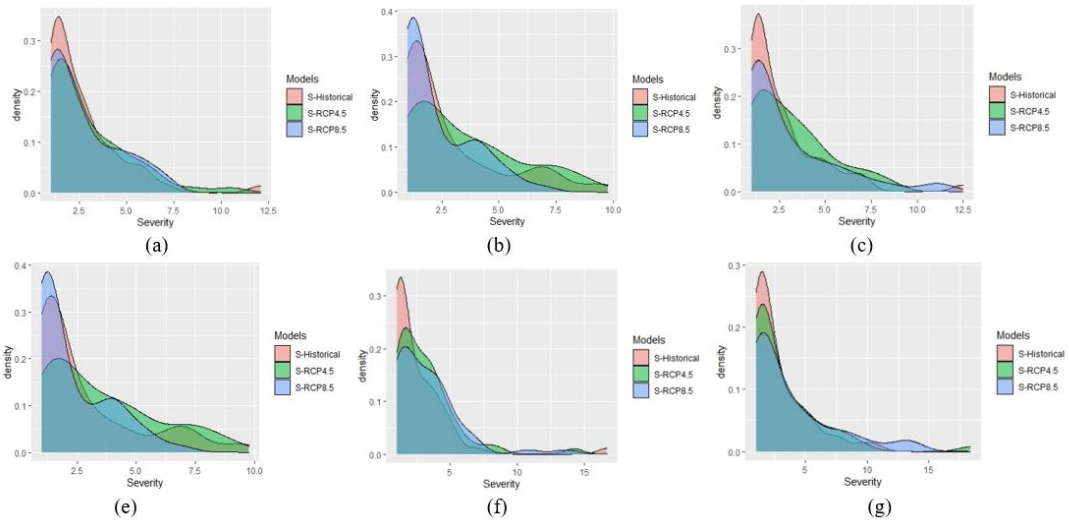

Fig.4.9 Comparison of Probability Density of severity for historical period (1971-2017) and future time period (2053-2099) under RCP4.5 and RCP 8.5 for climate division, (a) I; (b) II; and (c) III; (d) IV; (e) V; (f) VI.

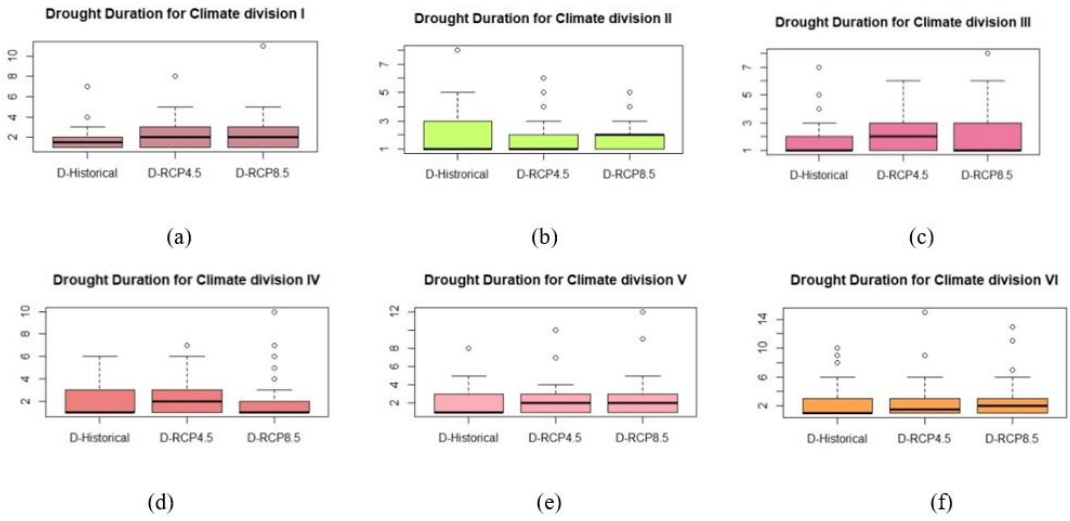

Fig. 4.10 Comparison of drought duration using box plots for historical period (1971-2017) and future time period (2053-2099) under RCP4.5 and RCP 8.5 for climate division, (a) I; (b) II; and (c) III; (d) IV; (e) V; (f) VI

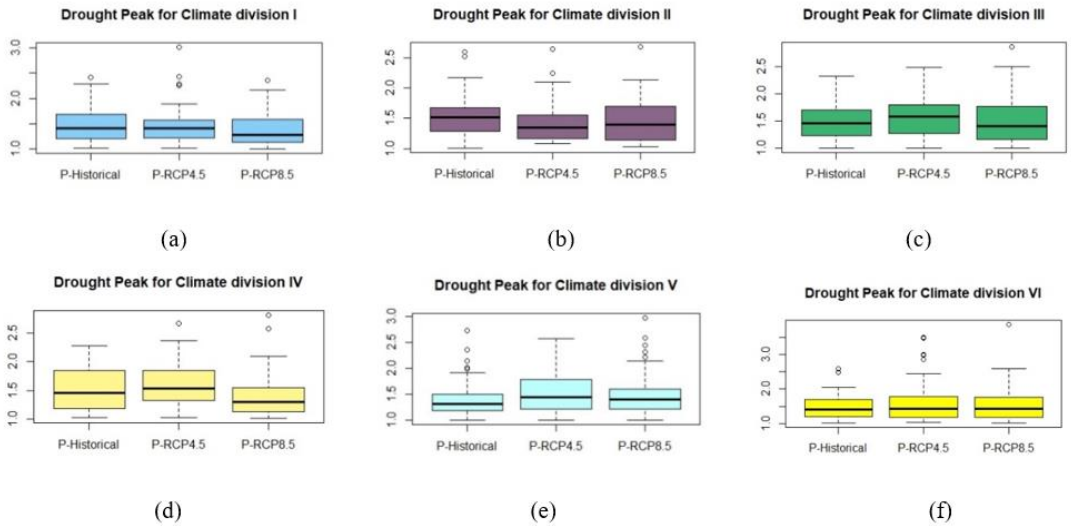

Fig. 4.11 Comparison of drought peak using box plots for historical period (1971-2017) and future time period (2053-2099) under RCP4.5 and RCP 8.5 for climate division, (a) I; (b) II; and (c) III; (d) IV; (e) V; (f) VI

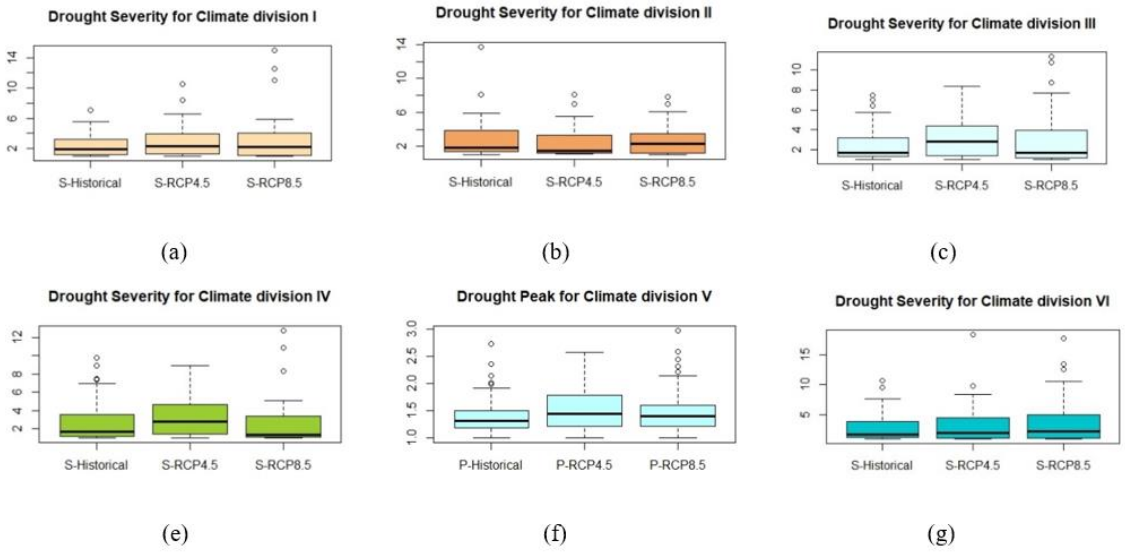

Fig.4.12 Comparison of drought severity using box plots for historical period (1971-2017) and future time period (2053-2099) under RCP4.5 and RCP 8.5 for climate division, (a) I; (b) II; and (c) III; (d) IV; (e) V; (f) VI

4.2.5 Mann Kendall Test of drought characteristics

Mann Kendall (MK) test and Sen's slope estimator were used for trend analysis for the six climate divisions. For determining the upward or downward trend of drought characteristics, the parameters of the MK test such as Kendall's τ, S, and Z statistics were calculated at 95% confidence level. Tables 4.2, 4.3 and 4.4 show the trend of drought

duration, peak and severity for historical and future periods for various climate divisions. Increasing trends in duration were observed in the case of climate divisions I, II and VI for reference periods whereas the decreasing trends were observed in the case of climate divisions III, IV and V. However, decreasing trends detected for duration were not significant for the reference period. The results of the MK test for future periods under two scenarios showed significant positive trends for durations in four climate division (I, II and IV and VI) for RCP4.5 and four climate division (III, IV, V and VI) for RCP8.5. Further, negative trends were observed for future periods for climate division III and V for RCP4.5, and climate division I and II for RCP8.5. The MK test for peak revealed positive trends in climate division I, III, VI and VI while negative trends were detected in climate divisions II and V for the reference period. Significant increasing trends in peaks were observed throughout the future period in the case of climate divisions I, II, III, IV, and VI and climate divisions II, III, VI, V and VI under RCP4.5 and RCP8.5 respectively. Downward trends were noticed in the case of climate division V for RCP4.5 and climate division I for RCP8.5. For reference period, the climate divisions I, II, III, IV, and VI showed positive Z values for the severity, indicating increasing trends. Negative Z value of climate division V indicate decreasing trends. The climate divisions IV and VI showed significant positive trends whereas the negative trends are no longer significant for reference period. Positive Z values were observed for the climate divisions II, II, IV and V for RCP4.5. Similarly, positive Z values indicate increasing trend in II, III, IV, V and VI for RCP8.5. Decreasing trends in drought severities were also observed in climate divisions I and III for RCP4.5 and climate division I for RCP8.5.

Table 4.2 Mann-Kendall test statistics of drought duration for historical and future periods

	Climate division I			**Climate division II**			**Climate division III**			**Climate division IV**			**Climate division V**			**Climate division VI**		
	His	**RCP4.5**	**RCP8.5**	**His**	**RCP4.5**	**RCP8.5**	**His**	**RCP4.5**	**RCP8.5**	**His**	**RCP4.5**	**RCP8.5**	**His**	**RCP4.5**	**RCP8.5**	**His**	**RCP4.5**	**RCP8.5**
τ	0.282	0.368	-0.15	0.218	0.403	-0.08	-0.047	-0.053	0.51	-0.083	0.31	0.584	-0.029	-0.042	0.29	0.12	0.13	0.24
Z	2.13	2.77	-1.75	1.98	2.84	-0.93	-0.56	-0.6	2.3	-0.99	2.29	3.043	-0.35	-0.48	2.25	1.45	1.56	1.98
Sen	0	0	0	0	0	0	0	0	0	0	0	0	0	0	0	0	0	0

Table 4.3 Mann-Kendall test statistics of drought peak for historical and future periods

	Climate division I			**Climate division II**			**Climate division III**			**Climate division IV**			**Climate division V**			**Climate division VI**		
	His	RCP4.5	RCP8.5	His	RCP4.5	RCP8.5	His	RCP4.5	RCP8.5	His	RCP4.5	RCP8.5	His	RCP4.5	RCP8.5	His	RCP4.5	RCP8.5
τ	0.09	0.03	-0.10	-0.02	0.17	0.05	0.11	0.09	0.27	0.25	0.13	0.16	-0.03	-0.07	0.07	0.08	0.17	0.21
Z	1.00	0.30	-1.08	-0.15	1.98	1.51	1.25	2.21	2.97	2.73	1.44	2.72	-0.30	-0.71	2.76	0.82	2.10	2.92
Sen	0.05	0.01	-0.02	0.00	0.05	0.04	0.05	0.04	0.16	0.09	0.06	0.12	-0.01	-0.03	0.02	0.03	0.15	0.14

Table 4.4 Mann-Kendall Test statistics of drought severity for historical and future periods

	Climate division I			Climate division II			Climate division III			Climate division IV			Climate division V			Climate division VI		
	His	RCP4.5	RCP8.5	His	RCP4.5	RCP8.5	His	RCP4.5	RCP8.5	His	RCP4.5	RCP8.5	His	RCP4.5	RCP8.5	His	RCP4.5	RCP8.5
τ	0.11	-0.05	-0.15	0.02	0.23	0.11	0.07	-0.02	0.19	0.12	0.14	0.23	-0.02	-0.06	0.03	0.20	0.22	0.27
Z	1.19	-0.53	-1.56	0.20	2.50	1.18	0.76	-0.21	2.12	1.20	1.58	2.47	-0.18	-0.63	0.27	2.19	2.11	2.88
Sen	0.11	-0.05	-0.09	0.02	0.02	0.06	0.06	-0.03	0.20	0.08	0.11	0.22	-0.01	-0.09	0.02	0.19	0.17	0.29

4.2.6 Trivariate copula models

Exponential and Gamma distributions have been used in many drought characterization studies to obtain the marginal distributions of drought properties (She et al. 2018). Gumbel, Gamma, Log-normal, Weibull and Exponential distributions were fitted to drought characteristics for evaluating the marginal distributions. Different statistical measures like AIC and log-likelihood functions were used for obtaining the best fitted distribution. The variations in drought characteristics could significantly affect the future drought phenomenon. Hence, trivariate copula analyses were implemented for reference and future periods by combining the dependency of drought characteristics to obtain copula parameter. The copula models namely Clayton, Gumbel and Frank were selected for modelling the trivariate drought characteristics. The copula parameters were estimated using MPL estimation method. CVM and KS were used for testing the goodness of fit for comparing the performance of different copula models based on their dependency between drought characteristics. The maximum p-values of statistics CVM and KS for 5000 sample runs, copula parameters and corresponding log likelihood function values and the best fitted copulas for a 3-month duration for six climate divisions are given in Tables 4.5, 4.6 and 4.7 for reference and future time periods. From the Tables, the drought characterization can be conducted using Frank Clayton, and Gumbel copulas that are verified at 5% significance level. Copula with the highest p-value was selected to find the dependence structure among drought characteristics. Overall, Frank and Gumbel copulas performed well when compared to other copulas. The best fitted parameters were used further to compute the joint return period

Table 4.5 Maximum likelihood, AIC values and p-values for using trivariate copula analysis based on drought characteristics for historical period.

	Climate division I	Climate division II	Climate division III	Climate division IV	Climate division V	Climate division VI
Copula selected	Frank	Gumbel	Gumbel	Frank	Frank	Gumbel
parameters	7.875	2.271	2.533	8.635	9.297	3.116
Maximum Likelihood	50.19	45.52	62.17	60.87	62.77	72.69
AIC	-98.3735	-89.05	-122.335	-119.745	-123.543	-143.379
KS	0.778	0.79	0.685	0.913	0.672	0.83
CVM	0.644	0.587	0.817	0.667	0.541	0.701

Table 4.6 Maximum likelihood, AIC values and p-values for the GoF tests using trivariate copula analysis based on drought characteristics future period under RCP4.5

	Climate division I	Climate division II	Climate division III	Climate division IV	Climate division V	Climate division VI
Copula selected	Clayton	Frank	Clayton	Frank	Frank	Gumbel
parameter	2.17	7.234	2.355	7.456	7.521	2.285
Max likelihood	79.09	93.24	74.3	86.52	85.21	76.54
AIC	-156.18	-184.49	-146.59	-171.04	-168.43	-151.08
KS	0.556	0.754	0.882	0.626	0.951	0.844
CVM	0.47	0.689	0.625	0.511	0.733	0.787

Table 4.7 Maximum likelihood, AIC values and p-values for the GoF using trivariate copula analysis based on drought characteristics future period under RCP8.5

	Climate division I	Climate division II	Climate division III	Climate division IV	Climate division V	Climate division VI
Copula selected	Frank	Frank	Gumbel	Frank	Frank	Frank
parameters	8.144	6.836	2.519	8.703	8.253	9.882
Max likelihood	101.4	84.67	104.5	113.5	87.03	93.04
AIC	-200.747	-167.341	-206.988	-224.979	-172.053	-184.083
KS	0.549	0.812	0.766	0.833	0.597	0.662
CVM	0.55	0.645	0.589	0.818	0.552	0.715

4.2.7 Drought risks assessment

The trivariate return levels for different return periods using the 'AND' and 'OR' criteria are presented in Tables 4.8 and 4.9 respectively. It can be seen from the Tables, that large uncertainties were present in future return periods for different climate divisions and the uncertainties will increase with the variation in return periods. This uncertainties of trivariate return period are because of the future variations in projected climatic parameters based on the increment in GHG and CO_2 under the two RCP scenarios. Comparable differences in the return periods between reference and future were also observed. It can be seen from the Tables that the joint return period of 'AND' case is more than the 'OR' case. The return period was less in climate division II compared to other climate divisions for reference period. It can, hence, be concluded that the climate division II showed more frequent drought events. Similarly, the drought events were more frequent

in climate divisions I, III, IV and V under RCP8.5 whereas climate division VI showed more frequent drought under RCP4.5 scenario for the period 2053-2099. The climate division VI will be more vulnerable with the increase in number of dry days and changing future climate condition. Overall, the return period analysis revealed that for a certain drought event, future drought return periods are expected to be lower than the reference period specifying the probable increase in drought occurrences than those detected in the past periods. Under the two RCP scenarios, the frequency of dry periods will increase during 2053-2099. This indicates that more severe and long-lasting droughts can be anticipated in the future in the GRB. Overall, the frequency, duration, severity, and peak of droughts will increase in the future. The trivariate copula analysis can be beneficial for a better management and planning of the water resources considering the extreme events.

Table 4.8 T^{AND} for drought characteristics of SPEI computed based on trivariate copula models

Reference Return Period (T)	Climate division I T^{AND}	Climate division II T^{AND}	Climate division III T^{AND}	Climate division IV T^{AND}	Climate division V T^{AND}	Climate division VI T^{AND}
5	18.01	10.7	15.66	12.91	10.88	8.15
10	41.33	17.63	37.14	23.54	27.41	14.21
20	86.63	36.97	61.28	53.14	81.12	51.11
50	454.32	184.13	334.72	310.57	213.54	198.53
RCP4.5 Return Period (T)	Climate division I T^{AND}	Climate division II T^{AND}	Climate division III T^{AND}	Climate division IV T^{AND}	Climate division V T^{AND}	Climate division VI T^{AND}
5	9.98	11.35	10.8	9.78	6.61	5.6
10	17.15	20.48	18.07	14.65	15.35	12.31
20	45.46	37.31	32.33	29.38	28.91	21.84
50	86.52	191.28	164.05	89.05	84.66	84.13
RCP8.5 Return Period (T)	Climate division I T^{AND}	Climate division II T^{AND}	Climate division III T^{AND}	Climate division IV T^{AND}	Climate division V T^{AND}	Climate division VI T^{AND}
5	8.15	14.14	8.96	8.67	6.2	7.11
10	15.19	31.03	13.46	12.51	14.26	17.82
20	37.68	78.85	31.34	26.35	24.15	39.11
50	79.69	302.37	125.57	72.13	77.31	96.42

Table 4.9 T^{OR} return periods for drought characteristics of SPEI computed based on trivariate copula models

Reference Return Period (T)	Climate division I T^{OR}	Climate division II T^{OR}	Climate division III T^{OR}	Climate division IV T^{OR}	Climate division V T^{OR}	Climate division VI T^{OR}
5	3.99	3.04	4.79	4.03	4.79	3.14
10	7.54	5.96	8.51	651	6.51	5.08
20	15.87	12.08	16.89	20.33	13.89	15.99
50	35.41	24.33	41.22	45.4	35.22	38.77
RCP4.5 Return Period (T)	Climate division I T^{OR}	Climate division II T^{OR}	Climate division III T^{OR}	Climate division IV T^{OR}	Climate division V T^{OR}	Climate division VI T^{OR}
5	3.02	3.2	3.51	5.88	4.27	2.39
10	6.56	6.77	6.86	9.47	9.33	5.04
20	11.38	13.54	15.09	18.12	18.25	10.52
50	25.6	29.91	33.83	39..66	34.12	23.78
RCP8.5 Return Period (T)	Climate division I T^{OR}	Climate division II T^{OR}	Climate division III T^{OR}	Climate division IV T^{OR}	Climate division V T^{OR}	Climate division VI T^{OR}
5	2.91	4.01	3.12	3.25	2.84	3.13
10	6.16	7.87	5.1	8.49	6.14	5.82
20	13.08	15.04	14.15	16.07	12.65	12.04
50	28.17	31.44	26.83	43.91	29.16	25.47

4.2.8 Conclusion

In this study, 3-month SPEI was derived by using the precipitation and the evapotranspiration data for the reference and future periods in the GRB. The bias adjusted RCMs individually showed large uncertainties in climate parameters. Hence, the REA method was implemented to reduce the uncertainties caused by individual RCMs. A comprehensive assessment of drought frequency was carried out using trivariate regional frequency analysis considering the inherent dependence between the drought characteristics. The main conclusions for objectives are as follows:

The temporal distribution of projected drought characteristics showed an increase in drought duration peak, and severity in future periods under the two RCPs in different climate divisions. The mean duration, severity, and peak for climate division V and VI showed increasing pattern having a longer duration, higher severity and peak than the other climate divisions.

Statistical homogeneity of the six climate divisions was tested by validation indices. SI and DI which identified most of the regions as homogenous.

Based on the drought characteristics, the non-parametric MK test was applied to assess the variability and pattern of drought characteristics. Most of the climate divisions

showed significant changes in trend of drought characteristics for future time period for two RCPs. The increase in drought events can be directly linked to increasing trend in the area.

The trivariate copula analysis showed that Gumbel and Frank copula performed well for most of the climate divisions using CVM and KS tests. After analyzing the trivariate return period for T^{AND} and T^{OR} cases, climate division V showed longer and severe drought events in comparison with other divisions. Further, frequent drought events were observed in case of climate divisions II, V and VI.

The return periods in future for different scenarios showed lower values of return periods than what are observed in the past for climate division VI in case of RCP 4.5, indicating more frequent drought events in the future periods. The risk of future droughts will become intensified with the changes of precipitation and evapotranspiration that are considered using SPEI-based drought index. It can be suggested that appropriate water resource planning and management activities should be implemented for climate divisions II, V and VI by considering the long-lasting behaviour and high severity characteristics of the drought events

On regional scale, the derived conclusions will be helpful for a precise and systematic understanding for managing the drought phenomenon. The identification the drought-prone areas will be useful for water managers for the planning and management of drought mitigation strategies. For a better management of drought, return period analysis is carried out for reference and future periods.

4.3 Assessment of Non-stationary Reconnaissance Drought Index (NRDI) and Non-stationary Standardized Precipitation Index (NSPI)

Daily precipitation datasets of resolution 0.25x0.25 were obtained for the period from 1950 to 2017 from the IMD website to develop non-stationary drought indices. Then precipitation data were converted to monthly scale for the GRB over 68 years (1950-2017). The NRDI requires both precipitation and evapotranspiration data to estimate the meteorological drought. Hence, the monthly 0.5x0.5 resolution evapotranspiration data were downloaded from the CRU 4.03TS data sites for the same period. The data were then extracted and regridded to the IMD grids. 3-, 6- and 12-month moving average were computed for cumulative precipitation and evapotranspiration. Further, aggregated global scale monthly climate indices were calculated aggregated based on 3-, 6- and 12- month

moving average. Then the lag value from 0 to 12 are computed for each of the four large scale climate indices. The non-stationary drought indices were developed and then compared to the stationary drought indices. The trivariate drought characterization were conducted based on copula analysis. Further, PCC model was also used for assessment of trivariate drought characteristics.

4.3.1 Non-stationary SPI and RDI indices

For demonstration of results, two sub-basins were selected i.e. Upper Godavari River Basin (UGRB) and Lower Godavari River Basin (LGRB). The basis for this study to incorporate large-scale climate indices that affect global climatology by variations of the phenomenon over the Pacific and Indian oceans (Rashid and Beecham, 2019). The large-scale climate indices are considered as external covariates for evaluating the NSPI and NRDI. For the LGRB and URGB, the monthly aggregation of precipitation and evapotranspiration data were prepared. In addition, the moving average of climate indices were obtained and then organized into 13 different lag values from 0 to 12. MLE method is used for the evaluation of parameters of Gamma and Log-normal distributions. Comparison between the stationary and non-stationary models was carried out by estimating the two stationary based indices namely SSPI and SRDI by keeping the parameters invariant with time.

Kendall correlation analysis was carried out at a significance level of 0.05 for the assessment of significant large-scale climate indices based on different lags for different time scales. Table 4.10 displays the dominant covariates for parameters of fitted distributions. It was observed that the 3-month cumulative precipitation and initial values(δ_0) showed a significant correlation with SOI and IOD for the UGRB and SOI for the LGRB for different lags respectively. Similarly, SOI was identified as the most influential covariate for 6-month aggregated precipitation and δ_0 series for the UGRB whereas SOI and SST showed a quantitative influence in the LGRB for different lag values. The MEI, SOI and SST are significantly associated with 12-month cumulative precipitation and δ_0 for both the sub-basins.

The stationary and non-stationary model performances were compared by minimizing the AIC. Table 4.11 represents the AIC values for non-stationary and stationary models. The AIC values obtained from non-stationary models were consistently lesser than those obtained from the stationary models. Hence, it can be concluded that the non-stationary models achieved better performance than the stationary models.

Table 4.10 Significant lag for different large-scale climate oscillations

NRDI	SOI	MEI	IOD	SST	NSPI	SOI	MEI	IOD	SST
UGRB					UGRB				
3-month	2		0		3-month	2		5	
6-month	2				6-month	2			
12-month	0	0		0	12-month	0	0		0
LGRB					LGRB				
3-month	4				3-month	4			
6-month	3			2	6-month	3	2		
12-month	3	4		3	12-month	3	3		5

Table 4.11 Comparison between stationary and non-stationary models using AIC values

Models	NRDI	SRDI	NSPI	SSPI
	UGRB		UGRB	
3-month	5272	5272	7119.57	7119.145
6-month	5615	5617	7591.586	7592.802
12-month	3759	3828	6175.181	6231.682
	LGRB		LGRB	
3-month	6923	6928	8935.202	8937.593
6-month	7268	7278	9266.781	9266.588
12-month	5061	5115	7343.492	7380.212

4.3.2 Spatio-temporal analysis of historical droughts

In the present study, comparison of stationary and nonstationary drought indices at 3-month scale is carried out for GRB. Stationary and nonstationary drought indices were plotted for the months of January to May to observe the temporal drought propagation from January to May. The non-stationary indices showed the actual drought situation since the large-scale climate indices were considered to construct these indices. From Fig. 4.13, it can be observed that the NSPI and SSPI showed slightly different drought propagation. For March, April and May, the western part of the basin showed higher tendency of drought events. Further, NRDI was computed considering the evapotranspiration and large-scale climate indices and then, NRDI and RDI were compared. The temporal propagation of the drought from January to May showed that the drought was propagating from eastern part to western part of the basin based on both NSPI and NRDI. The western part the basin is rain shadow region and is considered to be drought-prone. NRDI and RDI showed intense drought spots when compared to NRDI (Fig. 4.14). Although there were evidences of drought conditions in the basin, severe drought conditions were identified by NRDI compared to other drought indices. Moreover, the area under drought was larger

under NRDI compared to other indices. When PET is included, the NRDI captured more drought-affected areas compared to NSPI during the months of January to May.

Fig 4.15 showed the comparison between the severities of stationary and non-stationary indices. More severe most droughts occurred in the western part of the basin. The NRDI identified severe-most drought events compared to other indices as NRDI considered PET.

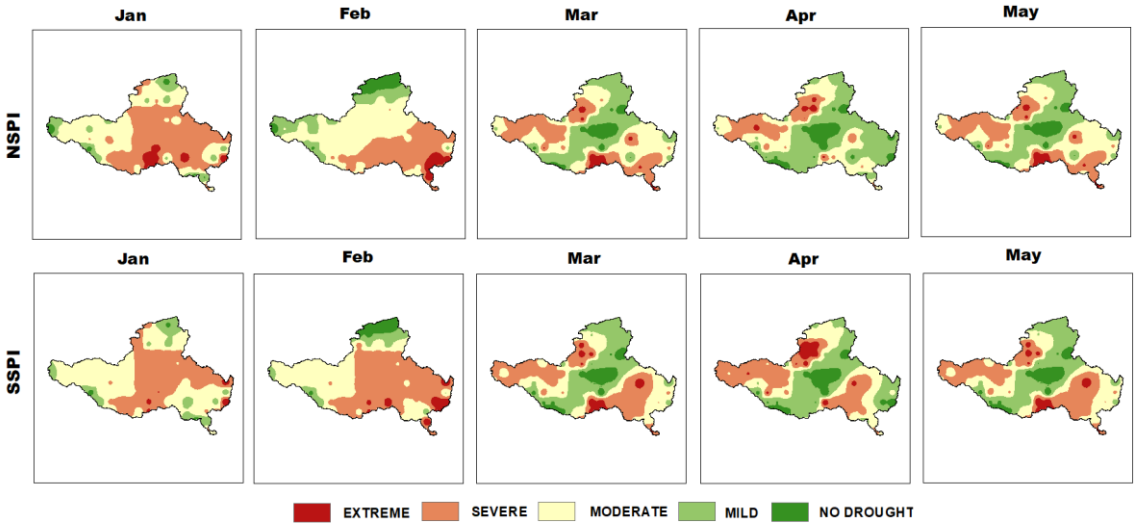

Fig 4.13 Temporal drought propagation of NSPI and SSPI - for 3-month time scale

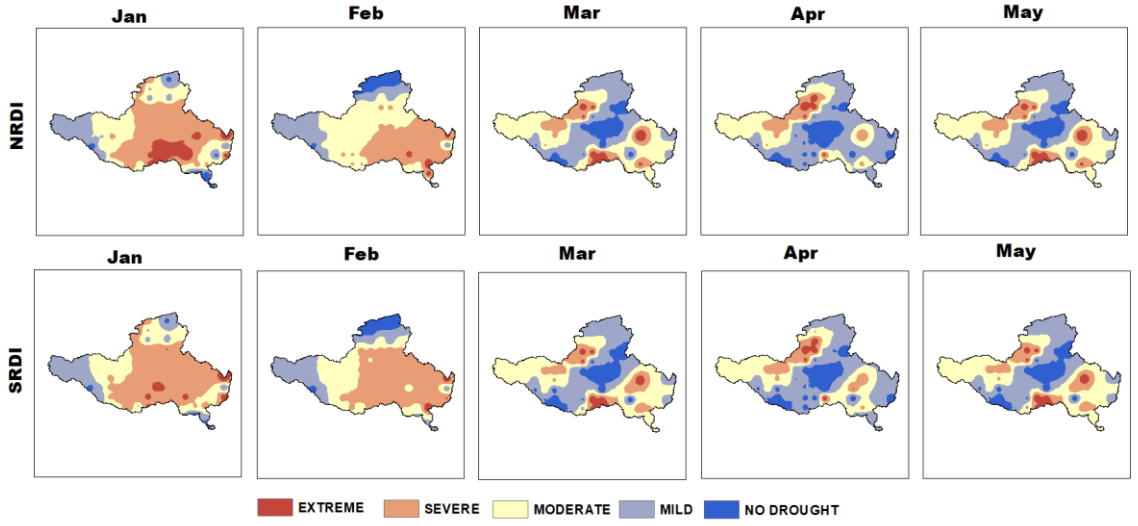

Fig 4.14. Temporal drought propagation of NRDI and SRDI – for 3-month time scale

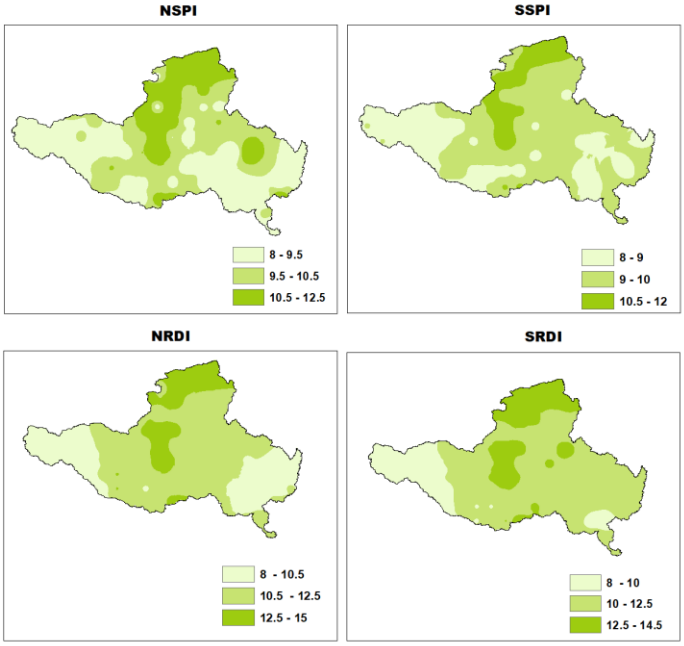

Fig 4.15 Non-stationary and stationary drought severities

4.3.4 Comparison of time series of historical drought

The outputs in the form of rationales were the drought indices that were transformed from the cumulative probability of rainfall and initial values (δ_0). Many differences of signals between the stationary and non-stationary time series were observed which were due to the inclusion of the external covariates. Large dissimilarities of signals were observed between NSPI and SSPI for 3-, 6- and 12-month aggregation levels for both the sub-basins as seen in Fig. 4.16 and Fig. 4.17. In these figures, the green line indicates the stationary drought while the red line indicates the non-stationary drought. These dissimilarities were apparent in case of SPI and RDI and were fairly different from the NSPI and NRDI. For comparing stationary and non-stationary models, box plots for 3-, 6-and 12-month time windows were prepared and shown in Fig. 4.18 and Fig. 4.19 for UGRB and LGRB to identify the variations of the drought characteristics. In these figures, P1, D1 and S1 refer to non-stationary drought characteristics while P2, D2 and S2 refer to stationary characteristics. After comparing 3-month NSPI and SSPI, significant differences were identified in the drought characteristics in the LGRB (Fig. 4.18(b)) compared to the UGRB (Fig 4.18(a)). Larger differences were evident in the drought severity and peak between NSPI and SSPI for the LGRB for 3-month time scale. In the case of duration, the UGRB showed significant variations between NSPI and SSPI for 3-month time scale whereas the LGRB showed less variations. Fig. 4.19 shows the

comparison between NRDI and SRDI for the spatial and temporal variability of drought characteristics for the 3-month time scale. The estimated severities of SRDI series were lower than the severity from NRDI series in the case of UGRB whereas the estimated peaks of SRDI series were higher than those estimated from the NRDI series ((Fig. 4.19(a)). In case of 3-month time series, for the LGRB, peak and severity estimated from SRDI were higher than that of the NRDI (Fig 4.19(b)). The comparison between NRDI and SRDI showed some variations in drought duration. From Fig. 4.18(c), it can be observed that the UGRB displayed significant changes in peak, duration and severity of the 6-month NSPI and SSPI series. For LGRB, there were significant variations of peak and severity whereas lesser variations of NSPI and SSPI were identified for the drought duration as can be seen from Fig. 4.18 (d). No significant variations of the drought characteristics were observed for NRDI and SRDI for both the sub-basins for the 6-month time scale as seen from Fig. 4.19(c) and Fig. 4.19(d). Comparison of the non-stationary and stationary approaches for the 12-month time scale for the drought events in both sub-basins showed significant deviations in drought characteristics (Fig 4.19 (e) and Fig. 4.19 (f)). It can, hence, be concluded that substantial variations of drought characteristics were evident in the case of 12-month time window compared to 3- and 6-month time window.

The differences observed in the drought characteristics between the stationary and non-stationary models have significant role in the implementation of sustainable water resources systems planning and management. In this study, non-stationary models have been considered for further analysis using trivariate and pairwise copula.

4.3.5 Trivariate copula models

The Archimedean copulas (Gumbel, Frank and Clayton) and elliptical copulas (Gaussian and Student's t) were used in this study to evaluate the dependence structure of drought characteristics. Different types of distributions namely Gumbel, Gamma, Log-normal, Weibull and Exponential distributions were fitted to the drought characteristics. The best fitted distributions for various time scales were obtained based on AIC criteria and the log-likelihood values to find the marginal distributions (Table 4.14 to Table 4.19).

The best fitted trivariate copula model among the copulas was decided by analysing the GoF measures - KS, CVM, Chsq considering 2000 sample runs including AIC, log-likelihood values and their estimated parameters are presented in Table 4.12 and Table 4.13. The results from Tables show that the Student's t copula performed better than the other trivariate copula models. The parameter estimation of trivariate copula analysis was

conducted using the MLE method. Parameters of Student's t copula show a single degree of freedom which is the driving force for the dependency of all other pair of variables. Because of this limitation, a unique method of copula construction named as vine copula was introduced. The conventional vine model was compared with the multivariate Student's t copula. The pairwise copula construction method was used in this study to find the copula parameters which further can be used to evaluate the frequency of non-stationary drought indices (NSPI and NRDI).

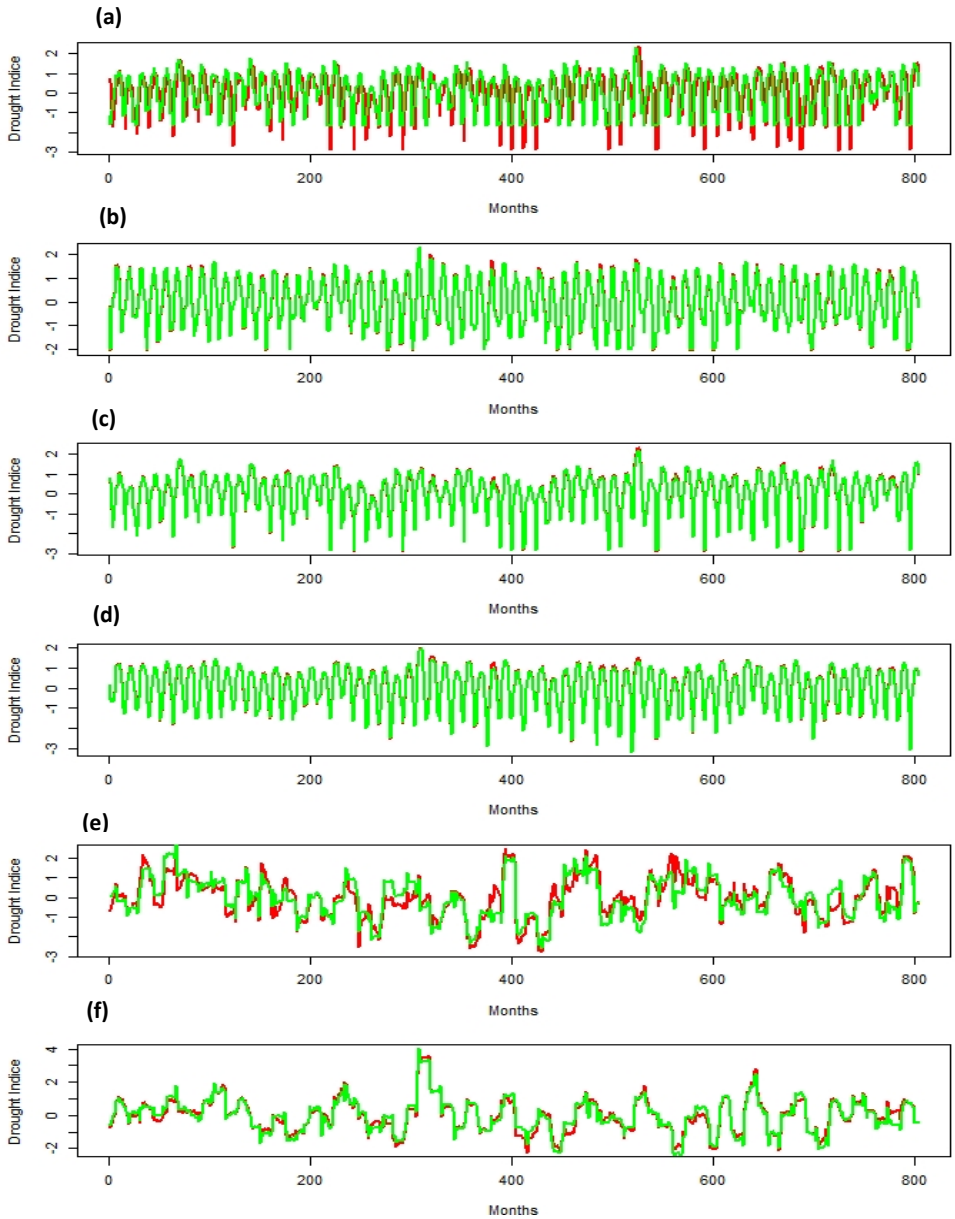

Fig. 4.16. NSPI and SSPI drought signals during 1951-2017 for 3-, 6- and 12-month time scales: (a) 3-month time scale for UGRB; (b) 3-month time scale for LGRB; (c) 6-month time scale for UGRB; (d) 6-month time scale for LGRB; (e) 12-month time scale for UGRB; (f) 12-month time scale for LGRB

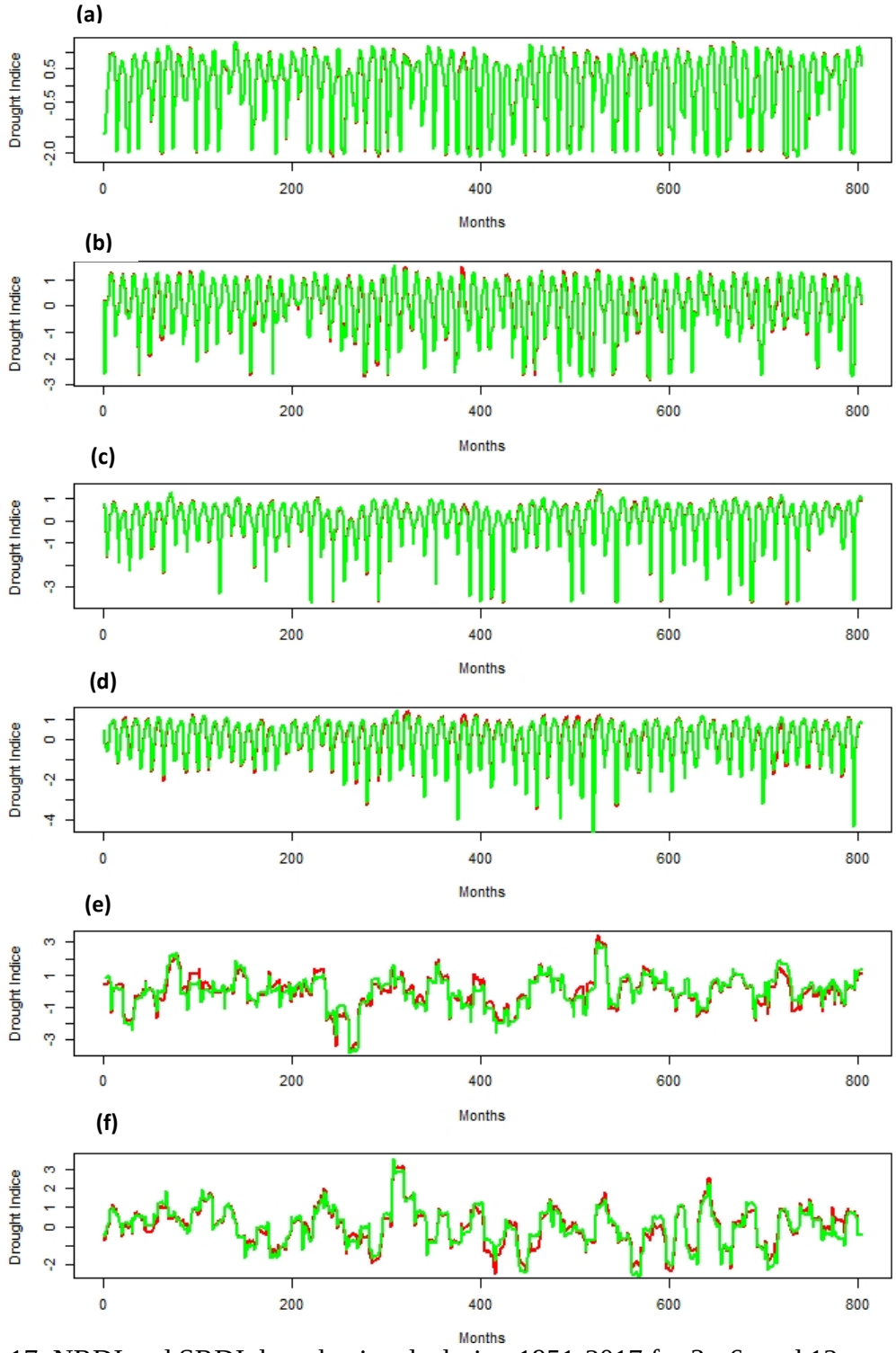

Fig. 4.17. NRDI and SRDI drought signals during 1951-2017 for 3-, 6- and 12-month time scales: (a) 3-month time scale for UGRB; (b) 3-month time scale for LGRB; (c) 6-month time scale for UGRB; (d)6-month time scale for LGRB; (e) 12-month time scale for UGRB; (f)12-month time scale for LGRB

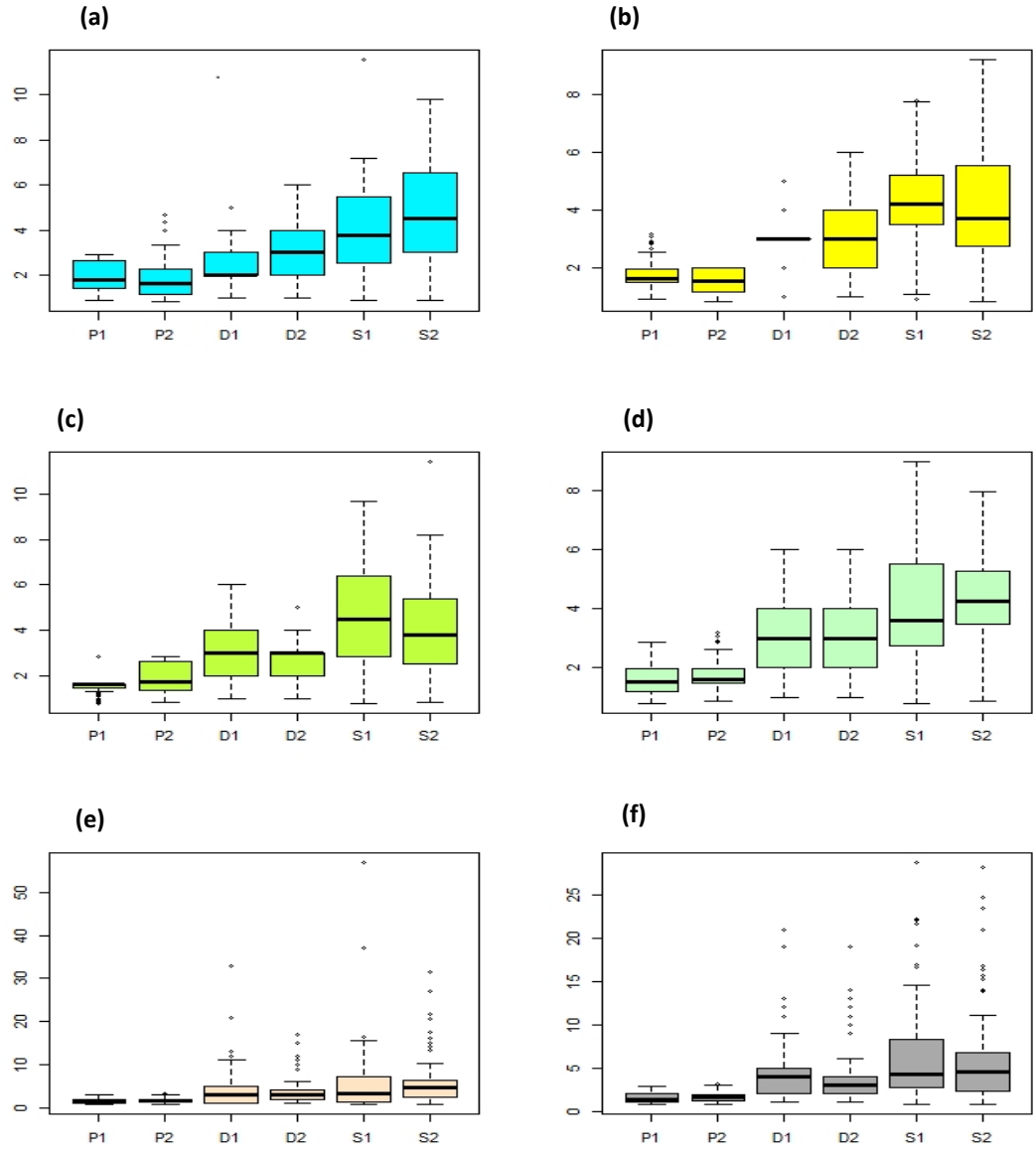

Fig.4.18 Comparison by box plots for drought variables peak (P), duration (D) and severity (S) for NSPI and SSPI for different time scales: (a) 3-month time scale for UGRB (b) 3-month time scale for LGRB; (c) 6-month time scale for UGRB (d) 6-month time scale for LGRB; (e) 12-month time scale for UGRB (f) 12-month time scale for LGRB.

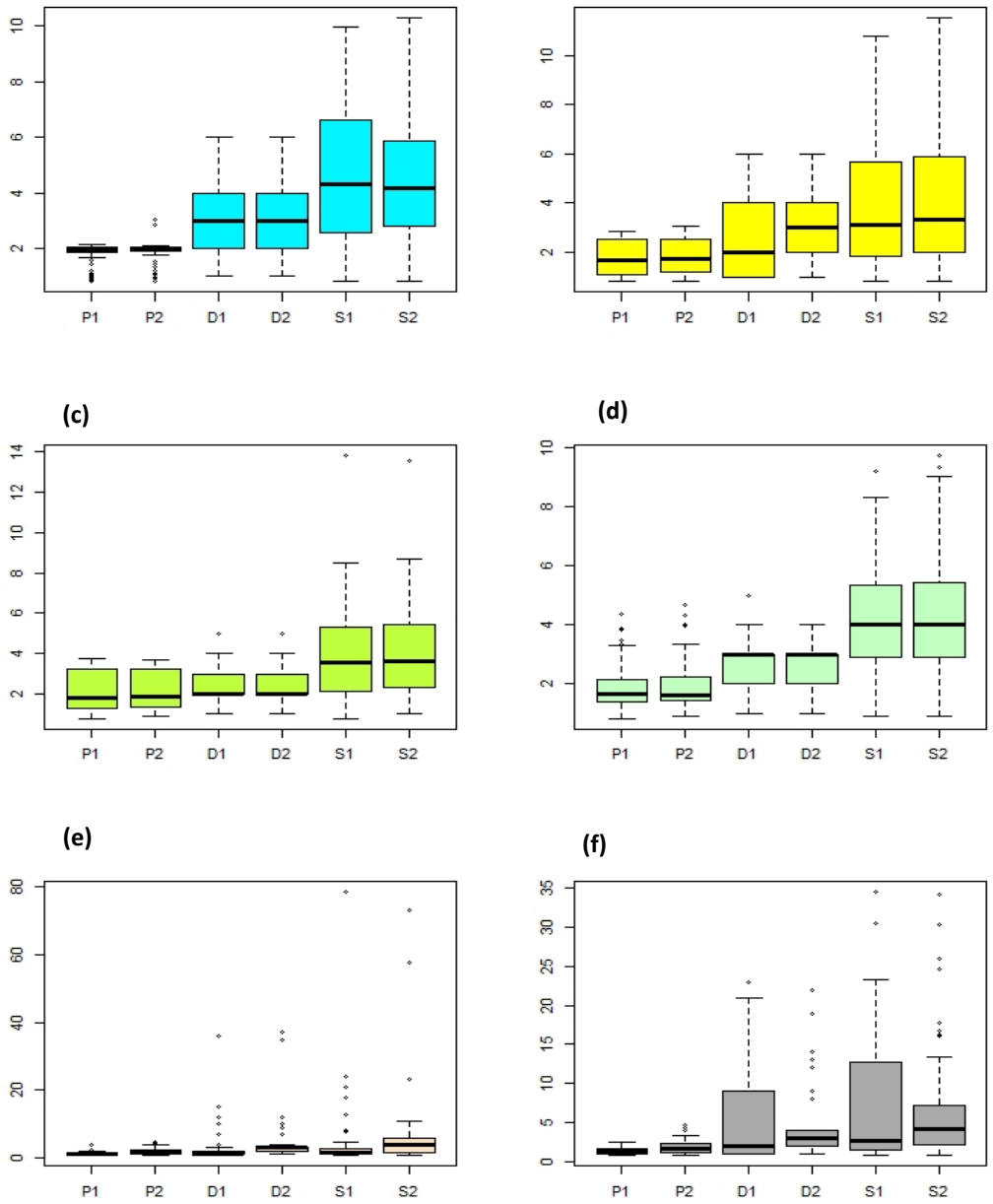

Fig. 4.19. Comparison by box plots for drought variables peak (P), duration (D) and severity (S) for NRDI and SRDI for different time scales (a) 3-month time scale for UGRB (b) 3-month time scale for LGRB; (c) 6-month time scale for UGRB (d) 6-month time scale for LGRB; (e) 12-month time scale for UGRB (f) 12-month time scale for LGRB

Table 4.12 Trivariate copula analysis for non-stationary reconnaissance drought characteristics

	3-month					6-month					12-month				
UGRB	Gumbel	Clayton	Frank	Normal	Student's t copula	Gumbel	Clayton	Frank	Normal	Student's t copula	Gumbel	Clayton	Frank	Normal	Student's t copula
Parameter	1.9	2.0	6.2	0.7	0.7	1.9	1.5	5.3	0.7	0.7	2.9	2.6	8.3	0.8	0.7
Loglikelihood	41.5	53.0	47.9	48.2	97.5	36.1	39.4	38.5	51.1	81.3	47.7	36.0	39.3	45.6	70.6
AIC	-81.0	-104.0	-93.8	-92.3	-187	-70.3	-76.7	-74.9	-98.2	-154	-93.4	-69.9	-76.6	-87.1	-133
KS	0.2	0.0	0.2	0.5	0.4	0.3	0.1	0.2	0.4	0.3	0.2	0.1	0.2	0.3	0.8
Chsq	0.4	0.1	0.3	0.4	0.7	0.1	0.0	0.1	0.1	0.2	0.1	0.0	0.0	0.0	0.1
CVM	0.2	0.1	0.1	0.2	0.5	0.1	0.1	0.1	0.4	0.6	0.0	0.0	0.0	0.0	0.2
LGRB															
Parameter	2.1	1.6	6.5	0.8	0.8	1.8	1.7	5.4	0.7	0.7	2.7	1.8	8.1	0.8	0.8
Loglikelihood	51.4	43.9	52.0	55.1	96.3	31.9	45.0	39.5	54.9	86.9	46.5	29.1	40.1	44.1	68.7
AIC	-100.8	-85.7	-102	-106.3	-184	-61.8	-87.9	-77.0	-105.7	-165	-91.1	-56.1	-78.1	-84.2	-129
KS	0.2	0.0	0.2	0.5	0.1	0.4	0.1	0.4	0.5	0.8	0.3	0.2	0.3	0.0	0.0
Chsq	0.1	0.0	0.2	0.3	0.4	0.1	0.1	0.2	0.0	0.4	0.2	0.0	0.1	0.1	0.5
CVM	0.1	0.0	0.0	0.0	0.0	0.0	0.0	0.0	0.4	0.6	0.2	0.1	0.1	0.2	0.1

Table 4.13 Trivariate copula analysis for non-stationary standardized precipitation drought characteristics

	3-month					6-month					12-month				
UGRB	Gumbel	Clayton	Frank	Normal	Student's t copula	Gumbel	Clayton	Frank	Normal	Student's t copula	Gumbel	Clayton	Frank	Normal	Student's t copula
Parameter	1.9	1.9	5.7	0.7	0.7	1.8	1.7	5.1	0.7	0.7	2.7	3.0	9.8	0.9	0.9
Loglikelihood	40.7	51.9	44.5	49.9	88.2	31.8	45.5	36.3	36.7	96	82.5	84.2	86.0	87.9	138.8
AIC	-79.5	-101.9	-87.1	-95.8	-168	-61.7	-89.1	-70.6	-69.4	-184	-163.1	-166.3	-169.9	-171.7	-269
KS	0.2	0.1	0.2	0.3	0.6	0.4	0.1	0.4	0.9	0.6	0.1	0.1	0.2	0.1	0.6
Chisq	0.0	0.2	0.2	0.1	0.3	0.2	0.1	0.1	0.0	0.5	0.0	0.0	0.0	0.0	0.2
CVM	0.1	0.0	0.0	0.8	0.5	0.5	0.2	0.3	0.6	0.9	0.4	0.3	0.3	0.1	0.3
LGRB															
Parameter	1.7	1.5	4.9	0.7	0.7	1.9	1.9	6.0	0.7	0.7	2.2	2.2	7.0	0.8	0.8
Loglikelihood	30.9	39.7	33.1	42.9	87.5	41.4	52.0	46.5	44.0	106	61.2	61.8	59.4	64.6	137.5
AIC	-59.7	-77.4	-64.2	-81.7	-167	-80.7	-102.0	-90.9	-84.0	-205	-120.3	-121.7	-116.8	-125.3	-267
KS	0.4	0.1	0.4	0.8	0.3	0.3	0.1	0.3	0.7	0.9	0.3	0.2	0.4	0.2	0.1
Chisq	0.0	0.0	0.0	0.0	0.0	0.0	0.0	0.0	0.0	0.5	0.0	0.0	0.1	0.0	0.3
CVM	0.0	0.0	0.0	1.0	1.0	0.3	0.1	0.2	0.2	0.6	0.2	0.1	0.1	0.1	0.5

Table 4.14. Fitted probability distribution functions, AIC and Log-likelihood for duration of NSPI series for different time scales and periods for UGRB and LGRB

UGRB	3-month		6-month		12-month	
Distribution	AIC	Log-likelihood	AIC	Log-likelihood	AIC	Log likelihood
Gumbel	190	-93.39	236.68	-116.34	335.86	-165.93
Gamma	188.41	-92.205	233.87	-114.93	318.24	-157.12
Lognormal	192.62	-94.31	239.89	-117.94	302.9	-149.49
Weibull	186.72	-91.36	229.31	-112.65	321.4	-158.7
Exponential	251.51	-124.75	281.32	-139.66	320.45	-159.22
LGRB	3-month		6-month		12-month	
Distribution	AIC	Log likelihood	AIC	Log likelihood	AIC	Log likelihood
Gumbel	165.45	-80.72	231.5	-113.75	346.53	-171.26
Gamma	155.52	-75.76	229.03	-112.51	334.18	-165.09
Lognormal	163.8	-79.9	236.09	-116.04	328.35	-162.17
Weibull	146.82	-71.41	223.5	-109.75	337.2	-166.6
Exponential	276.14	-137.07	280.68	-139.34	341.62	-169.81

Table 4.15. Fitted probability distribution functions, AIC and Log-likelihood for peak of NSPI series under different time scales and periods for UGRB and LGRB

UGRB	3-month		6-month		12-month	
Distribution	AIC	Log likelihood	AIC	Log likelihood	AIC	Log likelihood
Gumbel	133.43	-64.71	43.52	-19.76	91.78	-43.89
Gamma	131.34	-63.67	29.72	-12.86	94.35	-45.17
Lognormal	132.74	-64.373	33.96	-14.98	91.03	-43.51
Weibull	131.23	-63.61	38.02	-17.01	102.75	-49.37
Exponential	217.61	-107.8	187.1	-92.55	177.5	-87.75
LGRB	3-month		6-month		12-month	
Distribution	AIC	Log likelihood	AIC	Log likelihood	AIC	Log likelihood
Gumbel	85.816	-40.9	78.65	-37.32	83.73	-39.86
Gamma	90.623	-43.31	76.22	-36.11	83	-39.5
Lognormal	87.62	-41.81	77.25	-36.62	82.9	-39.45
Weibull	103.18	-49.59	78.58	-37.29	86.81	-41.4
Exponential	205.82	-101.91	187.22	-92.61	183.53	-90.769

Table 4.16. Fitted probability distribution functions, AIC and Log-likelihood for severity of NSPI series under different time scales and periods for UGRB and LGRB

Upper sub basin	3-month		6-month		12-month	
Distribution	AIC	Log likelihood	AIC	Log likelihood	AIC	Log likelihood
Gumbel	273.74	-134.87	294.89	-145.44	394.94	-195.47
Gamma	272.69	-134.34	293.06	-144.53	364.01	-180
Lognormal	278.61	-137.3	300.88	-148.441	347.51	-171.75
Weibull	272.05	-134.02	289.29	-142.64	363.43	-179.71
Exponential	-155.24	312.49	327.99	-162.99	362.05	-180.02
Lower sub basin	3-month		6-month		12-month	
Distribution	AIC	Log likelihood	AIC	Log likelihood	AIC	Log likelihood
Gumbel	241.33	-118.66	287.233	-141.61	393.384	-194.69
Gamma	239	-117.5	285.64	-140.82	375.87	-185.93
Lognormal	247.83	-121.91	291.72	-143.86	371.56	-183.78
Weibull	235.19	-115.59	284.31	-140.15	377.42	-186.71
Exponential	324.94	-161.47	-158.56	319.13	377.85	-187.92

Table 4.17. Fitted probability distribution functions, AIC and Log-likelihood for duration of NRDI series under different time scales and periods for UGRB and LGRB

Upper sub-basin	3-month		6-month		12-month	
Distribution	AIC	Log likelihood	AIC	Log likelihood	AIC	Log likelihood
Gumbel	221.22	-108.61	159.3	-77.65	203.23	-99.61
Gamma	218.25	-107.12	157.32	-76.66	175.59	-85.79
Lognormal	222.19	-109.09	159.86	-77.93	155.79	-75.89
Weibull	216.22	-106.11	158.33	-77.16	173.39	-84.69
Exponential	258.16	-128.08	223.4	-110.7	173.94	-85.97
Lower sub-basin	3-month		6-month		12-month	
Distribution	AIC	Log likelihood	AIC	Log likelihood	AIC	Log likelihood
Gumbel	214.03	-105.01	138.47	-67.23	-110.57	225.14
Gamma	210.27	-103.13	134.62	-65.31	-100.87	205.74
Lognormal	210.79	-103.39	136.69	-66.34	-97.58	199.16
Weibull	211.4	-103.7	138.42	-67.21	-100.86	205.72
Exponential	244.32	-121.16	250.34	-124.17	-100.88	203.76

Table 4.18. Fitted probability distribution functions, AIC and Log-likelihood for peak of NRDI series under different time scales and periods for UGRB and LGRB

Upper sub-basin	3-month		6-month		12-month	
Distribution	AIC	Log likelihood	AIC	Log likelihood	AIC	Log likelihood
Gumbel	90.76	-43.38	172.49	-84.24	41.83	-18.91
Gamma	76.42	-36.21	170.39	-83.19	48.96	-22.48
Lognormal	85.63	-40.81	169.9	-82.953	43.25	-19.62
Weibull	42.23	-19.116	172.24	-84.12	61.01	-28.5
Exponential	199.13	-98.56	222.75	-110.37	96.24	-47.12
Lower sub-basin	3-month		6-month		12-month	
Distribution	AIC	Log likelihood	AIC	Log likelihood	AIC	Log likelihood
Gumbel	128.87	-62.43	133.47	-64.73	48.51	-22.25
Gamma	126.96	-61.48	138.08	-67.04	49.48	-22.74
Lognormal	127.46	-61.73	132.83	-64.41	48.28	-22.14
Weibull	127.424	-61.712	149.66	-72.83	53.37	-24.68
Exponential	194.32	-96.16	208.92	-103.46	100.63	-49.31

Table 4.19. Fitted probability distribution functions, AIC and Log-likelihood for severity of NRDI series under different time scales and periods for UGRB and LGRB

Upper sub-basin	3-month		6-month		12-month	
Distribution	AIC	Log likelihood	AIC	Log likelihood	AIC	Log likelihood
Gumbel	292.67	-144.33	271.4	-133.7	247.01	-121.5
Gamma	290.31	-143.15	268.58	-132.29	202.69	-99.34
Lognormal	297.06	-146.53	269.22	-132.61	177.55	-86.77
Weibull	287.88	-141.94	271.47	-133.73	196.23	-96.11
Exponential	317.36	-157.68	296.99	-147.49	206.67	-102.33
Lower sub-basin	3-month		6-month		12-month	
Distribution	AIC	Log likelihood	AIC	Log likelihood	AIC	Log likelihood
Gumbel	298.1	-147.05	248.33	-122.16	254.08	-125.04
Gamma	288.77	-142.38	248.31	-122.15	226.92	-111.46
Lognormal	285.84	-140.92	249.69	-122.84	218.84	-107.42
Weibull	291.06	-143.53	251.55	-123.77	225.98	-110.99
Exponential	301.67	-149.83	307.73	-152.86	225.78	-111.89

4.3.6 Drought characteristics modelling using pair-copula models

Suitable vine structure between C-vine and D-vine models and the copula families must be selected for the dependent pair variables viz., peak (P) - duration (D), duration (D) - severity (S) and severity (S) - peak (P). The dependency measures between pair variables of drought events are given in Table 4.20, which explains stronger dependence between D and S. The next stronger dependency was observed between S and P. It can,

hence, be concluded that S must be present between D and P for the D-vine structure. D-vine structure was selected for further analysis since it had more flexibility towards forming the pair copula rather than the C-vine structure because it creates a relationship of variables with a particular root variable that defines the key elements of the structure (Aas et al. 2009). Kendall's plots and Chi-plots of the pair variables P - D, D - S and S - P are given in Fig. 4.20 to Fig. 4.31, which show positive dependencies between the pair variables. The dependency measures and the Kendall's and Chi-plots of the pair variables indicate that D and S showed the strongest dependency than other pairs. The copula families for the pair variables were selected from various copulas based on Clarke and Vuong tests (Table 4.20).

In the first phase of parameter estimation, the sequential parameters were estimated using the MLE method for pairs of drought variables D/S (θ_{DS}) and S/P (θ_{SP}). Then for the second phase of parameter estimation, the respective h functions (conditional distribution function) were computed between the pair variables D/S and S/P. The parameter, $\theta_{DP/S}$ was then estimated for drought variables (D/S, S/P). The copula families selected for the pair variables and the parameters estimated in the second phase ($\theta_{DP/S}$) considering the best fitted copula for the LGRB and UGRB for different time scales are given in Table 4.21.

Table 4.20. Dependence measurements among drought characteristics P - D, D - S and S - P using Kendall's τ and Spearman's ρ methods for NSPI and NRDI series under different time scales and periods for Upper and Lower Godavari River basins

NSPI UGRB	3-month			6-month			12-month		
	P-D	D-S	S-P	P-D	D-S	S-P	P-D	D-S	S-P
Kendall	0.31	0.697	0.601	0.2679	0.861	0.374	0.562	0.859	0.701
Spearman	0.403	0.83	0.782	0.353	0.954	0.5179	0.726	0.956	0.87
LGRB									
	P-D	D-S	S-P	P-D	D-S	S-P	P-D	D-S	S-P
Kendall	0.21	0.619	0.59	0.317	0.815	0.5	0.415	0.874	0.532
Spearman	0.265	0.737	0.76	0.412	0.923	0.664	0.569	0.96	0.737
NRDI UGRB									
	P-D	D-S	S-P	P-D	D-S	S-P	P-D	D-S	S-P
Kendall	0.34	0.81	0.53	0.28	0.604	0.67	0.51	0.81	0.73
Spearman	0.47	0.93	0.69	0.37	0.73	0.85	0.609	0.9	0.84
LGRB									
	P-D	D-S	S-P	P-D	D-S	S-P	P-D	D-S	S-P
Kendall	0.38	0.77	0.61	0.31	0.65	0.644	0.43	0.78	0.7
Spearman	0.5	0.89	0.79	0.4	0.79	0.83	0.52	0.84	0.81

Table 4.21. Pairwise Copula Construction (PCC) for NSPI and NRDI drought characteristics

NSPI UGRB	Clarke	Vuong	AIC	Selected Bivariate Copula			Parameter ($\theta_{DP/S}$)
3-month	0.62	0.914	-180.48	Clayton	Gaussian	Clayton	0.469
6-month	0.457	0.506	-197.83	Clayton	Frank	Gaussian	0.429
12-month	0.0248	0.984	-286.033	Frank	Gumbel	Frank	6.16
NSPI LGRB	Clarke	Vuong	AIC	Selected Bivariate Copula			Parameter ($\theta_{DP/S}$)
3-month	0.0026	0.0619	-169.575	Clayton	Clayton	Gumbel	0.244
6-month	0.62	0.692	-205.71	Clayton	Gaussian	Frank	0.46
12-month	0.024	0.0607	-273.98	Gaussian	Gumbel	Gaussian	0.623
NRDI UGRB	Clarke	Vuong	AIC	Selected Bivariate Copula			Parameter ($\theta_{DP/S}$)
3-month	0.703	0.6874	-199.82	Clayton	Frank	Gaussian	0.4855
6-month	0.526	0.358	-168.57	Gaussian	Gaussian	Clayton	0.291
12-month	0.511	0.556	-140.8	Gumbel	Gumbel	Gumbel	1.79
NRDI LGRB	Clarke	Vuong	AIC	Selected Bivariate Copula			Parameter ($\theta_{DP/S}$)
3-month	0.055	0.009	-224.66	Gaussian	Frank	Clayton	0.362
6-month	1	0.459	-171.19	Clayton	Clayton	Gaussian	0.338
12-month	1	0.418	-147.97	Gumbel	Gumbel	Gumbel	1.694

In the second phase of parameter estimation, the appropriate copula was selected from the first phase of copula families fitted for estimation of the sequential parameter. For example, in the case of the generated drought characteristics from 3- month NRDI, Gaussian copula was selected for estimation of the second phase of the parameter. Finally, the PCC model, accounting for the drought variables was compared with the derived trivariate copula using the AIC criteria. It can be observed from Table 4.22 that the AIC of the trivariate model showed higher AIC value compared to PCC based model. It can, hence, be justified that the PCC model can flexibly model the drought characteristics by transforming the bivariate model to a higher dimensional model.

Table 4.22. Comparison between Student's t copula and PCC model

UGRB	Student's t copula	PCC
3-month	-168.3	-180.5
6-month	-184.2	-197.8
12-month	-269.6	-286
LGRB	Student's t copula	PCC
3-month	-167	-169.6
6-month	-205.2	-205.7
12-month	-267.1	-273.98
UGRB	Student's t copula	PCC
3-month	-187.05	-199.8
6-month	-154.646	-168.57
12-month	-133.197	-140.8
LGRB	Student's t copula	PCC
3-month	-184.635	-224.66
6-month	-165.9	-171.19
12-month	-129.371	-147.97

4.3.7 Return period analysis of drought variables

The frequency analysis of droughts can be related to the occurrence of extreme events and their probability distributions. Here, the values of peak (P), duration (D) and severity (S) that exceed their truncation level ($S \geq s, D \geq d, P \geq p$) were considered for analysing the multivariate drought frequency. The joint return period analysis was carried out by using the two probability cases i.e. (i) ‘‘AND” and (ii) ‘‘OR” return periods for the drought variable using the approach suggested by Salvadori and Michele (2004).

Table 4.23 to Table 4.26 show the joint return periods (‘‘AND” and ‘‘OR” cases) obtained from the trivariate copula and PCC models using the drought characteristics for NSPI and NRDI for 3-, 6- and 12- month time scale. Here $T^{AND}_{(SDP)}TC$ and $T^{AND}_{(SDP)}$ PCC represent the joint return periods for trivariate Student’s t copula and PCC model respectively. Similarly, the joint return period of “OR” case can be denoted as $T^{OR}_{SDP}TC$ and $T^{OR}_{(SDP)}PCC$ for trivariate Student’s t copula and PCC models respectively. The ‘‘OR” joint return periods were less compared to ‘‘AND” return periods in both trivariate Student’s t copula and PCC models. It can, hence, be concluded that the frequency of drought was more in the "OR” case when compared to the "AND" case.

Table 4.23. Comparison of ‘AND ‘return periods for drought characteristics of NRDI computed based on trivariate student’s t copula (T_{ST}) and pair-copula model (T_{PC}) for Upper and Lower sub-basin

UGRB	3-month	T_{ST}	T_{PC}	6-month	T_{ST}	T_{PC}	12-month	T_{ST}	T_{PC}
	5	5.31	6.36	5	5.58	5.76	5	6.93	7.96
	10	13.14	14.89	10	12.45	14.61	10	15.85	18.02
	20	27.04	32.02	20	22.82	29.88	20	42.01	54.99
	50	68.74	77.54	50	57.55	66.25	50	76.55	91.27
LGRB	3-month	T_{ST}	T_{PC}	6-month	T_{ST}	T_{PC}	12-month	T_{ST}	T_{PC}
	5	5.86	6.41	5	5.26	6.11	5	6.83	8.41
	10	17.04	18.48	10	12.99	14.57	10	16.17	19.34
	20	32.08	38.5	20	25.42	31.84	20	36.74	48.11
	50	73.78	89.04	50	52.74	56.17	50	86.21	113.46

Table 4.24. Comparison of 'OR' return periods for drought characteristics of NRDI computed based on trivariate student's t copula (T_{ST}) and pair-copula model (T_{PC}) for Upper and Lower sub-basin

UGRB	3-month	T_{ST}	T_{PC}	6-month	T_{ST}	T_{PC}	12-month	T_{ST}	T_{PC}
	5	3.37	4.06	5	3.21	3.97	5	4.17	5.74
	10	7.95	8.04	10	6.99	7.48	10	8.74	9.31
	20	15.25	16.87	20	13.43	14.78	20	16.01	17.55
	50	35.28	41.09	50	29.08	36.01	50	38.29	44.88
LGRB	3-month	T_{ST}	T_{PC}	6-month	T_{ST}	T_{PC}	12-month	T_{ST}	T_{PC}
	5	3.54	3.95	5	3.21	3.55	5	4.14	4.68
	10	7.822	8.06	10	6.98	7.77	10	9.71	10.04
	20	13.99	14.96	20	12.09	13.57	20	17.21	19.71
	50	41.81	45.67	50	34.18	40.77	50	41.99	48..98

Table 4.25. Comparison of 'AND' return periods for drought characteristics of NSPI computed based on trivariate student's t copula (T_{ST}) and pair-copula model (T_{PC}) for Upper and Lower sub- basin

UGRB	3-month	T_{ST}	T_{PC}	6-month	T_{ST}	T_{PC}	12-month	T_{ST}	T_{PC}
	5	5.91	6.04	5	5.6	6.92	5	5.13	5.43
	10	13.87	14.31	10	11.96	13.16	10	11.29	15.23
	20	32.58	29.2	20	26.99	28.25	20	21.84	29.23
	50	73.8	78.96	50	69.08	71.28	50	62.71	69.9
LGRB	3-month	T_{ST}	T_{PC}	6-month	T_{ST}	T_{PC}	12-month	T_{ST}	T_{PC}
	5	5.52	5.91	5	6.47	7.62	5	6.65	6.79
	10	10.18	10.99	10	15.4	14.54	10	13.39	17.81
	20	23.81	25.24	20	35.28	38.41	20	22.4	37.43
	50	54.75	57.48	50	74.19	81.577	50	61.45	87.15

Table 4.26. Comparison of 'OR' return periods for drought characteristics of NSPI computed based on trivariate student's t copula (T_{ST}) and pair-copula model (T_{PC}) for Upper and Lower sub-basin

UGRB	3-month	T_{ST}	T_{PC}	6-month	T_{ST}	T_{PC}	12-month	T_{ST}	T_{PC}
	5	3.54	4.84	5	3.32	4.12	5	4.041	4.76
	10	8.81	9.77	10	7.89	9.02	10	6.47	9.87
	20	17.91	19.53	20	16.45	17.41	20	15.65	17.05
	50	44.42	48.33	50	38.88	40.18	50	36.05	45.21
LGRB	3-month	T_{ST}	T_{PC}	6-month	T_{ST}	T_{PC}	12-month	T_{ST}	T_{PC}
	5	4.16	4.85	5	3.99	4.99	5	3.07	4.71
	10	7.88	8.97	10	7.75	9.57	10	7.58	8.05
	20	16.84	14.02	20	14.87	16.88	20	13.52	17.99
	50	34.77	41.21	50	29.68	32.04	50	30.04	38.85

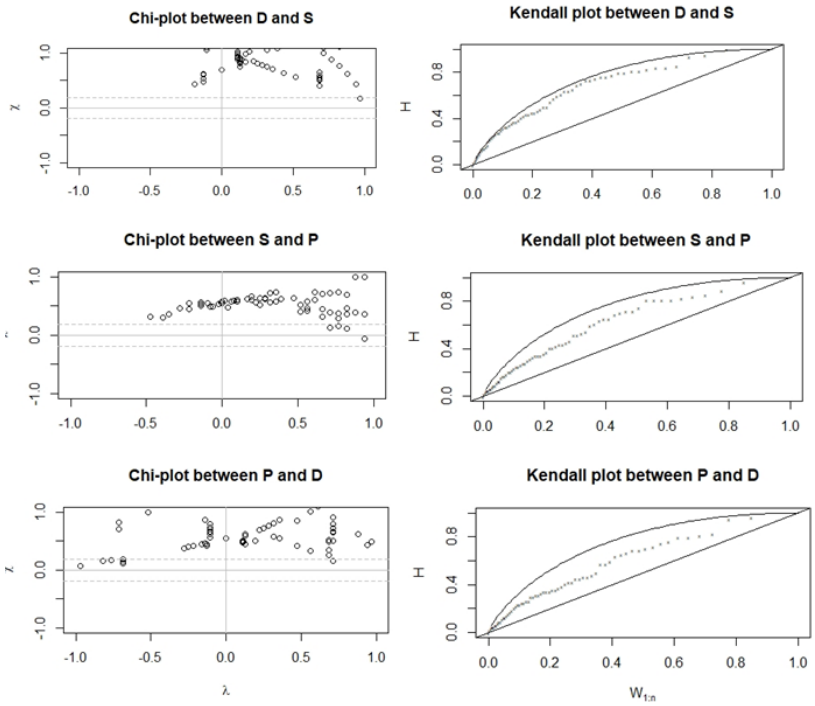

Fig. 4.20 Chi and Kendall plots of the pairwise drought characteristics D-S, S- P and P-D of NSPI for UGRB for 3-month time scale: Plots in 1st column represent the Chi-plots of pairwise characteristics and 2nd column represent the Kendall plots of the pairwise drought characteristics

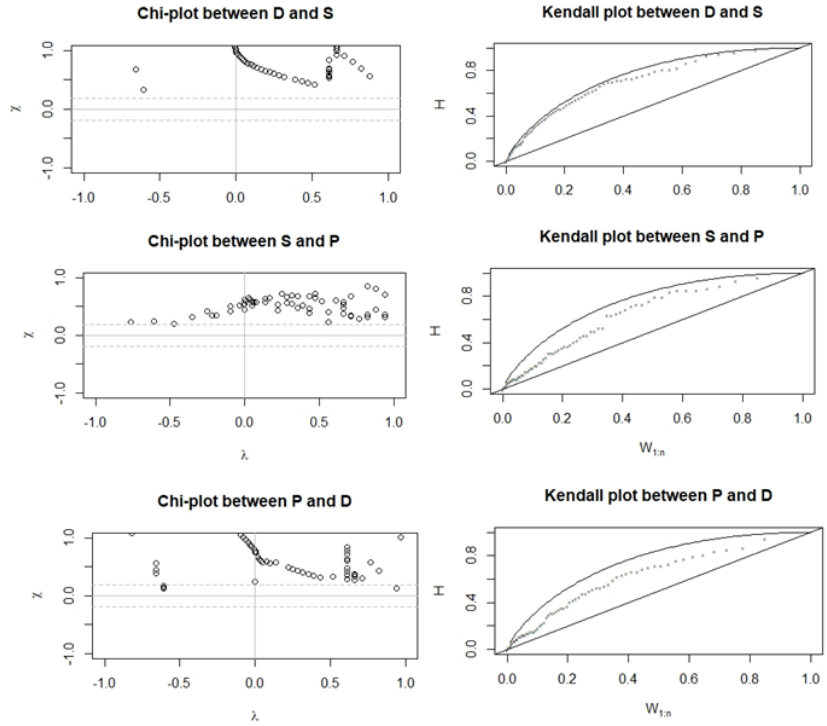

Fig. 4.21 Chi and Kendall plots of the pairwise drought characteristics D-S, S- P and P-D of NSPI for LGRB for 3-month time scale: Plots in 1st column represent the Chi-plots of pairwise characteristics and 2nd column represent the Kendall plots of the pairwise drought characteristics

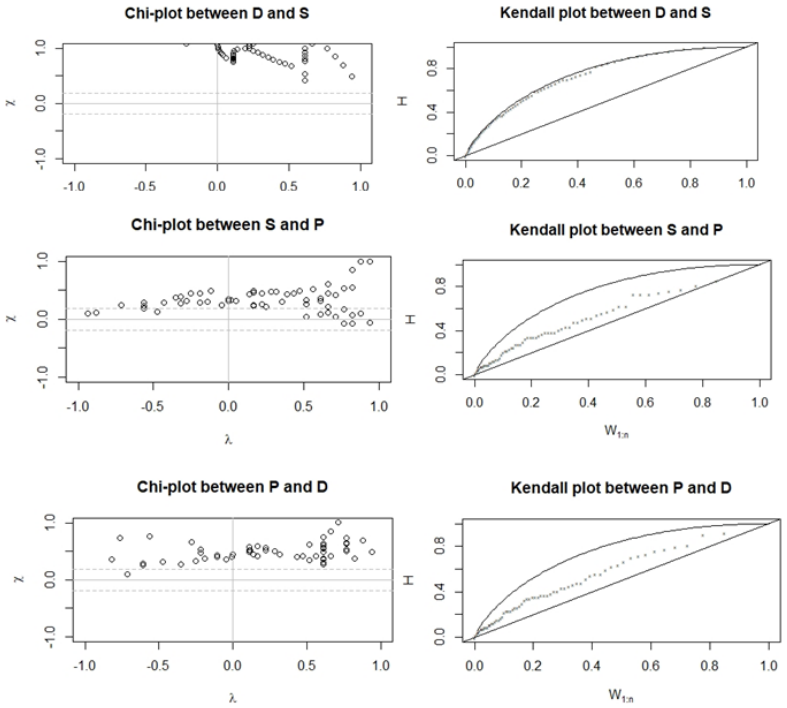

Fig. 4.22. Chi and Kendall plots of the pairwise drought characteristics D-S, S- P and P-D of NSPI for UGRB for 6-month time scale: Plots in 1st column represent the Chi-plots of pairwise characteristics and 2nd column represent the Kendall plots of the pairwise drought characteristics

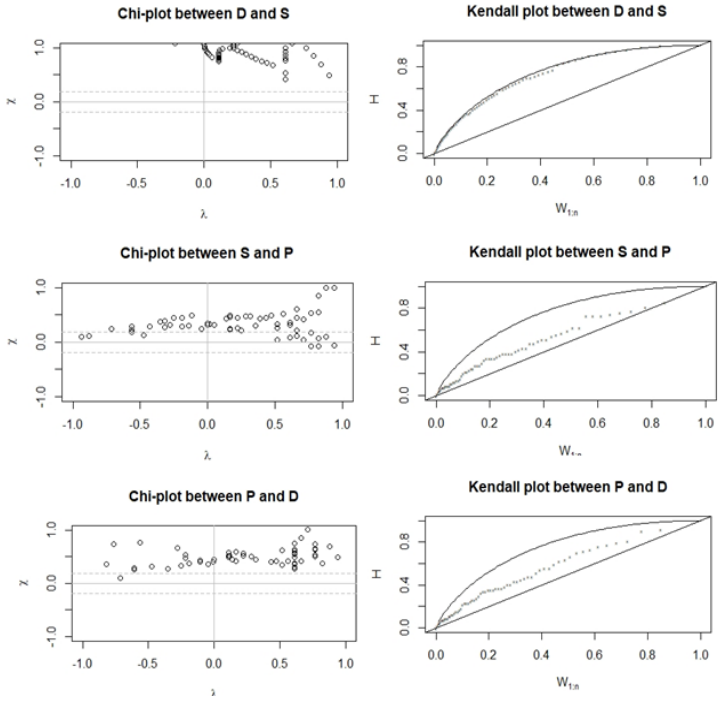

Fig. 4.23. Chi and Kendall plots of the pairwise drought characteristics D-S, S- P and P-D of NSPI for LGRB for 6-month time scale: Plots in 1st column represent the Chi-plots of pairwise characteristics and 2nd column represent the Kendall plots of the pairwise drought characteristics

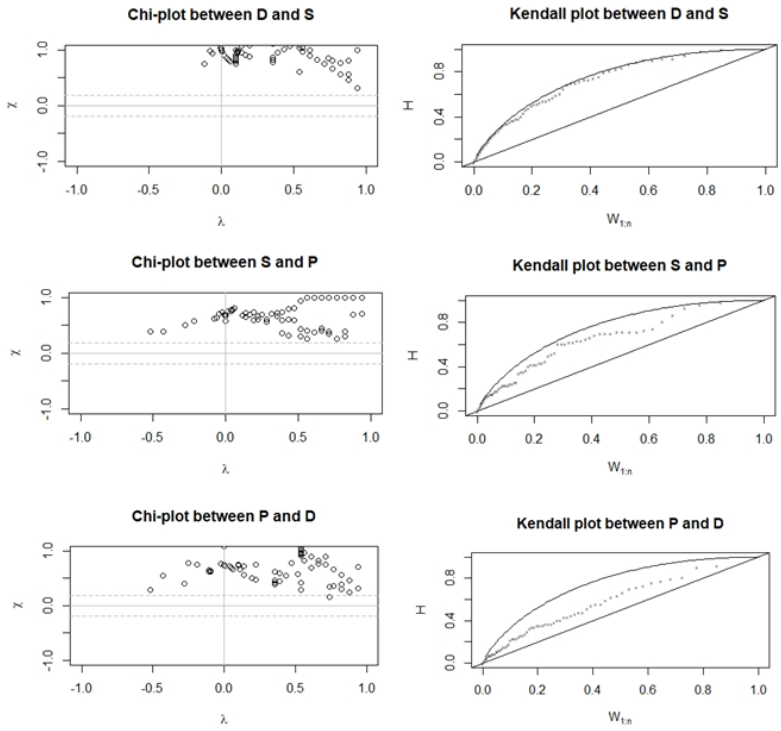

Fig. 4.24. Chi and Kendall plots of the pairwise drought characteristics D-S, S- P and P-D of NSPI for UGRB for 12-month time scale: Plots in 1st column represent the Chi-plots of pairwise characteristics and 2nd column represent the Kendall plots of the pairwise drought characteristics

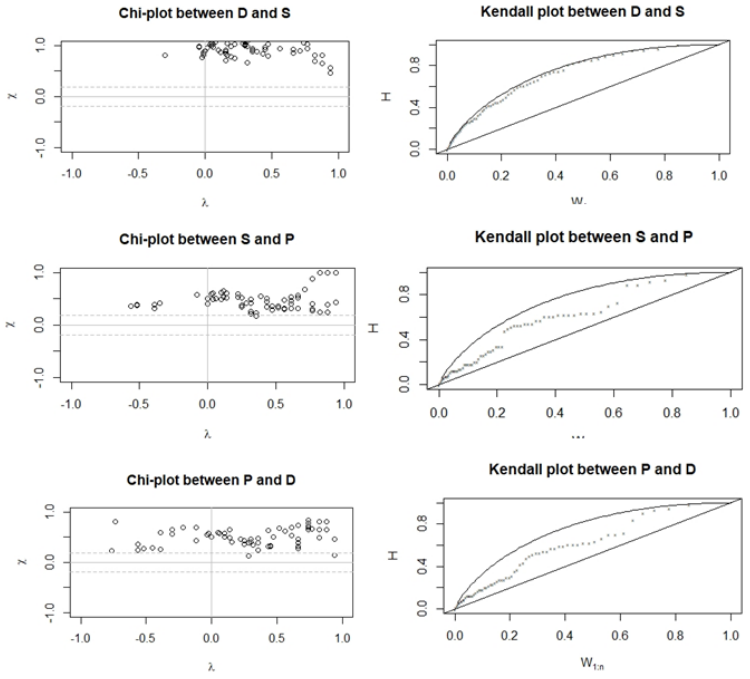

Fig. 4.25. Chi and Kendall plots of the pairwise drought characteristics D-S, S- P and P-D of NSPI for LGRB for 12-month time scale: Plots in 1st column represent the Chi-plots of pairwise characteristics and 2nd column represent the Kendall plots of the pairwise drought characteristics

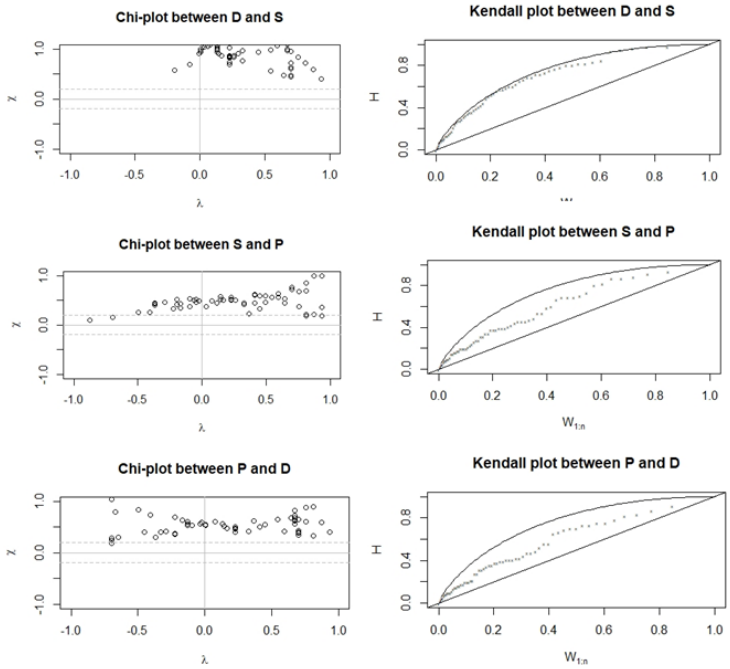

Fig. 4.26. Chi and Kendall plots of the pairwise drought characteristics D-S, S- P and P-D of NRDI for UGRB for 3-month time scale: Plots in 1st column represent the Chi-plots of pairwise characteristics and 2nd column represent the Kendall plots of the pairwise drought characteristics

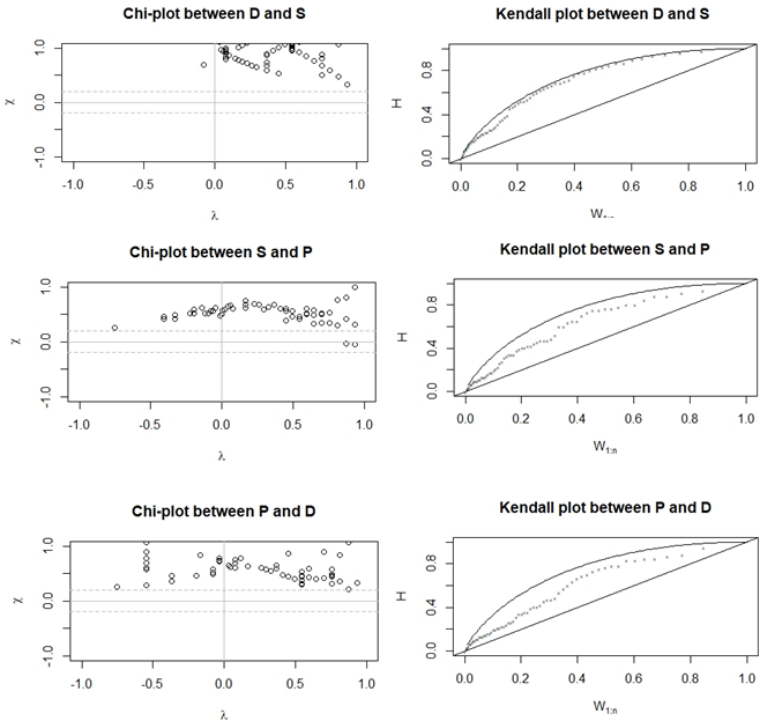

Fig. 4.27. Chi and Kendall plots of the pairwise drought characteristics D-S, S- P and P-D of NRDI for LGRB for 3-month time scale: Plots in 1st column represent the Chi-plots of pairwise characteristics and 2nd column represent the Kendall plots of the pairwise drought characteristics

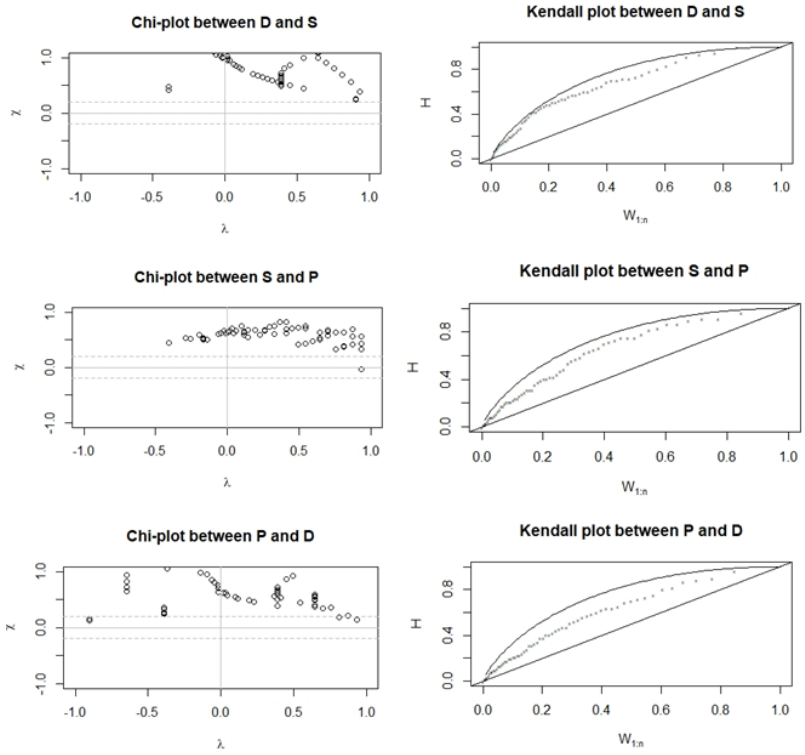

Fig. 4.28. Chi and Kendall plots of the pairwise drought characteristics D-S, S- P and P-D of NRDI for UGRB for 6-month time scale: Plots in 1st column represent the Chi-plots of pairwise characteristics and 2nd column represent the Kendall plots of the pairwise drought characteristics

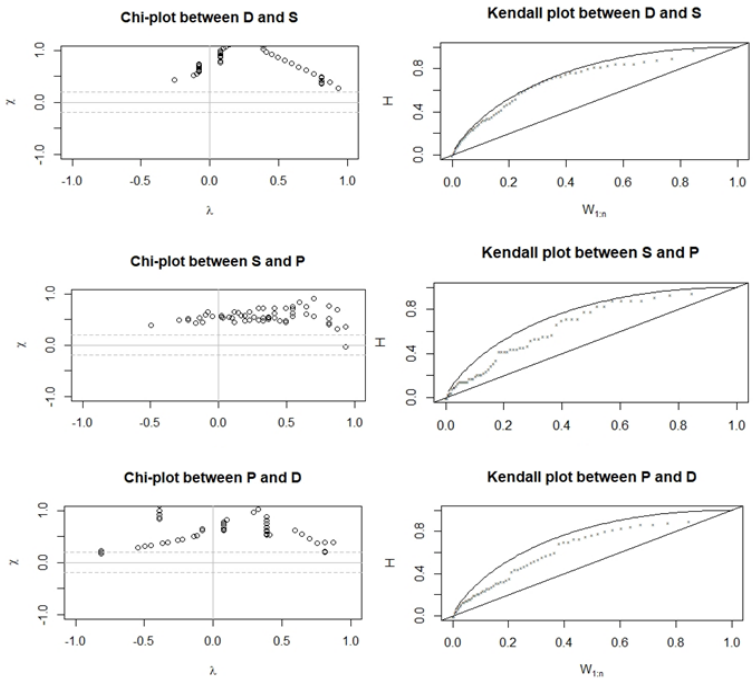

Fig. 4.29. Chi and Kendall plots of the pairwise drought characteristics D-S, S- P and P-D of NRDI for LGRB for 6-month time scale: Plots in 1st column represent the Chi-plots of pairwise characteristics and 2nd column represent the Kendall plots of the pairwise drought characteristics

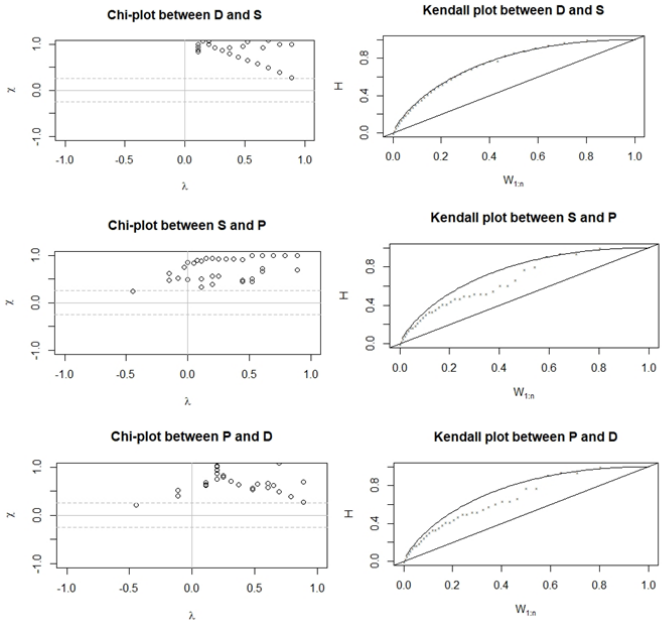

Fig. 4.30. Chi and Kendall plots of the pairwise drought characteristics D-S, S- P and P-D of NRDI for UGRB for 12-month time scale: Plots in 1st column represent the Chi-plots of pairwise characteristics and 2nd column represent the Kendall plots of the pairwise drought characteristics

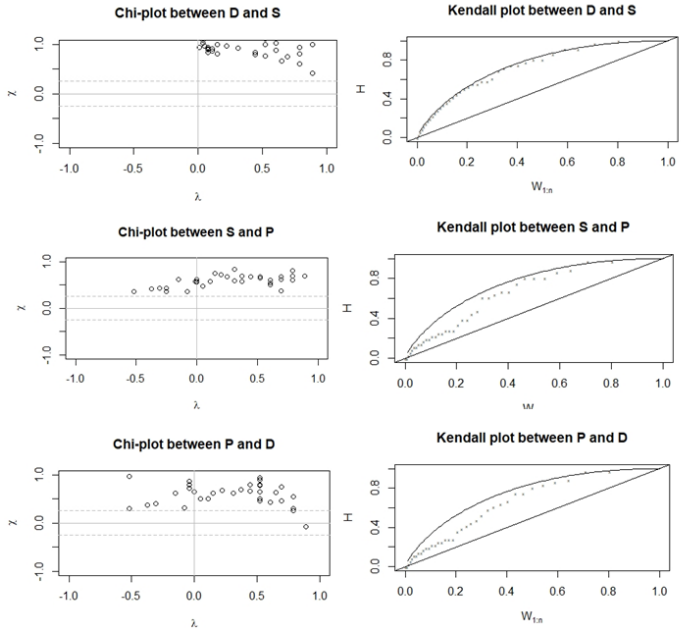

Fig. 4.31. Chi and Kendall plots of the pairwise drought characteristics D-S, S- P and P-D of NRDI for LGRB for 12-month time scale: Plots in 1st column represent the Chi-plots of pairwise characteristics and 2nd column represent the Kendall plots of the pairwise drought characteristics

4.3.8 Conclusions

The concept of non-stationarity was employed by aggregating the precipitation and initial value series with the large-scale climate indices with lag time of 0-12 months. It can be concluded that the non-stationary meteorological droughts considering the large-scale climate indices are capable of capturing the drought events in comparison with stationary drought indices. Both precipitation and evapotranspiration based non-stationary drought indices can be applied to identify more complex aspect of drought occurrence. The probabilistic estimation of drought characteristics must be carried out to estimate the recurrence intervals of droughts. The standard multivariate copulas were not flexible enough to model the higher dimensional copula for assessment of extreme events. The drawbacks of multivariate copulas can be removed using D-vine copula models. PCC model was also used to find the drought return periods. The conclusions derived for objective 2 are:

i. The non-stationary models performed better compared to the stationary models as the AIC values were lower in case of non-stationary models. UGRB, showed a significant influence at various lags for 3-, 6- and 12- month time scales. SOI, MEI and SST were the most influential large-scale covariates at different time scales.
ii. The non-stationary and stationary models showed variations in their time signals. The box plots between drought variables revealed that the drought properties significantly varied under stationary and non-stationary conditions in the both the basins for 12-month time scale.
iii. The "AND" and "OR' joint return periods for PCC models were higher compared to those obtained from the trivariate Student's t copula model for both the non-stationary models. The drought frequencies for PCC model were higher as compared to the trivariate copula model.
iv. After analysing the trivariate and PCC models, the return periods showed variations between "AND" and "OR" return periods for drought in different time scales. The variations of return periods between trivariate Student's t copula and PCC model are significant in case of 12-month time scale for both the non-stationary drought events. To summarize, the 'AND' and 'OR' return periods predicted by PCC model are more reliable compared to trivariate Student's t copula model as PCC model performed better than the trivariate Student's t copula.

4.4 Multivariate Bivariate and Trivariate Drought Assessment

The CRU precipitation and evapotranspiration data were downloaded from the site. GLDAS VIC soil moisture data was obtained from the site and then soil moisture data was gridded to CRU grids to maintain spatial uniformity. The multivariate drought indices such as MSDI and RTDI were constructed. MSDI integrates the precipitation and soil moisture while RTDI defines the integration of precipitation, soil moisture and evapotranspiration. The SPI and SSI were taken for cross comparison with MSDI. Similarly, a comparison of RDI and SSI with RTDI was carried out to identify the variations in multivariate drought conditions. Similar to SPI, the MSDI and RTDI can also have negative values, which imply the dry period. Positive values imply the wet period and the zero values of the drought refer to normal climate conditions.

4.4.1 Computation of SPI, RDI and SSI

SPI, RDI and SSI were computed by using the method discussed previously. The values of these indices lying between 0 and -0.99, -1.00 and -1.49, -1.50 and -1.8, and greater than

-1.8, define mild, moderate, severe, and extreme droughts. The negative drought index values were considered for estimation of dry events and the positive drought values were considered for wet periods. Run theory analysis was carried out in this study to characterize the drought events such as drought peak, duration and severity.

4.4.2 Bivariate dependency measurement

Dependencies between precipitation and evapotranspiration, precipitation and soil moisture and evapotranspiration- soil moisture were obtained using rank based dependency measurement techniques like Kendall's τ and Spearman's ρ rank correlation coefficients. Table 4.27 shows that best correlation was observed between precipitation and soil moisture whereas negative correlation was exhibited between both precipitation-evapotranspiration and evapotranspiration - soil moisture. However, it may be argued that the dependence pairs (precipitation -evapotranspiration and evapotranspiration- soil moisture) are not significantly positive and does not indicate that it was independent because other than normality condition, the zero correlation was similar to the dependency of parameters (Genest et al. 2007). Moreover, from a hydrological point of view, precipitation, evapotranspiration and soil moisture were dependent upon each other.

MSDI and RTDI were then developed based on the parameters obtained for the best fitted copula.

Table 4.27 Dependency measurements of precipitation-soil moisture, evapotranspiration-precipitation and evapotranspiration and soil moisture

Variable	Kendall's τ	Spearman's ρ
Precipitation and soil moisture	0.307	0.477
Evapotranspiration and precipitation	-0.123	-0.164
Evapotranspiration and soil moisture	-0.34	-0.517

4.4.3 Copula based joint probability bivariate and trivariate analysis

The bivariate model was derived using the joint probability distribution of the precipitation and soil moisture. The information on precipitation and soil moisture were combined using Frank, Gumbel and Clayton copulas. Trivariate analysis was carried out using the joint probability distribution of precipitation, soil moisture and evapotranspiration using Meta elliptical copulas (Student's t copula and Normal copula) as the process of evapotranspiration cannot be neglected from climatological point of view. The parameters of copulas were estimated using a rank-based Pseudo Likelihood Estimation (MPL). The GoF tests - S_{ks}, T_{cvm}, Ch_{sq} (for 1000 sample runs) and AIC justified the best copula for both bivariate and trivariate formulation of drought indices. The estimated parameters for copulas and their respective values are given in Table 4.28 and Table 4.29. The dependence between precipitation and soil moisture can be modelled by Frank copula since the GoF measures showed higher values and AIC showed lower values (Table 4.28). This can further be used for the computation of MSDI based on the parameters obtained from Frank copula. Table 4.29 shows the trivariate analysis modelled by Student's t copula. Though the p-value greater than 0.05 cannot be ignored in the copula formation, but in this case the best fitted copulas (Frank and Student's t copula) were selected for further analysis of MSDI and RTDI.

Table 4.28 P-values for the GoF tests - S_{ks}, T_{cvm} and Ch_{sq} for deriving 3-month and 6-month based on Gumbel, Frank and Clayton copulas using precipitation and soil moisture

3-month	Gumbel	Frank	Clayton	6-month	Gumbel	Frank	Clayton
S_{ks}	0.7	0.81	0.4	S_{ks}	0.66	0.74	0.41
Ch_{sq}	0.1	0.21	0.3	Ch_{sq}	0.19	0.46	0.3
T_{cvm}	0.5	0.9	0.2	T_{cvm}	0.36	0.27	0.29
AIC	-105.9	-117.9	-32.7	AIC	-135.87	-143.1	-63.96
θ^{PML}	1.4	3.2	0.4	θ^{PML}	1.5	3.69	0.58

Table 4.29 p-values for the GoF tests - S_{ks}, T_{cvm} and Ch_{sq} for deriving 3-month and 6-month based on Student's t copula and Normal copula using precipitation, soil moisture and evapotranspiration

3-month	Student's t	Normal	6- month	Student's t	Normal
S_{ks}	0.35	0.02	S_{ks}	0.26	0.25
Ch_{sq}	0.4	0.39	Ch_{sq}	0.41	0.4
T_{cvm}	0.46	0.31	T_{cvm}	0.28	0.11
AIC	-272.8	-149.16	AIC	-277.31	-189.52
θ^{PML}	0.55	0.54	θ^{PML}	0.54	0.54

4.4.4 Spatial variation of drought severities

For spatial distribution of drought severities in the region, the inverse distance weighting interpolation (IDW) method was implemented for interpolating the maximum drought severities at each station, subsequently, the distribution of the spatial map of the study area were obtained. Furthermore, the spatial distribution of drought severities of MSDI and RTDI were compared in Fig. 4.32. Based on Fig. 4.32, during 1971 to 2017, the maximum drought was high in central to western part of the region while, a lower drought severity was observed in the eastern part of the basin. The eastern part of the basin belongs to the low- drought incidence area. After comparing MSDI-3 and MSDI-6, it was observed that the areal extent of MSDI-6 was larger than MSDI-3 in the western part of the basin. Similarly, severities of RTDI-6 showed larger areal extent compared to severities of RTDI-3 throughout western part of the region. When comparing MSDI and RTDI, it was observed that drought severities of RTDI-6 showed severe-most events compared to other indices for different time scales. Furthermore, the western part of the basin was recognized as the region with the highest drought severities.

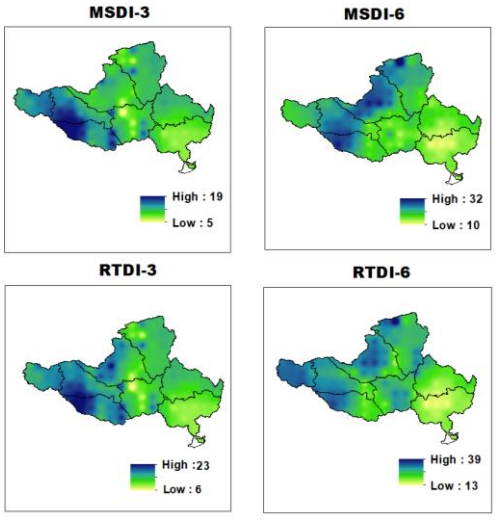

Fig 4.32. Maximum drought severities of MSDI and RTDI

4.4.5 Comparison between SPI, SSI and MSDI

SPI shows the behaviour of meteorological drought which has a faster onset and offset of drought behaviour. SSI is used for the agricultural drought which depends on the temperature, soil characteristics and soil groups dominant in the particular area. The combination of SPI, SSI and MSDI can be understood in a better way by dividing the whole time series into two parts, viz. (1981-1999, and 2000-2017). However, perfect correlations may not exist between SPI, SSI and MSDI, but they may follow the similar drought evolution pattern. Fig. 4.33(a) shows that some there are some signals which showed agreements and some which showed disagreements between SPI, SSI and MSDI. SSI-3 showed a moderate drought condition in April 1987 while MSDI showed an extreme drought condition for the same time period. October-1986 showed a severity in drought behaviour with respect to SPI-3, SSI-3 and MSDI-3. More fluctuations in drought signals occurred in the 3-month MSDI time series. It can be observed that the 3-month MSDI and SSI drought condition continued from September 1996 to May 1998 from the Fig. 4.33 (a). For the period from 2001 to 2010, the SPI-3 showed recovery from drought when compared to SSI-3 and MSDI-3. The negative values that indicated that the drought continued from the year 2011 to 2013, whereas wet events continued between September 2013 and September 2014. Severe drought conditions were observed again in the year June 2015-2016. It can be seen that the MSDI showed combined effect of SPI and SSI.

In the time window of 1981-1999, SSI-6 showed early recovery of drought when compared to SPI-6 while the MSDI-6 showed higher negative drought trend when compared to SSI and SPI. Severe drought was observed during May 1985 since both the precipitation and soil moisture had negative trend and as a result of this, the MSDI-6 showed a severe drought condition (a combination of SPI and SSI). The SPI-6 showed moderate drought condition whereas MSDI-6 showed severe drought conditions during the period January 1992 to May 1992 and May 1997 to September 1997. SPI-6 showed that most of the drought signals were having positively trending values, while SSI-6 showed most of the signals have negative drought conditions for the time period 2001-2010. MSDI-6 showed peak drought conditions from May to September 2001 and January to May 2005. The severity of drought can clearly be noticed during May 2012, April 2013 to May 2013 and December 2015 for MSDI-6 whereas SPI-6 showed moderate drought conditions. It is evident that when the drought time scale increased from 3-month to 6-

month, less difference in drought trend is observed between SPI and SSI, whereas the MSDI showed more fluctuating drought conditions.

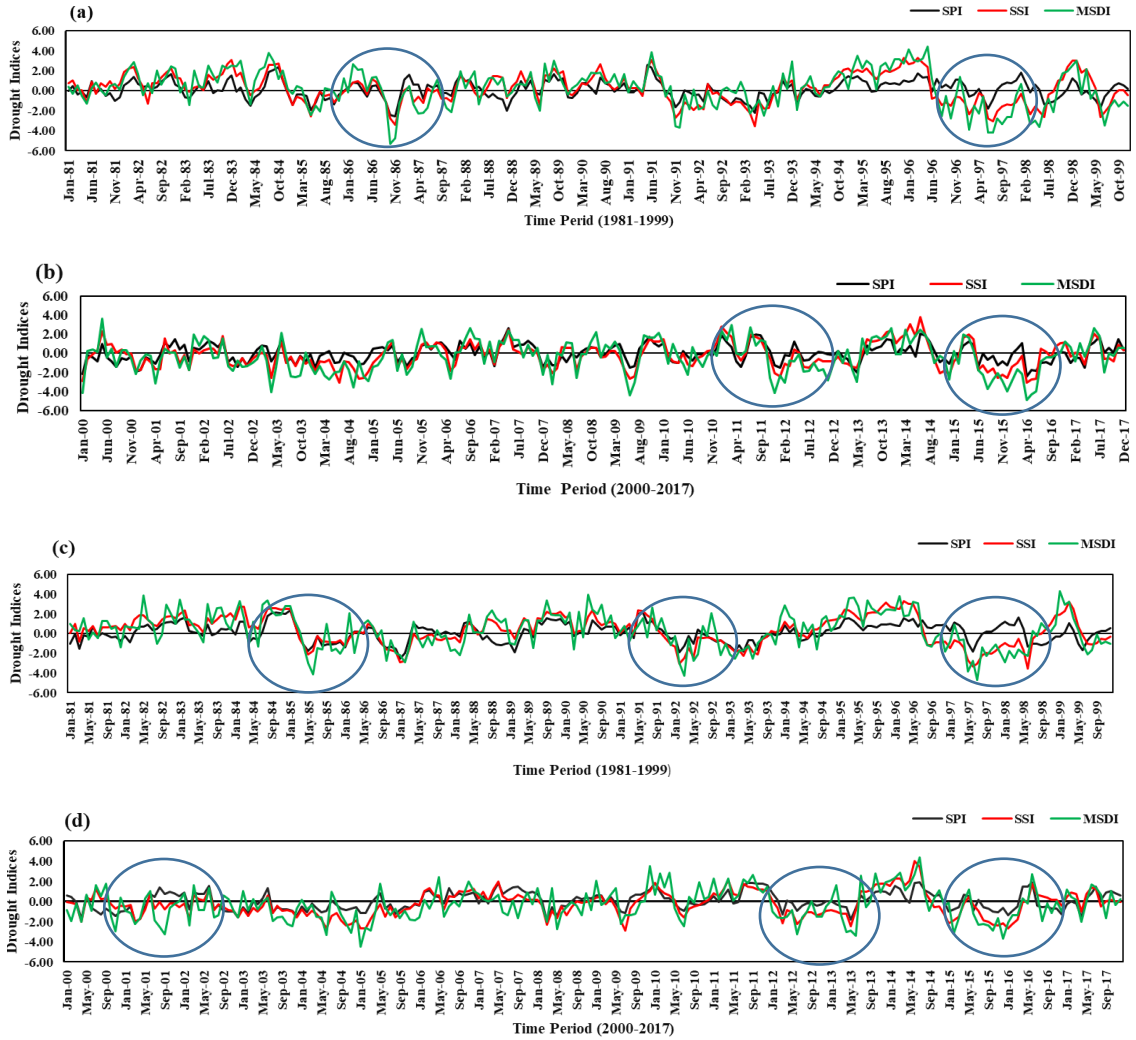

Fig. 4.33. Comparisons of SPI, SSI and MSDI for 3-month and 6-month time scale; (a) 3-month time scales during the time window 1981-1999; (b) 3-month time scales during the time window 2000-2017; (c) 6-month time scales during the time window 1981-1999; (d)6-month time scales during the time window 2000-2017

4.4.6 Comparison of RDI, SSI and RTDI

The RTDI is compared with RDI and SSI. RDI was chosen because it gave combined drought information of precipitation and evapotranspiration. Precipitation alone cannot be used for the detection of drought. The RDI-3 and SSI-3 are generally consistent but discontinuity was also observed between time signals. It can be observed from Fig 4.34 (a), that the time signals showed that positive and negative drought signals were different. For example, May 1998 showed a positive trend in RDI-3 and a negative trend for SSI-3. Ultimately, a negative RTDI-3 emerged in this case. If the average rainfall is more and

evapotranspiration is less (RDI>0) and the soil moisture was dry (SSI<0) for that period of time, then the combination of the three variables (RTDI) can create a negative drought trend (RTDI <0). For a 3-month time scale, the drought duration of RTDI signals was similar to SSI. The severity aspect of drought must not be neglected in this circumstance. During the years 1981 to1999, it can be observed that SSI showed more negative drought trends than RDI. So, RTDI showed a drought event whichever was lower between RDI and SSI. The peak drought was seen in May 1984, April 1985, and September 2016 for RTDI-3. However, the extremely dry months for RDI were May 1985, December 2000, January 2001 and May 2014 and for SSI, they were for the periods of June 1980, March 1987, August to November 1997, January to May 1998. May 2006.

The initial drought was captured by RTDI-6 as shown in Fig. 4.34 (c). The drought peaks were more prominent in RTDI-6 as compared to RDI-6 and SSI-6. In January 1986, it was observed that negative signals of drought were captured for both RDI-6 and SSI-6. So, the RTDI-6 also followed these negative trends of the drought indices. For the year 2016, negative drought effect of RTDI was identified due to the combined effects of the RDI and SSI. RTDI captured drought earlier than SSI and RDI. In most of the cases, the drought condition was captured well for RTDI and SSI whereas RDI was not efficient in capturing the dry events in the chosen 38 years of time frame. The drought duration and severity of the drought were different for RDI-6, SSI-6 and RTDI-6. The drought was more severe in the case of RTDI-6.

4.4.7 Comparison between MSDI and RTDI

MSDI and RTDI have been estimated using copula functions for 3, 6- month time scales during the period 1981–2017. Here the hypothesis contained a comparison between MSDI and RTDI for better understanding of droughts based on different climatic parameters. Similar evolution pattern between MSDI and RTDI was observed during the period 1981-1999 (Fig. 4.35(a)). After analysing the data, it can be observed that there was an agreement and disagreement of drought signals between the MSDI and RTDI. Further, soil moisture anomaly status can influence the drought persistence and continuity between MSDI and RTDI. For example, an agreement between signals were visible in the time period of (1991-1992) and disagreements of time signals were visible in the time period of (1984-1985). Moreover, the onset and offset of drought events for MSDI and RTDI were different. So there is a probability that the drought characteristics must be different for these two indices. For example, RTDI-3 conveyed a severe drought condition

in September 1985, whereas MSDI-3 showed a mild drought phenomenon. September 2004 and 2011 showed severe drought conditions for MSDI-3 and RTDI-3. So, the drought indices showed consistency with each other. It is evident that the 3-month drought signals displayed more variations when compared to 6-months drought signals. For example, January 1986 showed severity drought pattern for MSDI-6 and RTDI-6. More consistency between signals were observed in the case of 6-month MSDI and RTDI as seen from Fig. 4.35(c) and Fig. 4.35(d).

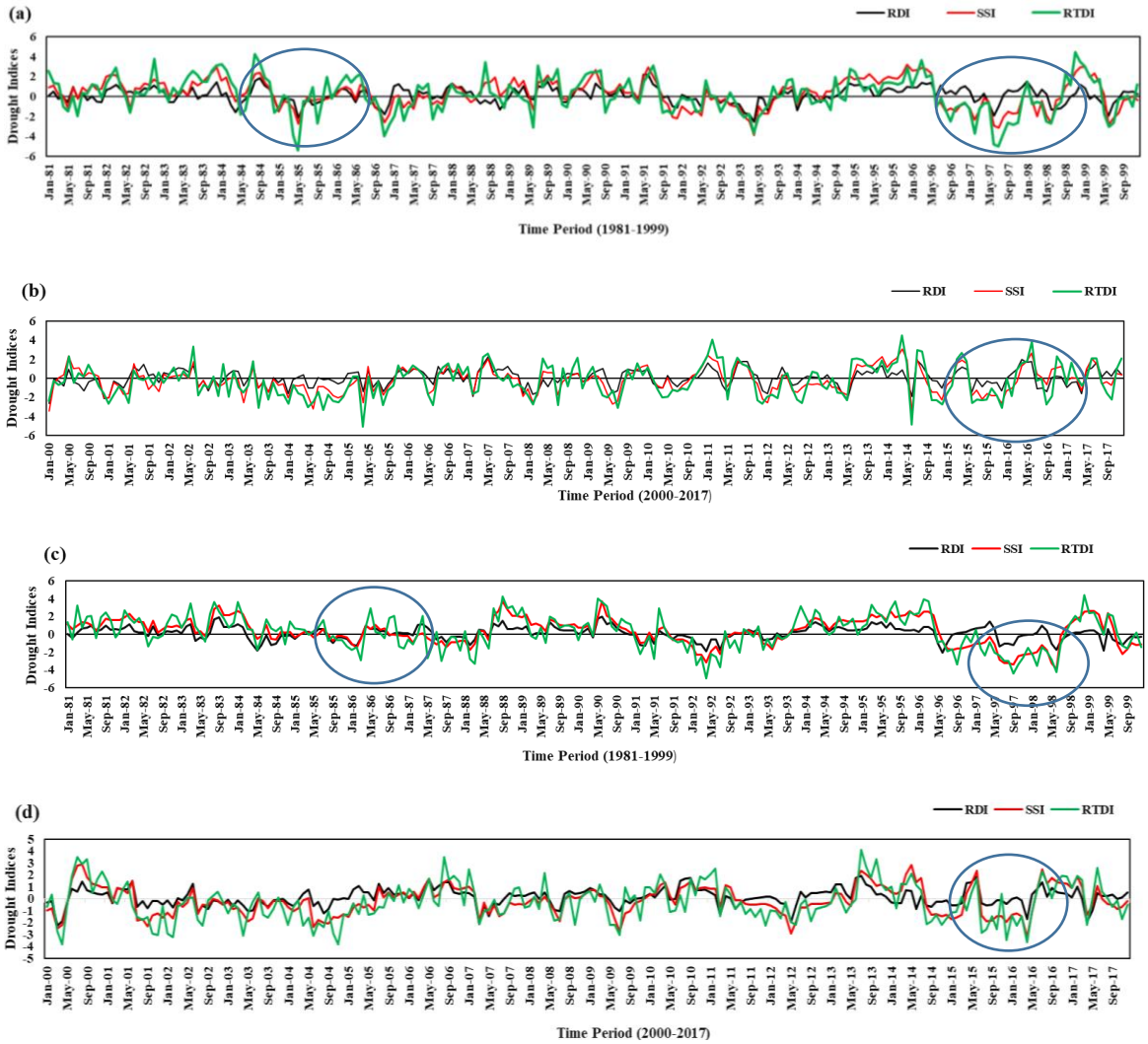

Fig. 4.34. Comparisons of RDI, SSI and RTDI for 3-month and 6-month time scale. (a) represents 3-month time scales during the time window 1981-1991; (b) represents 3-month time scales during the time window 2000-2017; (c) represents 6-month time scales during the time window 1981-1991; (d) represents 6-month time scales during the time window 2000-2017.

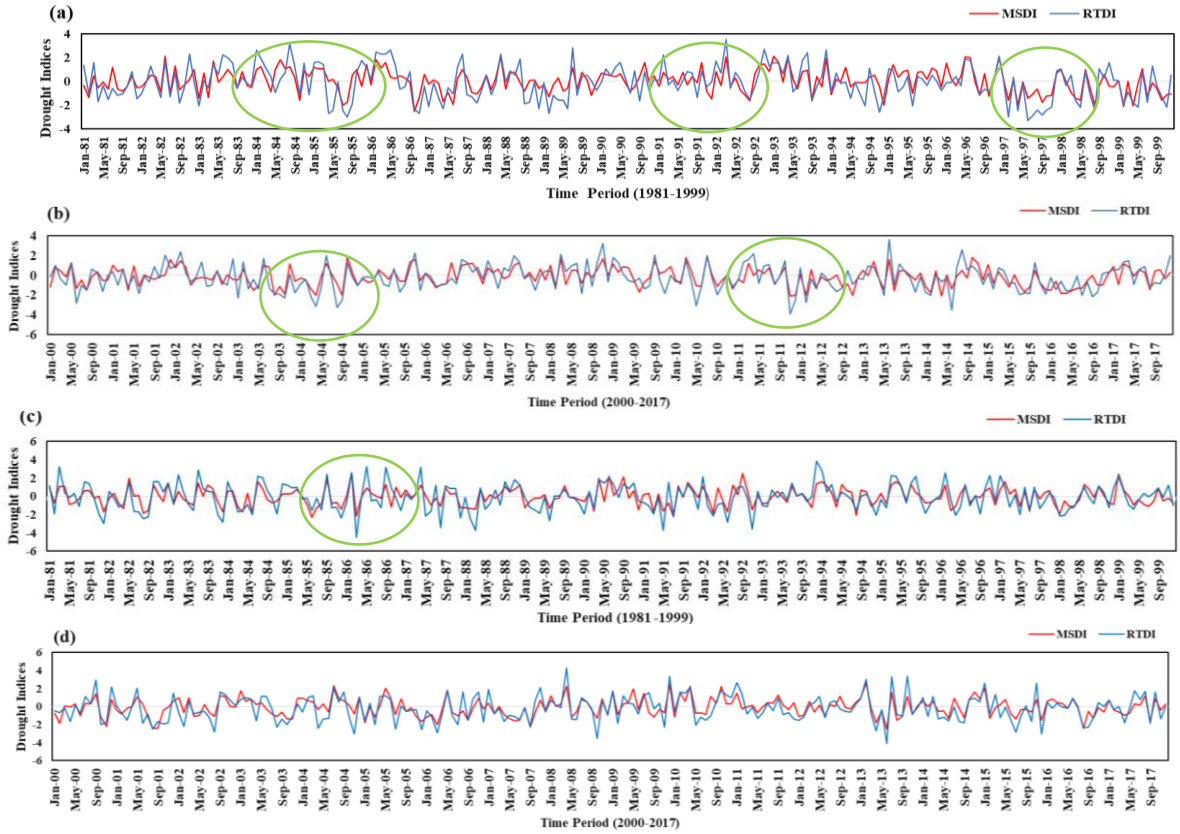

Fig. 4.35 Comparisons of MSDI and RTDI for 3-month and 6-month time scale. (a) represents 3-month time scales during the time window 1981-1999; (b) represents 3-month time scales during the time window 2000-2017; (c) represents 6-month time scales during the time window 1981-1999; (d) represents 6-month time scales during the time window 2000-2017.

4.4.8 Teleconnection between MSDI and RTDI with large scale climate indices

The study focussed on the effect of ENSO events, IOD and ISMR on MSDI and RTDI (3 and 6-month) for the GRB. The teleconnection between the MSDI and RTDI climate indices with ENSO events, IOD and ISMR will be helpful for understanding the variability of meteorological and agricultural drought. Hence, Cross Wavelet Analysis (CWA) was implemented in this study for investigation of the association among drought indices and large-scale climate indices. The wavelet coherences between monthly MSDI and RTDI with climate indices (MEI/SST/SOI/IOD/ISMR) in the region are illustrated in Fig. 4.36 and Fig. 4.37 respectively for 3-month time scale for the time period of 1981-2015. For 6-month time scale MSDI and RTDI are represented in Fig. 4.38 and Fig. 4.39 respectively. The energy densities are represented by the colour bars. The arrows represent the phase relationship. The arrows pointing left show anti-phase relationship while the

right pointed arrows define in-phase relationship and the 95% confidence level against red noise is given as a thick contour. Fig 4.36 (a) displays correlation pattern with MEI signals during 1991-1998 and 2013-2011. It can be observed from Fig. 4.36 (b) that the SOI signals showed a strong coherence pattern with MSDI-3 during the periods 1988-1998 and 2012-2015 in the basin. Fig. 4.36 (c) display correlation of SST with drought signals (MSDI-3) during 1991-2007 whereas IOD exhibited a significant correlation with MSDI-3 during 1981-1985, 1988-1994 and 2011-2015 represented in Fig. 4.36(d). Fig. 4.36(e) show that ISMR has a strong correlation with MSDI-3. ISMR displayed a strongest teleconnection pattern with MSDI-3 among all the large-scale climate indices.

The RTDI-3 showed teleconnections with MEI and SOI as can be observed from Fig. 4.37 (a) and Fig. 4.37 (b). In Fig. 4.37 (b), SOI showed a statically significant coherence with RTDI-3 during 1992-1997 and 2010-2015 at the 95% significance level. For RTDI-3, the teleconnections with SST were observed in Fig 4.37(c). The most evident teleconnection with SST and RTDI-3 was observed during the period 2006-2015 and SST confirmed a strongest correlation pattern with RTDI-3, when compared to other climate indices. IOD also demonstrated a strong teleconnection pattern with RTDI-3 during 1983-1990 and 2013-2015 illustrated in Fig. 4.37 (d). As given in Fig. 4.37 (e), the ISMR signals showed a fairly good association with RTDI-3 series. The coherence patterns of MSDI-6 and large-scale climate indices are given in Fig. 4.38(a) to Fig. 4.38(e). It can be seen that MEI exhibited a statistically significant teleconnection with MSDI-6 during 1988-2010 at 95% significance level as seen in Fig. 4.38(a). From Fig. 4.38(c), the strongest correlation was identified between the MSDI-6 and SST signals. The SOI, IOD and ISMR showed fairly good correlation with MSDI-6 drought events in the region. Fig. 4.39(a) describes a good correlation of RTDI-6 with MEI during 1981-2001 and 2011-2015. RTDI-6 also exhibited a good teleconnection with SOI, SST, IOD and ISMR. From the Fig. 4.39(c) and Fig. 4.39(e), it can be confirmed that the RTDI-6 showed a significant and strong correlations with SST and ISMR. Hence it can be concluded based on the observations from CWA that SST and ISMR emerged as the most significant indices which can impact the meteorological and agricultural droughts in this region. These are reflected in the variations of MSDI and RTDI, which have been developed in the study.

4.4.9 Conclusions

The integration of agricultural and meteorological drought plays a vital role in the prediction and reliable monitoring of drought. In this study, copula based MSDI and RTDI

were developed for a clear representation of meteorological and agricultural features of drought in the hydrological process.

From the study, it is observed that MSDI and RTDI are important for capturing a quantitative and qualitative drought which consists of both agricultural and meteorological drought occurrences to examine the evolution of drought phenomenon.

These indices are applied to study the drought in the GRB. Further, copula analysis showed that the parameters of Frank copula can be used for obtaining the MSDI while Student's t-copula can used for obtaining RTDI.

The resultant MSDI and RTDI are based on the joint probability cumulative distribution function whose sensitivity towards capturing the persistence, onset, and termination of drought is more prominent than SPI, RDI and SSI. This can help in understanding the real-time spatial as well as temporal drought mechanism. It also can help in early detection of drought condition rather than SPI, RDI and SSI.

The MSDI and RTDI exhibited comparable performance when compared to the corresponding SPI and RDI, and it is more sensitive to capturing the onset, persistence, and termination of droughts.

CWA was performed in this study to identify the teleconnections between large scale climate indices and the drought events. CWA showed MSDI and RTDI (3- and 6-month) had been significantly influenced by ENSO, IOD and ISMR patterns. Among all the climate indices, ISMR showed a strong and effective association with MSDI-3 whereas SST showed strong teleconnection with RTDI-3. Additionally, SST had strong influence on MSDI-6, while RTDI-6 showed a strong association with SST and ISMR signals. So, it can be suggested that the ENSO events, IOD and ISMR play a major role in drought variability over the basin.

MSDI and RTDI can capture the meteorological and agricultural drought variability detecting the onset and termination of droughts. These multivariate drought indices will be beneficial in deeper understanding of the drought mechanisms and further enhance the drought monitoring technology. Overall, the study showed the teleconnection of MSDI and RTDI with large scale climate indices can be potentially used for drought monitoring and assessment under the climate variability in India.

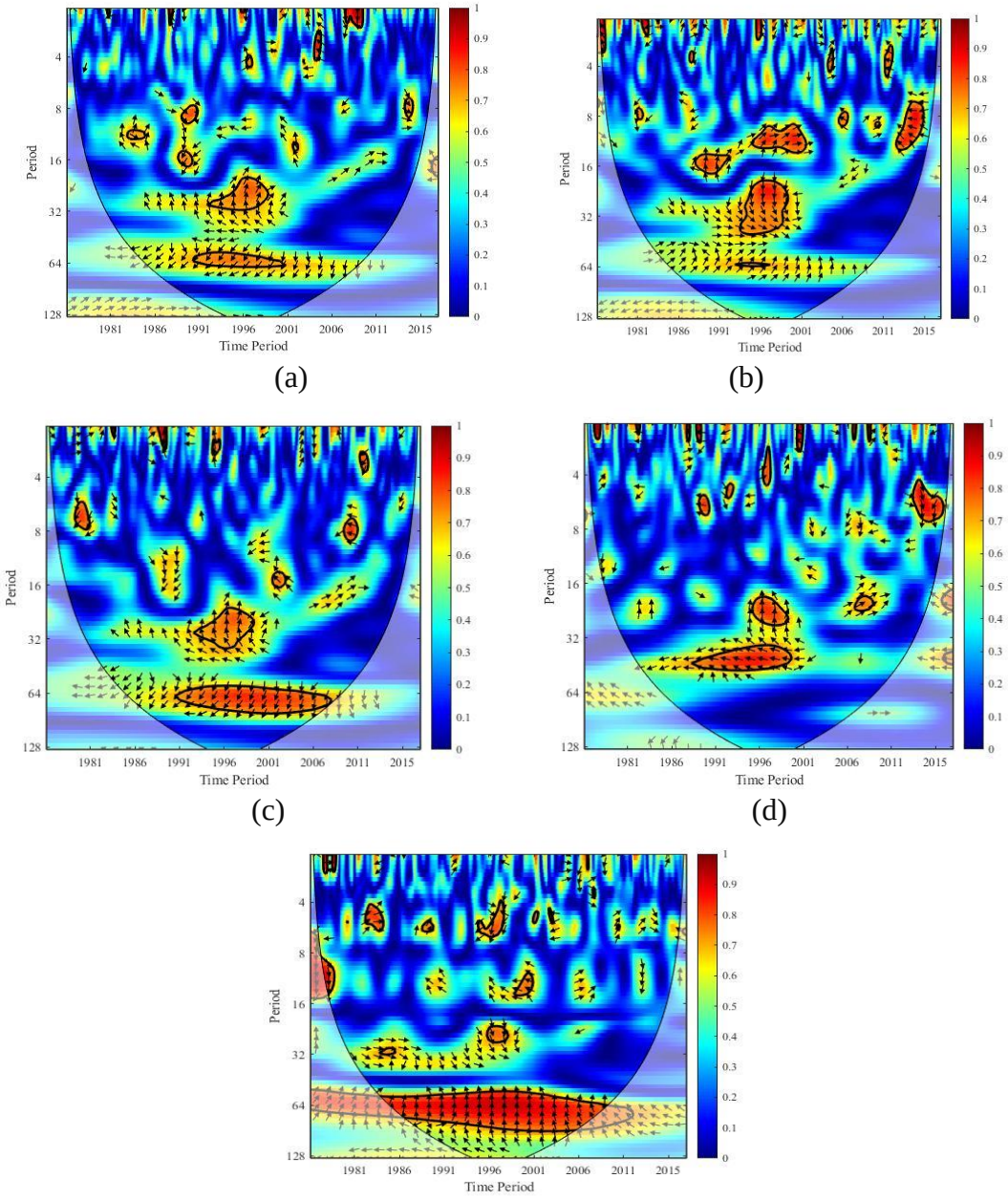

Fig. 4.36. The wavelet coherences between MSDI and large-scale climate indices for 3-month time scale. (a)-(c) wavelet coherences between MSDI and MEI/SOI/SST; (d)-(e) wavelet coherences between MSDI and IOD/ISMR.

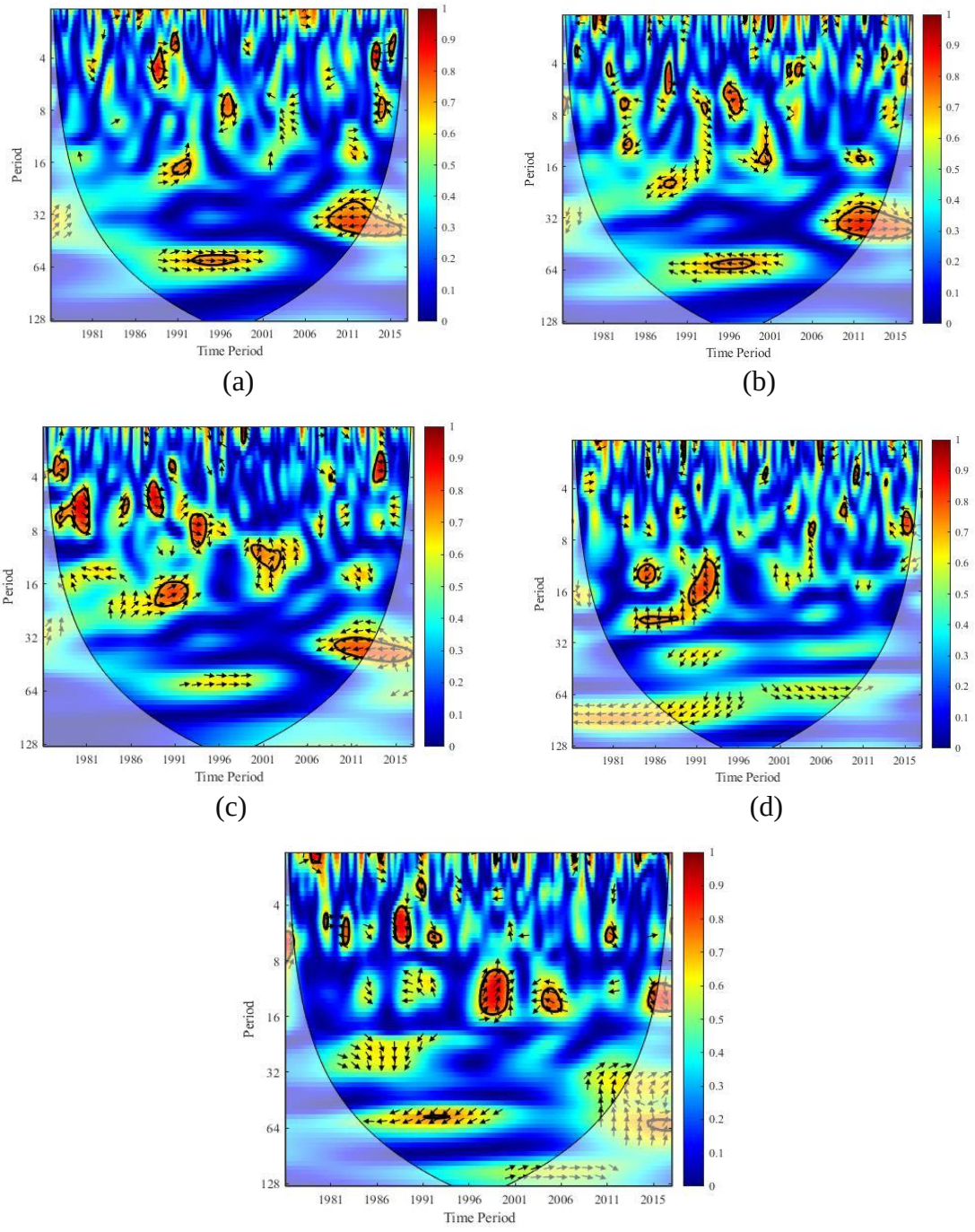

(a) (b) (c) (d) (e)

Fig. 4.37. Wavelet coherences between RTDI and large-scale climate indices for 3-month time scale; (a) -(c) wavelet coherences between RTDI and MEI/SOI/SST; (d)-(e) wavelet coherences between RTDI and IOD/ISMR.

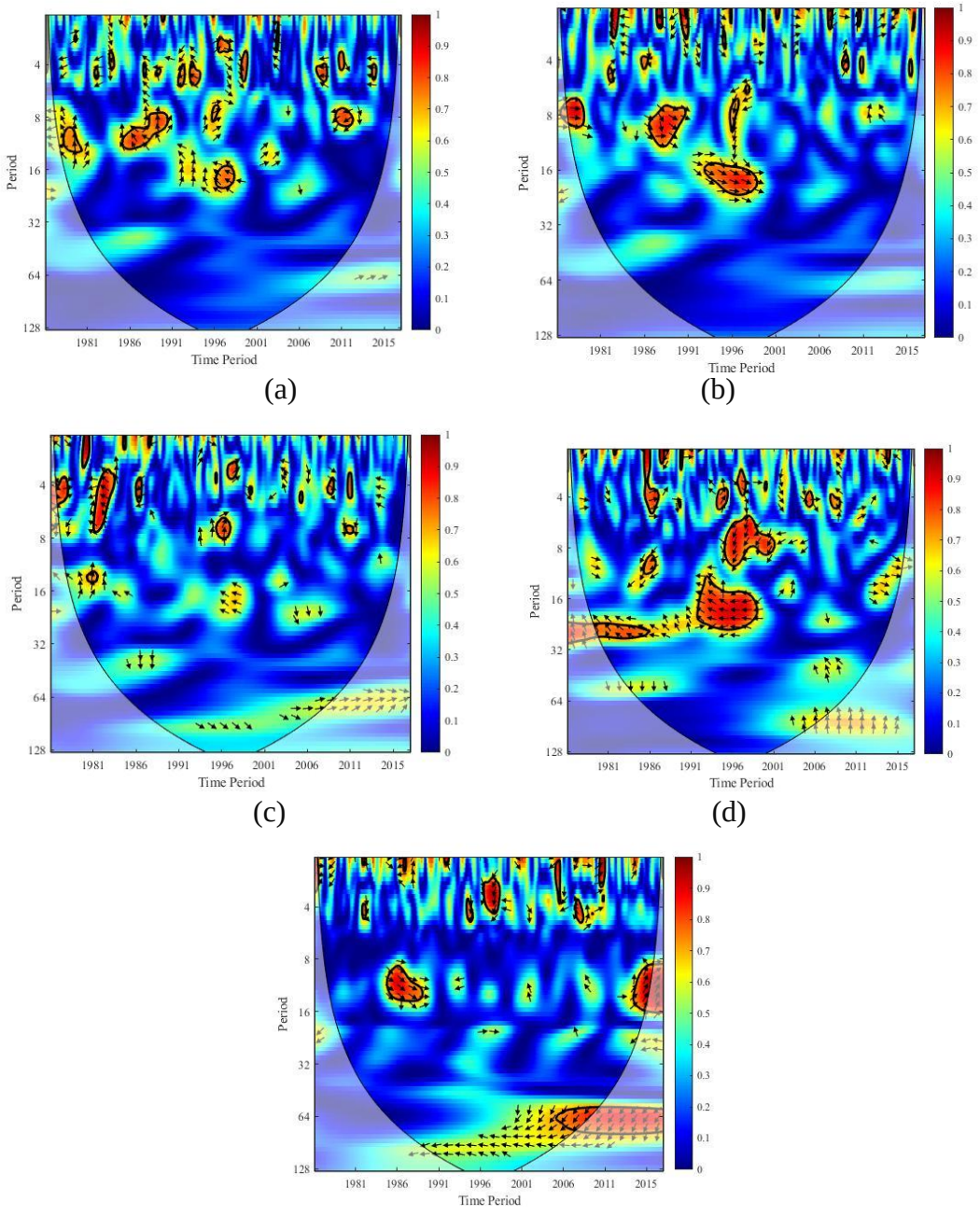

Fig. 4.38. Wavelet coherences between MSDI and large-scale climate indices for 6-month time scale. (a) -(c) wavelet coherences between MSDI and MEI/SOI/SST; (d) - (e) wavelet coherences between MSDI and IOD/ISMR.

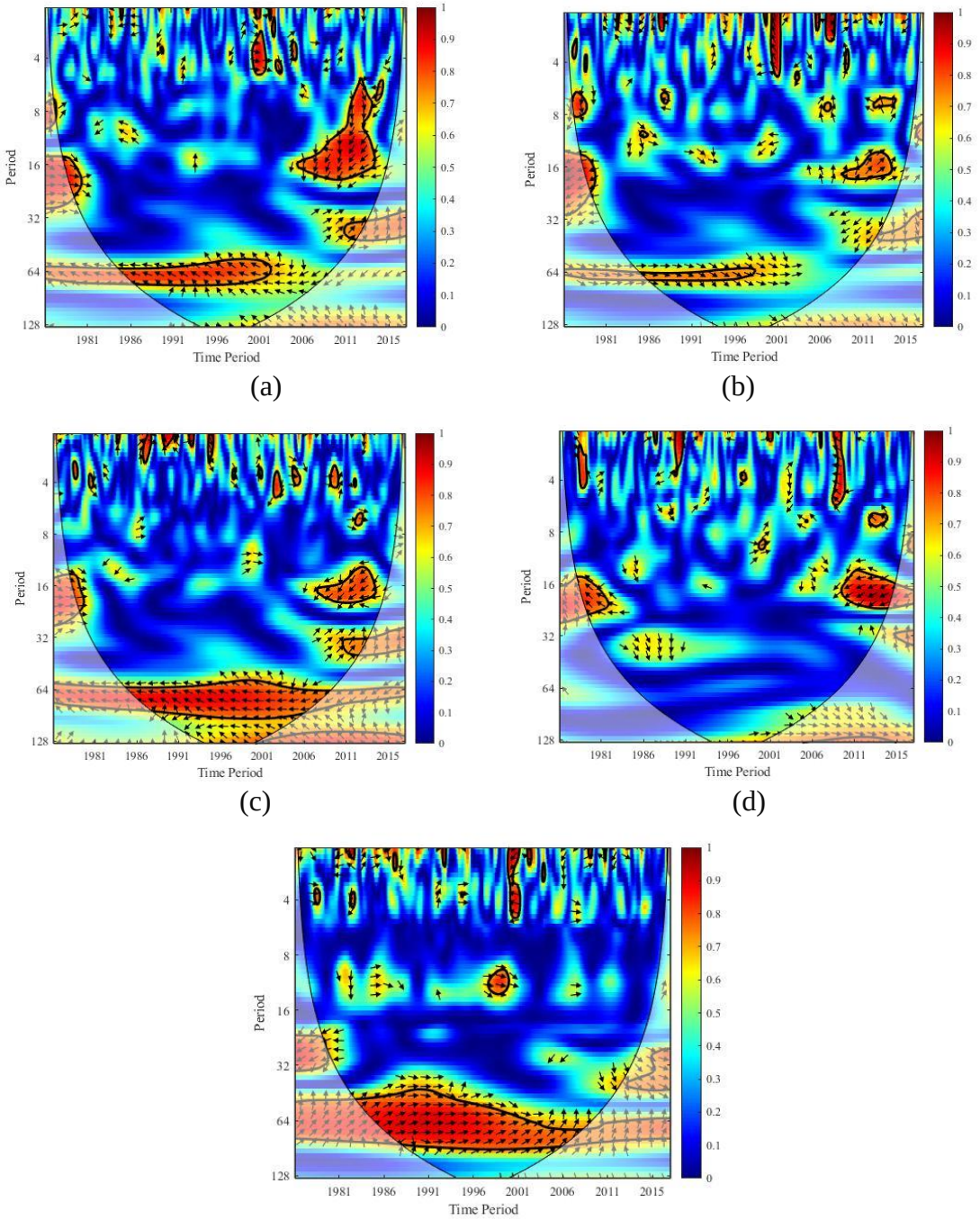

Fig. 4.39. Wavelet coherences between RTDI and large-scale climate indices for 6-month time scale; (a) -(c) wavelet coherences between RTDI and MEI/SOI/SST; (d) - (e) represent the wavelet coherences between RTDI and IOD/ISMR.

4.5 Impact of Climate Change on Multivariate Drought

IMD precipitation, minimum and maximum temperature data of resolution 0.25x0.25 were downloaded from the site. SWAT model was calibrated and validated based on streamflow observations for WRB and IRB. The future water balance components were estimated based on

the ensemble bias corrected CMIP6-GCM. Then the water balance components like evapotranspiration, soil moisture and streamflow variables were obtained from the model for future and historical period. Further, MDI was constructed considering precipitation and SWAT simulated variables for both reference and future periods. Drought characteristics were then compared to detect the changes in different scenarios.

4.5.1 Calibration and validation of SWAT

Sensitive analysis is essential for identifying the most sensitive key parameters, which can accurately calibrate the model. Redundant parameters during calibration process can be reduced by sensitivity analysis. Selected parameters were auto calibrated and validated using SUFI2 optimization algorithm in the SWAT-CUP (Arnold, 2012). Parameter ranges were initialized and then the uncertainties were reduced by optimizing these ranges using SUFI2 algorithm that can be quantified through 95% prediction uncertainty (95PPU) bands. After calibration, parameters were updated in SWAT-CUP with new parameter values obtained from the best simulation. The parameters used for calibration and validation and fitted parameters are presented in Table 4.30 and Table 4.31 for WRB and IRB respectively. Then, the model was validated using newly obtained parameters for the particular validation periods. Model performance criteria like coefficient of determination (R^2), PBIAS (Percentage Bias), Nash-Sutcliffe Efficiency (NSE) (Nash and Sutcliff, 1970), R- and P-factor were employed to analyse the performance status of the model. The 95PPU band indicated that the simulated streamflows were well captured at Pathagudem and Ashti outlet points (Fig. 4.40). The NSE, R^2, PBIAS, R and P-factor for calibration and validation for both the basins are presented in Table 4.32. The performance statistics of WRB and IRB watershed models indicated that observed streamflows were well simulated and the peaks and troughs were well captured by the simulated streamflows. The calibrated model was then simulated using gridded ensemble mean GCM data for the period between 1920 and 2100 by considering 5 years of warm-up period. Four future SSP scenarios have been considered in this study by dividing the time period into future1 (2025-2062) and future2 (2063-2100). The drought condition during the baseline period (1976-2013) was then compared to the future projections.

Table 4.30 Calibrated parameters of Wainganga (Ashti)
(*R denotes replaced parameter and V denotes relative parameter)

Parameter*	Fitted Value	Min value	Max value
R__CN2.mgt	0.1	-0.2	0.2
V__ALPHA_BF.gw	0.5	0	1
V__GW_DELAY.gw	17.1	0	450
V__GWQMN.gw	715.3	0	1000
V__OV_N.hru	0.1	0	1
V__EPCO.hru	0.5	0	1
V__CH_K2.rte	15.1	0	100
V__CH_N2.rte	0.1	0	0.3
V__CH_K1.sub	3.8	0	300
V__CH_N1.sub	12.6	0	30
V__ESCO.hru	0.2	0	1
V__REVAPMN.gw	329	0	500
R__SOL_K(..).sol	0.1	-0.2	0.2
R__SOL_AWC(..).sol	-0.1	-0.2	0.2
R__SOL_BD(..).sol	0	-0.2	0.2
R__SOL_Z(..).sol	0.1	-0.2	0.2
V__GW_REVAP.gw	0.1	0	0.2
V__CANMX.hru	65	0	100
V__RCHRG_DP.gw	0.7	0	1
V__SURLAG.bsn	8	0.1	24

Table 4.31 Calibrated parameters of streamflow of Indravati (Pathagudem)
(*R denotes replaced parameter and V denotes relative parameter)

Parameter	Fitted value	Min	Max
R__CN2.mgt	0.149	-0.2	0.2
V__ALPHA_BF.gw	0.9975	0	1
A__GW_DELAY.gw	151.875	0	450
V__GW_REVAP.gw	0.08525	0.02	0.2
A__GWQMN.gw	707.5	0	1000
A__REVAPMN.gw	233.75	0	500
V__ESCO.hru	0.0825	0	1
R__SOL_AWC(..).sol	0.113	-0.2	0.2
V__EPCO.hru	0.7175	0	1
R__SOL_K(..).sol	-0.2	-0.2	-0.2
R__SOL_Z(..).sol	0.143	-0.2	0.2
R__SOL_BD(..).sol	0.141	-0.2	0.2
V__CH_N2.rte	0.20625	0	0.3
V__CH_K2.rte	36.54087	0.05	200
V__CANMX.hru	9.75	0	100
R__CH_N1.sub	10.35	0	20
R__CH_K1.sub	58.75	0	100

Table 4.32 Performance evaluation SWAT model calibration and validation of IRB and WRB

Pathagudem	P-factor	R-factor	PBIAS	R^2	NSE
Calibration	0.54	0.56	-15	0.88	0.89
Validation	0.68	0.70	-9	0.93	0.94
Ashti					
Calibration	0.51	0.74	-17	0.86	0.82
Validation	0.58	0.81	-13	0.94	0.93

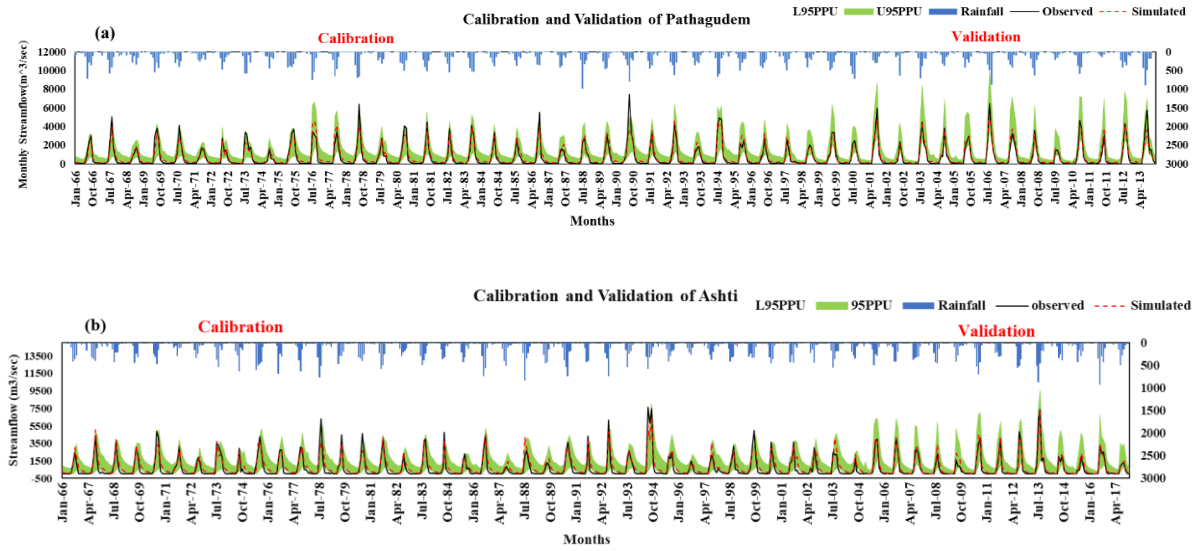

Fig. 4.40 (a) 95 PPU plot for Indravati basin; (b) 95 PPU plot for Wainganga basin

4.5.2 Projected changes in annual mean precipitation, and maximum and minimum temperatures

MDI will be highly influenced by the changes in precipitation, evapotranspiration, streamflow and soil moisture for the sub-basins. So, the variation in the climatic pattern need to be investigated. The spatial distributions of projected changes in ensemble averaged precipitation, maximum and minimum temperature under four SSPs are given in Fig. 4.41 (a) to 4.41 (f). The spatial distributions of mean annual % changes in precipitation, minimum and maximum temperatures are presented in Fig. 4.42 (a) to Fig. 4.42 (f). For IRB and WRB, there will be an increased annual mean precipitation for future period with respect to the reference period. The spatial dispersion of WRB and IRB are similar to the reference climate under four scenarios. There will also be an increase in the areal extension of precipitation over WRB and IRB. The spatial pattern of mean annual precipitation over WRB under all SSPs revealed that the projected precipitation significantly will increase in the south-eastern part of WRB under all the SSP scenarios as can be seen in Fig. 4.41 (a). For the future 1 period, the projected annual mean precipitation over WRB is likely to increase by 4 to 18%, -10 to 14 %, 10 to 27% and 14 to 27% under SSP126, SSP245, SSP370 and SSP585 respectively. Similarly, for future 2 period, the mean

annual precipitation over WRB is likely to increase by 13 to 30%, 15 to 32%, 16 to 35 % and 21 to 37% under SSP126, SSP245, SSP370 and SSP585, respectively presented in the Fig.4.42 (a). A major change is expected in projected annual mean precipitation over the northern part of WRB. For the rest of the WRB, a steady change for future1 and future 2 period under all the SSP scenarios is expected.

Spatial plot of IRB shown in Fig. 4.41 (b) suggests that the annual mean precipitation will be high in the southern parts whereas in the north-eastern region, the annual mean precipitation will be low. The areal extent of precipitation will increase for all future scenarios. Simulation from future1 showed that mean annual precipitation will increase by 12 to 20%, -5 to 13%, 10 to 24% and 8 to 27 % under the four scenarios. The mean annual precipitation will have significant increments of 10 to 27%, 11 to 29%, 15 to 29% and 20 to 35% in future 2 under the four scenarios for IRB (Fig. 4.42 (b)). It can, hence, be concluded that the large increase in the projected mean annual precipitation over WRB and IRB is expected to occur under SSP585 scenario in future 2 period. In future 2 also, an increase in the projected annual mean annual precipitation can be expected over both the basins.

The projected changes in the annual mean maximum and minimum temperature over WRB and IRB showed spatial variability when compared to the reference period. The analysis of spatial plots for mean annual maximum and minimum temperature showed that the northern part of WRB showed lower temperature, while the southern parts of the basin showed higher annual maximum and minimum temperature under all scenarios (Fig 4.41 (c)). The western parts of the IRB will experience an increase in annual mean maximum temperature for the future scenarios while the mean annual minimum temperature will have an increasing pattern over south-eastern part of the basin (Fig 4.41(d)). During future1 scenario, the projected mean annual maximum temperature over WRB is expected to show significant variation ranging from -0.8 to 1.8 °C, 0 to 2 °C, -0.7 to 2 °C and -0.04 to 2.1 °C and for future 2 scenario, the variations will be in ranges of -0.4 to 2°C, 0.1 to 2.5°C, 1 to 4 °C and 2.8 to 4 °C under the four SSP scenarios respectively (Fig. 4.42 (c)). On the other hand, the mean annual minimum temperature showed increase of 0.3 to 2°C, -0.1 to 2.5°C, -0.1 to 2.5 °C and 0.6 to 2.5 °C for future 1 and 0.5 to 2.5°C, 1 to 3°C, 2 to 4 °C and 2 to 4 °C future 2 scenario under SSP respectively, relative to the present climate (Fig. 4.42 (e)). Similarly, it can be seen from Fig. 4.42 (d) that the projected annual mean maximum temperature for IRB had increments of -1 to 1.7 °C, -1 to 1.5°C, -0.2 to 1.8 °C and -0.5 to 2°C for future1 and -1 to 2 °C, -0.5 to 2.5 °C, 0.1 to 3 °C and 1.2 to 4 °C for future 2 respectively for the four SSPs. The mean annual minimum temperature is expected to increase by -0.2 to 2°C, -0.2 to 2.3°C, -0.3

to 2.4 °C and -.24 to 2.5 °C for future1 and -0.4 to 2.3°C, 0.31 to 3°C, 1.2 to 4 °C and -.1.7 to 5 °C for future 2 respectively under the four scenarios as can be observed from Fig. 4.42 (f). The mean annual maximum and minimum temperature will have consistent changes in the future time scales in the IRB as the time progresses except under the SSP245 scenario. It is clear that under future climate scenarios, the largest increase of around 4°C in annual maximum temperature is projected to occur over southern parts of WRB and western part of the IRB. Under the high-emission SSP585 scenario, WRB and IRB exhibited a significant increase in annual mean maximum and minimum temperature. A clear picture of an increasing pattern in annual mean precipitation, maximum and minimum temperature are observed for SSP585 (high-emission scenario) throughout the 21st century.

As mentioned earlier, the entire catchment area of the WRB is full of valleys and hills and it is a major sub-basin of Godavari. The IRB spreads from the Kalahandi district of Odisha up to the confluence of the rivers Indravati and Godavari. So, these sub-basins are vulnerable to climate change which can be attributed to the topographic and climate pattern over the WRB and IRB. Further, likely increase in the temperature will accelerate the climate variability. Although the mean temperature is expected to increase in the future scenarios, the precipitation also is expected to increase. Precipitation is the dominant parameter influencing the streamflow pattern for this region. The evapotranspiration and streamflow pattern over these basins will vary in future scenarios. Mishra et al. (2020a) observed that precipitation and temperature of GRB will be increasing in the future periods under different scenarios and the highest increase is attributed to the large emission scenario i.e. SSP585. Here, significant and robust changes in the precipitation, minimum and maximum temperature were observed for the two sub-basins in the SSP585 scenario.

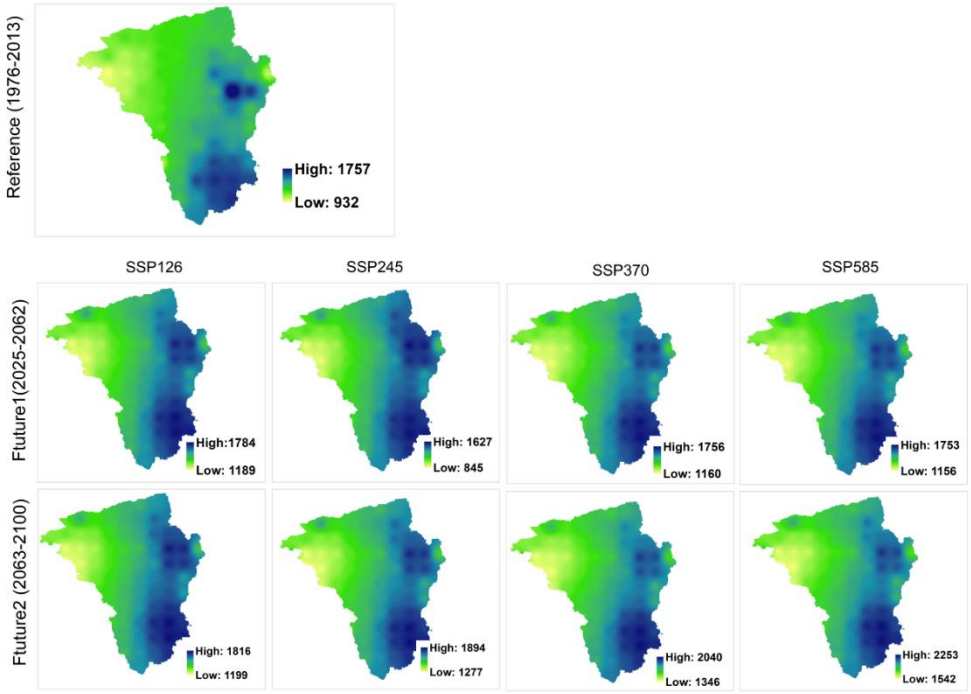
Reference (1976-2013)
High: 1757
Low: 932
SSP126
SSP245
SSP370
SSP585
Ftuture1(2025-2062)
High:1784
Low: 1189
High: 1627
Low: 845
High: 1756
Low: 1160
High: 1753
Low: 1156
Ftuture2 (2063-2100)
High: 1816
Low: 1199
High: 1894
Low: 1277
High: 2040
Low: 1346
High: 2253
Low: 1542

(a)

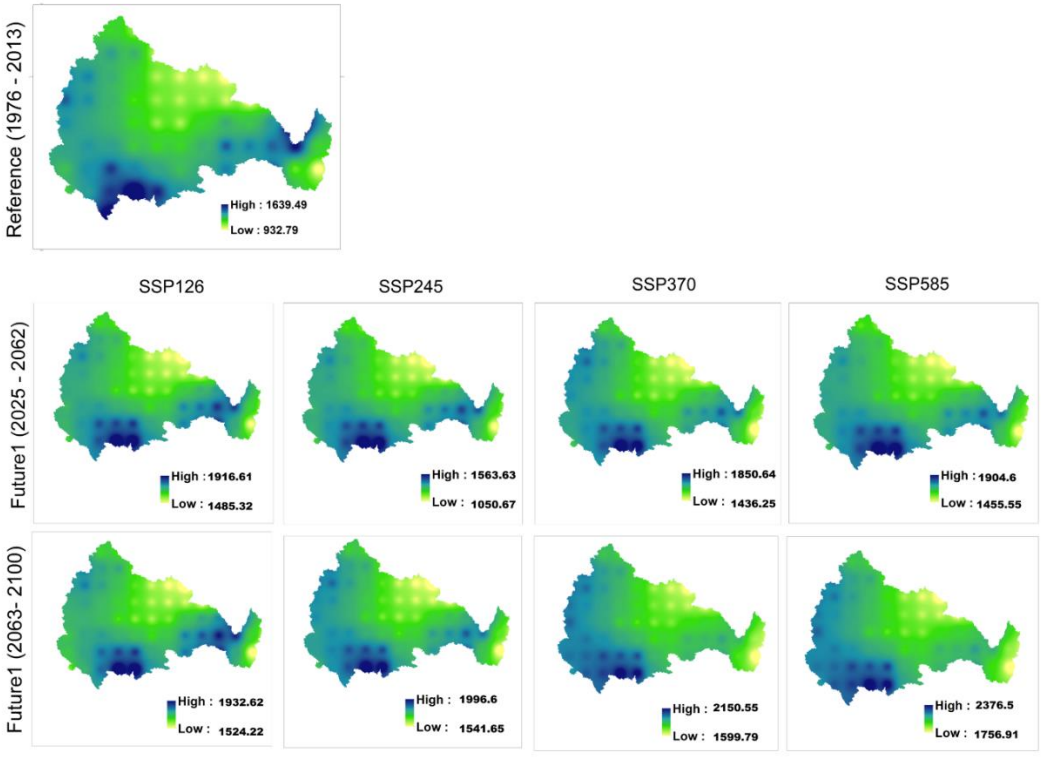
Reference (1976 - 2013)
High : 1639.49
Low : 932.79
SSP126
SSP245
SSP370
SSP585
Future1 (2025 - 2062)
High :1916.61
Low : 1485.32
High : 1563.63
Low : 1050.67
High : 1850.64
Low : 1436.25
High :1904.6
Low : 1455.55
Future1 (2063- 2100)
High : 1932.62
Low : 1524.22
High : 1996.6
Low : 1541.65
High : 2150.55
Low : 1599.79
High : 2376.5
Low : 1756.91

(b)

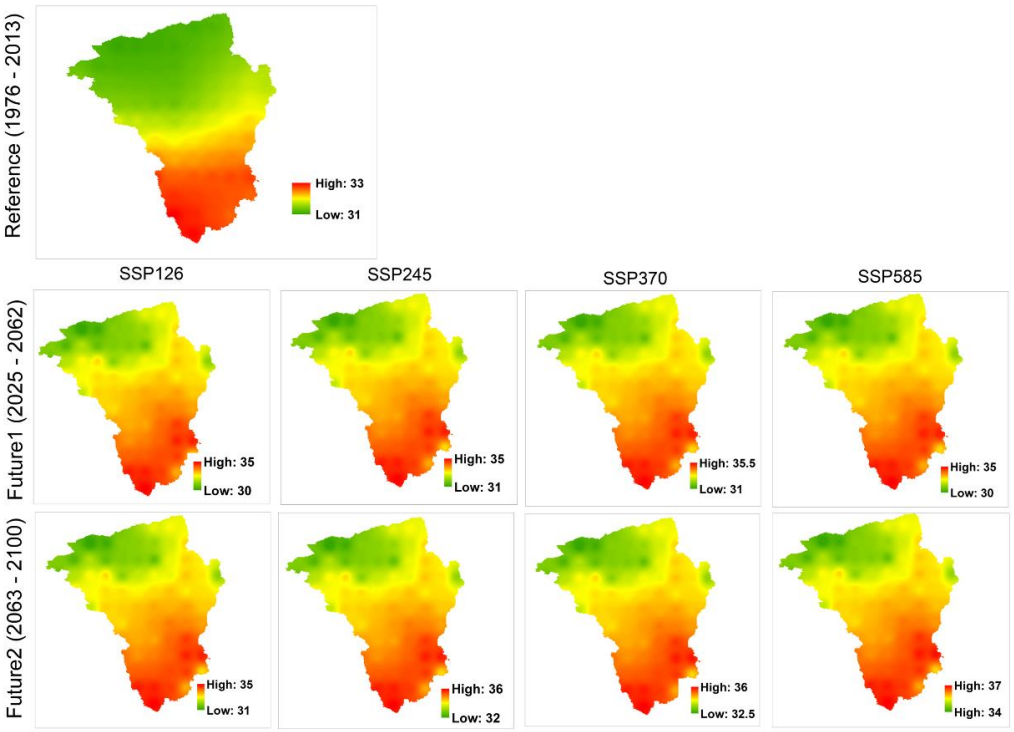
Reference (1976 - 2013)
High: 33
Low: 31
SSP126
SSP245
SSP370
SSP585
Future1 (2025 - 2062)
High: 35
Low: 30
High: 35
Low: 31
High: 35.5
Low: 31
High: 35
Low: 30
Future2 (2063 - 2100)
High: 35
Low: 31
High: 36
Low: 32
High: 36
Low: 32.5
High: 37
High: 34

(c)

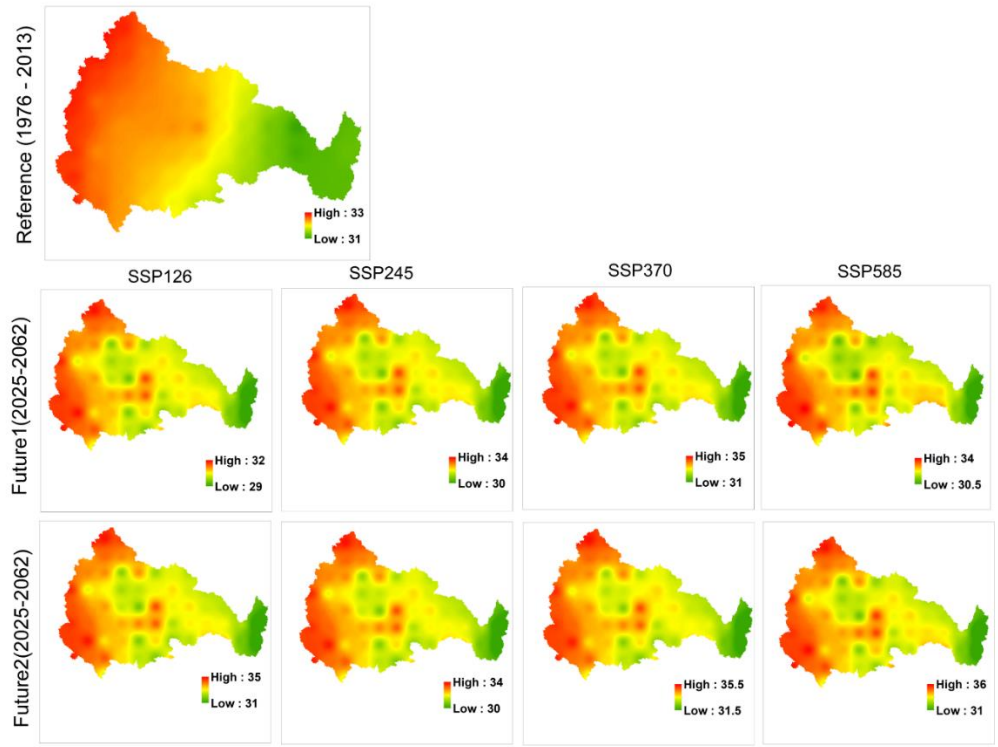
Reference (1976 - 2013)
High : 33
Low : 31
SSP126
SSP245
SSP370
SSP585
Future1(2025-2062)
High : 32
Low : 29
High : 34
Low : 30
High : 35
Low : 31
High : 34
Low : 30.5
Future2(2025-2062)
High : 35
Low : 31
High : 34
Low : 30
High : 35.5
Low : 31.5
High : 36
Low : 31

(d)

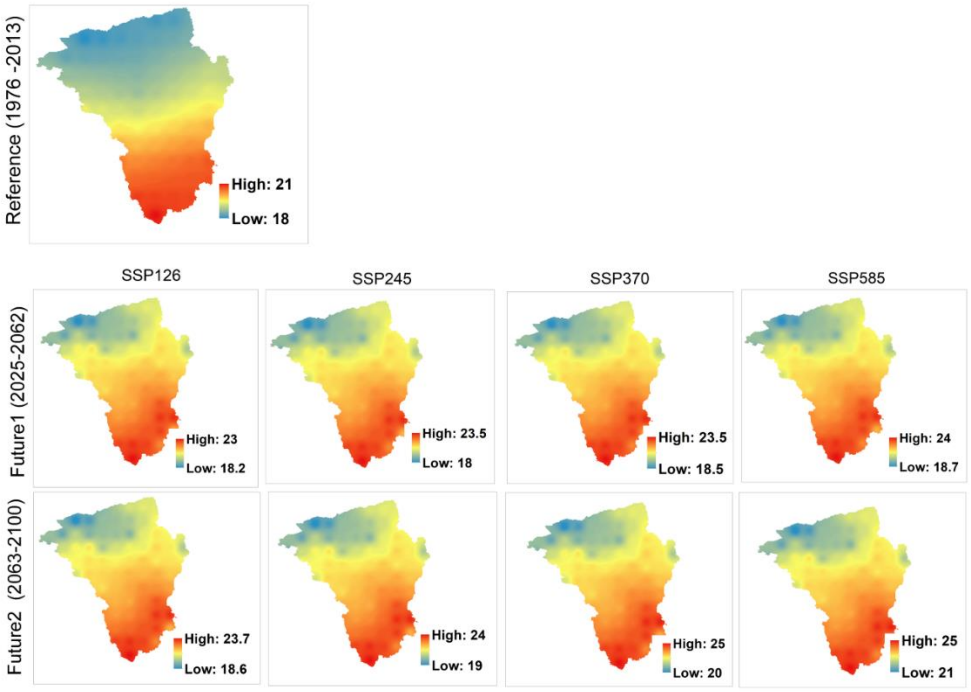

(e)

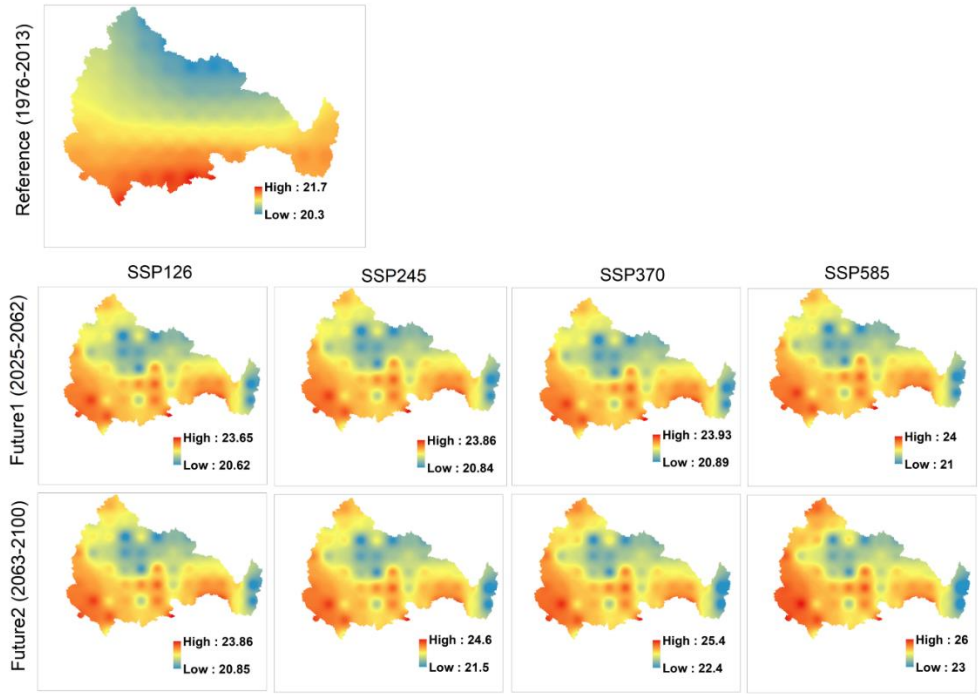

(f)

Fig. 4.41: Mean annual climate parameter over both the basins for reference (1976-2013) and future periods under four SSPs; (a) Mean annual precipitation over WRB; (b) Mean annual precipitation over IRB (c) Mean annual maximum temperature over WRB; (d) Mean annual maximum temperature over IRB; (e) Mean annual minimum temperature over WRB; (f) mean annual minimum temperature over IRB

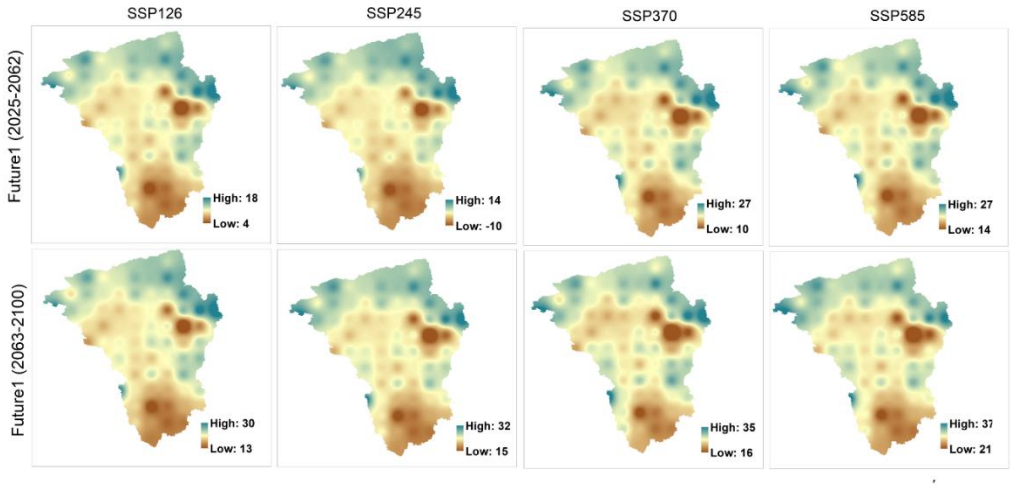
SSP126
SSP245
SSP370
SSP585
Future1 (2025-2062)
Future1 (2063-2100)
High: 18
Low: 4
High: 14
Low: -10
High: 27
Low: 10
High: 27
Low: 14
High: 30
Low: 13
High: 32
Low: 15
High: 35
Low: 16
High: 37
Low: 21

(a)

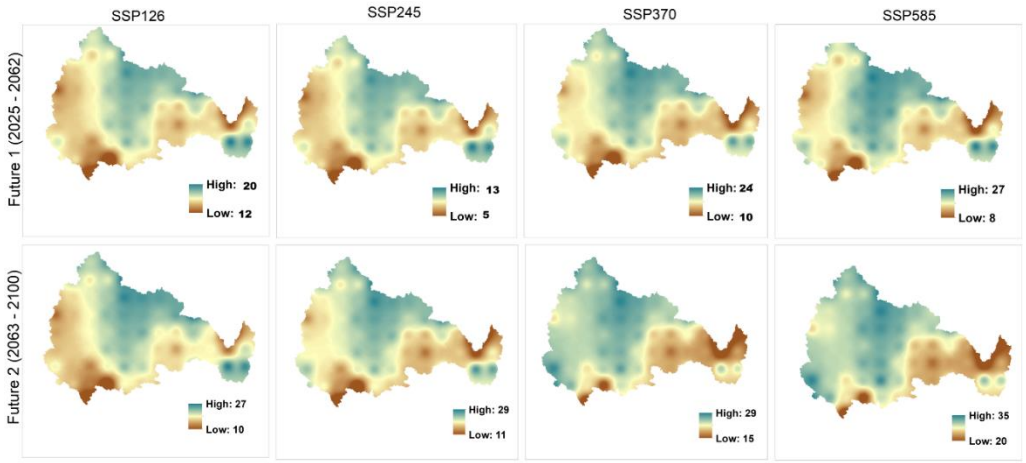
SSP126
SSP245
SSP370
SSP585
Future 1 (2025 - 2062)
Future 2 (2063 - 2100)
High: 20
Low: 12
High: 13
Low: 5
High: 24
Low: 10
High: 27
Low: 8
High: 27
Low: 10
High: 29
Low: 11
High: 29
Low: 15
High: 35
Low: 20

(b)

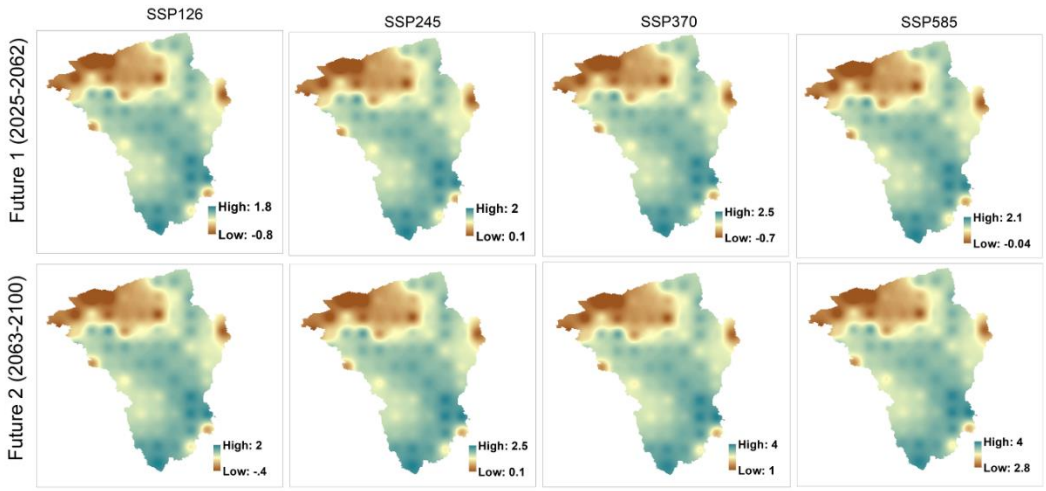
SSP126
SSP245
SSP370
SSP585
Future 1 (2025-2062)
Future 2 (2063-2100)
High: 1.8
Low: -0.8
High: 2
Low: 0.1
High: 2.5
Low: -0.7
High: 2.1
Low: -0.04
High: 2
Low: -.4
High: 2.5
Low: 0.1
High: 4
Low: 1
High: 4
Low: 2.8

(c)

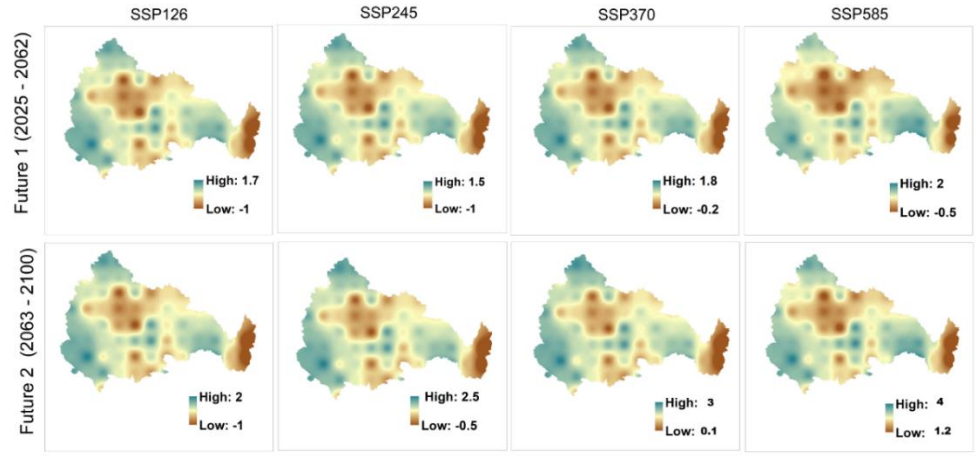

(d)

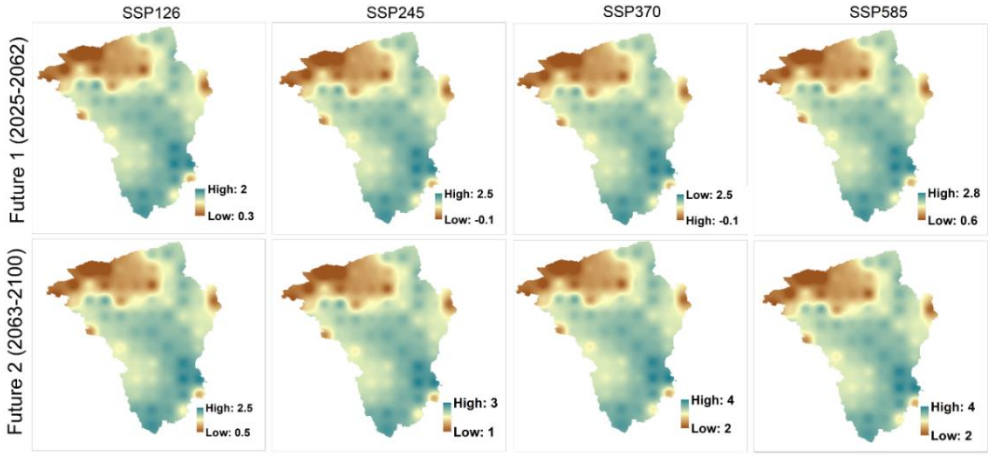

(e)

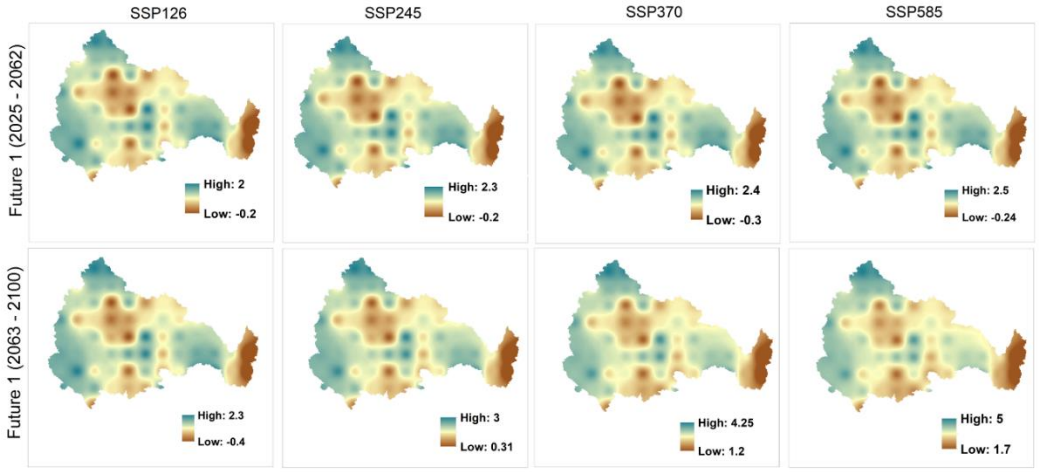

(f)

Fig. 4.42: Mean annual precipitation, maximum and minimum temperature changes over both the basins for reference (1976-2013) and future periods under four SSPs; (a) % Change in mean annual precipitation over WRB; (b) % Change in mean annual precipitation over IRB (c) %Change in mean annual maximum temperature over WRB; (d) Change in mean annual maximum temperature over IRB; (e) Change in mean annual minimum temperature over WRB; (f) Change in mean annual minimum temperature over IRB

4.5.3 Projected changes in evapotranspiration and streamflow

Spatial changes of evapotranspiration and streamflow in future periods relative to reference period are presented in Fig. 4.43 (a) to Fig. 4.43 (d). The mean annual evapotranspiration showed a decreasing pattern while an increasing pattern is observed in the mean annual streamflow over future periods for both the basins. For instance, SSP126, SSP370 and SSP585 show decline in the evapotranspiration under the warming climate while the SSP245 scenario (future1) show an increase in the evapotranspiration. A decline in evapotranspiration is found in the south-eastern and north-western part of WRB. The streamflow showed a large increment in the south-west part of WRB. With respect to the reference period, IRB showed a decline in the evapotranspiration while increase of streamflow is observed in the northern part of IRB. Higher variations in streamflow and evapotranspiration pattern were observed in future 2 when compared to future1 scenario. Interestingly, by the end of the 21st century, for SSP585, significant changes are anticipated in the annual mean evapotranspiration and streamflow over both the basins. These differences in the projected evapotranspiration and streamflows can be attributed to variations associated with precipitation and temperatures in the catchment area. The results from this study would be helpful in suggesting different strategies required to manage the water resources in different watersheds with response to climate change.

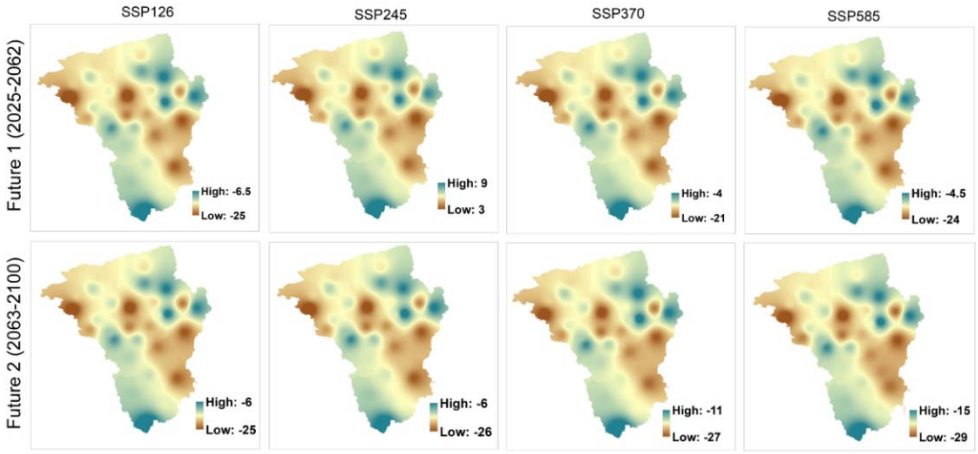

(a)

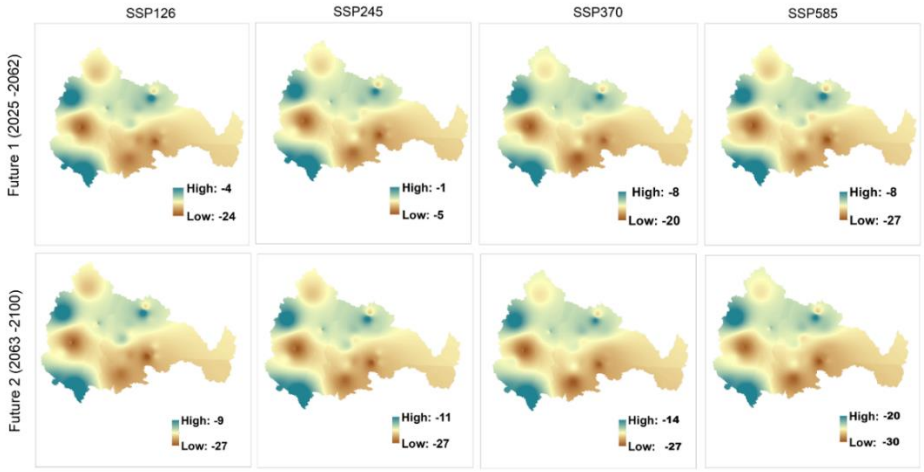

(b)

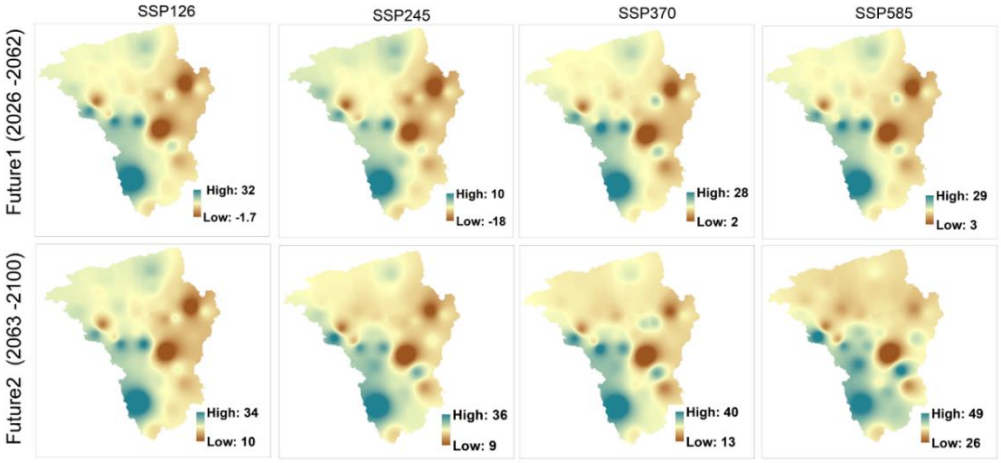

(c)

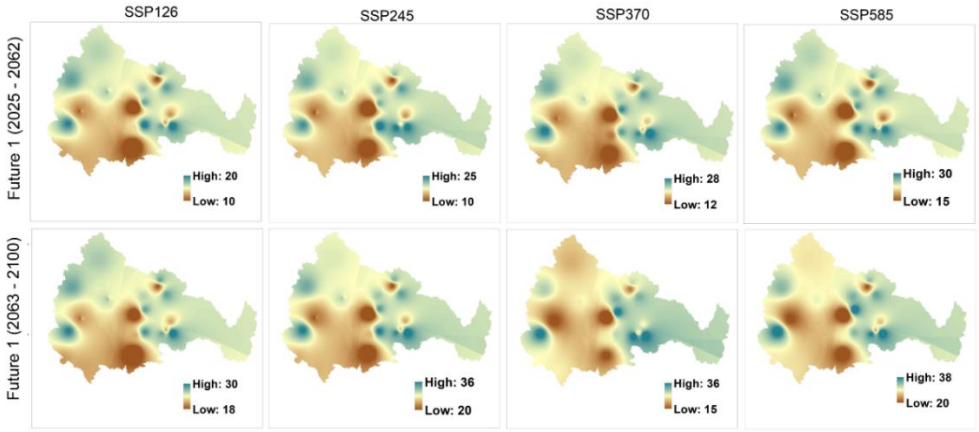

(d)

Fig. 4.43. Mean annual evapotranspiration and streamflow changes over both the basins for reference (1976-2013) and future periods under four SSPs; (a) % Change in evapotranspiration over the WRB; (b) % Change in evapotranspiration over the IRB; (c) % Change in streamflow over the WRB; (d) % Change in streamflow over the IRB

4.5.4 Projected changes in drought severity and duration

Drought characteristics play a major role in water resources management. Hence, a detailed investigation on these during reference and future periods under all SSPs were carried out to identify the relative variations in drought phenomenon. Drought severities were computed based on the sub-basins generated by the SWAT model. The maximum drought severity for reference and future periods over WRB and IRB are presented in Fig. 4.44(a) and Fig. 4.44(c). Significant variations in maximum severities between the reference period and future period are observed in Fig. 4.44(a). The maximum drought severities are also found to have decreasing pattern under all future scenarios except in SSP245. The severe-most drought events under SSP245 scenario are observed for the future1 scenario. The maximum severity hotspots are found to increase in the south-western part of the WRB for SSP245. Fig. 4.44(c) suggests an intensification in drought severity over the northern part of the basin under SSP245 scenario for IRB. Drought hotspots in the middle region of IRB are observed during the reference period and the northern part of IRB showed maximum severity hotspots in the future scenarios. It is to be noted that, the future scenarios have projected less drought events towards the end of the 21st century especially for SSP585.

The relative changes in drought duration between future and reference periods were then compared and presented in Fig. 4.44(b) and Fig. 4.44(d). From the MDI analysis under various SSPs, the projected drought durations are seen to mainly decrease in the WRB for future scenarios (Fig. 4.44 (b)). From the low emission to high emission, the drought with shorter durations are visible in the IRB under SSP126, SSP370 and SSP585 (future1), while droughts with a longer duration are projected in under the SSP245 (Fig. 4.44(d)). The spatial dispersion of maximum drought characteristics across WRB and IRB are more in the reference period and SSP245 scenario. Hence the reference period and SSP245 scenario are more vulnerable to drought, since relatively higher maximum duration and severities were observed than other future scenarios. SSP585 scenario showed lower maximum drought durations since the precipitation and streamflow are increasing and evapotranspiration showing decreasing tendency over the WRB and IRB. It can be concluded that, by the end of the century, the drought incidences are going to be decreasing based on the CMIP6 projections for all the scenarios. All the SSPs showed that there will be changes in the drought pattern and the spatial extension for all the scenarios. It is also observed that the number of drought events are expected to decrease in future 2 period. These

changes in the projected drought severity and durations are due to the associated variability in the climate under different scenarios.

However, the pattern of drought characteristics varies for future with the reference period due to variation in the climatic variables in the future projection based on CMIP6 model simulation from SWAT. Hence the precipitation, streamflow, evapotranspiration and soil moisture play a crucial role in governing the local meteorological, hydrological and agricultural drought phenomenon.

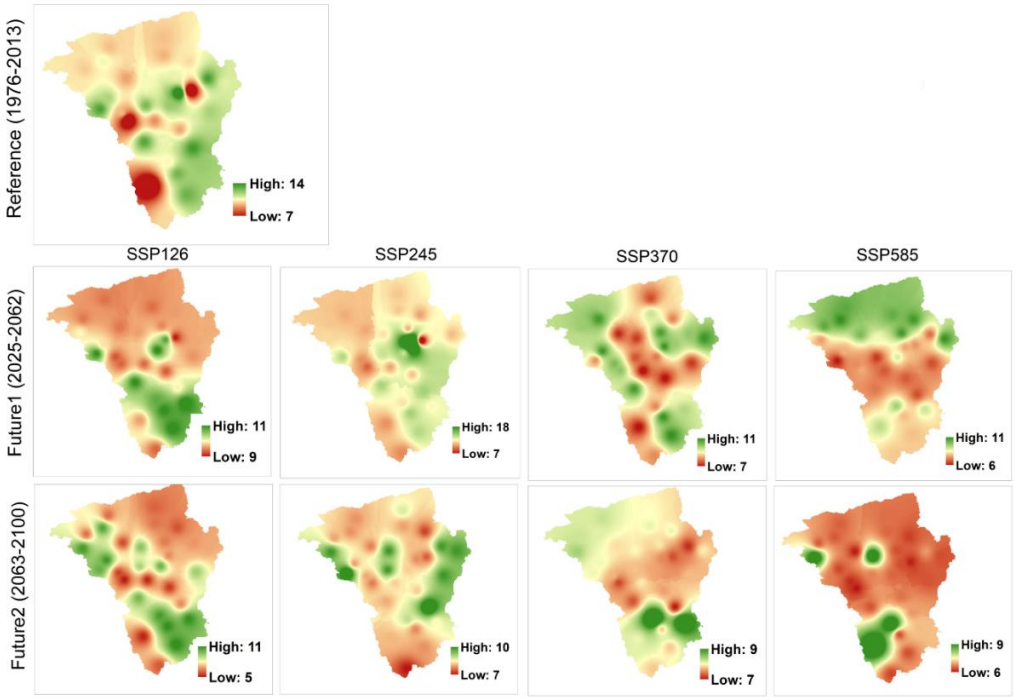

(a)

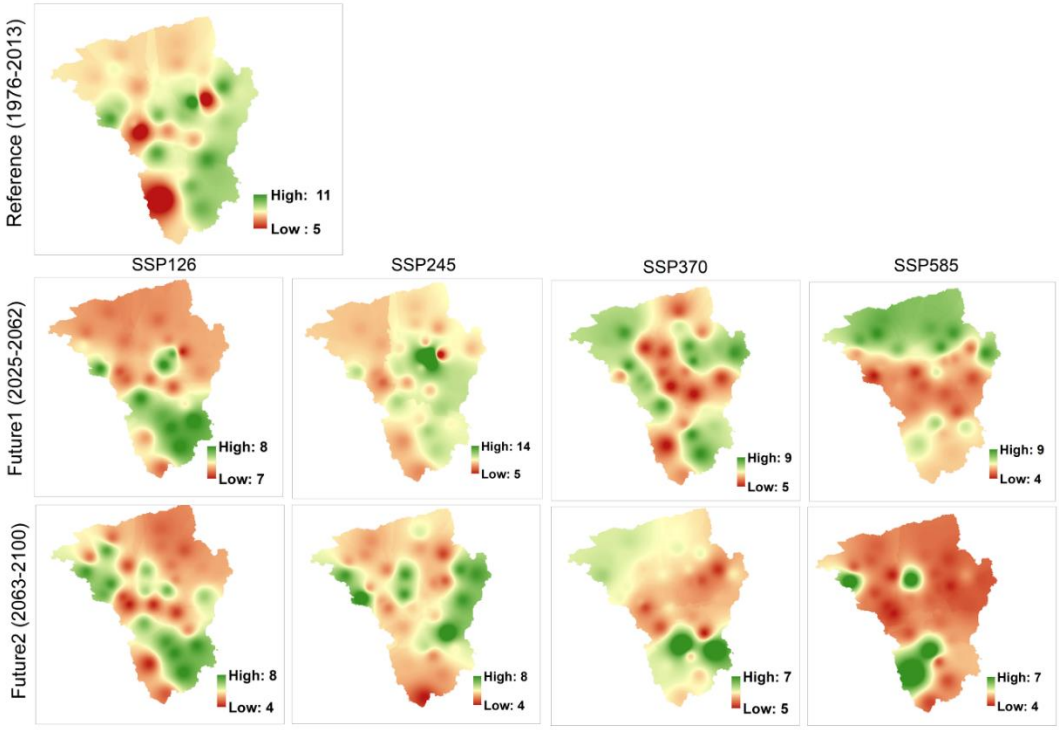
Reference (1976-2013)
High: 11
Low : 5
SSP126
SSP245
SSP370
SSP585
Future1 (2025-2062)
High: 8
Low: 7
High: 14
Low: 5
High: 9
Low: 5
High: 9
Low: 4
Future2 (2063-2100)
High: 8
Low: 4
High: 8
Low: 4
High: 7
Low: 5
High: 7
Low: 4

(b)

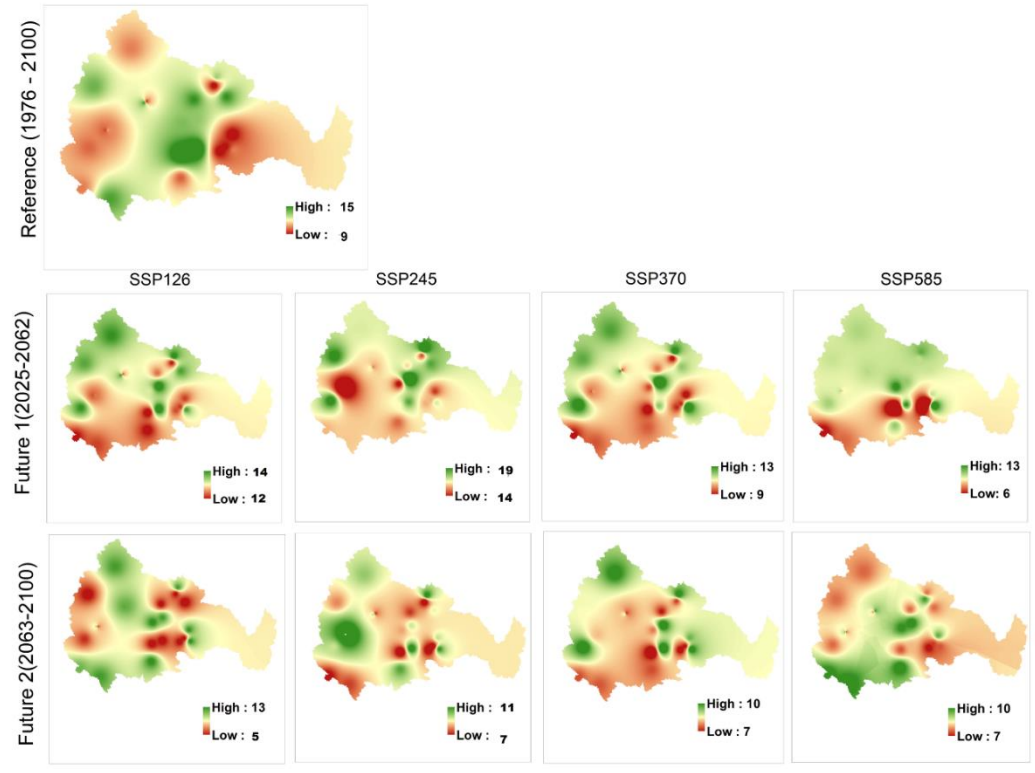
Reference (1976 - 2100)
High : 15
Low : 9
SSP126
SSP245
SSP370
SSP585
Future 1(2025-2062)
High : 14
Low : 12
High : 19
Low : 14
High : 13
Low : 9
High: 13
Low: 6
Future 2(2063-2100)
High : 13
Low : 5
High : 11
Low : 7
High : 10
Low : 7
High : 10
Low : 7

(c)

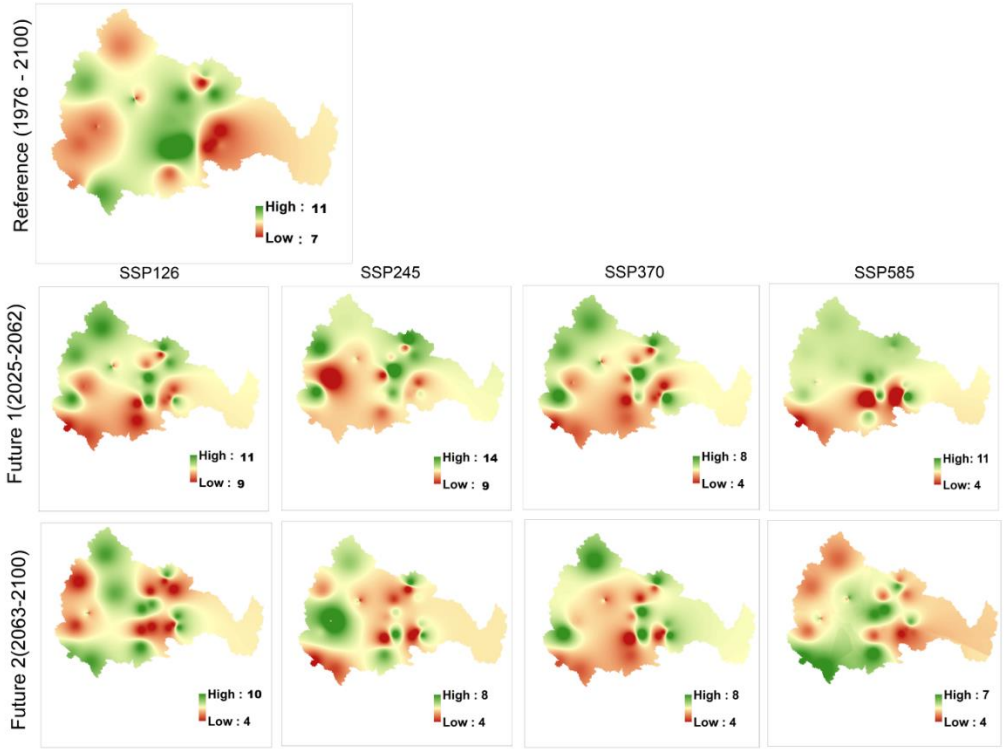

(d)

Fig. 4.44: Maximum drought severities and durations changes over both the basins for reference (1976-2013) and future periods under four SSPs; (a) maximum drought severities over WRB; (b) maximum drought durations over WRB; (c) maximum drought severities over IRB; (d) % maximum drought durations over IRB

4.5.5 Conclusion

A multivariate formulation of drought is essential for jointly representing all forms of drought events that can simultaneously affect a particular region. In this study, a new copula based probabilistic multivariate drought index has been developed for reference and future scenarios. All variables like precipitation, evapotranspiration, streamflow and soil moisture are involved for the multivariate drought assessment. The key findings based on this objective of the study are discussed.

The observed variability of the SWAT streamflow anomalies was well captured in the Wainganga and Indravati basins. The model was calibrated and validated using SWAT-CUP SUFI2 algorithm. The performance of the model was evaluated based on NSE, R^2 and PBIAS. The performance indicators showed that the model performed well for both calibration and validation period.

An increase in spatial extent of annual precipitation is observed for future scenarios. The south-eastern part of WRB and southern part of IRB are expected to receive a large amount of annual precipitation. The annual maximum and minimum temperature show an increasing pattern under all the future scenarios.

The spatial analysis of changes in mean annual evapotranspiration and streamflow suggested decrease in evapotranspiration and high increase in streamflow for both the sub-basins under consideration. An intensification in precipitation, streamflow and a reduction in evapotranspiration indicate a reduction in droughts events in future periods.

The drought severities and durations will be in decreasing tendency for future scenarios compared to the reference period. SSP585 indicates lesser drought severity for both the basins while SSP245 and reference period emerged as the most vulnerable to drought conditions. The large variations in the drought properties can be attributed to the variation in the climate variables.

To summarize, MDI can be useful in an efficient way for drought monitoring under the reference and future climate. Moreover, MDI overcomes the required variability to identify simultaneous variability of climate parameters to access drought phenomenon as it integrates the response of several climatic parameters.

4.6 Impact of Climate Change on Crop Yield and Crop-Drought Relationship with Varying Climate

Data regarding precipitation, minimum and maximum temperature were downloaded from the IMD website. Evapotranspiration was calculated using ET calculator in AquaCrop model. AquaCrop model was then calibrated and validated based on the observed yield depending on the parameters for Aurangabad region. The future water crop yields were estimated for four SSPs (SSP126, SSP245, SSP370 and SSP585) based on the ensemble mean of bias corrected CMIP6-GCMs namely ACCESS-CM2, BCC-CSM2-MR, CanESM5, INM-CM4-8 and MPI-ESM1-2-HR. The crop yields were then obtained from the model for future period. SYRS were obtained from the yield series for future and reference periods. SPEI values at different lags were then correlated with the SYRS to obtain the crop-drought relationship for reference and future periods.

4.6.1 AquaCrop model performance evaluation and estimated CO_2

In this study, the mean CO_2 concentration of 364 ppm was used for the period 1997-2014 and for the future period, value of CO_2 concentration is taken according to the scenarios. The average CO_2 concentrations in SSP126, SSP245, SSP370 and SSP585 scenarios are 434 ppm, 500 ppm, 528 ppm and 630 ppm respectively.

The model was calibrated and validated using the observed crop yield series for the period of 1998 to 2014. The cultivars specific parameters were used for simulating the yield by considering the meteorological parameters. The model was calibrated and validated for cotton, maize and

wheat for the Aurangabad region of UGRB. The parameters and the fitted values for calibration and validation periods are provided in Table 4.33. The relation between observed and simulated crops for calibration and validation periods are plotted for different crops are given in Fig. 4.45 and Fig. 4.46 for the region. RMSE obtained between the observed and simulated yield values indicated that the model accuracy was quite good during calibration and validation processes. Moreover, in most of the cases, simulated yield captured observed yield well during the calibration and validation period. On the basis of model performance, the calibrated model was used to project the crop yield for future scenarios.

Table 4.33 Parameters for calibration and validation periods in AquaCrop model

Crop Parameters	Units
Time from sowing to maturity	Days
Maximum effective rooting depth	M
Reference Harvest Index	%
Length of the flowering stage	Days
Time from sowing to emergence	Days
Time from sowing to maximum rooting depth	Days
Time from sowing to start senescence	Days
Time from sowing to flowering	Days
Building up of the Harvest index	Days
Soil surface covered by an individual seedling	cm^2/plant
Number of plants per hectare	--
Canopy growth coefficient	% /day
Maximum canopy cover	%
Canopy decline coefficient	%/day
Shape factor for water stress limiting stomatal conductance	--
Shape factor describing root zone expansion	--
Soil Parameters	
Curve number and readily evaporable water	--, mm
Hydraulic conductivity, root zoon expansion rate, gravel mass	mm/day, %, %
Number of soil layers, their texture and thickness	--, --, m

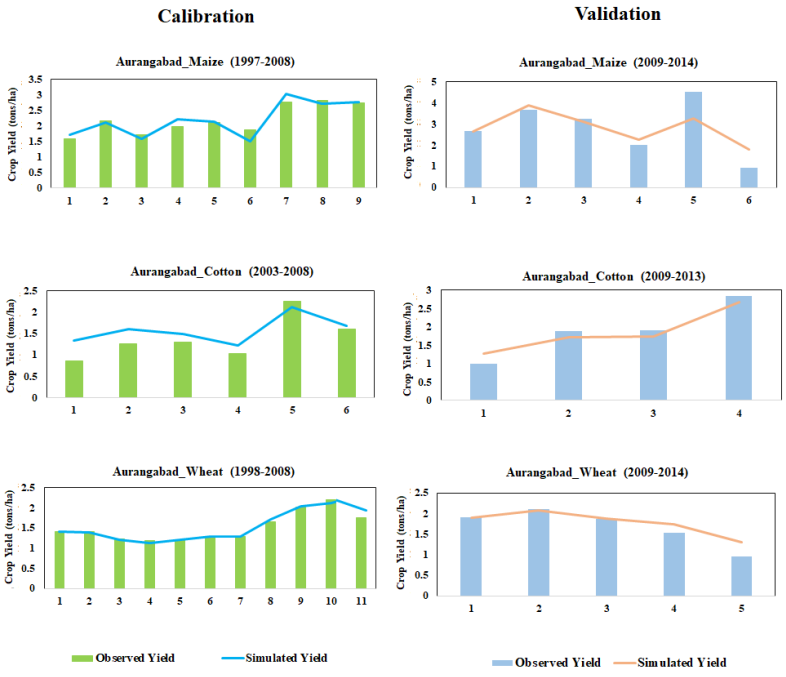

Fig 4.45 Observed and simulated yield for Aurangabad region for calibration and validation period

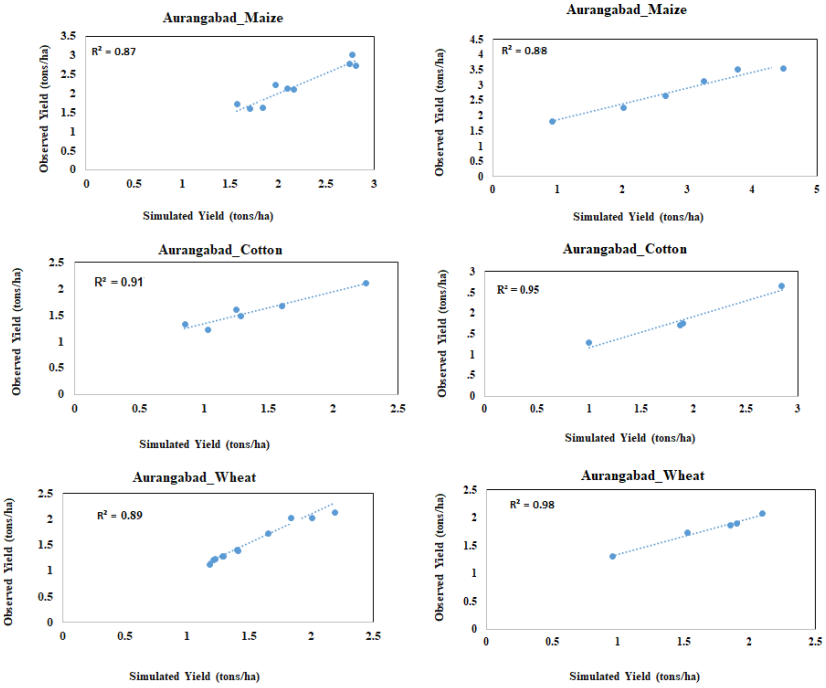

Fig 4.46 Observed and simulated R^2 values for Aurangabad region for calibration and validation period

4.6.2 Future projection of yield

All crops monitored during 1997-2014 showed an increase in growth trend. The yield increased considerably during the period 1997-2014 due to improved technologies for crop production. For future yield prediction, four emission scenarios viz., SSP126, SSP245, SSP370 and SSP585 were selected. The future yields of maize, cotton and wheat are predicted for Aurangabad region. Similar to the observed time period, for better representation of results, the future period was also sub divided into different divisions for a specified crop. The yield of maize, cotton and wheat increased significantly over the future scenarios with respect to the observed for the SSP585 scenario. For comparison between the box plots for observed and future scenarios for different crops are presented in Fig. 4.47. From the Fig. 4.47, it can be observed that there is a significant increase in the maize, cotton and wheat yield for all the future scenarios especially in the high emission scenarios (SSP370 and SSP585) in the end of 21st century. It is also observed that there is significant variability in the yield variability with respect to the observed period.

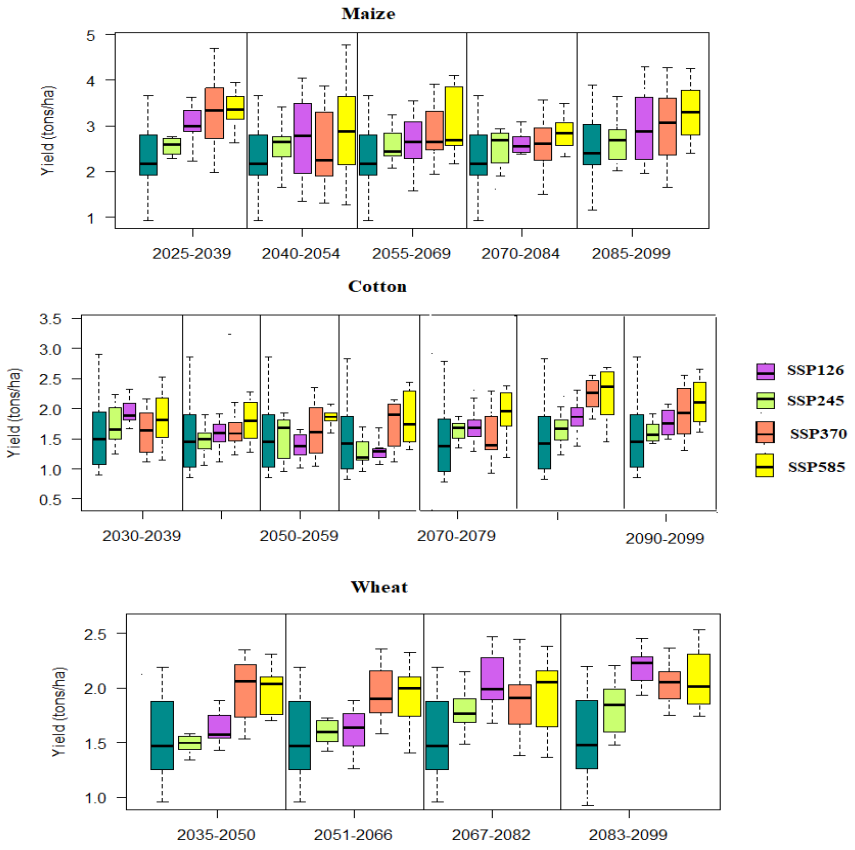

Fig. 4.47. Projected crop yield for maize, cotton and wheat under SSP126, SSP245,SSP370 and SSP585

4.6.3 Crop yield response to the climate variability

This research considered crop growth seasons for maize (April to September), cotton (May to December), and wheat (October to February). As previously mentioned, yield projections for various crops are based only on changes in climatic factors, and hence, it is important to establish a relationship between the climate variability of various crops and their yields. Non-climatic factors like fertilisation and cultivar impacts, irrigation techniques, and other technological developments were not considered in this study. The evolution of temperature fluctuations, as well as their anomalies, under observed and perspective scenarios will aid in determining their influence on climate change on crop productivity in the Aurangabad region. For different crops, the temporal differences in precipitation, minimum and maximum temperatures of future scenarios with regard to the reference period for different crops are shown in Figs. 4.48, Fig. 4.49, and Fig 4.50. The projected average yield for maize (Fig. 4.47), is expected to increase in the future scenarios during 2025-2099. The threshold temperature (cold and heat stress) for maize should be between 27 °C and 33 °C (Bhatt et al. 2014). According to Fig. 4.48, the monthly average precipitation during crop growing season is predicted to rise considerably. In addition, the maximum and minimum temperatures is expected to increase in the future scenarios. Higher emission scenarios, such as SSP370 and SSP585, show significant variations in comparison to the reference period. The optimal temperature range has a beneficial impact on crop yield if other elements such as soil condition and available water content remain in favourable condition (Bhatt et al. 2014). The projected cold and heat stress during the growing period of wheat is expected to remain in optimal range. Therefore, wheat production is likely to increase during 2025-2099 (Fig 4.47). Temperature influences the photosynthesis and respiration processes (Lobell and Gourdji, 2012). Similarly, for cotton, the optimum thermal range is between 32° C (hot stress) to 23.5° C (cold stress) with optimum temperature of 28° C (Bhatt et al. 2014) and temperature ranges showed favourable condition for cotton production. Therefore, under the favourable climatic conditions, the projected average yield for cotton (Fig. 4.50), is expected to increase in the future scenarios during 2025-2099. The significant increase in maize yields under climate change scenarios are due to favorable temperature conditions related to cotton and wheat. Similarly, the CO_2 concentration tends to increase in the future scenarios. Significant increase in the CO_2 concentration is expected in SSP370 and SSP585 scenarios for the growing period of crops. Generally, increased CO_2 concentration will directly affect the crop yield for C4 plants through enhanced photosynthesis (Kumar, 2016). The average water productivity (WP) is also expected to

have an increasing effect in the future scenarios compared to reference period. WP directly affects the biomass production which is directly proportional to crop yield. The average WP varies with crop type (Table 4.34). The cold temperature stress has minimal effect on the crop yield. Hence it can be observed that the WP increases with progress of time possibly resulting in the increment in the crop productivity. To summarize, the appropriate range of cold and heat stress, higher CO_2 concentration and increased WP could be attributed for the increment in the mean crop yield over the region.

Table 4.34 Average WP for different crops

Crops	WP(gm/m^2)
Maize	
Reference Period	6.6
2025-39	7.9
2040-54	8.8
2055-69	10.1
2070-84	9.5
2085-99	10.2
Cotton	
Reference Period	7.1
2030-39	7.8
2040-49	9.5
2050-59	8.4
2060-69	8.7
2070-79	8.8
2080-89	7.1
2090-99	10.4
Wheat	
Reference Period	6.8
2035-50	7.8
2051-66	7.9
2067-82	8.1
2083-98	8.8

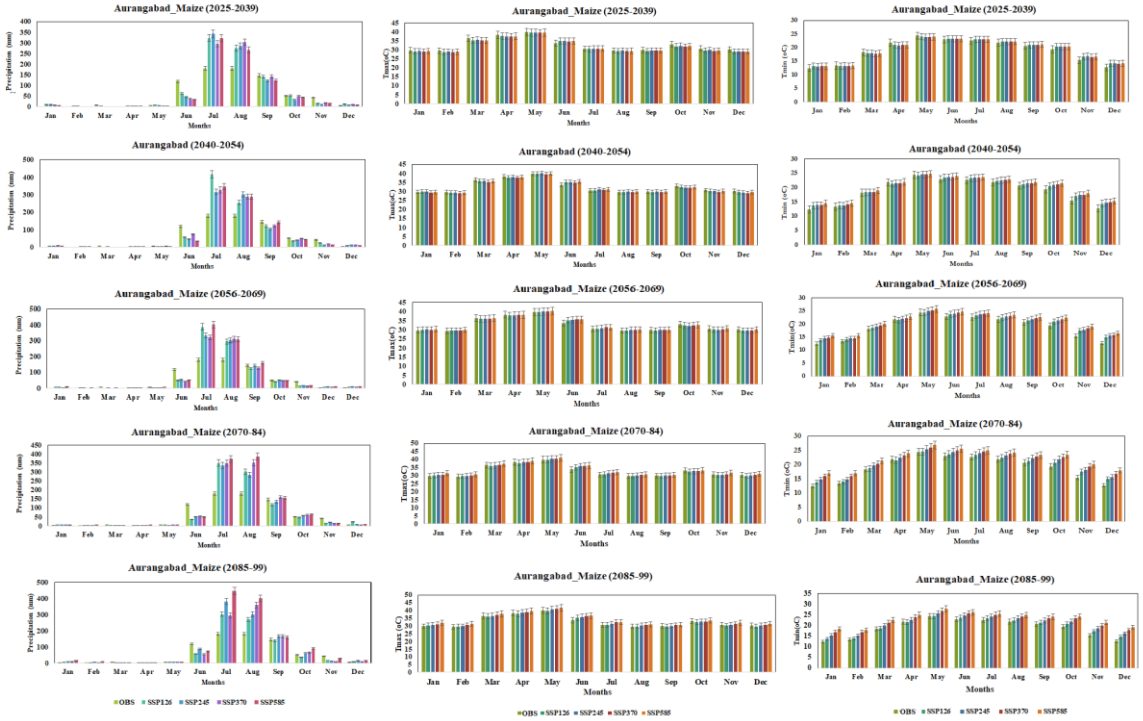

Fig 4.48 Mean monthly precipitation, maximum and minimum temperature for reference and future scenarios for maize

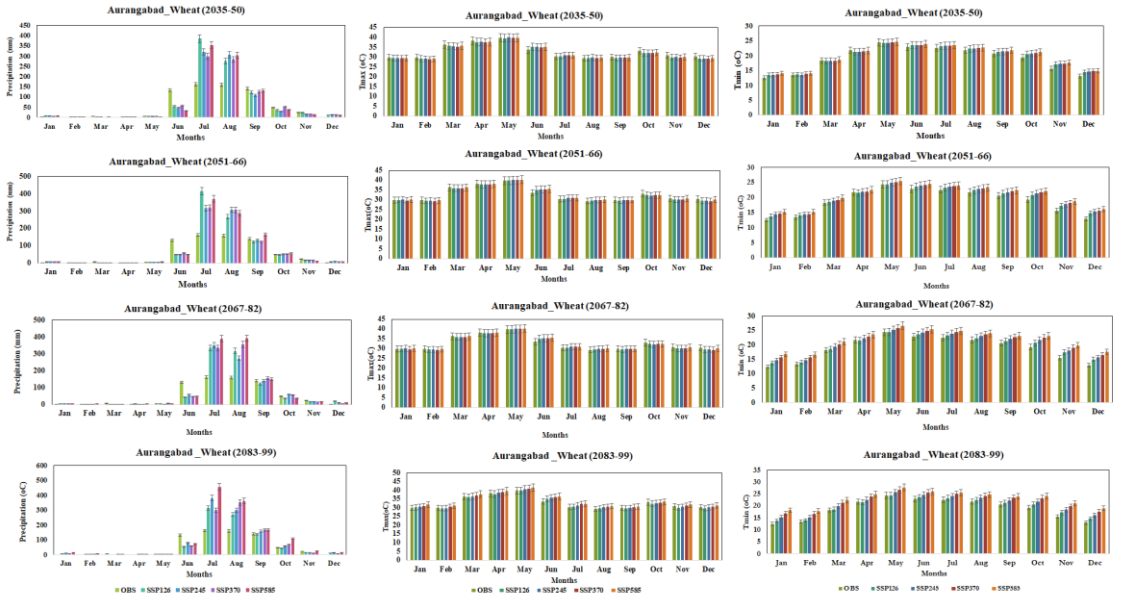

Fig 4.49 Mean monthly precipitation, maximum and minimum temperature for reference and future scenarios for wheat

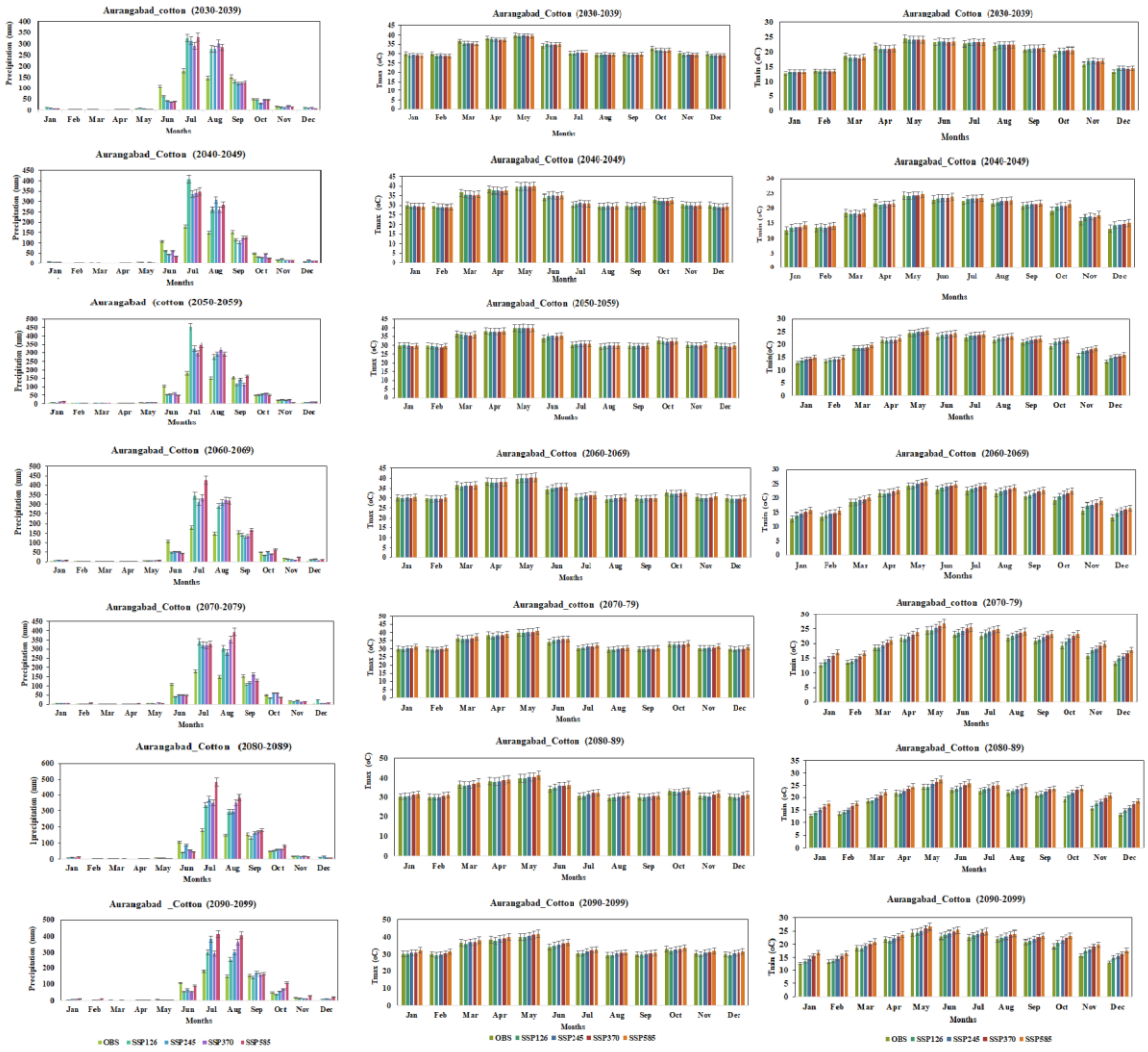

Fig 4.50 Mean monthly precipitation, maximum and minimum temperature for reference and future scenarios for cotton

4.6.4 Standardised yield residuals series (SYRS) evolution as a loss/gain indicator

The temporal evolution of the SYRS of maize, cotton and wheat for reference period is presented in Fig. 4.51. The agricultural yield could be categorized depending on the SYRS values as <- 1.5 indicating high loss and >1.5 indicating high gain. The reference period revealed that moderate to high losses for maize occurred in the years 2003, 2004, and 2011 for the region. SYRS for cotton revealed moderate to significant losses throughout the years 2003, 2004, 2005, 2006 and 2009. For wheat, moderate to high losses occurred in the years 2003, 2004 and 2013. The year 2013 showed mild losses in wheat for this region. Considering the SYRS condition, the largest crop failure occurred in the years 2004 for maize, 2003 for cotton, and 2003 for wheat within the reference period. Thus, 2003 scored first in terms of crop losses for winter wheat, maize, and cotton. Cotton had the most low-yielding years during the reference period, followed

by maize and then wheat. The evolution pattern of SYRS for future scenarios are presented in the Fig. 4.52, Fig. 4.53 and Fig. 4.54 for maize, cotton and wheat respectively. From the figures, it can be observed that the highest loss in crop production is expected to occur during the years of 2050-59 and 2060-69 for maize, 2060-69 and 2080-89 for cotton and 2035-2050 and 2067-2082 for wheat in terms of the intensity of the SYRS. For future scenarios, SSP245 showed greatest number of low yielding years. In terms of crops, the greatest number of low yielding years were observed in the case of wheat, followed by cotton and then maize. For future, the following features are expected for production in crop: (i) the highest yield variability recorded in the SYRS for wheat, then maize and the least for cottons; (ii) the prevalence of high-yielding years for all of the crops was detected; the relatively stable yield for cotton is expected to prevail.

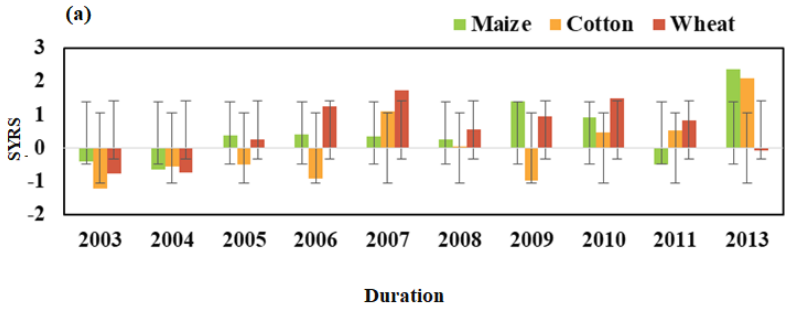

4.51 SYRS for maize.cotton and wheat for reference period

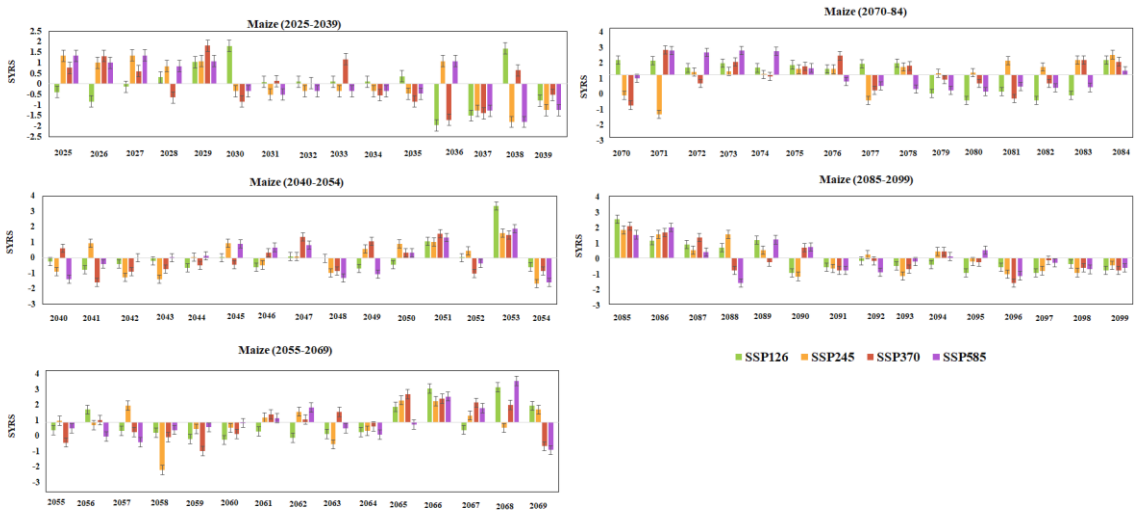

Fig. 4.52 SYRS for maize for SSP126, SSP245, SSP370 and SSP585

Fig. 4.53 SYRS for cotton for SSP126, SSP245, SSP370 and SSP585

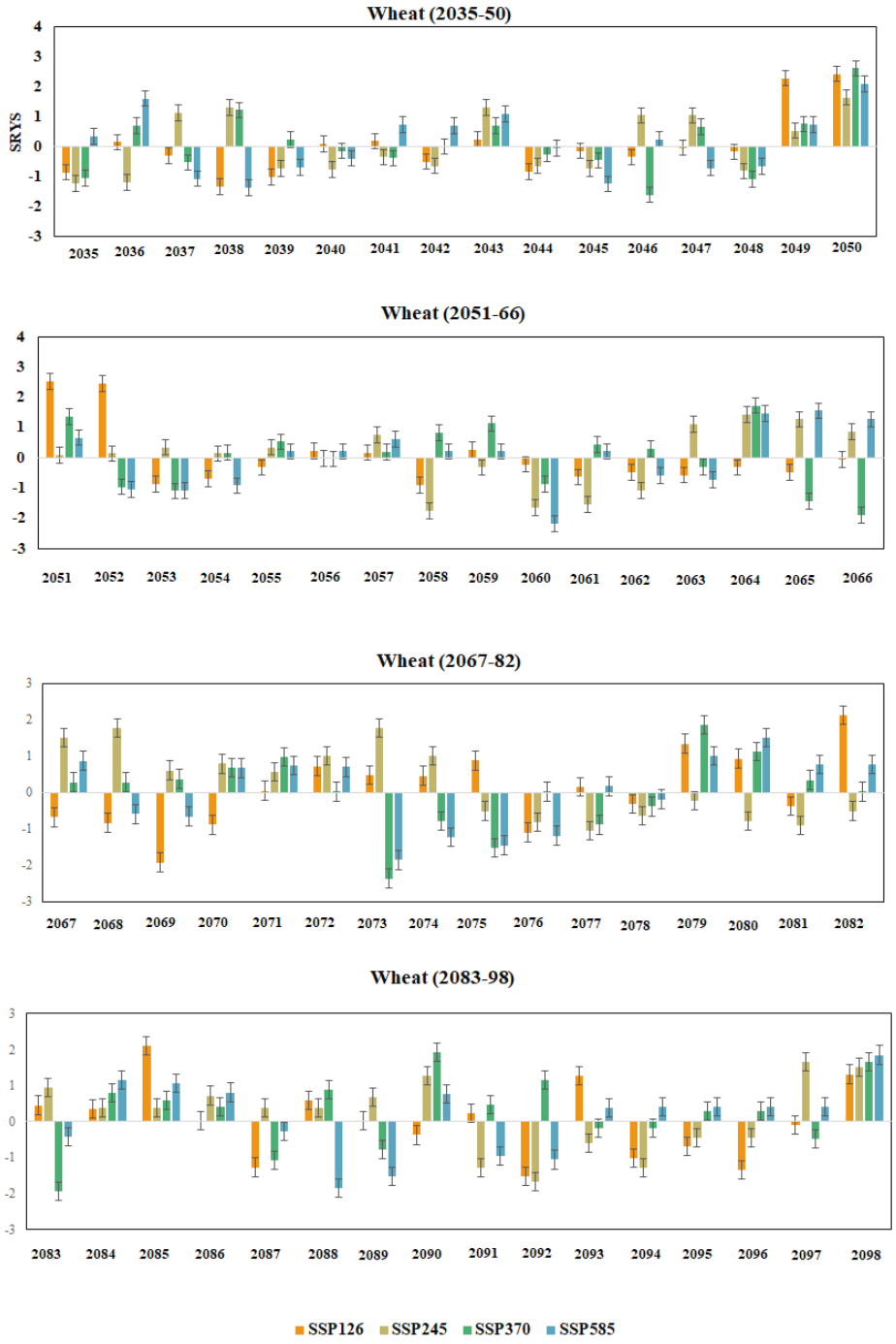

Fig.4.54 SYRS for wheat for SSP126, SSP245, SSP370 and SSP585

4.6.5 Yield-responses to drought conditions

Kendall τ correlation coefficients between the monthly de-trended SPEI series at 1-12-month lags and SYRS of three crops were computed for the reference and future scenarios. Basically, correlations between SPEI and SRYS signify the year-to-year variations in crop yield and are related to the year-to-year variation of drought time series. This interpretation can assess the

impact of drought on crop patterns for various scenarios over a specified time scale and month. Drought, according to Sharma et al. (2016), can reduce crop productivity by preventing cell enlargement leading to reduced leaf size, reduced relative leaf water content, reduced tillering and plant height, and increased crop root length. Further, when compared to non-stress conditions, multi-stage drought led to a potential reduction in crop production and a reduction in yield qualities, as well as a worsening of physiological parameters such as chlorophyll content, relative water content, rate of transpiration and photosynthesis, and lipid peroxidation. However, during drought events, changes occur primarily among growth stages and genotypes (Kumar et al. 2020). For reference period, differences in the responses of crops to different lags of the SPEI were observed in this study (Fig. 4.55). From Fig. 4.55, it can be seen that for maize, the months from April to June are highly sensitive to onset of drought events. Similarly, for cotton, the most sensitive period is during February to May. Wheat showed the greatest yield sensitivity for the period of January to May. The results for cumulative drought impact on yield series for different crops for future scenarios are given in Fig. 4.56, Fig. 4.57 and Fig. 4.58.

Based on SPEI values, drought is expected to significantly affect maize production in April-May and October- November in the SSP126 scenario at short-term drought. The next damaging effect of drought is expected in the SSP245 scenario. Conversely, SSP585 scenario is expected to have less profound positive correlation than other scenarios. Cotton showed sensitivity to drought condition, especially in the early growth stages in the SSP126 scenario. The greatest correlation was recorded for the SPEI at 5-6-month lags in July to October. Wheat is highly sensitive to drought during the April-May in the SSP126 scenario. Zhang et al. (2018) studied that the growth stage of wheat is highly sensitive to drought conditions because of reduction in leaf area due to reduced root growth, reduction in leaf number per plant, size and longevity of leaves. Drought reduces chlorophyll content, membrane stability, relative water content, chlorophyll fluorescence and yield and yield components, NPK uptake, and increases catalase, peroxidase, and superoxide dismutase content (Sheoran et al. 2015), but the effect was more pronounced with late season drought stress than early season drought stress (Nawaz et al. 2012). A positive correlation is expected between the SYRS of wheat and the de-trended SPEI at time scales from 2 to 4 months during March, April, and May ($r = 0.1$-0.7), which corresponds with the highest moisture demands. In the SSP585 scenario, crops showed less sensitive to drought condition, leading to low yield losses (SYRS ≤ -1.5). The greatest yield-drought correlation was for wheat, the least for maize for the observed period. For future scenarios,

cotton is expected to be more sensitive to drought onset. During the observed period, crops are more sensitive to drought condition rather than future periods.

Maize
SPEI in different time scales

	1-month	2-month	3-month	4-month	5-month	6-month	7-month	8-month	9-month	10-month	11-month	12-month
Dec	0	0	0.0	0.00	0.00	0.00	0.00	0.00	0.00	0	0	0
Nov	0.2	0	0.0	0.00	0.00	0.00	0.00	0.00	0.00	-0.2	-0.2	-0.2
Oct	0.3	0.4	0.0	0.00	0.00	0.00	0.00	0.00	0.00	-0.3	-0.3	-0.4
Sept	0.0	-0.01	0.0	0.00	0.00	0.00	0.00	0.00	0.00	0.00	0.00	0.00
Aug	0.27	-0.2	0.37	0.00	0.00	0.00	0.00	0.00	0.00	0.00	0.00	0.00
July	0.0	0.0	0.0	0.00	0.00	0.00	0.00	0.00	0.00	0.00	0.00	0.00
Jun	0.1	0.1	0.1	0.00	0.00	-0.20	-0.20	-0.20	0.00	0.00	0.00	0.00
May	0.2	0.27	0.27	0.00	0.00	0.00	0.00	0.00	0.00	0.00	0.00	0.00
Apr	0.4	0.5	0.5	0.00	0.00	0.00	0.00	0.00	0.00	0.00	0.00	0.00
Mar	0.0	0.0	0.0	0.00	0.00	0.00	0.00	0.00	0.00	0.00	0.00	0.00
Feb	0.2	0.0	0.0	0.00	0.00	0.00	0.00	0.00	0.00	0.00	0.00	0.00
Jan	-0.10	0.0	0.0	0.00	0.00	0.00	0.00	-0.2	-0.4	-0.1	0.00	0.00

Cotton
SPEI in different time scales

	1-month	2-month	3-month	4-month	5-month	6-month	7-month	8-month	9-month	10-month	11-month	12-month
Dec	0.50	0.0	0.0	0.0	0.0	0.0	0.0	0.0	0.0	0.2	0.3	0.4
Nov	0.30	0.0	0.0	0.3	0.0	0.1	0.4	0.6	0.4	0.1	-0.1	0.3
Oct	0.60	0.0	0.0	0.0	0.0	0.0	0.0	0.0	0.0	0.0	0.4	0.5
Sept	0.00	0.0	0.0	0.0	0.0	0.0	0.0	0.0	0.0	0.0	0.0	0.0
Aug	0.00	0.0	0.0	0.0	0.0	0.0	0.0	0.0	-0.2	-0.2	-0.1	0.0
July	0.00	0.0	0.0	0.6	0.6	0.0	0.0	0.0	-0.1	-0.2	-0.2	-0.3
Jun	0.00	0.0	0.0	0.0	0.0	0.0	0.0	0.0	0.0	0.0	0.0	0.0
May	0.45	0.4	0.0	0.1	0.0	-0.2	-0.3	0.0	0.0	0.0	-0.1	-0.1
Apr	0.40	0.6	0.0	0.2	0.0	0.6	0.3	0.0	0.0	0.0	-0.1	0.0
Mar	0.50	0.3	0.0	0.0	0.0	0.0	0.0	0.0	0.0	0.0	0.0	0.0
Feb	0.21	0.1	0.0	0.0	0.0	0.0	0.0	0.0	0.0	0.0	0.0	0.0
Jan	0.00	0.00	0.0	0.0	0.0	0.0	0.0	0.0	0.0	0.0	0.0	0.0

Wheat
SPEI in different time scales

	1-month	2-month	3-month	4-month	5-month	6-month	7-month	8-month	9-month	10-month	11-month	12-month
Dec	0.1	0.2	-0.1	-0.1	-0.2	-0.3	-0.1	0.0	0.5	0.3	0.2	-0.2
Nov	0.2	0.0	0.4	0.3	-0.1	-0.2	-0.1	0.4	0.4	0.2	0.1	0.3
Oct	-0.1	0.4	0.0	0.6	0.0	0.0	0.0	0.0	0.2	0.1	0.1	0.4
Sept	-0.1	0.3	0.6	0.0	0.0	0.0	0.0	0.0	0.0	0.0	0.1	0.3
Aug	-0.2	-0.1	0.2	0.4	0.0	0.0	0.0	0.0	-0.1	-0.2	-0.1	0.0
July	-0.3	-0.2	0.1	0.3	0.0	0.0	0.0	0.0	-0.2	0.5	0.2	0.2
Jun	-0.1	-0.1	0.1	0.0	0.0	0.0	0.0	0.0	-0.3	0.0	-0.3	-0.2
May	0.2	0.2	0.3	0.0	0.0	0.0	0.0	0.0	0.0	0.0	0.0	0.0
Apr	0.3	0.4	0.3	0.0	0.0	0.0	0.0	0.0	0.0	0.0	0.0	0.0
Mar	-0.6	0.4	0.2	0.0	-0.1	-0.3	-0.3	0.3	0.0	0.0	0.0	0.0
Feb	0.3	0.2	0.1	0.0	0.0	0.0	0.0	0.0	0.0	0.0	0.0	0.0
Jan	0.2	0.1	0.1	0.1	0.0	0.0	0.0	0.0	0.0	0.0	0.0	0.0

Fig. 4.55 SYRS and de-trended SPEI relationship for maize, cotton and wheat, during reference period

SSP126

SPEI in different time scales

	1-month	2-month	3-month	4-month	5-month	6-month	7-month	8-month	9-month	10-month	11-month	12-month
Dec	0.0	0.0	0.0	0.0	0.0	0.0	0.0	0.0	0.0	0.0	0.0	0.0
Nov	0.1	0.0	0.5	0.4	0.1	0.0	0.0	0.0	0.0	0.0	0.0	0.0
Oct	0.0	0	0.4	0.4	0.1	0.0	0.0	0.0	0.0	0.0	0.0	0.0
Sept	0.0	0.0	0.0	0.0	0.0	0.0	0.0	0.0	0.0	0.0	0.0	0.0
Aug	0.1	0.0	0.0	0.0	0.0	0.0	0.0	0.0	0.0	0.0	0.0	0.0
July	0.1	-0.1	-0.2	-0.3	0.5	0.0	0.0	0.0	0.0	0.0	0.0	0.0
Jun	0.0	-0.2	-0.4	-0.3	0.1	0.0	0.0	0.0	0.0	0.0	0.0	0.0
May	0.3	0.5	0.0	0.0	0.0	0.0	0.0	0.0	0.0	0.0	0.0	0.0
Apr	0.5	0.4	0.0	0.0	0.0	0.0	0.3	0.2	0.0	0.0	0.0	0.0
Mar	0.0	0.1		0.0	0.0	0.0	0.1	0.1	0.0	0.0	0.0	0.0
Feb	0.0	0.0	0.0	0.0	-0.4	-0.1	-0.2	0.0	0.0	0.0	0.0	0.0
Jan	0.2	0	0	0	-0.3	-0.2	-0.3	0.0	0.0	0.0	0.0	0.0

SSP245

SPEI in different time scales

	1-month	2-month	3-month	4-month	5-month	6-month	7-month	8-month	9-month	10-month	11-month	12-month
Dec	0.0	0.0	0.0	0.0	0.0	0.0	0.0	0.0	0.0	0.0	0.0	0.3
Nov	0.0	0.0	0.0	0.0	0.3	0.2	0.0	0.0	0.0	0.0	0.0	0.2
Oct	0.0	0.0	0.0	0.0	0.4	0.4	0.0	0.0	0.0	0.0	0.0	0.0
Sept	0.0	0.0	0.0	0.0	0.0	0.0	0.0	0.0	0.0	0.0	0.0	0.0
Aug	0.0	0.0	0.0	0.0	0.0	0.0	0.0	0.0	0.0	0.0	0.0	0.0
July	0.0	0.0	-0.4	-0.3	0.0	0.0	0.0	0.0	0.0	0.0	0.0	0.0
Jun	0.0	0.0	-0.4	-0.3	0.0	0.0	0.0	0.0	0.0	0.0	0.0	0.0
May	0.5	0.6	0.4	0.0	0.0	0.0	0.0	0.0	0.0	0.0	0.0	0.0
Apr	0.2	0.3	0.2	0.0	0.3	0.2	0.0	0.0	0.0	0.0	0.0	0.0
Mar	0.0	0.0		0.0	0.1	0.1	0.0	0.0	0.0	0.0	0.0	0.0
Feb	0.0	0.0	-0.1	-0.2	0.0	0.0	0.0	0.0	0.0	0.0	0.0	0.0
Jan	-0.2	-0.3	-0.2	-0.3	0	0.0	0.0	0.0	0.0	0.0	0.0	0

SSP370

SPEI in different time scales

	1-month	2-month	3-month	4-month	5-month	6-month	7-month	8-month	9-month	10-month	11-month	12-month
Dec	0.6	0.5	0.0	0.0	0.0	0.0	0.0	0.0	0.0	0.0	0.0	0.3
Nov	0.3	0.3	0.0	0.0	0.0	0.0	0.0	0.0	0.0	0.0	0.0	0.2
Oct	0.2	0.1	0.0	0.0	0.0	0.0	0.0	0.0	0.0	0.0	0.0	0.0
Sept	0.0	0.0	0.0	0.0	0.0	0.0	0.0	0.0	0.0	0.0	0.0	0.0
Aug	0.0	0.0	0.0	0.0	0.0	0.0	0.0	0.0	0.0	0.0	0.0	0.0
July	0.0	0.0	0.0	0.0	0.0	-0.3	-0.3	0.0	0.0	0.0	0.0	0.0
Jun	0.0	0.0	0.0	0.0	0.0	-0.2	-0.2	0.0	0.0	0.0	0.0	0.0
May	0.5	0.3	0.0	0.0	0.0	0.0	0.0	0.0	0.0	0.0	0.0	0.0
Apr	0.2	0.1	0.0	0.0	0.0	0.0	0.0	0.0	0.0	0.0	0.0	0.0
Mar	0.0	0.0	0.0	0.0	0.0	0.0	0.0	0.0	0.0	0.0	0.0	0.0
Feb	0.0	-0.1	-0.4	-0.2	0.0	0.0	0.0	0.0	0.0	0.0	0.3	0.6
Jan	0.0	-0.2	-0.2	0	0.0	0.0	0.0	0.0	0.0	0.0	0.0	0.0

SSP585

SPEI in different time scales

	1-month	2-month	3-month	4-month	5-month	6-month	7-month	8-month	9-month	10-month	11-month	12-month
Dec	0.0	0.0	0.0	0.0	0.0	0.0	0.0	0.0	0.0	0.0	0.0	0.3
Nov	0.4	0.3	0.0	0.0	0.0	0.0	0.0	0.0	0.0	0.0	0.0	0.2
Oct	0.1	0.1	0.0	0.0	0.0	0.0	0.0	0.0	0.0	0.0	0.0	0.0
Sept	0.0	0.0	0.0	0.0	0.0	0.0	0.0	0.0	0.0	0.0	0.0	0.0
Aug	0.0	0.0	0.0	0.0	0.0	0.0	0.0	0.0	0.0	0.0	0.0	0.0
July	0.0	0.0	0.0	0.0	0.0	0.0	0.0	0.0	0.0	0.0	0.0	-0.4
Jun	0.0	0.0	0.0	0.0	0.0	0.0	0.0	0.0	0.0	0.0	0.0	-0.1
May	0.0	0.0	0.0	0.0	0.6	0.4	0.0	0.0	0.0	0.0	0.0	0.0
Apr	0.0	0.0	0.0	0.0	0.1	0.1	0.0	0.0	0.0	0.0	0.0	0.0
Mar	0.0	0.0	0.0	0.0	0.0	0.0	0.0	0.0	0.0	0.0	0.0	0.0
Feb	0.0	0.0	0.0	0.0	-0.1	-0.4	-0.3	0.0	0.0	0.0	0.1	0.1
Jan	0.0	0.0	0.0	0.0	-0.2	-0.2	-0.2	0.0	0.0	0.0	0.2	0.2

Fig. 4.56 SYRS and de-trended SPEI relationship for maize under different scenarios

SSP126
SPEI for different time scale

	1-month	2-month	3-month	4-month	5-month	6-month	7-month	8-month	9-month	10-month	11-month	12-month
Dec	0.0	0.0	0.0	0.0	0.0	0.0	0.0	0.0	0.0	0.0	0.0	0.0
Nov	0.1	0.0	0.0	0.0	0.0	0.0	0.0	0.0	0.1	0.0	0.0	0.0
Oct	0.4	0.4	0.0	0.0	0.0	0.0	0.0	0.0	-0.1	-0.1	0.0	0.0
Sept	0.1	0.4	0.0	0.4	0.6	0.0	0.0	0.0	-0.2	-0.2	0.0	0.0
Aug	0.5	0.0	0.0	0.6	0.0	0.0	0.0	0.0	-0.3	-0.3	0.0	0.0
July	0.1	0.0	0.0	0.5	0.5	0.0	0.0	0.3	0.0	0.0	0.0	0.0
Jun	-0.2	0.0	0.0	0.1	0.1	0.0	0.0	0.3	0.0	0.0	0.0	0.0
May	-0.1	0.0	0.0	0.0	0.0	0.0	0.0	0.5	0.0	0.0	0.0	0.0
Apr	-0.1	0.0	0.0	0.0	0.0	0.0	0.0	0.3	0.0	0.0	0.0	0.0
Mar	0.0	0.0	0.0	0.0	0.0	0.0	0.0	0.0	0.0	0.0	0.0	0.0
Feb	0.0	0.0	0.0	-0.1	-0.2	0.0	0.0	0.0	0.0	0.2	0.0	0.0
Jan	0.0	0.0	0.0	-0.2	-0.3	0.0	0.0	0.0	0.0	0.0	0.0	0.0

SSP245
SPEI for different time scale

	1-month	2-month	3-month	4-month	5-month	6-month	7-month	8-month	9-month	10-month	11-month	12-month
Dec	0.0	0.0	0.0	0.0	0.0	0.0	0.0	0.0	0.0	0.0	0.0	0.0
Nov	0.1	0.0	0.0	0.0	0.1	0.0	0.0	0.0	0.1	0.0	0.0	0.0
Oct	0.0	0.0	0.0	0.0	0.0	0.0	0.0	0.0	0.1	0.1	0.0	0.0
Sept	0.0	0.0	0.5	0.0	0.6	0.0	0.0	0.0	0.2	0.2	0.0	-0.2
Aug	0.0	0.0	0.4	0.5	0.0	0.0	0.0	0.0	0.0	0.0	0.0	-0.6
July	0.1	0.0	0.4	0.3	0.4	0.0	0.0	0.0	-0.3	-0.3	0.0	0.0
Jun	0.3	0.0	0.2	0.1	0.1	0.0	0.0	0.0	0.3	0.2	0.0	0.0
May	-0.2	0.0	0.0	-0.1	-0.4	0.0	0.0	0.0	0.3	0.3	0.0	0.0
Apr	-0.2	0.0	-0.1	-0.2	-0.3	0.0	0.0	0.0	0.0	0.0	0.0	0.0
Mar	0.0	0.0		0.0	0.0	0.0	0.0	0.0	-0.3	-0.3	0.0	0.0
Feb	0.0	0.0	0.0	0.0	0.0	0.0	0.0	0.0	-0.2	-0.1	0.0	0.0
Jan	0.0	0.0	-0.2	-0.1	0.0	0.0	0.0	0.0	0.0	0.0	0.0	0.0

SSP370
SPEI for different time scale

	1-month	2-month	3-month	4-month	5-month	6-month	7-month	8-month	9-month	10-month	11-month	12-month
Dec	-0.1	-0.3	0.0	0.0	0.0	0.0	0.0	0.0	0.0	0.0	0.0	0.0
Nov	0.1	0.0	0.0	0.0	0.1	0.0	0.0	0.0	0.0	0.0	0.0	0.0
Oct	0.0	0.0	0.0	0.0	0.0	0.0	0.0	0.0	0.0	0.0	0.0	0.0
Sept	0.6	0.2	0.4	0.0	0.0	0.0	0.0	0.0	0.2	0.1	0.0	0.1
Aug	0.0	0.0	0.3	0.2	0.0	0.0	0.0	0.0	0.0	0.0	0.0	0.2
July	0.0	0.0	0.2	0.1	0.0	0.0	0.0	0.0	0.0	0.0	0.0	0.0
Jun	0.3	0.2	0.2	0.1	0.1	0.0	0.0	0.0	0.0	0.0	0.0	0.0
May	-0.2	0.0	-0.1	-0.2	-0.3	0.0	0.0	0.0	0.0	0.0	0.0	0.0
Apr	-0.2	0.1	0.0	0.0	0.0	0.0	0.0	0.0	0.0	0.0	0.0	0.0
Mar	0.0	0.1		0.0	0.0	0.0	0.0	0.0	0.0	-0.4	-0.3	0.0
Feb	0.0	0.0	0.0	0.0	0.0	0.0	0.0	0.0	0.0	-0.1	-0.2	-0.3
Jan	0.0	0.0	0.0	0.0	0.0	0.0	0.0	0.0	0.0	0.0	0.0	0.0

SSP585
SPEI for different time scale

	1-month	2-month	3-month	4-month	5-month	6-month	7-month	8-month	9-month	10-month	11-month	12-month
Dec	0.0	0.0	0.0	0.0	0.0	0.0	0.0	0.0	0.0	0.0	0.1	0.2
Nov	0.0	0.0	0.0	0.0	0.0	0.0	0.0	0.0	0.0	0.0	0.4	0.3
Oct	0.0	0.0	0.0	0.0	0.0	0.0	0.0	0.0	0.0	0.0	0.0	0.0
Sept	0.6	0.2	0.4	0.0	0.0	0.0	0.0	0.0	-0.1	-0.3	0.0	0.0
Aug	-0.1	-0.2	0.0		0.0	0.0	0.0	0.0	-0.2	-0.1	0.0	0.0
July		-0.3	0.0	0.0	0.0	0.0	0.0	0.0	0.0	0.0	0.0	0.0
Jun	0.3	0.2	0.2	0.1	0.1	0.0	0.0	0.0	0.0	0.0	0.0	0.0
May	0.6	0.5	0.1	0.0	0.0	0.0	0.0	0.0	0.0	0.0	0.0	0.0
Apr	0.0	0.0	0.0	0.4	0.2	0.0	0.0	0.0	0.0	0.0	0.0	0.0
Mar	0.0	0.0		0.0	0.0	0.0	0.0	0.0	0.0	-0.2	-0.1	0.0
Feb	0.0	0.0	0.0	0.0	0.0	0.0	0.0	0.0	0.0	-0.3	-0.4	0.0
Jan	0.0	0.0	0.0	0.0	0.0	0.0	0.0	0.0	0.0	0.0	0.0	0.0

Fig. 4.57 SYRS and de-trended SPEI relationship for wheat under different scenarios

SSP16
SPEI for different time scales

	1-month	2-month	3-month	4-month	5-month	6-month	7-month	8-month	9-month	10-month	11-month	12-month
Dec	0.0	0.0	0.0	0.0	0.0	0.0	0.0	0.0	0.0	0.0	0.0	0.0
Nov	0.1	0.0	0.0	0.0	0.1	0.1	0.0	0.0	0.0	0.0	0.0	0.0
Oct	0.0	0.0	0.0	0.0	0.1	0.2	0.0	0.0	0.0	0.0	0.0	0.0
Sept	0.0	0.0	0.0	0.0	0.0	0.0	0.0	0.0	0.0	0.0	0.0	0.0
Aug	0.1	0.1	0.0	0.0	0.0	0.0	0.0	0.0	0.0	0.0	0.0	0.0
July	0.1	0.1	0.0	0.0	0.5	0.0	0.0	0.0	0.0	0.0	0.0	0.0
Jun	0.0	0.0	0.0	0.0	0.1	0.0	0.0	0.0	0.0	0.0	0.0	0.0
May	0.7	0.5	0.0	0.0	0.0	0.0	0.0	0.0	0.0	0.0	0.0	0.0
Apr	0.5	0.4	0.0	0.0	0.0	0.0	0.3	0.2	0.0	0.0	0.0	0.4
Mar	0.0	0.1	0.0	0.0	0.0	0.0	0.1	0.1	0.0	0.0	0.0	0.5
Feb	0.0	0.0	0.0	0.0	-0.4	-0.1	-0.2	0.0	0.0	0.0	0.0	0.0
Jan	0.2	0	0.0	0.0	-0.3	-0.2	-0.3	0.0	0.0	0.0	0.0	0.0

SSP245
SPEI for different time scales

	1-month	2-month	3-month	4-month	5-month	6-month	7-month	8-month	9-month	10-month	11-month	12-month
Dec	-0.2	-0.2	-0.2	0.0	0.0	0.0	0.0	0.0	0.0	0.0	0.2	0.0
Nov	-0.3	-0.3	-0.1	0.0	0.0	0.0	0.0	0.0	0.0	0.0	0.2	0.0
Oct	0.0	0.0	0.0	0.0	0.0	0.0	0.0	0.0	0.0	0.0	0.0	0.0
Sept	0.0	0.0	0.0	0.0	0.0	0.0	0.0	0.0	0.0	0.0	0.0	0.0
Aug	0.0	0.0	0.0	0.0	0.0	0.0	0.0	0.0	0.0	0.0	0.0	0.0
July	0.0	0.0	0.0	0.0	0.0	0.0	0.0	0.0	0.0	0.0	0.0	0.0
Jun	0.0	0.0	0.0	0.0	0.0	0.0	0.0	0.0	0.0	0.0	0.0	0.1
May	0.0	0.7	0.3	0.5	0.0	0.0	0.0	0.0	0.6	0.2	0.0	0.0
Apr	0.0	0.6	0.5	0.4	0.0	0.0	0.0	0.0	0.4	0.2	0.0	0.0
Mar	0.0	0.2	0.2	0.1	0.0	0.0	0.0	0.0	0.0	0.0	0.0	0.0
Feb	0.0	0.0	0.0	0.0	0.0	0.0	0.0	0.0	0.0	0.0	0.0	-0.1
Jan	0.0	0.0	0.0	0.0	0.0	0.0	0.0	0.0	0.0	0.0	0.0	-0.1

SSP370
SPEI for different time scales

	1-month	2-month	3-month	4-month	5-month	6-month	7-month	8-month	9-month	10-month	11-month	12-month
Dec	0.0	0.0	0.0	0.0	0.0	0.0	0.0	0.0	0.0	0.0	0.0	0.3
Nov	0.0	0.0	0.0	0.0	0.0	0.0	0.0	0.0	0.0	0.0	0.0	0.0
Oct	0.0	0.0	0.0	0.0	0.0	0.0	0.0	0.0	0.0	0.0	0.0	0.0
Sept	0.0	0.0	0.0	0.0	0.0	0.0	0.0	0.0	0.0	0.0	0.0	0.0
Aug	0.0	0.0	0.0	0.0	0.0	0.0	0.4	0.3	0.0	0.0	0.0	0.0
July	0.0	0.0	0.0	0.0	0.0	0.0	0.0	0.0	0.0	0.0	0.0	0.0
Jun	0.0	0.0	0.0	0.0	0.0	0.0	0.0	0.0	0.0	0.0	-0.3	-0.2
May	0.6	0.3	0.0	-0.2	0.0	0.0	0.0	0.0	0.0	0.0	-0.1	0.0
Apr	0.4	0.6	0.0	-0.1	-0.1	0.0	0.0	0.0	0.0	0.0	0.0	0.0
Mar	0.0	0.2	0.0	0.0	0.0	0.0	0.0	0.0	0.0	0.0	0.0	0.0
Feb	0.0	0.0	0.0	0.0	0.0	0.0	0.0	0.0	0.0	0.0	0.0	0.0
Jan	0.0	0.0	0.0	0.0	0.0	0.0	0.0	0.0	0.0	0.0	0.0	0.0

SSP585
SPEI for different time scales

	1-month	2-month	3-month	4-month	5-month	6-month	7-month	8-month	9-month	10-month	11-month	12-month
Dec	0.0	0.0	-0.1	-0.2	0.0	0.0	0.0	0.0	0.0	0.0	0.2	0.0
Nov	0.0	0.0	-0.1	0.0	0.0	0.0	0.0	0.0	0.0	0.0	0.2	0.0
Oct	0.0	0.0	0.0	0.0	0.0	0.0	0.0	0.0	0.0	0.0	0.0	0.0
Sept	0.0	0.0	0.0	0.0	0.0	0.0	0.0	0.0	0.0	0.0	-0.1	-0.4
Aug	0.0	0.0	0.0	0.0	0.0	0.0	0.0	0.0	0.0	0.0	-0.1	-0.1
July	0.0	0.0	0.0	0.0	0.0	0.0	0.0	0.0	0.0	0.0	0.0	0.0
Jun	0.0	0.0	0.0	0.0	0.0	0.0	0.0	0.0	0.0	0.0	0.0	0.0
May	0.3	0.6	0.0	0.0	0.0	0.0	0.0	-0.2	-0.1	0.0	0.0	0.0
Apr	0.5	0.6	0.0	0.0	0.0	0.0	0.0	0.0	0.0	0.0	0.0	0.0
Mar	0.2	0.2	0.0	0.0	0.0	0.0	0.0	0.0	0.0	0.0	0.0	0.0
Feb	0.0	0.0	0.0	0.0	0.0	0.0	0.0	0.0	0.6	0.2	0.0	0.0
Jan	0.0	0.0	-0.2	-0.3	0.0	0.0	0.0	0.0	0.4	0.2	0.0	0.0

Fig. 4.58 SYRS and de-trended SPEI relationship for cotton under different scenarios

4.6.5 Conclusion

As a part off the research, the present study investigated the impact of climate change on yield of maize, cotton and wheat in the semi-arid region of Upper Godavari River Basin (UGRB) using AquaCrop model. Ensemble mean of five climate GCMs taken from CMIP6 model were given as input crop model to project future crop yield. Further, the crop-drought relationship status was obtained in varying climate scenarios. The key findings of the study are:

i. The AquaCrop model performed well for both calibration and validation period for maize, cotton and wheat crops based on the performance measures.
ii. Climate changes including increased temperatures, changes in seasonal precipitation amount and patterns, and elevated atmospheric CO_2 concentration have important impacts on crop productivity and water use. Precipitation, maximum and minimum temperature is expected to increase under future scenarios. Basically, temperature and CO_2 affect the crop production rather than precipitation. Moreover, the monthly average precipitation showed significant change as compared to the reference period. For four SSPs, future ensemble climatic models predict warmer climate change scenarios and increased atmospheric CO_2.
iii. The climate change impact analysis of four scenarios on crop yield, indicated significant increase in the maize, cotton and wheat crops for future scenarios. The most significant increase crop yield is expected in the maize followed by wheat and cotton in the SSP585 scenario. At the end of the 21st century, the crop yield is expected to increase significantly for SSP585 scenarios. The average yield will increase, but this will occur in a non-linear manner.
iv. The increase in the mean crop yield with respect to the reference period showed that the highest increase is expected during the far future (2081-2099) in most of the cases.
v. De-trended SPEI has a relatively strong association with the SYRS at important crop productive stages in observed period.
vi. The magnitudes of the correlations between various agricultural crops clearly showed that yield-drought correlation values tended to be higher for the SPEI at the 1- 4-month lags in the future scenarios.

vii. The yield-response to drought also varied among crops: the greatest yield-drought correlation was for wheat and the least for maize for observed period. In future scenarios, cotton is expected to be more sensitive to drought onset.

viii. The results of the study are important in understanding the possible impact of climate change on crop yield and helpful in developing knowledge for stakeholders and planners to develop appropriate plans and strategies. Apart from assessing the potential impacts of climate change on crop productivity and assessing the impacts, modelling can helpful updating agricultural adaptation strategies for managing these risks and beginning to tease out which adaptations are more robust under future conditions.

CHAPTER5

SUMMARY AND CONCLUSIONS

5.1 Summary

Climate change affects hydrological cycle, sea levels and sea surface temperature patterns and agricultural production. The extent, frequency and occurrences of extreme events like droughts and floods could be attributed to the global changes on climatic pattern (IPCC, 2013). It is reported that that the impact of climate change will affect the drought pattern over GRB. Hence, the impact of climate change on drought pattern must be studied in GRB scale. Further, onset and offset criteria of drought affect cropping pattern, cultivation period, and crop productivity. Uneven rainfall distributions and dry months may have an impact on crop production. However, drought footprints have a correlation with crop productivity. As a result, assessing the crop-drought relationship in the context of climate change is unavoidable for long-term development in agricultural practices.

SPEI for the 3-month time scale was calculated using precipitation and evapotranspiration data from the GRB for the reference and future periods. Individually, bias-adjusted RCMs revealed significant uncertainties in climate parameters. As a result, the REA method was used to reduce the uncertainties caused by individual RCMs. Drought return, peak, severity, and durations were evaluated for two emission scenarios, RCP4.5 and RCP8.5. The trivariate regional frequency analysis was used to conduct a comprehensive assessment of drought frequency, considering the inherent dependence between the drought characteristics.

The non-stationarity drought indices such as NSPI and NRDI were developed by considering precipitation and initial value series with the large-scale climate indices as covariates. Both NSPI and NRDI could be applied to identify more complex aspect of drought occurrence. The probabilistic estimation of drought characteristics was carried out to estimate drought return periods. Drought return periods were also calculated using the D-vine PCC model and trivariate copula model. Then trivariate copula model and PCC model were compared.

The integration of agricultural and meteorological drought plays a vital role in the prediction and reliable monitoring of drought. The single variable dependent drought cannot adequately define the onset and withdrawal characteristics of drought. MSDI was developed based on precipitation and soil moisture considering bivariate copulas. Similarly, RTDI was

developed, which incorporated precipitation, soil moisture, and evapotranspiration. MSDI and RTDI effectively represent meteorological and agricultural droughts by considering the complex climate pattern.

Drought monitoring is a difficult subject due to its reliance on various climatic variables. To address this, a copula-based probabilistic MDI that represent the meteorological, hydrological, and agricultural droughts simultaneously has been developed. Four variate Clayton copula was the best fit copula model that used to combine precipitation, evapotranspiration, soil moisture and streamflow. Evapotranspiration, soil moisture and streamflow were estimated using the SWAT model. The future changes of precipitation, evapotranspiration, soil moisture and streamflow were estimated based on five ensemble bias corrected CMIP6-GCMs. The future MDI was also assessed to identify the impact of climate change on drought using CMIP6-GCMs under four SSPs. Drought characteristics like severity and duration were evaluated to identify the changes in future drought events.

The calibrated and validated AquaCrop model was used to evaluate the climate change impact on crop yields of maize, cotton and wheat over semi-arid region of UGRB. The future crop yield was projected by considering the bias-corrected ensemble CMIP6-GCM outputs under four SSP scenarios (SSP126, SSP245, SSP370 and SSP585) using AquaCrop model. Drought and its relationship to crop characteristics are complicated because the increasing occurrence of drought events caused due to climate variability affects productivity of crops. The temporal SYRS in the study area was investigated, and further, the impact of the de-trended SPEI on maize, cotton and wheat crops were investigated.

5.2 Conclusions

Based on the study, the following conclusions were arrived

i. The drought durations, peaks and severities are expected to increase in the future scenarios of for the basin based on the projections in RCMs.
ii. The spatial variations in the non-stationary indices showed that the western part of the basin is highly susceptible to drought. From the month of January to May, the drought propagated from eastern part to the western part of the basin.
iii. The non-stationary drought models performed better than the stationary drought model.
iv. The PCC model is more reliable than trivariate student's t copula model for obtaining the drought return period.

v. Based on Multivariate Standardised Drought Index (MSDI) and Reconnaissance Trivariate Drought Index (RTDI), the western part of the basin is highly vulnerable to drought.

vi. The multivariate droughts are related to the large-scale climate indices. Hence it could be justified that the large-scale climate indices must be incorporated in the drought assessment studies.

vii. SSP585 scenario indicated lesser drought severity while SSP245 indicated the most vulnerable drought conditions for Wainganga and Indravati river basins.

viii. The climate change impact analysis on crop yield considering the ensemble model showed significant increase in the crop yields for all the major crops for future scenarios. The highest increase in crop yield is expected during the far future (2081-2099) in most of the cases.

ix. The yield-response to drought also varied among crops: the greatest yield-drought correlation was for wheat and the least for maize for observed period. For future scenarios, cotton is expected to be more sensitive to drought onset.

5.3 Contribution from the Study

i. With the understanding of adverse effect of climate change on regional drought mechanism, the present study evaluated the potential climate change impact on drought on a river basin scale, encompassing different climate models. The study analyses the impact of climate change over river Godavari using bias corrected climate projections from Regional Climate Models (RCMs) considering different homogeneous region based on K-means clustering algorithm. The intermodal uncertainties were addressed using Reliability Ensemble Averaging (REA) method considering the performance and convergence criteria. Furthermore, the drought characterization and return period analysis have been carried out based on copula based multivariate techniques.

ii. Non-stationary drought assessment plays a significant role in drought mitigation strategies. Understanding the large-scale climate indices and its teleconnection with climate pattern, the non-stationary drought assessment was carried out for Godavari basin. Drought characteristics were investigated and then compared based on stationary and non-stationary models. A novel approach, Vine copula model was opted and compared with traditional form of trivariate copula modelling for drought return period analysis.

iii. Precipitation, minimum, maximum temperatures were projected based on bias corrected CMIP6-GCMs under four scenarios (SSP126, SSP245, SSP370and SSP585). REA method is implemented to obtain the model ensemble to tackle the uncertainty with in the model. Further, a semi-distributed calibrated hydrological model, SWAT is implemented to project the water balance components such streamflow, evapotranspiration, soil moisture spatially and temporally over two large river basins in Godavari, i.e. Wainganga and Indravati river basins. Further, qualitative association among meteorological, hydrological and agricultural drought is not adequately understood on a river basin scale in India. Hence, the precipitation (P) and the simulated climate variables, like, evapotranspiration (ET), soil moisture (SM) and runoff (Q) from the SWAT have been used to obtain a new copula-based MDI.

iv. Crop growth models like AquaCrop are useful in understanding the impact of climate change on crop production considering the various projections from GCMs and RCMs. In this study, climate change impact on crop yield of major crops of Aurangabad region, i.e., maize, cotton and wheat were studied. AquaCrop model is used to simulate the yield of all the three crops for a historical period (1997-2014) and then compared with observed yield data. The future yield is projected based on calibrated AquaCrop model. Further, a new approach has been developed to obtain crop-drought relationship status considering SPEI and yield series (SYRS) with changing climate condition.

v. Agricultural management strategies and crop monitoring at various scales require a necessary supporting activity to quantify the complexity of crop-climate-soil interactions. This study is aimed to provide useful information to researchers and policymakers in order to better understand the effects of climate change on food security and to develop appropriate adaptation and mitigation options to achieve the desired goals.

5.4 Limitations of the Study

i. LULC is assumed to be constant during SWAT simulations for periods of 2025-2100. This indicates that the climate is the only factor influencing the streamflow variability during future scenarios. The combined impact of LULC and climate could give a better knowledge about the hydrological processes in the basin.

ii. Only major crops have been considered to arrive the yield rather than the actual crop pattern. Crop pattern study would enhance the idea of crop development in this area.

iii. More information from field data can improve regional projections considering crop models.

5.5 Scope for further Studies

Based on the research, the scope for the further studies are identified as:

i. The future projections of LULC will give insight into the future changes in the LULC pattern.
ii. The future projections of non-stationary drought assessment with time as covariate can be considered.
iii. The SWAT model can be calibrated and validated for evapotranspiration and soil moisture based on data availability of this area.
iv. Drought hazard assessment of the basin can be carried out to identify the potential drought prone area.
v. The drought and crop relations must be found for different drought indices obtained for further analysis
vi. Socioeconomic and agricultural droughts must be studied in the entire basin in further studies.

REFERENCES

Aadhar, S., Mishra, V., 2020. On the projected decline in droughts over South Asia in CMIP6 multimodel ensemble. J. Geophys. Res. Atmos. 125(20), e2020JD033587. https://doi.org/10.1029/2020JD033587

Aas, K., Czado, K.C., Frigessi, A., Bakken, H., 2009. Pair-copula constructions of multiple dependence. Insur. Math. Econ. 44:182–198.

Abbaspour, K. C., Rouholahnejad, E., Vaghefi, Srinivas, B., Srinivasan, R., Yang, H., Kløve, B., 2015. A continental-scale hydrology and water quality model for Europe: Calibration and uncertainty of a high-resolution large-scale SWAT model. J. Hydrol, 524, 733-752. https://doi.org/10.1016/j.jhydrol.2015.03.027

Abedinpour, M., Sarangi, A., Rajput, T. B. S., Singh, M., Pathak, H., Ahmad, T., 2012. Performance evaluation of AquaCrop model for maize crop in a semi-arid environment. Agric. Water Manag. 110, 55-66. https://doi.org/10.1016/j.agwat.2012.04.001

Ahmadalipour, A., Moradkhani, H., Svoboda, M., 2017. Centennial drought outlook over the CONUS using NASA-NEX downscaled climate ensemble. Int. J. Climatol. 37(5), 2477-2491. https://doi.org/10.1002/joc.4859

Ahmed, K., Shahid, S., Chung, E. S., Wang, X. J., Harun, S. B., 2019. Climate change uncertainties in seasonal drought severity-area-frequency curves: Case of arid region of Pakistan. J. Hydrol. 570, 473-485. https://doi.org/10.1016/j.jhydrol.2019.01.019

Anand, J., Gosain, A. K., Khosa, R., 2018. Prediction of land use changes based on Land Change Modeler and attribution of changes in the water balance of Ganga basin to land use change using the SWAT model. Sci. Total Environ. 644, 503-519. https://doi.org/10.1016/j.scitotenv.2018.07.017

Angeles, M. E., Gonzalez, J. E., Erickson III, D. J., Hernández, J. L, 2007. Predictions of future climate change in the Caribbean region using global general circulation models. International Journal of Climatology: A Journal of the Royal Meteorological Society. 27(5), 555-569. https://doi.org/10.1002/joc.1416

Arnold, J. G., Moriasi, D. N., Gassman, P. W., Abbaspour, K. C., White, M. J., Srinivasan, R., Santhi C., Harmel R. D., Griensven A. V., Van Liew M. W. , Kannan. N., Jha, M. K., 2012. SWAT: Model use, calibration, and validation. Transactions of the ASABE, 55(4), 1491-1508. https://digitalcommons.unl.edu/biosysengfacpub/406

Bazrafshan, J., Hejabi, S., 2018. A non-stationary reconnaissance drought index (NRDI) for drought monitoring in a changing climate. Water. Resour. Manag. 32(8):2611-2624. https://doi.org/10.1007/s11269-018-1947-z.

Bergström, S., Forsman, A., 1973. Development of a conceptual deterministic rainfall-runoff mode. Nord. Hydrol, 4, 240-253.

Bhatta, B., Shrestha, S., Shrestha, P. K., Talchabhadel, R., 2019. Evaluation and application of a SWAT model to assess the climate change impact on the hydrology of the Himalayan River Basin. Catena, 181, 104082. https://doi.org/10.1016/j.catena.2019.104082

Bird, D. N., Benabdallah, S., Gouda, N., Hummel, F., Koeberl, J., La Jeunesse, I., Meyer, S., Prettenthaler, F., Soddu A., Woess-Gallasch, S., 2016. Modelling climate change impacts on and adaptation strategies for agriculture in Sardinia and Tunisia using AquaCrop and value-at-risk. Sci. Total Environ. 543, 1019-1027. https://doi.org/10.1016/j.scitotenv.2015.07.035

Bisht, D. S., Mohite, A. R., Jena, P. P., Khatun, A., Chatterjee, C., Raghuwanshi, N. S., Singh, R., Sahoo, B., 2020. Impact of climate change on streamflow regime of a large Indian river basin using a novel monthly hybrid bias correction technique and a conceptual modeling framework. J. Hydrol, 590, 125448.

Bisht, D. S., Sridhar, V., Mishra, A., Chatterjee, C., Raghuwanshi, N. S., 2019. Drought characterization over India under projected climate scenario. Int. J. Climatol. 39(4), 1889-1911. https://doi.org/10.1002/joc.5922

Bocchiola, D.A., Nana, E.S., Soncini, A.N., 2013. Impact of climate change scenarios on crop yield and water footprint of maize in the Po valley of Italy. Agric. Water Manag. 116:50-61. https://doi.org/10.1016/j.agwat.2012.10.009

Chawla, I., Mujumdar, P. P., 2015. Isolating the impacts of land use and climate change on streamflow. Hydrol. Earth Syst. Sci. 19(8), 3633-3651. https://doi.org/10.5194/hess-19-3633-2015

Chen, J., Brissette, F. P., Zhang, X. J., Chen, H., Guo, S., Zhao, Y., 2019. Bias correcting climate model multi-member ensembles to assess climate change impacts on hydrology. Clim. Change. 153(3), 361-377. https://doi.org/10.1007/s10584-019-02393-x

Chen, Y., Liu, A., Cheng, X., 2020. Quantifying economic impacts of climate change under nine future emission scenarios within CMIP6. Sci. Total Environ. 703: 134950. https://doi.org/10.1016/J.SCITOTENV.2019.134950

Choudhary, A., Dimri, A. P., Maharana, P., 2018. Assessment of CORDEX-SA experiments in representing precipitation climatology of summer monsoon over India. Theor. Appl. Climatol. 134(1), 283-307. https://doi.org/10.1007/s00704-017-2274-7

Clarke, K.A., 2007. A simple distribution-free test for non-nested model selection. Polit. Anal. 15 (3):347-363. DOI: https://doi.org/10.1093/pan/mpm004.

Das, J., Jha, S., Goyal, M. K., 2020a. On the relationship of climatic and monsoon teleconnections with monthly precipitation over meteorologically homogenous regions in India: Wavelet & global coherence approaches. Atmos. Res. 238, 104889. https://doi.org/10.1016/j.atmosres.2020.104889

Das, J., Jha, S., Goyal, M.K., 2020b. Non-stationary and copula-based approach to assess the drought characteristics encompassing climate indices over the Himalayan states in India. J. Hydrol. 580:24356. https://doi.org/10.1016/j.jhydrol.2019.124356.

Das, J., Poonia, V., Jha, S., Goyal, M. K., 2020c. Understanding the climate change impact on crop yield over Eastern Himalayan Region: ascertaining GCM and scenario uncertainty. Theor. Appl. Climatol. 142(1), 467-482. https://doi.org/10.1007/s00704-020-03332-y

Das, J., Umamahesh, N. V., 2018. Assessment of uncertainty in estimating future flood return levels under climate change. Nat. Hazards. 93(1), 109-124.

Dash, S. S., Sahoo, B., Raghuwanshi, N. S., 2020. A novel embedded pothole module for soil and water assessment tool (SWAT) improving streamflow estimation in paddy-dominated catchments. J. Hydrol. 588, 125103. https://doi.org/10.1016/J.JHYDROL.2020.125103

Deb, P., Kiem, A.S., Babel, M.S., Chu, S.T., Chakma, B., 2015. Evaluation of climate change impacts and adaptation strategies for maize cultivation in the Himalayan foothills of India. J. Water Clim. Chang. 6:596– 614. https://doi.org/10.2166/wcc.2015.070

Debele, S. E., Strupczewski, W. G., Bogdanowicz, E., 2017. A comparison of three approaches to non-stationary flood frequency analysis. Acta. Geophysica, 65(4), 863-883. https://doi.org/10.1007/s11600-017-0071-4

DHI., 2017. Mike zero user's guide. MIKE by DHI. Harsholm, Denmark. Accessed 11 Oct 2020, https://manuals.mikepoweredbydhi.help/2017/MIKE_Zero_ General.htm.

Doorenbos, J., Kassam, A.H., 1979. Yield response to water. FAO Irrigation and Drainage Paper No. 33. Food and Agriculture Organization of the United Nations, Rome, Italy

Duan, K., Wang, X., Liu, B., Zhao, T., Chen, X., 2021. Comparing Bayesian model averaging and reliability ensemble averaging in post-processing runoff projections under climate change. Water. 13(15), 2124. https://doi.org/10.3390/w13152124

Dubey, S. K., Sharma, D., 2018. Assessment of climate change impact on yield of major crops in the Banas River Basin, India. Sci. Total Environ. 635, 10-19. https://doi.org/10.1016/j.scitotenv.2018.03.343

Eyring, V., Bony, S., Meehl, G.A., Senior, C.A., Stevens, B., Stouffer, R.J., Taylor, K.E. 2016 Overview of the Coupled Model Intercomparison Project Phase 6 (CMIP6) experimental design and organization. Geosci. Model Dev. 9:1937–1958. https://doi.org/10.5194/GMD-9-1937-2016

Fan, X., Jiang, L., Gou, J., 2021. Statistical downscaling and projection of future temperatures across the Loess Plateau, China. Weather. Clim. Extremes. 32, 100328. https://doi.org/10.1016/j.wace.2021.100328

Fang, G. H., Yang, J., Chen, Y. N., Zammit, C. 2015. Comparing bias correction methods in downscaling meteorological variables for a hydrologic impact study in an arid area in China. Hydrol Earth Syst Sci. 19(6), 2547-2559. https://doi.org/10.5194/hess-19-2547-2015

Fang, W., Huang, S., Huang, Q., Huang, G., Wang, H., Leng, G., Wang, L., Li, P., Ma, L., 2019. Bivariate probabilistic quantification of drought impacts on terrestrial vegetation

dynamics in mainland China. J. Hydrol. 577, 123980. https://doi.org/10.1016/j.jhydrol.2019.123980.

Farahani, H. J., Izzi, G., Oweis, T. Y., 2009. Parameterization and evaluation of the AquaCrop model for full and deficit irrigated cotton. Agronomy journal, 101(3), 469-476. https://doi.org/10.2134/agronj2008.0182s

Farahmand, A., AghaKouchak, A., 2015. A generalized framework for deriving nonparametric standardized drought indicators. Adv. Water. Resour. 76:140-14 http://dx.doi.org/10.1016/j.advwatres.2014.11.012

Feng, S., Hao, Z., 2020. Quantifying likelihoods of extreme occurrences causing maize yield reduction at the global scale. Sci. Total Environ. 704, 135250. https://doi.org/10.1016/j.scitotenv.2019.135250.

Feng, S., Hao, Z., Zhang, X., Hao, F., 2019. Probabilistic evaluation of the impact of compound dry-hot events on global maize yields. Sci. Total Environ. 689, 1228–1234. https://doi.org/10.1016/j.scitotenv.2019.06.373.

Foster, T., Brozović, N., Butler, A. P., Neale, C. M. U., Raes, D., Steduto, P., Fereres E, Hsiao, T. C., 2017. AquaCrop-OS: An open source version of FAO's crop water productivity model. Agric. Water Manag. 181, 18-22. https://doi.org/10.1016/j.agwat.2016.11.015

Fowler, H. J., Blenkinsop, S., Tebaldi, C. 2007. Linking climate change modelling to impacts studies: recent advances in downscaling techniques for hydrological modelling. International Journal of Climatology: A Journal of the Royal Meteorological Society, 27(12), 1547-1578. https://doi.org/10.1002/joc.1556

Gaitán, E., Monjo, R., Pórtoles, J., Pino-Otín, M. R. 2020. Impact of climate change on drought in Aragon (NE Spain). Sci. Total Environ. 740, 140094. https://doi.org/10.1016/j.scitotenv.2020.140094

Gao, S., Huang, D., Du, N., Ren, C., Yu, H., 2022. WRF ensemble dynamical downscaling of precipitation over China using different cumulus convective schemes. Atmos. Res. 106116. https://doi.org/10.1016/j.atmosres.2022.106116

Genest, C., Favre, A.C., Béliveau, J., Jacques, C., 2007. Metaelliptical copulas and their use in frequency analysis of multivariate hydrological data. Water Resour. Res. 43(9). https://doi.org/10.1029/2006WR005275

Genest, C., Rémillard, B., Beaudoin, D., 2009. Goodness-of-fit tests for copulas: A review and a power study. Insur. Math. Econ 44(2):199-213. https://doi.org/10.1016/j.insmatheco.2007.10.005

Ghosh, S., Mujumdar, P. P., 2008. Statistical downscaling of GCM simulations to streamflow using relevance vector machine. Adv. Water Resour. 31(1), 132-146. https://doi.org/10.1016/j.advwatres.2007.07.005

Giorgi, F., Mearns, L. O., 1991. Approaches to the simulation of regional climate change: a review. Rev. Geophys. 29(2), 191-216. https://doi.org/10.1029/90RG02636

Giorgi, F., Mearns, L. O., 2003. Probability of regional climate change based on the Reliability Ensemble Averaging (REA) method. Geophys. Res. Lett. 30(12). https://doi.org/10.1029/2003GL017130

Grinsted, A., Moore, J.C., Jevrejeva, S, 2004. Application of the cross wavelet transform and wavelet coherence to geophysical time series. Nonlinear Process. Geophys. 11(5/6), 561-566. https://doi.org/10.5194/npg-11-561-2004

Gu, H., Wang, G., Yu, Z., Mei, R., 2012. Assessing future climate changes and extreme indicators in east and south Asia using the RegCM4 regional climate model. Clim. Change 114(2), 301-317. https://doi.org/10.1007/s10584-012-0411-y

Guo, Q., Chen, J., Zhang, X., Shen, M., Chen, H., Guo, S., 2019. A new two-stage multivariate quantile mapping method for bias correcting climate model outputs. Clim. Dyn. 53(5), 3603-3623. https://doi.org/10.1007/s00382-019-04729-w

Guo, Y., Huang, S., Huan, Q., Wang, H., Wang, L., Fang, W., 2019. Copulas-based bivariate socioeconomic drought dynamic risk assessment in a changing environment. J. Hydrol. 575: 1052-1064. https://doi.org/10.1016/j.jhydrol.2019.06.010

Gupta, V., Jain, M. K., 2018. Investigation of multi-model spatiotemporal mesoscale drought projections over India under climate change scenario. J. Hydrol. 567, 489-509. https://doi.org/10.1016/j.jhydrol.2018.10.012

Gupta, V., Jain, M. K., 2021. Unravelling the teleconnections between ENSO and dry/wet conditions over India using nonlinear Granger causality. Atmos. Res. 247, 105168. https://doi.org/10.1016/j.atmosres.2020.105168

Gupta, V., Kumar Jain, M., Singh, V. P., 2020. Multivariate modeling of projected drought frequency and hazard over India. J. Hydrol. Eng. 25(4), 04020003. OI: 10.1061/(ASCE)HE.1943-5584.0001893.

Gusain, A., Ghosh, S., Karmakar, S., 2020. Added value of CMIP6 over CMIP5 models in simulating Indian summer monsoon rainfall. Atmos. Res. 232:104680. https://doi.org/10.1016/J.ATMOSRES.2019.104680

Hao, Z., AghaKouchak, A., 2013. Multivariate standardized drought index: a parametric multi-index model. Adv. Water Resour. 57, 12-18. DOI 10.1016/j.advwatres.2013.03.009

Hao, Z., Hao, F., Singh, V.P., Zhang, X., 2018. Quantifying the relationship between compound dry and hot events and El Niño–southern Oscillation (ENSO) at the global scale. J. Hydrol. 567:332–338. https://doi.org/10.1016/j.jhydrol.2018.10.022

Hargreaves, G. H., Samani, Z. A., 1985. Reference crop evapotranspiration from temperature. Appl. Eng. Agric. 1(2), 96-99.

Harris, I. P. D. J., Jones, P. D., Osborn, T. J., Lister, D. H., 2014. Updated high-resolution grids of monthly climatic observations–the CRU TS3. 10 Dataset. Int. J. Climatol. 34(3), 623-642. https://doi.org/10.1002/joc.3711

Hengade N., Eldho T. I., Ghosh S., 2018. Climate change impact assessment of a river basin using CMIP5 climate models and the VIC hydrological model. Hydrol. Sci. J. 63(4), 596-614. https://doi.org/10.1080/02626667.2018.1441531

Hirabayashi, Y., Tanoue, M., Sasaki, O., Zhou, X., Yamazaki, D., 2021. Global exposure to flooding from the new CMIP6 climate model projections. Sci. Rep. 11(1), 1-7. https://doi.org/10.1038/s41598-021-83279-w

Holzworth, D. P., Snow, V., Janssen, S., Athanasiadis, I. N., Donatelli, M., Hoogenboom, G., White J.W., Thorburn, P., 2015. Agricultural production systems modelling and software: current status and future prospects. Environ. Model. Softw. 72, 276-286. https://doi.org/10.1016/j.envsoft.2014.12.013

Holzworth, D., Huth, N. I., Fainges, J., Brown, H., Zurcher, E., Cichota, R, Verrall S, Herrmann N.I, Zhen B & Snow, V., 2018. APSIM Next Generation: Overcoming challenges in modernising a farming systems model. Environ. Model. Softw. 103, 43-51. https://doi.org/10.1016/j.envsoft.2018.02.002

Hsiao, T. C., Heng, L., Steduto, P., Rojas-Lara, B., Raes, D., Fereres, E., 2009. AquaCrop—the FAO crop model to simulate yield response to water: III. Parameterization and testing for maize. Agronomy Journal, 101(3), 448-459. https://doi.org/10.2134/agronj2008.0218s

Huang, S., Huang, Q., Leng, G., Liu, S. 2016. A nonparametric multivariate standardized drought index for characterizing socioeconomic drought: A case study in the Heihe River Basin. J. Hydrol. 542:875-883. https://doi.org/10.1016/j.jhydrol.2016.09.059

Huang, S., Huang, Q., Leng, G., Liu, S., 2016. A nonparametric multivariate standardized drought index for characterizing socioeconomic drought: A case study in the Heihe River Basin. J. Hydrol. 542, 875-883. https://doi.org/10.1016/j.jhydrol.2016.09.059

Huang, S., Krysanova, V., Hattermann, F., 2015. Projections of climate change impacts on floods and droughts in Germany using an ensemble of climate change scenarios. Reg. Environ. Change. 15(3), 461-473. https://doi.org/10.1007/s10113-014-0606-z

Jasrotia, A. S., Baru, D., Kour, R., Ahmad, S., Kour, K., 2021. Hydrological modeling to simulate stream flow under changing climate conditions in Jhelum catchment, western Himalaya. J. Hydrol. 593, 125887. https://doi.org/10.1016/j.jhydrol.2020.125887

Jehanzaib, M., Shah, S. A., Yoo, J., Kim, T. W., 2020. Investigating the impacts of climate change and human activities on hydrological drought using non-stationary approaches. J. Hydrol. 588, 125052. https://doi.org/10.1016/j.jhydrol.2020.125052

Jha, S., Das, J., & Goyal, M. K., 2021. Low frequency global-scale modes and its influence on rainfall extremes over India: Nonstationary and uncertainty analysis. Int. J. Climatol. 41(3), 1873-1888. https://doi.org/10.1002/joc.6935

Jones, J. W., Hoogenboom, G., Porter, C. H., Boote, K. J., Batchelor, W. D., Hunt, L. A., Wilkens P. W, Singh U, Gijsman A.J., Ritchie, J. T., 2003. The DSSAT cropping system model. Eur. J. Agron. 18(3-4), 235-265. https://doi.org/10.1016/S1161-0301(02)00107-7

Kahya, E., Dracup, J. A., 1993. US streamflow patterns in relation to the El Niño/Southern Oscillation. Water Resour. Res. 29(8), 2491-2503. https://doi.org/10.1029/93WR00744

Karim, M. R., Rahman, M. A., 2015. Drought risk management for increased cereal production in Asian least developed countries. Weather. Clim. Extremes. 7, 24-35. https://doi.org/10.1016/j.wace.2014.10.004

Kendall, M.G., 1975. Rank Correlation Methods. Griffin, London.

Keyantash, J.A., Dracup, J.A., 2004. An aggregate drought index: assessing drought severity based on fluctuations in the hydrologic cycle and surface water storage. Water Resour. Res. 40 (9). doi:10.1029/2003WR002610, 2004

Krishnan, R., Sabin, T.P., Madhura, R.K., Vellore, R.K., Mujumdar, M., Sanjay, J., Rajeevan, M., 2019. Non-monsoonal precipitation response over the Western Himalayas to climate change. Clim. Dyn. 52(8): 4091-4109. https://doi.org/10.1007/s00382-018-4357-2

Kumar, K.S, Anand Raj, P., Sreelatha, K., Sridhar, V., 2021a. Regional analysis of drought severity-duration-frequency and severity-area-frequency curves in the Godavari River Basin, India. Int. J. Clim. 41(12), 5481-5501. https://doi.org/10.1002/joc.7137

Kumar, M., 2016. Impact of climate change on crop yield and role of model for achieving food security. Environ. Monit. Assess. 188(8), 1-14. https://doi.org/10.1007/s10661-016-5472-3

Kumar, N., Poonia, V., Gupta, B. B., Goyal, M. K., 2021b. A novel framework for risk assessment and resilience of critical infrastructure towards climate change. Technol. Forecast. Soc. Change. 165, 120532. https://doi.org/10.1016/j.techfore.2020.120532

Kumar, P., Sarangi, A., Singh, D. K., Parihar, S. S., 2014. Evaluation of AquaCrop model in predicting wheat yield and water productivity under irrigated saline regimes. Irrig. Drain. 63(4), 474-487. https://doi.org/10.1002/ird.1841

Kumar, S., Mishra, A. K., Pramanik, S., Mamidanna, S., Whitbread, A., 2020. Climate risk, vulnerability and resilience: Supporting livelihood of smallholders in semiarid India. Land Use Policy, 97, 104729. https://doi.org/10.1016/j.landusepol.2020.104729

Kurowicka D, Cooke R (2006) Uncertainty Analysis with High Dimensional Dependence Modeling. John Wiley.

Leng, G., Hall, J., 2019. Crop yield sensitivity of global major agricultural countries to droughts and the projected changes in the future. Sci. Total Environ. 654, 811-821. https://doi.org/10.1016/j.scitotenv.2018.10.434

Leng, G., Tang, Q., Rayburg, S., 2015. Climate change impacts on meteorological, agricultural and hydrological droughts in China. Glob. Planet. Change. 126, 23-34. https://doi.org/10.1016/j.gloplacha.2015.01.003

Leung, L. R., Qian, Y., Bian, X., 2003. Hydroclimate of the western United States based on observations and regional climate simulation of 1981-2000. Part I: Seasonal statistics.

J. Clim. 16(12), 1892-1911. https://doi.org/10.1175/1520-0442(2003)016<1892:HOTWUS>2.0.CO;2

Li, F., Zhang, Y., Xu, Z., Teng, J., Liu, C., Liu, W., Mpelasoka, F., 2013. The impact of climate change on runoff in the southeastern Tibetan Plateau. J. Hydrol. 505, 188-201. https://doi.org/10.1016/j.jhydrol.2013.09.052

Liang, X., D. P. Lettenmaier, E. F. Wood, Burges S. J., 1994. A simple hydrologically based model of land surface water and energy fluxes for general circulation models, *J. Geophys. Res.* **99**(D7), 14415–14428, doi: 10.1029/94JD00483.

Lin, G. F., Chang, M. J., Wang, C. F., 2017. A novel spatiotemporal statistical downscaling method for hourly rainfall. Water Resour. Manag. 31(11), 3465-3489. https://doi.org/10.1007/s11269-017-1679-5

Liu, W. T., Kogan, F. N., 1996. Monitoring regional drought using the vegetation condition index. Int. J. Remote Sens. 17(14), 2761-2782. https://doi.org/10.1080/01431169608949106

Liu, X., Pan, Y., Zhu, X., Yang, T., Bai, J., & Sun, Z., 2018. Drought evolution and its impact on the crop yield in the North China Plain. J. Hydrol. 564, 984-996. https://doi.org/10.1016/j.jhydrol.2018.07.077

Liu. S., Zhang. J., Wang. N., Wei. N., 2020. Large-Scale Linkages of Socioeconomic Drought with Climate Variability and Its Evolution Characteristics in Northwest China. Adv. in Meteorol. 2020. https://doi.org/10.1155/2020/2814539

López, J., Francés, F., 2013. Non-stationary flood frequency analysis in continental Spanish rivers, using climate and reservoir indices as external covariates. Hydrol. Earth Syst. Sci. 17(8), 3189-3203. https://doi.org/10.5194/hess-17-3189-2013

Ma, Y., Hong, Y., Chen, Y., Yang, Y., Tang, G., Yao, Y., Tang G., Yao Y, Long D, Li C, Han Z., Liu, R., 2018. Performance of optimally merged multisatellite precipitation products using the dynamic Bayesian model averaging scheme over the Tibetan Plateau. J. Geophys. Res. Atmos. 123(2), 814-834. https://doi.org/10.1002/2017JD026648

Mabhaudhi, T., Modi, A. T., Beletse, Y. G., 2014. Parameterisation and evaluation of the FAO-AquaCrop model for a South African taro (Colocasia esculenta L. Schott) landrace. Agric. For Meteorol. 192, 132-139. https://doi.org/10.1016/j.agrformet.2014.03.013

MacQueen, J., 1967. Some methods for classification and analysis of multivariate observations. In Proceedings of the fifth Berkeley symposium on mathematical statistics and probability (Vol. 1, No. 14, pp. 281-297).

Mancosu, N., Spano, D., Orang, M., Sarreshteh, S., Snyder, R. L., 2016. SIMETAW#-a model for agricultural water demand planning. Water Resour. Manag. 30(2), 541-557. https://doi.org/10.1007/s11269-015-1176-7

Manfreda, S., Fiorentino, M., Iacobellis, V., 2005. DREAM: distributed model for runoff, evapotranspiration, and antecedent soil moisture simulation. Adv. Geosci. 2, 31-39. https://doi.org/10.5194/adgeo-2-31-2005

Mann, H.B., 1945. Nonparametric tests against trend. Econometrica. 13, 245–259.

Masia, S., Trabucco, A., Spano, D., Snyder, R. L., Sušnik, J., Marras, S., 2021. A modelling platform for climate change impact on local and regional crop water requirements. Agric. Water Manag. 255, 107005. https://doi.org/10.1016/j.agwat.2021.107005

Masroor M., Rehman S., Avtar R., Sahan, M., Ahmed R., Sajjad H., 2020. Exploring climate variability and its impact on drought occurrence: Evidence from Godavari Middle sub-basin, India. Weather. Clim. Extremes. 30, 100277. https://doi.org/10.1016/j.wace.2020.100277

Masud M. B., Khaliq M. N., Wheater H. S., 2017. Future changes to drought characteristics over the Canadian Prairie Provinces based on NARCCAP multi-RCM ensemble. Clim. Dyn. 48(7-8), 2685-2705. https://doi.org/10.1007/s00382-016-3232-2

Masud, M. B., Qian, B., Faramarzi, M., 2020. Performance of multivariate and multiscalar drought indices in identifying impacts on crop production. Int. J. Clim. 40(1), 292-307. https://doi.org/10.1002/joc.6210

Mishr. V., 2020. Long-term (1870-2018) drought reconstruction in context of surface water security in India. J. Hydrol. 580:124228. https://doi.org/10.1016/j.jhydrol.2019.124228

Mishra, A. K., Singh, V. P., 2010. A review of drought concepts. J. Hydrol. 391(1-2), 202-216. https://doi.org/10.1016/j.jhydrol.2010.07.012

Mishra, S. K., Sahany, S., Salunke, P., Kang, I. S., Jain, S., 2018. Fidelity of CMIP5 multi-model mean in assessing Indian monsoon simulations. NPJ Clim. Atmos. Sci. 1(1), 1-8. https://doi.org/10.1038/s41612-018-0049-1

Mishra, V., Bhatia, U., Tiwari, A.D., 2020a. Bias-corrected climate projections for South Asia from Coupled Model Intercomparison Project-6. Sci. data, 7(1), 1-13. https://doi.org/10.6084/m9.figshare.12963008

Mishra, V., Shah, H., López, M., Lobanova, A., Krysanova, V., 2020b. Does comprehensive evaluation of hydrological models influence projected changes of mean and high flows in the Godavari River basin? Clim. Change, 163(3), 1187-1205. https://doi.org/10.1007/s10584-020-02847-7

Mishra, V., Tiwari, A. D., Aadhar, S., Shah, R., Xiao, M., Pai, D. S., Lettenmaier, D., 2019. Drought and famine in India, 1870–2016. Geophys. Res. Lett. 46(4), 2075-2083. https://doi.org/10.1029/2018GL081477

Mishra. V., Shah. R., Thrasher, B., 2014. Soil moisture droughts under the retrospective and projected climate in India. J. Hydrometeorol. 15(6): 2267-2292. DOI: 10.1175/JHM-D-13-0177.1. https://doi.org/10.1175/JHM-D-13-0177.1

Monteith, J.L., 1965. Evaporation and environment. In: The state and movement of water in living organisms. XIXth symposium, Soc Exp Biol, Swansea. Cambridge University Press, Cambridge, pp 205–234

Montoya, F., Camargo, D., Ortega, J. F., Córcoles, J. I., Domínguez, A., 2016. Evaluation of Aquacrop model for a potato crop under different irrigation conditions. Agric. Water Manag. 164, 267-280. https://doi.org/10.1016/j.agwat.2015.10.019

Mukherjee, S., Mishra, A., Trenberth, K. E., 2018. Climate change and drought: a perspective on drought indices. Curr. Clim. Change Rep. 4(2), 145-163. https://doi.org/10.1007/s40641-018-0098-x

Muthuvel, D., Amai, M., 2021. Multivariate analysis of concurrent droughts and their effects on Kharif crops-A copula-based approach. Int. J. Clim. https://doi.org/10.1002/joc.7390

Myers, C. G., Oster, J. L., Sharp, W. D., Bennartz, R., Kelley, N. P., Covey, A. K., Breitenbach, S. F., 2015. Northeast Indian stalagmite records Pacific decadal climate change: Implications for moisture transport and drought in India. Geophys. Res. Lett. 42(10), 4124-4132. https://doi.org/10.1002/2015GL063826

Narasimhan, B., & Srinivasan, R. (2005). Development and evaluation of Soil Moisture Deficit Index (SMDI) and Evapotranspiration Deficit Index (ETDI) for agricultural drought monitoring. Agric For Meteorol. 133(1-4), 69-88. https://doi.org/10.1016/j.agrformet.2005.07.012

Nilawar, A. P., Waikar, M. L., 2019. Impacts of climate change on streamflow and sediment concentration under RCP 4.5 and 8.5: A case study in Purna river basin, India. Sci. Total Environ, 650, 2685-2696.

Nyathi, M. K., Van Halsema, G. E., Annandale, J. G., Struik, P. C., 2018. Calibration and validation of the AquaCrop model for repeatedly harvested leafy vegetables grown under different irrigation regimes. Agric. Water Manag. 208, 107-119. https://doi.org/10.1016/j.agwat.2018.06.012

O'neill, B.C., Tebaldi, C., Van Vuuren, D.P., Eyring, V., Friedlingstein, P., Hurtt, G., Knutti, R., Kriegler, E., Lamarque, J.F., Lowe, J., Meehl, G.A., Moss, R., Riahi, K., Sanderson, B.M., 2016. The Scenario Model Intercomparison Project (ScenarioMIP) for CMIP6. Geosci. Model. Dev. 9, 3461–3482. https://doi.org/10.5194/gmd-9-3461-2016

Ojha, R., Nagesh Kumar, D., Sharma, A., Mehrotra, R., 2013. Assessing severe drought and wet events over India in a future climate using a nested bias-correction approach. J. Hydrol. Eng. 18(7), 760-772. DOI:10.1061/(ASCE)HE.1943-5584.0000585

Osorio, J.G., Galiano, S.G., 2012. Non-stationary analysis of dry spells in monsoon season of Senegal River Basin using data from Regional Climate Models (RCMs). J. Hydrol. 450:82-92. https://doi.org/10.1016/j.jhydrol.2012.05.029.

Pai, D. S., Rajeevan, M., Sreejith, O. P., Mukhopadhyay, B., Satbha, N. S, 2014. Development of a new high spatial resolution (0.25× 0.25) long period (1901-2010) daily

gridded rainfall data set over India and its comparison with existing data sets over the region. Mausam. 65(1), 1-18. https://doi.org/10.54302/mausam.v65i1.851

Palmer, W. C., 1965. Meteorological drought. US Department of Commerce, Weather Bureau. 30. Washington, DC, USA.

Pathak, A. A., Dodamani, B. M., 2019. Trend analysis of groundwater levels and assessment of regional groundwater drought: Ghataprabha River Basin, India. Nat. Resour. Res. 28(3), 631-643. https://doi.org/10.1007/s11053-018-9417-0

Paul, S., Ghosh, S., Oglesby, R., Pathak, A., Chandrasekharan, A., Ramsankaran, R. A. A. J., 2016. Weakening of Indian summer monsoon rainfall due to changes in land use land cover. Sci. rep. 6(1), 1-10. https://doi.org/10.1038/srep32177

Pawar, G. S., Kale, M. U., Lokhande, J. N., 2017. Response of AquaCrop model to different irrigation schedules for irrigated cabbage. Agric. Res. 6(1), 73-81. https://doi.org/10.1007/s40003-016-0238-2

Penman, H.L., 1948. Natural evaporation from open water, bare soil and grass. Proc R Soc Lond A193:120–145

Perrin, C.; Michel, C.; Andréassian, V., 2003. Improvement of a parsimonious model for streamflow simulation. J. Hydrol. 279, 275–289. https://doi.org/10.1016/S0022-1694(03)00225-7

Pervez, M. S., Henebry, G. M., 2014. Projections of the Ganges–Brahmaputra precipitation-Downscaled from GCM predictors. J. Hydrol. 517, 120-134. https://doi.org/10.1016/j.jhydrol.2014.05.016

Potop, V., Možný, M., Soukup, J., 2012. Drought evolution at various time scales in the lowland regions and their impact on vegetable crops in the Czech Republic. Agric. For. Meteorol. 156, 121-133. https://doi.org/10.1016/j.agrformet.2012.01.002

Potopová, V., Štěpánek, P., Možný, M., Türkott, L., Soukup, J., 2015. Performance of the standardised precipitation evapotranspiration index at various lags for agricultural drought risk assessment in the Czech Republic. Agric. For. Meteorol. 202, 26-38. https://doi.org/10.1016/j.agrformet.2014.11.022

Pranuthi, G., Tripathi, S. K., 2018. Assessing the climate change and its impact on rice yields of Haridwar district using PRECIS RCM data. Clim. Change. 148(1), 265-278. https://doi.org/10.1007/s10584-018-2176-4

Qi, J., Zhang, X., Yang, Q., Srinivasan, R., Arnold, J.G., Li, J., Waldholf, S.T., Cole, J., 2020. SWAT ungauged: Water quality modeling in the Upper Mississippi River Basin. J. Hydrol. 584, 124601. https://doi.org/10.1016/J.JHYDROL.2020.124601

Quan, H., Ding, D., Wu, L., Qiao, R., Zhang, T., Feng, H., Wu, L., Siddique, K. H., 2022. Future climate change impacts on mulched maize production in an arid irrigation area. Agric.Water Manag. 266, 107550. https://doi.org/10.1016/j.agwat.2022.107550

Raftery, A. E., Gneiting, T., Balabdaoui, F., Polakowski, M., 2005. Using Bayesian model averaging to calibrate forecast ensembles. Mon. Weather Rev. 133(5), 1155-1174. https://doi.org/10.1175/MWR2906.1

Rajbanshi, J., Das S., 2021. The variability and teleconnections of meteorological drought in the Indian summer monsoon season: Implications for staple crop production. J. Hydrol. 603: 126845. https://doi.org/10.1016/J.JHYDROL.2021.126845

Raje, D., Mujumdar, P. P., 2011. A comparison of three methods for downscaling daily precipitation in the Punjab region. Hydrol. Process. 25(23), 3575-3589. https://doi.org/10.1002/hyp.8083

Rajsekhar, D., Singh, V.P., Mishra, A.K., 2015. Multivariate drought index: An information theory based approach for integrated drought assessment. J. Hydrol. 526:164-182. http://dx.doi.org/10.1016/j.jhydrol.2014.11.031

Raoufi, R. S., Soufizadeh, S., 2020. Simulation of the impacts of climate change on phenology, growth, and yield of various rice genotypes in humid sub-tropical environments using AquaCrop-Rice. Int. J. Biometeorol. 64(10), 1657-1673. https://doi.org/10.1007/s00484-020-01946-5

Rashid, M.M., Beecham, S., 2019. Development of a non-stationary Standardized Precipitation Index and its application to a South Australian climate. Sci. Total Environ. 657, 882-892. https://doi.org/10.1016/j.scitotenv.2018.12.052.

Roushangar, K., Nourani, V., Alizadeh, F. 2018. A multiscale time-space approach to analyze and categorize the precipitation fluctuation based on the wavelet transform and information theory concept. Hydrol. Res., 49(3), 724-743. https://doi.org/10.2166/nh.2018.143

Russo, S., Dosio, A., Sterl, A., Barbosa, P., Vogt, J. 2013. Projection of occurrence of extreme dry-wet years and seasons in Europe with stationary and nonstationary Standardized Precipitation Indices. J. Geophys. Res. Atmos. 118:7628–7639. https://doi:10.1002/jgrd.50571, 2013.

Sahai, A.K, Grimm, A.M., Satyan, V., Pant, G.B. 2003. Long-lead prediction of Indian summer monsoon rainfall from global SST evolution. Clim. Dyn. 20(7-8):855-863. https://DOI 10.1007/s00382-003-0306-8.

Salvadori, G., De Michele, C., 2004. Frequency analysis via copulas: Theoretical aspects and applications to hydrological events. Water Resour. Res. 40(12). https://doi.org/10.1029/2004WR003133

Samimi, M., Mirchi, A., Moriasi, D., Ahn, S., Alian, S., Taghvaeian, S., Sheng, Z., 2020. Modeling arid/semi-arid irrigated agricultural watersheds with SWAT: Applications, challenges, and solution strategies. J. Hydrol. 590, 125418. https://doi.org/10.1016/J.JHYDROL.2020.125418

Sengupta, A., Rajeevan, M., 2013. Uncertainty quantification and reliability analysis of CMIP5 projections for the Indian summer monsoon. Curr. Sci. 1692-1703.

Shafer, B. A., Dezman, L.E., 1982. Development of a Surface Water Supply Index (SWSI) to assess the severity of drought conditions in snowpack runoff areas. In: Proceedings of the Western Snow Conference, Colo. State Univ. Fort Collins, pp. 164–175

Shah, D., Mishra, V., 2020. Drought onset and termination in India. J. Geophys. Res. Atmos. 125(15):e2020JD032871. https://doi.org/ 10.1029/2020JD032871

Shao, S., Zhang, H., Singh, V. P., Ding, H., Zhang, J., Wu, Y. 2022. Nonstationary analysis of hydrological drought index in a coupled human-water system: Application of the GAMLSS with meteorological and anthropogenic covariates in the Wuding River basin, China. J. Hydrol. 127692. https://doi.org/10.1016/j.jhydrol.2022.127692

Sharma, S., Hamal, K., Khadka, N., Shrestha, D., Aryal, D., Thakuri, S., 2021. Drought characteristics over Nepal Himalaya and their relationship with climatic indices. Meteorol. Appl. 28(2), e1988. https://doi.org/10.1002/met.1988

Sharma, T., Vittal, H., Chhabra, S., Salvi, K., Ghosh, S., Karmakar, S., 2018. Understanding the cascade of GCM and downscaling uncertainties in hydro-climatic projections over India. Int. J. Clim. 38, e178-e190. https://doi.org/10.1002/joc.5361

She D., Mishra A. K., Xia J., Zhang L. Zhang X., 2016. Wet and dry spell analysis using copulas. Int. J. Clim. 36(1), 476-491. https://doi.org/10.1002/joc.4369

Shirazi, S. Z., Mei, X., Liu, B., Liu, Y., 2022. Estimating potential yield and change in water budget for wheat and maize across Huang-Huai-Hai Plain in the future. Agric. Water Manag. 260, 107282. https://doi.org/10.1016/j.agwat.2021.107282

Shrestha, S., Chapagain, R., Babel, M. S., 2017. Quantifying the impact of climate change on crop yield and water footprint of rice in the Nam Oon Irrigation Project, Thailand. Sci. Total Environ. 599, 689-699. https://doi.org/10.1016/j.scitotenv.2017.05.028

Shukla, S., Wood, A. W., 2008. Use of a standardized runoff index for characterizing hydrologic drought. Geophys. Res. Lett. 35(2). https://doi.org/10.1029/2007GL032487

Srivastava, A. K., Rajeevan, M., Kshirsagar, S. R., 2009. Development of a high resolution daily gridded temperature data set (1969–2005) for the Indian region. Atmos. Sci. Lett. 10(4), 249-254. https://doi.org/10.1002/asl.232

Stasinopoulos, M., Rigby, R.A., 2008. Generalized Additive Models for Location Scale and Shape (GAMLSS) in R. J. Stat. Softw. 223:1–46. https://doi.org/10.1111/j.1467-9876.2005.00510.x.

Steduto, P., Hsiao, T. C., Raes, D., Fereres, E., 2009. AquaCrop-The FAO crop model to simulate yield response to water: I. Concepts and underlying principles. Agronomy Journal, 101(3), 426-437. https://doi.org/10.2134/agronj2008.0139s

Stöckle, C. O., Donatelli, M., Nelson, R., 2003. CropSyst, a cropping systems simulation model. Eur. J. Agron. 18(3-4), 289-307. https://doi.org/10.1016/S1161-0301(02)00109-0

Subburayan S., Murugappan A., Mohan S., 2011. Modified Hargreaves equation for estimation of ET_o in a hot and humid location in Tamilnadu State, India. Int. J. Eng. Sci. Tech. 3(1), 592-600.

Swain, S. S., Mishra, A., Sahoo, B., Chatterjee, C., 2020. Water scarcity-risk assessment in data-scarce river basins under decadal climate change using a hydrological modelling approach. J. Hydrol, 590, 125260. https://doi.org/10.1016/j.jhydrol.2020.125260

Tabari, H., Paz, S. M., Buekenhout, D., Willems, P., 2021. Comparison of statistical downscaling methods for climate change impact analysis on precipitation-driven drought. Hydrol. Earth Syst. Sci. 25(6), 3493-3517. https://doi.org/10.5194/hess-25-3493-2021

Tamaddun, K.A., Kalra, A., Bernardez, M., Ahmad, S., 2019. Effects of ENSO on temperature, precipitation, and potential evapotranspiration of North India's monsoon: An analysis of trend and entropy. Water. 11(2):189.https:// doi:10.3390/w11020189.

Tarek, M., Brissette, F., Arsenault, R., 2021. Uncertainty of gridded precipitation and temperature reference datasets in climate change impact studies. Hydrol. Earth Syst. Sci. 25(6), 3331-3350. https://doi.org/10.5194/hess-25-3331-2021

Tegegne, G., Melesse, A. M., Worqlul, A. W., 2020. Development of multi-model ensemble approach for enhanced assessment of impacts of climate change on climate extremes. Sci. Total Environ. 704, 135357. https://doi.org/10.1016/j.scitotenv.2019.135357

Tehrani, M. J., Helfer, F., Jenkins, G., 2021. Impacts of climate change and sea level rise on catchment management: A multi-model ensemble analysis of the Nerang River catchment, Australia. Sci. Total Environ. 777, 146223. https://doi.org/10.1016/j.scitotenv.2021.146223

Teutschbein, C., Seibert, J., 2012. Bias correction of regional climate model simulations for hydrological climate-change impact studies: Review and evaluation of different methods. J. Hydrol. 456, 12-29. https://doi.org/10.1016/j.jhydrol.2012.05.052

Thornthwaite, C.W., 1948. An approach toward a rational classification of climate. Geogr. Rev. 38, 55-94.

Tirivarombo, S., Osupile, D., Eliasson, P. 2018. Drought monitoring and analysis: standardised precipitation evapotranspiration index (SPEI) and standardised precipitation index (SPI). Physics and Chemistry of the Earth, Parts A/B/C, 106, 1-10. https://doi.org/10.1016/j.pce.2018.07.001

Tiwari, P. R., Kar, S. C., Mohanty, U. C., Dey, S., Sinha, P., Shekhar, M. S., Sokhi, R. S. (2019). Comparison of statistical and dynamical downscaling methods for seasonal-scale winter precipitation predictions over north India. Int. J. Clim. 39(3), 1504-1516. https://doi.org/10.1002/joc.5897

Tong, Y., Gao, X., Han, Z., Xu, Y., Xu, Y., Giorgi, F., 2021. Bias correction of temperature and precipitation over China for RCM simulations using the QM and QDM methods. Clim. Dyn. 57(5), 1425-1443. https://doi.org/10.1007/s00382-020-05447-4

Torma C., Giorgi F. Coppola E., 2015. Added value of regional climate modeling over areas characterized by complex terrain-Precipitation over the Alps. J. Geophys. Res. Atmos. 120(9), 3957-3972. https://doi.org/10.1002/2014jd022781

Trenberth, K.E., Dai, A., Van Der Schrier, G., Jones, P.D., Barichivich, J., Briffa, K.R., Sheffield, J. 2014. Global warming and changes in drought. Nat. Clim. Change. 4(1):17-22.https:// DOI: 10.1038/NCLIMATE2067.

Tsakiris, G., Pangalou, D., Vangelis, H., 2007. Regional drought assessment based on the Reconnaissance Drought Index (RDI). Water. Resour. Manag. 21(5), 821-833. https://doi.org/10.1007/s11269-006-9105-4

Ukkola, A. M., De Kauwe, M. G., Roderick, M. L., Abramowitz, G., Pitman, A. J., 2020. Robust future changes in meteorological drought in CMIP6 projections despite uncertainty in precipitation. Geophys. Res. Lett. 47(11), e2020GL087820. https://doi.org/10.1029/2020GL087820

Van Diepen, C. V., Wolf, J. V., Van Keulen, H., Rappoldt, C., 1989. WOFOST: a simulation model of crop production. Soil Use Manag. 5(1), 16-24. https://doi.org/10.1111/j.1475-2743.1989.tb00755.x

Veettil, A. V., Mishra, A. K., 2020. Multiscale hydrological drought analysis: Role of climate, catchment and morphological variables and associated thresholds. J. Hydrol, 582, 124533. https://doi.org/10.1016/j.jhydrol.2019.124533

Verma, S., Bhatla, R., 2021. Performance of RegCM4 for dynamically downscaling of El Nino/La Nina events during Southwest Monsoon over India and its regions. Earth Space Sci. 8(3), e2020EA001474. https://doi.org/10.1029/2020EA001474

Vicente-Serrano S. M., Beguería S., López-Moreno J. I., 2010. A multiscalar drought index sensitive to global warming: the standardized precipitation evapotranspiration index. J. clim. 23(7), 1696-1718. https://doi.org/10.1175/2009jcli2909.1

Villarini, G., Smith, J.A., Serinaldi, F., Bales, J., Bate, P.D., Krajewski, W.F. 2009. Flood frequency analysis for non-stationary annual peak records in an urban drainage basin. Adv. Water Resour. 32(8):1255-1266. https://doi.org/10.1016/j.advwatres.2009.05.003.

Vuong, Q.H., 1989. Likelihood ratio tests for model selection and non-nested hypotheses. Econometrica 57 (2):307–333. https://www.jstor.org/stable/1912557.

Wang D., Hejazi M., Cai X. Valocchi A. J., 2011. Climate change impact on meteorological, agricultural, and hydrological drought in central Illinois. Water Resour. Res. 47(9). https://doi.org/10.1029/2010wr009845

Wang, B., Jin, C., Liu, J., 2020. Understanding Future Change of Global Monsoons Projected by CMIP6 Models. J. Clim. 33:6471–6489. https://doi.org/10.1175/JCLI-D-19-0993.1

Wang, D., Hejazi, M., Cai, X., Valocchi, A. J., 2011. Climate change impact on meteorological, agricultural, and hydrological drought in central Illinois. Water Resour. Res. 47(9). https://doi.org/10.1029/2010WR009845

Wang, H., Kumar, A., 2015. Assessing the impact of ENSO on drought in the US Southwest with NCEP climate model simulations. J. Hydrol. 526:30-41. http://dx.doi.org/10.1016/j.jhydrol.2014.12.012.

Wang, Y., Li, J., Feng, P., Hu, R. 2015. A Time-Dependent Drought Index for Non-Stationary Precipitation Series. Water Resour. Manag. 29:5631–5647. https:// DOI 10.1007/s11269-015-1138-0

Wilby, R. L., Hay, L. E., Gutowski Jr, W. J., Arritt, R. W., Takle, E. S., Pan, Z., Leaves G.H., Clark, M. P., 2000. Hydrological responses to dynamically and statistically downscaled climate model output. Geophys. Res. Lett. 27(8), 1199-1202. https://doi.org/10.1029/1999GL006078

Wilhite D. A., Glantz M. H., 1985. Understanding: the drought phenomenon: the role of definitions. Water Int. S10 (3), 111-120. https://doi.org/10.4324/9780429301735-2

Wilhite, D. A., 2000. Drought as a natural hazard: concepts and definitions. Published in Drought: A Global Assessment, Vol. I, edited by Donald A. Wilhite, chap. 1, pp. 3–18, London: Routledge

Willmott, C.J., Rowe, C.M., Mintz, Y., 1985. Climatology of the terrestrial seasonal water cycle. J. Climatol. 5, 589–606.

Won, J., Choi, J., Lee, O., Kim, S., 2020. Copula-based Joint Drought Index using SPI and EDDI and its application to climate change. Sci. Total Environ. 744, 140701. https://doi.org/10.1016/j.scitotenv.2020.140701

Xu, L., Chen, N., & Zhang, X., 2018. A comparison of large-scale climate signals and the North American Multi-Model Ensemble (NMME) for drought prediction in China. J. Hydrol. 557, 378-390. https://doi.org/10.1016/j.jhydrol.2017.12.044

Yang, Y., Cui, Y., Bai, K., Luo, T., Dai, J., Wang, W., Luo, Y., 2019. Short-term forecasting of daily reference evapotranspiration using the reduced-set Penman-Monteith model and public weather forecasts. Agric. Water Manag. 211, 70-80. https://doi.org/10.1016/j.agwat.2018.09.036

Yevjevich, V. M., 1967. Objective approach to definitions and investigations of continental hydrologic droughts, An (Doctoral dissertation, Colorado State University. Libraries).

Zarch, M. A. A., Sivakumar, B., Sharma, A., 2015. Droughts in a warming climate: A global assessment of Standardized precipitation index (SPI) and Reconnaissance drought index (RDI). J. Hydrol. 526, 183-195. https://doi.org/10.1016/j.jhydrol.2014.09.071

Zhai, J., Mondal, S. K., Fischer, T., Wang, Y., Su, B., Huang, J., Tao, H., Wang, G., Ullah, W., Uddin, M. J., 2020. Future drought characteristics through a multi-model ensemble from CMIP6 over South Asia. Atmos. Res. 246, 105111. https://doi.org/10.1016/j.atmosres.2020.105111

Zhang, H., Wu, C., Yeh, P. J. F., Hu, B. X., 2020. Global pattern of short-term concurrent hot and dry extremes and its relationship to large-scale climate indices. Int. J. Clim. 40(14), 5906-5924. https://doi.org/10.1002/joc.6555

Zhang, T., Su, X., Feng, K., 2021. The development of a novel nonstationary meteorological and hydrological drought index using the climatic and anthropogenic indices as

covariates. Sci. Total Environ. 786, 147385. https://doi.org/10.1016/j.scitotenv.2021.147385

Zhang, Y., You, Q., Chen, C., Ge, J., 2016. Impacts of climate change on streamflows under RCP scenarios: A case study in Xin River Basin, China. Atmos. Res. 178, 521-534. https://doi.org/10.1016/j.atmosres.2016.04.018

Zou, L., Zhou, T., 2021. Mean and extreme precipitation changes over China under SSP scenarios: results from high-resolution dynamical downscaling for CORDEX East Asia. Clim. Dyn.1-17.

PUBICATIONS FROM THE RESEARCH

Peer Reviewed Journals:

1. **Soumyashree Dixit** and K V Jayakumar (2022), "A Non-stationary and Probabilistic Approach for Drought Characterization using Trivariate and Pairwise Copula Construction (PCC) Model". Water Resources Management (SCI). DOI: 10.1007/s11269-022-03069-5

2. **Soumyashree Dixit** and K V Jayakumar (2021) "Spatio-temporal analysis of copula based probabilistic Multivariate drought index using CMIP6 model". International Journal of Climatology (SCI). https://doi.org/10.1002/joc.7469

3. **Soumyashree Dixit** and K V Jayakumar (2021) "A Study on Copula Based Bivariate and Trivariate Drought Assessment in Godavari River Basin and the Teleconnection of Drought with Large Scale Climate Indices. Theoretical and Applied Climatology (SCI). https://doi.org/10.1007/s00704-021-03792-w

4. **Soumyashree Dixit**, Syed Tayyaba and K V Jayakumar (2021) "Spatio-temporal variation and future risk assessment of projected drought events in the Godavari River basin using Regional Climate Models". Journal of Water and Climate change (SCI). doi: 10.2166/wcc.2021.093

5. **Soumyashree Dixit**, Bindu Madhavi Atla, and K V Jayakumar (2022), "Evolution and drought hazard mapping of future meteorological and hydrological droughts using CMIP6 model", May 2022, Stochastic Environmental Research and Risk Assessment, DOI: 10.1007/s00477-022-02230-1

Conference Presentations:

1. **Soumyashree Dixit** and K V Jayakumar (2018), "Climate change impact on Munneru River basin using SWAT", International Conference International Conference on Soil and Water Assessment Tool 2018, IIT Madras. 10-12 Jan.

2. **Soumyashree Dixit,** Pooja Singh and K V Jayakumar (2018)**, "**Spatio-temporal Analysis of Drought across Warangal Region based on Multisource Remote Sensing Data", HYDRO 2019- International conference on Hydraulics, Water Resources and Coastal Engineering 2019, Osmania University, Hyderabad 10-20 Dec.